POLITECHNIKA KRAKOWSKA
im. Tadeusza Kościuszki

Bogumił Wrana

Soil Dynamics – Computation Models

KRAKÓW 2016

ISBN 978-83-7242-888-2

Wydawnictwo PK, ul. Skarżyńskiego 1, 31-866 Kraków; tel.: 012 628 37 25, fax: 012 628 37 60
e-mail: wydawnictwo@pk.edu.pl ☐ www.wydawnictwo.pk.edu.pl
Adres do korespondencji: ul. Warszawska 24, 31-155 Kraków

Druk i oprawę wykonano w Dziale Poligrafii Politechniki Krakowskiej
Ark. wyd. 11,00.

Zam. 166/2016 Cena zł 29,40 zł z VAT

Table of Contents

Preface

This book is intended for use as a text in advanced soil mechanics that focuses on the description of dynamic waves in soil which are of interest mainly to practicing and research engineers. Although soil mechanics involves soil statics and dynamics, only soil statics have become well established while soil dynamics remained in a rudimentary stage until recent developments in the field of earthquake engineering.

Dynamic loads are imposed on soils and geotechnical structures by several sources, such as human activities (bomb blasts, the operation of machinery, construction operations, mining, traffic) or by natural factors such as earthquakes, wind, and wave actions. It is well known that the stress–strain properties of a soil and its behaviour depend upon several model parameters. In the book, the author considers different soil models such as one-, two- and three-phase soil models in the range of homogeneous mixture theory of continuous mechanics over the space-time domain.

The author proposes strategies to solve continuous dynamics problems in a soil using the finite element method (FEM) with the influence of fluid and air flow through a soil. A nonlinear stress-strain relationship with rate-dependent deformation based on a plasticity model was proposed. In soil dynamics calculated by numerical methods a major task is obtain the solution (displacement, velocity and acceleration) over time with acceptable error. The author considers and compares some advance time integration methods based on signal analysis.

I hope that this book can be a useful reference for students, researchers, and modellers interested in soil dynamics as one-two- and three phase mixture material.

Bogumił Wrana

Chapter 1

INTRODUCTION

1.1. Preliminary discussion

Soil is a heterogeneous material consisting primarily of mineral, organic or anthropogenic granular particles of different sizes and pores occupied by fluid (mainly water) and gas (mainly air). Soil is thus a three-phase material consisting of a solid phase (the structure made of the particles), a liquid phase and a gas phase. Currently, three models of soil material are considered: a single-phase model as a mixture of grains and pores; two-phase model, consisting of a solid (skeleton) and the fluid phase in the pores; a three-phase material with interaction forces between three phases.

Some researchers recognise the work of Karl von Terzaghi' "*Erdbaumechanik auf bodenphysikalischer Grundlage*" issued in Vienna in 1925 as the beginning of classical study of the mechanics of soil. However, the initial work should be recognised as that of Charles Coulomb in 1776 on the basic principles of limit equilibrium in soil.

The beginning of the development of the theory of porous media of soil is recognised as the work of Maurice Anthony Biot in 1956. Biot considered the wave propagation in a porous soil medium using generalised Lagrangian displacement. He decided to separate the soil skeleton displacement $\mathbf{u}^s$ with fluid displacement $\mathbf{u}^f$ and considered kinetic energy and dissipation energy on the relative motion of fluid to the skeleton.

On the development of the theory of porous media, a significant impact has the following researchers:

- Heinrich and Desoyer (1956) – studying stationary and non-stationary water flow in pores, taking into account the anisotropy of the skeleton;
- Frenkel (1944) – describing the quantitative effects associated with the spread of elastic vibrations in soil;
- Derski (1978) – providing a set of four equations: mass conservation of two-phase medium; liquid mass; balance of skeleton with pore water and slowly flowing water in pores;

– Smith (1979) – proving the equivalence of Biot and Derski equations;
– Szefer (1980) – developing the consolidation theory in the nonlinear static problems;
– Gryczmański (1995) – collecting and comparing the current elastic–plastic soil models;
– Kubik with co–workers (2000) – presenting the principles of porous soil dynamics in the elastic range;
– Sikora (2008, 2009) – collecting and comparing the current problems of porous soil modelling.

In 1996, Rene de Boer presented the history of the development of porous soil models in a review article.

Description of the soil structure (consist with randomly distributed grain, pore water and gas) as the continuum function is a still open problem. This is a problem of scale, described as the ratio l_0/d, where l_0 – the characteristic dimension of the average area, d – average equivalent diameter of the soil particles.

1.2. Dynamic load

The loads acting on the soil can be static, unchanging over time and/or dynamic loads varying over time. This book relates to dynamic loads which extends (relative to the static load) to identify the inertial forces dependent on the density and the soil acceleration. Moreover, it relates to the determination of damping forces, which in essence is defined by the local phenomenon of pore water flow and viscous damping associated with models of the theory of elastic-viscoplasticity.

Based on the dynamic characteristics of the force, dynamic load (Figure 1.1) acting on the soil can be grouped as follows:
– periodic (often called cyclic in soil dynamics), e.g. from a vibrating compaction or vibration of rotating machines installed on foundations, such as turbines, fans, screens, etc.;
– impact or impulse, which act directly on the soil or through the foundation on which shock devices, such as hammers, presses, etc. are mounted;
– seismic, which result from earthquakes and paraseismic originate from human activities, such as explosions in mines and moving vehicles.

These loads are different amplitudę-frequency characteristics, and may be stationary with a constant spectrum over time or nonstationary with the spectrum changing over time.

In the half-space soil area, the load can be found at:
– the ground surface level – caused by moving loads (e.g. from traffic vehicles, rail, ...) or by the soil compaction machine;

– the bottom foundation level – resulting from dynamic forces of machinery or from the dynamic execution of sheet piling, ...;
– below the ground level in tunnels – caused by moving vehicles or tunnel works technology,
– on the edge of the calculation model area – caused by earthquakes.

The yellow area on Figure 1.1 presents the dynamic loads acting during several minutes, in which are exist the two different phenomena depending on the type of soil. In the case of cohesive soils where the permeability coefficient is small (e.g. silt or clay), the undrainage dynamics analysis is considered. In the case of cohesionless soil where the permeability coefficient is large (e.g. sand or gravel), the dynamic analysis with drainage is considered, which includes the soil liquefaction problem (especially in the case of semi–compacted sand). It should be noted that this book does not cover the soil liquefaction problem.

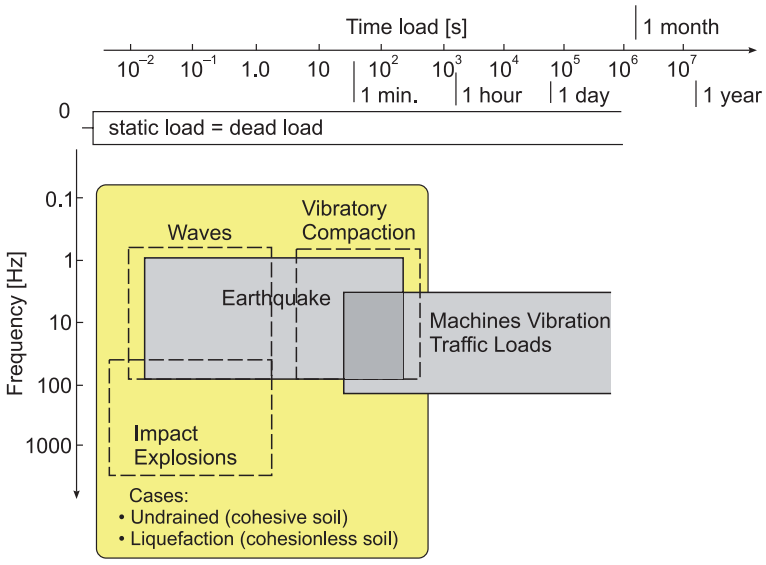

Fig. 1.1. Load types acting on the soil area

In the dynamic analysis of buildings, the problem of soil structure interaction with the surrounding soil should be considered. Currently, in most practical calculations the simplification is used. The above-ground structure is separated from the soil by introducing appropriate supports into the model structure. Next, the wave propagation problem in a soil (as a separate half-space area) with the building foundations only is considered.

The main objective of this book is to provide a scientific basis for modelling problems of soil dynamics with particular reference to the phenomenon of wave

propagation. This problem is considered in many scientific disciplines, such as the dynamics of building structures resting on the soil (soil structure interaction for dynamic loading) and paraseismic engineering, geophysics, and the numerical modelling of the soil area.

In the case of soil dynamic, the soil model as the constitutive relationship between strain and stress played the decisive role. Based on results of field tests of shear strain, the specified ranges of the constitutive models can be considered, as shown in Table 1.1. The ranges can vary depending on the type of soil and the conditions, e.g. the plasticity index or compacting index, the water content, the content of clay fraction, the current history of stress, and the degree of consolidation.

Table 1.1

Soil constitutive models depend on the shear strain amplitude under cyclic loading Davidovici (1995)

Soil constitutive equation	Values of shear strain γ						
	10^{-6}	10^{-5}	10^{-4}	10^{-3}	10^{-2}	10^{-1}	1
	Small		Average		Large	Destroying	
Elastic							
Elastic-plastic							
Destruction							
Effects of cyclic loading							
Effects of load speed							

Table 1.1 shows that:

- with $\gamma < 10^{-4}$, soil deformations do not depend on the frequency of dynamic forces, and its behaviour can be described by a single-phase, linear-elastic model;
- at $10^{-4} < \gamma < 10^{-1}$, soil behaviour can be described by a two-phase, elastic-plastic mode;
- with $\gamma > 10^{-3}$, shear amplitude and frequency of the dynamic forces changes the shape of the hysteresis loop. In the non-cohesive, semi-compacted soils, increases in pore pressure leads to the phenomenon of liquefaction, and in compacted soil, to the phenomenon of dilatancy.

1.3. Soil modelling problems in the finite element method (FEM)

In dynamic analysis, by using the finite element method, one can find three main stages: idealisation, discretisation, and solution of equations of motion. At the stage of idealisation, it is necessary to enter the soil layers with the same material parameters (Figure 1.2a).

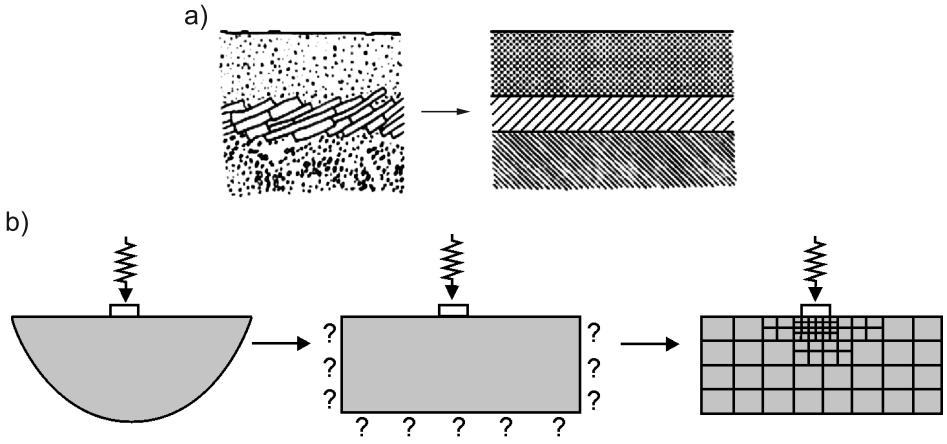

Fig. 1.2. Stages of numerical modelling (Gaussmann, 2002): a) separation of soil layers; b) reduction in the amount of unbounded area of soil and the selection of mesh elements

In the discretisation stage (Figure 1.2b), the unbounded half-space area of soil (naturally occurring) should be restricted to a limited area, then the finite element mesh should be determined. For a proper mesh with a finite number of degrees of freedom, matrix calculations are carried out which solve the equations of motion. Element mesh density can vary over time and location, taking into account the thickness of the individual layers of soil.

1.4. The scope of applicability of one-, two- and three-phase models

Three levels of accuracy of soil models due to the number of phases can be considered in dynamic analysis: a) a single-phase model; b) a two-phase model, consisting of the skeleton and pore fluid; c) a three-phase, consisting of the soil skeleton gas and liquid in the pores.

The single-phase soil model is described by parameters of mixture material model with regard to their physical and mechanical properties. This model is mainly used to the seismic waves propagation problem in the linear-elastic material soil model.

The two-phase model is mainly used in the case of fully saturated soil, in the analysis of dams, embankments or slopes, and in the case of dry soil.

The three-phase model, taking into account the interaction of the soil skeleton, fluid and gas in the pores, is currently being developed and is a field of research in many scientific centres. This model leads to a large complex system of equations of motion, and practical numerical calculation requires high-powered hardware.

Figure 1.3 shows an example of the areas to which the model is applied. The single-phase model is most commonly applied to assess the propagation of vibrations from their source to points of interest, e.g. a building. If there is a need to analyse vibrations of the soil around a building, a two-phase model is need. A three-phase model is often used in the analysis of local phenomena (Figure 1.3).

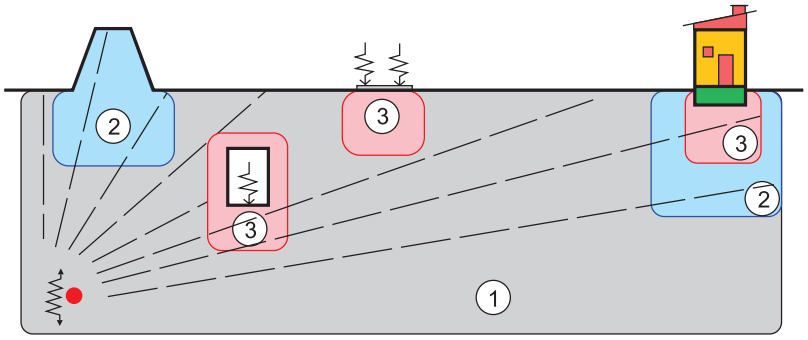

Fig. 1.3. Examples of areas of application models: (1) the single-phase model; (2) the two--phase model; (3) the three-phase model

1.5. Description of chapters of the book

The book contains seven chapters – the first chapter provides a general introduction, which aims to familiarise the reader with the description of dynamic problems taking place in the book. The second chapter is devoted to the problems of wave propagation in the single-phase isotropic elastic half-space: dilatational wave, shear waves, surface waves Rayleigh and Love's. Next, a formula often used in seismic and paraseismic wave propagation problems is presented.

The third chapter presents the problems of wave propagation in the two-phase soil model consisting of the solid phase (skeleton) and fluid phase fully saturated the pores. This model was first described by Biot in 1956 and is still being developed. This section presents the solution of the wave equation with two dilatational waves and two shear waves.

In the fourth chapter, the equation of motion of soil as the three-phase model is considered: a) a skeleton phase; b) a water phase and c) an air phase – this is defined

as an unsaturated or partially saturated soil. This model is the subject of many scientific papers. The main problems in this model are the definition of the variables that describe the behaviour of the soil under the dynamic load and the problems with both laboratory and in-situ measurements of parameters. In this chapter, the set of problem equations which describe wave propagation is presented – there are three dilatational waves and three shear waves.

The fifth chapter contains an introduction to the description of elastic-plastic and elastic-viscoplastic soil models. The Mohr-Coulomb, Drucker-Prager and Cam-Clay elastic-plastic models are described. Moreover, elastic-viscoplastic models, which take into account the dynamic loads (time-varying) according to the theory of overstress, and the nonstationary flow theory are presented. Remarks and comments about the advantages and disadvantages of describing the time-varying load theory are listed.

The sixth chapter presents the numerical calculation methods used to differential equations motion described the multiphase soil. The following sets of variables of the three-phase medium are presented:

a) displacement of skeleton, water and air ($\mathbf{u}^s$, $\mathbf{u}^w$, $\mathbf{u}^a$);
b) displacement of skeleton, velocity of water flow and pore water pressure ($\mathbf{u}^s$, $\mathbf{w}$, p);
c) displacement of skeleton and pore water pressure ($\mathbf{u}^s$, p).

Next in this chapter, the problem of boundary conditions in the unbounded soil area is considered. At the end of this chapter, a description of the experiences of the VELACS research project carried out in order to verify the computational models developed in the dynamics of soil issues is provided.

Chapter seven is devoted to the presentation of numerical problems and the solving of equations of motion by the finite element method. The two main characteristics of time integration methods are shown: the modal method and the direct method of integration over time. Error measurement of the numerical methods used for the integration of the equation of motion are presented. The spectral radius, the definition of the amplitude error and the error period are presented with comments. Methods, such as the central difference method, the method of Wilson, the Newmark method, HHT-α method and the method of TDG are analysed. Also methods used to non--linear equations of motion are presented.

The book includes four appendices. Appendix A shows the matrices and vectors operations and definitions of differential operators. Appendix B contains the analytical equation of gradients of the potential function theory of plasticity. Appendix C presents the basic equation dynamics of discrete systems. Tables of dynamic parameters of soil, construction and building materials are presented in Appendix D.

Different aspects of wave propagation in the soil are considered. Many scientists in many research centres have considered this problem and have made significant contributions; therefore, I have made attempts to limit the number of references. I would like to extend my apologies to all those researchers whose work I have omitted.

Finally, I would to like to express my gratitude to Prof Zbigniew Sikora (Gdańsk University of Technology, Poland) and Prof Roman Lewandowski (Poznań University of Technology, Poland) for their valuable comments in the final editing of this textbook.

1.6. References to Chapter 1

Biot M.A. (1956a): *Theory of Propagation of Elastic Waves in a Fluid – Saturated Porous Solid. Low – Frequency Range*, Journal of the Acoustical Society of America 28 (2), 168-178.

Biot M.A. (1956b): *Theory of Propagation of Elastic Waves in a Fluid – Saturated Porous Solid. Higher – Frequency Range*, Journal of the Acoustical Society of America 28 (2), 179-191.

Boer R. de (1996): *Highlights in the historical development of the porous media theory – toward a consistent macroscopic theory*, Applied Mechanics Reviews vol. 49, 201-262.

Chmilewski T., Zembaty Z. (1998): *Podstawy dynamiki budowli*, Arkady.

Couomb C.A. (1776): *Essai sur une application des r`egles des maximis et minimis `a quelques problemes de statique relatifs `a l'architecture*, Mem. Acad. Roy. Pres. divers Sav., 5, 7.

Davidvici V. et al. (1995): *Genie Parasismique*, Presses des Ponts et Chaussées, Paris.

Frenkel J. (1944): *On the Theory of Seismic and Seismoelectric Phenomena in Moist Soil*, J. Phys., 8, 230-241.

Gaussann P., Schad H., Smith I. (2002): *Numerical Methods in Geotechnical Engineering Handbook*, Ernst & Sohn, Berlin.

Gryczański M. (1995): *Wprowadzenie do opisu sprężysto – plastycznych modeli gruntów*, Wydawnictwo PAN, Studia z zakresu inżynierii, nr 40, Warszawa.

Kubik J., Cieszko M., Kaczmarek M. (2000): *Podstawy dynamiki nasyconych ośrodków porowatych, Biblioteka mechaniki stosowanej*, Seria A. Monografie.

Langer J. (1980): *Dynamika budowli*, Politechnika Wrocławska.

Lewandowski R. (2006): *Dynamika konstrukcji budowlanych*, Wydawnictwo Politechniki Poznańskiej.

Nowacki W. (1972): *Dynamika budowli*, Arkady.

Sikra Z. (2008): *Geo-engineering computer simulation seems attractive but it is the real word?*, Studia Geotechnica et Mechanica, Vol. XXX, Nr 1–2.

Siora Z. (2009): *Symulacje komputerowe w geotechnice. Problem szacowania parametrów materiałowych i ważności rozwiązań numerycznych*, Mat. XXIV Ogólnopolskie warsztaty pracy projektanta konstrukcji, Wisła 17–20 marzec, 2009, Tom II, 337-394.

Sefer G. (1980): *Nonlinear problems of consolidation theory*, Mat. Konf. Problems nonlineares de mecanique, PWN, Warszawa.

Teraghi K. (1925): *Erdbaumechanik auf bodenphysikalischer Grundlage*, Leipzig, F. Deuticke.

Wodarczyk E. (1991): *Modele gruntów i skał w zagadnieniach falowych*, *A*rchiwum Inżynierii Lądowej, t. XXXVII, z. 3–4.

Chapter 2

ELASTIC WAVES IN HALF–SPACE

2.1. Notations used in Chapter 2

A – matrices, tensors,

a – vectors

$\nabla \mathbf{u} = \mathrm{div}\mathbf{u} = \dfrac{\partial u_1}{\partial x_1} + \dfrac{\partial u_2}{\partial x_2} + \dfrac{\partial u_3}{\partial x_3} = \varepsilon_v$ – dilatation, volumetric strain, displacement field divergence

$\Delta = \nabla^2 = \nabla\nabla = \left\{ \dfrac{\partial^2}{\partial x^2}, \dfrac{\partial^2}{\partial y^2}, \dfrac{\partial^2}{\partial z^2} \right\}$ – Laplace's operator, e.g. $\nabla^2 u = \dfrac{\partial^2 u}{\partial x_1^2} + \dfrac{\partial^2 u}{\partial x_2^3} + \dfrac{\partial^2 u}{\partial x_3^2}$,

$\lambda = \dfrac{vE}{(1+\nu)(1-2\nu)}$ – Lamé's constant

$\mu = G = \dfrac{E}{2(1+\nu)}$ – shear modulus, Kirchhoff's modulus, Lamé's constant

$v = \dfrac{\lambda}{2(\lambda + G)}$ – Poisson's ratio

$E = \dfrac{G(3\lambda + 2G)}{\lambda + G}$ – Young's modulus

ρ – volume density

$V_L = \sqrt{\dfrac{M}{\rho}} = \sqrt{\dfrac{E(1-\nu)}{(1+\nu)(1-2\nu)\rho}}$ – dilatational wave velocity, $M = \lambda + 2G$

$V_S = \sqrt{\dfrac{G}{\rho}} = \sqrt{\dfrac{E}{2(1+\nu)\rho}}$ – shear wave velocity, distortion wave velocity

2.2. Introduction

The propagation of elastic waves problem in a half-space soil due to dynamic loads is considered (Figure 2.1). Loads can be placed on the soil surface (e.g. a passing car, train), they can also be caused by mechanical device resting on the foundation (e.g. harmonic excitation by electric turbines, impact loads by hammers etc.) or can be derived from loads inside a half-space (e.g. traffic in a tunnel). Loads causing a wave phenomenon can be periodic or aperiodic.

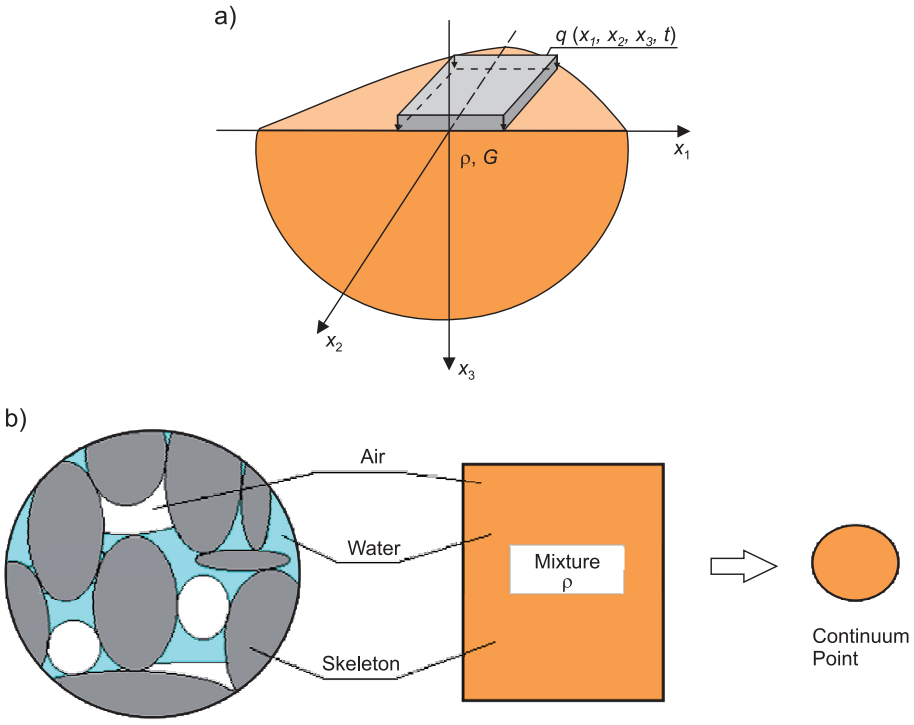

Fig. 2.1. a) Elastic half-space, b) Continuum point of the single-phase soil model

An analytical solution of the wave problem in the case of concentrated force acting on elastic half-space was first provided by Lamb (1904). The same problem was considered by Pekeris (1955) and by De Hoop (1970). In the case of vertical loads, an approximation solution is often used – this is in order to omit horizontal components. This solution is called *confined elasticity* and it was proposed by Westergaard (1938) in static loads and by Barend (1980) in dynamic loads. This approximation solution is often applied in engineering calculations to determine a displacement or a stress field in the elastic half-space under dynamic load.

This chapter is devoted to the wave propagation problem in elastic half-space soil. The different parts of the chapter are devoted to the description of a dilatational wave, shear waves, a Rayleigh's and a Love's surface waves.

2.3. The basic wave equations in the single-phase elastic half-space soil model

The basic equations of the dynamics problem in the single-phase soil model are a set of Navier equations with include inertia forces. In the Cartesian coordinate system, the equations are:

$$(\lambda+G)\frac{\partial}{\partial x_1}\left(\frac{\partial u_1}{\partial x_1}+\frac{\partial u_2}{\partial x_2}+\frac{\partial u_3}{\partial x_3}\right)+G\left(\frac{\partial^2 u_1}{\partial x_1^2}+\frac{\partial^2 u_1}{\partial x_2^2}+\frac{\partial^2 u_1}{\partial x_3^2}\right)+b_1=\rho\frac{\partial^2 u_1}{\partial t^2} \quad (2.1a)$$

$$(\lambda+G)\frac{\partial}{\partial x_2}\left(\frac{\partial u_1}{\partial x_1}+\frac{\partial u_2}{\partial x_2}+\frac{\partial u_3}{\partial x_3}\right)+G\left(\frac{\partial^2 u_2}{\partial x_1^2}+\frac{\partial^2 u_2}{\partial x_2^2}+\frac{\partial^2 u_2}{\partial x_3^2}\right)+b_2=\rho\frac{\partial^2 u_2}{\partial t^2} \quad (2.1b)$$

$$(\lambda+G)\frac{\partial}{\partial x_3}\left(\frac{\partial u_1}{\partial x_1}+\frac{\partial u_2}{\partial x_2}+\frac{\partial u_3}{\partial x_3}\right)+G\left(\frac{\partial^2 u_3}{\partial x_1^2}+\frac{\partial^2 u_3}{\partial x_2^2}+\frac{\partial^2 u_3}{\partial x_3^2}\right)+b_3=\rho\frac{\partial^2 u_3}{\partial t^2} \quad (2.1c)$$

or

$$(\lambda+G)\frac{\partial}{\partial x_1}\nabla\mathbf{u}+G\nabla^2 u_1+b_1=\rho\frac{\partial^2 u_1}{\partial t^2} \quad (2.1d)$$

$$(\lambda+G)\frac{\partial}{\partial x_2}\nabla\mathbf{u}+G\nabla^2 u_2+b_2=\rho\frac{\partial^2 u_2}{\partial t^2} \quad (2.1e)$$

$$(\lambda+G)\frac{\partial}{\partial x_3}\nabla\mathbf{u}+G\nabla^2 u_3+b_3=\rho\frac{\partial^2 u_3}{\partial t^2} \quad (2.1f)$$

where:

ρ – volume density of soil,

b_1, b_2, b_3 – components of mass force in the direction x_1, x_2, x_3.

2.4. Constitutive equations

Constitutive equations of elastic half-space soil model are Hooke's equations with isotropic elastic soil parameters, determining normal stress:

$$\sigma_{11} = \lambda\varepsilon_v + 2G\frac{\partial u_1}{\partial x_1} \tag{2.2a}$$

$$\sigma_{22} = \lambda\varepsilon_v + 2G\frac{\partial u_2}{\partial x_2} \tag{2.2b}$$

$$\sigma_{33} = \lambda\varepsilon_v + 2G\frac{\partial u_3}{\partial x_3} \tag{2.2c}$$

shear stress:

$$\tau_{12} = G\left(\frac{\partial u_1}{\partial x_2} + \frac{\partial u_2}{\partial x_1}\right) = \tau_{21} \tag{2.2d}$$

$$\tau_{13} = G\left(\frac{\partial u_1}{\partial x_3} + \frac{\partial u_3}{\partial x_1}\right) = \tau_{31} \tag{2.2e}$$

$$\tau_{23} = G\left(\frac{\partial u_2}{\partial x_3} + \frac{\partial u_3}{\partial x_2}\right) = \tau_{32} \tag{2.2f}$$

In the consideration of wave propagation, it is assumed that $b_1 = b_2 = b_3 = 0$, so that equation (2.1) reduces the homogeneous differential equation:

$$(\lambda + G)\frac{\partial}{\partial x_1}\varepsilon_v + G\nabla^2 u_1 = \rho\frac{\partial^2 u_1}{\partial t^2} \tag{2.3a}$$

$$(\lambda + G)\frac{\partial}{\partial x_2}\varepsilon_v + G\nabla^2 u_2 = \rho\frac{\partial^2 u_2}{\partial t^2} \tag{2.3b}$$

$$(\lambda + G)\frac{\partial}{\partial x_3}\varepsilon_v + G\nabla^2 u_3 = \rho\frac{\partial^2 u_3}{\partial t^2}. \tag{2.3c}$$

2.5. Dilatational wave equation

Differentiating equation: (2.1a) with respect to x_1, (2.1b) with respect to x_2, (2.1c) with respect to x_3, obtained:

$$\lambda\frac{\partial^2}{\partial x_1^2}\left(\frac{\partial u_1}{\partial x_1} + \frac{\partial u_2}{\partial x_2} + \frac{\partial u_3}{\partial x_3}\right) + G\frac{\partial^2}{\partial x_1^2}\left(\frac{\partial u_1}{\partial x_1} + \frac{\partial u_2}{\partial x_2} + \frac{\partial u_3}{\partial x_3}\right) + \\ + G\frac{\partial}{\partial x_1}\left(\frac{\partial^2 u_1}{\partial x_1^2} + \frac{\partial^2 u_1}{\partial x_2^2} + \frac{\partial^2 u_1}{\partial x_3^2}\right) = \rho\frac{\partial}{\partial x_1}\frac{\partial^2 u_1}{\partial t^2} \tag{2.4a}$$

$$\lambda\frac{\partial^2}{\partial x_2^2}\left(\frac{\partial u_1}{\partial x_1}+\frac{\partial u_2}{\partial x_2}+\frac{\partial u_3}{\partial x_3}\right)+G\frac{\partial^2}{\partial x_2^2}\left(\frac{\partial u_1}{\partial x_1}+\frac{\partial u_2}{\partial x_2}+\frac{\partial u_3}{\partial x_3}\right)+$$
$$+G\frac{\partial}{\partial x_2}\left(\frac{\partial^2 u_2}{\partial x_1^2}+\frac{\partial^2 u_2}{\partial x_2^2}+\frac{\partial^2 u_2}{\partial x_3^2}\right)=\rho\frac{\partial}{\partial x_2}\frac{\partial^2 u_2}{\partial t^2} \tag{2.4b}$$

$$\lambda\frac{\partial^2}{\partial x_3^2}\left(\frac{\partial u_1}{\partial x_1}+\frac{\partial u_2}{\partial x_2}+\frac{\partial u_3}{\partial x_3}\right)+G\frac{\partial^2}{\partial x_3^2}\left(\frac{\partial u_1}{\partial x_1}+\frac{\partial u_2}{\partial x_2}+\frac{\partial u_3}{\partial x_3}\right)+$$
$$+G\frac{\partial}{\partial x_3}\left(\frac{\partial^2 u_3}{\partial x_1^2}+\frac{\partial^2 u_3}{\partial x_2^2}+\frac{\partial^2 u_3}{\partial x_3^2}\right)=\rho\frac{\partial}{\partial x_3}\frac{\partial^2 u_3}{\partial t^2} \tag{2.4c}$$

Summing parties' equation (2.4), we obtained:

$$(\lambda+2G)\frac{\partial^2}{\partial x_1^2}\left(\frac{\partial u_1}{\partial x_1}+\frac{\partial u_2}{\partial x_2}+\frac{\partial u_3}{\partial x_3}\right)+(\lambda+2G)\frac{\partial^2}{\partial x_2^2}\left(\frac{\partial u_1}{\partial x_1}+\frac{\partial u_2}{\partial x_2}+\frac{\partial u_3}{\partial x_3}\right)+$$
$$+(\lambda+2G)\frac{\partial^2}{\partial x_3^2}\left(\frac{\partial u_1}{\partial x_1}+\frac{\partial u_2}{\partial x_2}+\frac{\partial u_3}{\partial x_3}\right)=\rho\frac{\partial^2}{\partial t^2}\left(\frac{\partial u_1}{\partial x_1}+\frac{\partial u_2}{\partial x_2}+\frac{\partial u_3}{\partial x_3}\right) \tag{2.5a}$$

or

$$\frac{(\lambda+2G)}{\rho}\left(\frac{\partial^2}{\partial x_1^2}\varepsilon_v+\frac{\partial^2}{\partial x_2^2}\varepsilon_v+\frac{\partial^2}{\partial x_3^2}\varepsilon_v\right)-\frac{\partial^2}{\partial t^2}\varepsilon_v=0 \tag{2.5b}$$

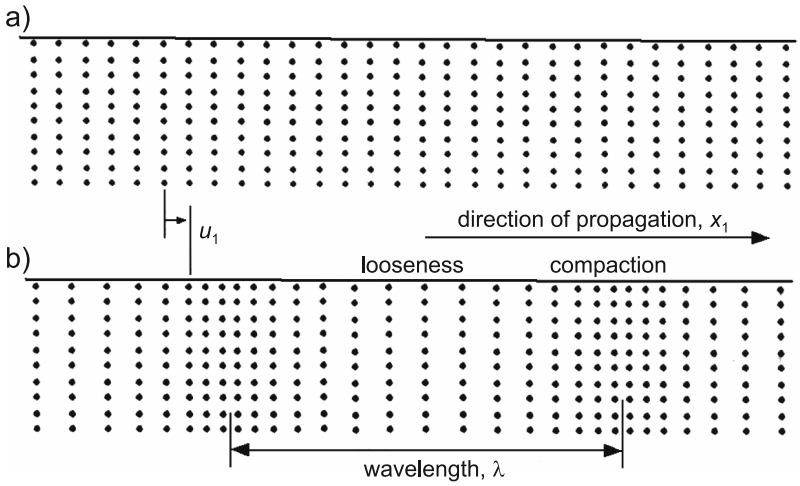

Fig. 2.2. The dilatational wave: a) before the wave propagation; b) during the wave propagation

or

$$\frac{(\lambda+2G)}{\rho}\nabla^2\varepsilon_v-\frac{\partial^2}{\partial t^2}\varepsilon_v=0 \tag{2.5c}$$

Equation (2.5c) is a homogeneous differential equation that describes the eigen--vibrations of half-space soil as a homogeneous isotropic elastic area. The first part defines the elasticity of soil, and the second part determines the inertia of a soil area by the ε_v variable. The equation describes the propagation of the dilatational wave, the volumetric wave or the pressure wave (flat or spherical, depending on the space dimension), see Figure 2.2. The constant in equation (2.5c) is:

$$V_L^2=\frac{(\lambda+2G)}{\rho}=\frac{M}{\rho}=\frac{E(1-\nu)}{(1+\nu)(1-2\nu)\rho}\ -\text{dilatational wave speed} \tag{2.6}$$

2.6. Shear wave equations

Shear wave equations are obtained from equation (2.3) by reducing the dilatation part ε_v. Next differentiating it successively in respect to the variables: x_1, x_2, x_3.

The shear wave equation in the plane x_2 – x_3 obtained by differentiating equation (2.3b) with respect to x_3, (2.3c) with respect to x_2, and then adding the parties to give:

$$\frac{G}{\rho}\nabla^2\left(-\frac{\partial u_2}{\partial x_3}+\frac{\partial u_3}{\partial x_2}\right)-\frac{\partial^2}{\partial t^2}\left(-\frac{\partial u_2}{\partial x_3}+\frac{\partial u_3}{\partial x_2}\right)=0 \tag{2.7a}$$

or

$$\frac{G}{\rho}\nabla^2\omega_1-\frac{\partial^2\omega_1}{\partial t^2}=0 \tag{2.7b}$$

where:

$$\omega_1=-\frac{\partial u_2}{\partial x_3}+\frac{\partial u_3}{\partial x_2}\ -\text{rotation in the plane } x_2-x_3. \tag{2.7c}$$

The shear wave equation in the plane x_1 – x_3 obtained by differentiating equation (2.3a) with respect to x_3, (2.3c) with respect to x_1, and then adding the parties to give:

$$\frac{G}{\rho}\nabla^2\omega_2-\frac{\partial^2\omega_2}{\partial t^2}=0 \tag{2.8a}$$

where:

$$\omega_2 = -\frac{\partial u_1}{\partial x_3} + \frac{\partial u_3}{\partial x_1} \text{ – rotation in the plane } x_1 - x_3 \tag{2.8b}$$

The shear wave equation in the plane $x_1 - x_2$ obtained by differentiating equation (2.3a) with respect to x_2, (2.3b) with respect to x_1, and then adding the parties to give:

$$\frac{G}{\rho}\nabla^2\omega_3 - \frac{\partial^2\omega_3}{\partial t^2} = 0 \tag{2.9a}$$

where:

$$\omega_3 = -\frac{\partial u_1}{\partial x_2} + \frac{\partial u_2}{\partial x_1} \text{ – rotation in the plane } x_1 - x_2 \tag{2.9b}$$

Shear wave equations (2.7), (2.8), (2.9) are homogeneous differential equations that describe the eigen-vibrations of half-space soil as a homogeneous isotropic elastic area. The first part defines the elasticity of soil, and the second part determines the rotation inertia of a soil area in the plane $(x_2 - x_3)$, $(x_1 - x_3)$ and $(x_1 - x_2)$. These are the equations of the dynamics of the variables ω_1, ω_2, ω_3, and therefore, describe the propagation of shear, rotating and distortion waves. In equations (2.7), (2.8) and (2.9) V_S – the shear wave velocity, is constant:

$$V_S = \sqrt{\frac{G}{\rho}} = \sqrt{\frac{E}{2(1+\nu)\rho}} \tag{2.10a}$$

and the relation

$$V_S = V_L\sqrt{\frac{1-2\nu}{2(1-\nu)}} \tag{2.10b}$$

Comments

1. From equation (2.10b) it appears that, the dilatational waves velocity V_L is greater than the shear wave velocity V_S because $V_L = \sqrt{\frac{(\lambda+2G)}{\rho}} > V_S = \sqrt{\frac{G}{\rho}}$.
2. The dilatational wave is called the primary wave – *P*.
3. The shear wave is called the distortion wave, the secondary waves – *S* (Figure 2.3).

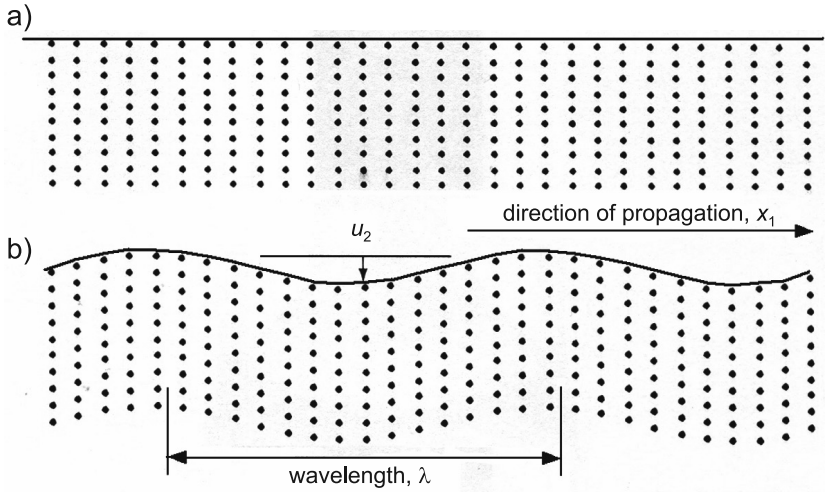

Fig. 2.3. The shear wave: a) before the wave propagation; b) during the wave propagation

2.7. Spherical wave equation

Wave equations presented in sections 2.5 and 2.6 can be written in the general form

$$c^2 \nabla^2 \eta - \frac{\partial^2 \eta}{\partial t^2} = 0, \tag{2.11}$$

where:

$c^2 = \dfrac{(\lambda + 2G)}{\rho}$, $\eta = \varepsilon_v$ – in the case of dilatational wave,

$c^2 = \dfrac{G}{\rho}$, $\eta = \omega_1$ or $\eta = \omega_2$ or $\eta = \omega_3$ – in the case of shear waves.

The solution to this equation was given by d'Alembert in the form of

$$\eta\,(x_1, x_2, x_3, t) = f\,(x_1 - ct, x_2 - ct, x_3 - ct) + g\,(x_1 + ct, x_2 + ct, x_3 + ct), \tag{2.12}$$

where:

f – a wave propagating in the direction $(+x_1, +x_2, +x_3)$,

g – a wave propagating in the direction $(-x_1, -x_2, -x_3)$.

If the wave propagates in the radial direction $r = \sqrt{x_1^2 + x_2^2 + x_3^3}$, then derivatives in equation (2.11) have the form:

$$\frac{\partial^2 \eta}{\partial x_1^2} = \frac{x_1^2}{r}\frac{\partial^2 \eta}{\partial r^2} + \frac{r^2 - x_1^2}{r^3}\frac{\partial \eta}{\partial r} \tag{2.13a}$$

$$\frac{\partial^2 \eta}{\partial x_2^2} = \frac{x_2^2}{r}\frac{\partial^2 \eta}{\partial r^2} + \frac{r^2 - x_2^2}{r^3}\frac{\partial \eta}{\partial r} \tag{2.13b}$$

$$\frac{\partial^2 \eta}{\partial x_3^2} = \frac{x_3^2}{r}\frac{\partial^2 \eta}{\partial r^2} + \frac{r^2 - x_3^2}{r^3}\frac{\partial \eta}{\partial r} \tag{2.13c}$$

Adding equation (2.13) parties, we received

$$\nabla^2 \eta = \frac{\partial^2 \eta}{\partial r^2} + \frac{2}{r}\frac{\partial \eta}{\partial r}. \tag{2.13d}$$

Substituting (2.13d) to (2.11), we obtained the spherical wave equation in the radial direction

$$c^2\left(\frac{\partial^2 \eta}{\partial r^2} + \frac{2}{r}\frac{\partial \eta}{\partial r}\right) - \frac{\partial^2 \eta}{\partial t^2} = 0 \tag{2.14a}$$

or

$$c^2 \frac{\partial^2 (r\eta)}{\partial r^2} - \frac{\partial^2 (r\eta)}{\partial t^2} = 0. \tag{2.14b}$$

Equation (2.14b) is called spherical wave equation, the solution is in a form similar to (2.12):

$$r\eta = f(r - ct) + g(r + ct). \tag{2.15}$$

The spherical wave propagates radially. The first term in equation (2.15) defines a wave running in the positive direction, the second in the negative direction.

2.8. Rayleigh surface wave

In addition to the dilatational and shear waves that propagate inside the half--space, there are also waves that propagate on the surface called surface waves. Rayleigh was the first to described this wave in 1885 – this wave is named after him. These waves occur during earthquakes, explosions, etc., and play an important role in seismic studies. The wave propagates at a free surface of half-space and is strongly damped at depth. Derivation of the Rayleigh wave equation can be found in many books on soil dynamics (e.g. Kolsky, 1963; Richart, Hall & Woods, 1970; Achenbach, 1975; Das, 1993; Kramer, 1996). The next part of the chapter presents

the derivation of the Rayleigh wave equation proposed by Achenbach (1975) with some modifications of the author.

The Rayleigh wave is a shear plane wave, so it is considered as a plane strain model in the plane $x_1 - x_3$ (Figure 2.1), i.e. with the assumptions: $\varepsilon_2 = \gamma_{21} = \gamma_{23}=0$.

Solution of wave equations in the displacement variable was presented in the base of exponential functions, as a product solution in space and in time:

$$u_1 = [A_1 \exp(-d_1 x_3) + A_2 \exp(-d_2 x_3)] \exp[ik(x_1 - V_R t)] \tag{2.16a}$$

$$u_3 = [B_1 \exp(-d_1 x_3) + B_2 \exp(-d_2 x_3)] \exp[ik(x_3 - V_R t)] \tag{2.16b}$$

or

$$u_1 = \mathbf{a} \exp(-\mathbf{d} x_3) \exp[ik(x_1 - V_R t)] \tag{2.16c}$$

$$u_3 = \mathbf{b} \exp(-\mathbf{d} x_3) \exp[ik(x_3 - V_R t)], \tag{2.16d}$$

where:

$\mathbf{a} = \{A_1, A_2\}$, $\mathbf{b} = \{B_1, B_2\}$ – vectors (row), containing complex numbers determined from the boundary conditions,

$\mathbf{d} = \{d_1, d_2\}^T$ – vector (column), containing positive real variables, indicating the disappearance of wave amplitudes in the direction x_3 when x_3 tends to infinity,

k – real variable, the wave number.

The sequence of transformations

Step I – Constants delimitation: B_1, B_2

Substituting a solution form (2.16a) into equation (2.1a) and (2.16b) to (2.1c), the following characteristic equation is obtained:

$$\left[(V_S^2\mathbf{m})\mathbf{d}^2 - (V_L^2 - V_R^2)k^2\mathbf{m}\right]\mathbf{a}^T + \left[-i(V_L^2 - V_S^2)k\mathbf{d}^T\right]\mathbf{b}^T = 0 \tag{2.17a}$$

$$\left[-i(V_L^2 - V_S^2)k\mathbf{d}^T\right]\mathbf{a}^T + \left[(V_L^2\mathbf{m})\mathbf{d}^2 - (V_S^2 - V_R^2)k^2\mathbf{m}\right]\mathbf{b}^T = 0, \tag{2.17b}$$

where:

V_L, V_S – are dilatational and shear waves speeds,

$\mathbf{m} = \{1, 1\}$ – unit vector (row).

The non-trivial solution of equations (2.17) obtained from the condition of zero determinant of the coefficient matrix:

$$\left[(V_L^2\mathbf{m})\mathbf{d}^2 - (V_L^2 - V_R^2)k^2\right]\left[(V_S^2\mathbf{m})\mathbf{d}^2 - (V_S^2 - V_R^2)k^2\right] = 0 \tag{2.18}$$

Assuming that $V_R < V_S < V_L$, two, real positive roots are obtained:

$$d_1 = k\sqrt{1-\frac{V_R^2}{V_L^2}}, \quad d_2 = k\sqrt{1-\frac{V_R^2}{V_S^2}}. \tag{2.19a, b}$$

Substituting (2.19) to (2.17) received amplitude relationships A_1, A_2, B_1, B_2:

$$\left(\frac{B_1}{A_1}\right) = -\frac{d_1}{ik}, \quad \left(\frac{B_2}{A_2}\right) = \frac{ik}{d_2}. \tag{2.20a, b}$$

Relationships (2.20) allow the introduction of the new constants as: $C_1 = A_1$, $C_2 = A_2$, $B_1 = -d_1C_1/ik$, $B_2 = ikC_2/d_2$. Substituting new constants to equation (2.16), we obtained solution forms:

$$u_1(x_1, x_3, t) = [C_1 \exp(-d_1x_3) + C_2 \exp(-d_2x_3)] \exp[ik(x_1 - V_Rt)] \tag{2.21a}$$

$$u_3(x_1,x_3,t) = \left[-\frac{d_1}{ik}C_1\exp(-d_1x_3) + \frac{ik}{d_2}C_2\exp(-d_2x_3)\right]\exp[ik(x_1 - V_Rt)] \tag{2.21b}$$

Step II – Constants delimitation: C_1, C_2, d_1, d_2 from boundary conditions.

Free surface boundary condition limiting elastic half-space: for $x_3 = 0$: $\sigma_{33} = \tau_{31} = \tau_{32} = 0$

according to (2.2c) $$\sigma_{33} = \lambda\left(\frac{\partial u_1}{\partial x_1} + \frac{\partial u_3}{\partial x_3}\right) + 2G\frac{\partial u_3}{\partial x_3} = 0 \tag{2.22a}$$

according to (2.2e) $$\sigma_{31} = G\left(\frac{\partial u_3}{\partial x_1} + \frac{\partial u_1}{\partial x_3}\right) = 0. \tag{2.22b}$$

The solution form for displacement (2.21) substituted into equations (2.22) and taking into account that: $G = \rho V_S^2$, $\lambda = \rho(V_L^2 - 2V_S^2)$ we obtained:

$$-2d_1C_1 - \left(d_2 + \frac{k^2}{d_2}\right)C_2 = 0 \tag{2.23a}$$

$$\left(V_L^2 - 2V_S^2 - V_L^2\frac{d_1^2}{k^2}\right)C_1 - 2V_S^2C_2 = 0. \tag{2.23b}$$

Then, taking into account (2.19a, b) we received:

$$2d_1C_1 + \left(2 - \frac{V_R^2}{V_S^2}\right)k^2\frac{C_2}{d_2} = 0 \tag{2.24a}$$

$$\left(2-\frac{V_R^2}{V_S^2}\right)C_1+2C_2=0. \tag{2.24b}$$

The non-trivial solution of equations (2.24) obtained from the condition of zero determinant of the coefficient matrix:

$$\left(2-\frac{V_R^2}{V_S^2}\right)^2=4\sqrt{1-\frac{V_R^2}{V_L^2}}\sqrt{1-\frac{V_R^2}{V_S^2}}. \tag{2.25}$$

The equation (2.25) can be represented, depending on the variable $\frac{V_R^2}{V_S^2}$, i.e.

$$\frac{V_R^2}{V_S^2}\left[\frac{V_R^6}{V_S^6}-8\frac{V_R^4}{V_S^4}+V_R^2\left(\frac{24}{V_S^2}-\frac{16}{V_L^2}\right)-16\left(1-\frac{V_S^2}{V_L^2}\right)\right]=0 \tag{2.26a}$$

or

$$\frac{V_R^6}{V_S^6}-8\frac{V_R^4}{V_S^4}+V_R^2\left(\frac{24}{V_S^2}-\frac{16}{V_L^2}\right)-16\left(1-\frac{V_S^2}{V_L^2}\right)=0. \tag{2.26b}$$

Comments

1. The trivial root of (2.26) is $V_R = 0$, for which $u_1(x_1,x_3,t)$ and $u_3(x_1,x_3,t)$ does not depend on time, and from (2.24), we obtained $C_1 = C_2 = 0$.
2. Assuming variable $p=\frac{V_R^2}{V_S^2}$ and taking into account (2.10b) $\frac{V_S^2}{V_L^2}=\frac{1-2\nu}{2(1-\nu)}$, equation (2.26b) can be written as:

$$p^3-8p^2+8p\left[\frac{2-\nu}{1-\nu}\right]-\frac{16}{2(1-\nu)}=0. \tag{2.27}$$

The solution of equation (2.27) as $\sqrt{p}=\frac{V_R}{V_S}$ – the Rayleigh wave speed to the shear wave speed factor is shown in Figure 2.4a.

Knowing $p=\frac{V_R^2}{V_S^2}$, the coefficients β_1, β_2 can be calculated according to (2.19a, b):

$$\beta_1=\frac{d_1}{k}=\sqrt{1-\frac{V_R^2}{V_L^2}}=\sqrt{1-p\frac{1-2\nu}{2(1-\nu)}},\quad \beta_2=\frac{d_2}{k}=\sqrt{1-\frac{V_R^2}{V_S^2}}=\sqrt{1-p}.$$

From (2.24b) one can obtain the relationship $\frac{C_1}{C_2} = \frac{-2}{2-p}$.

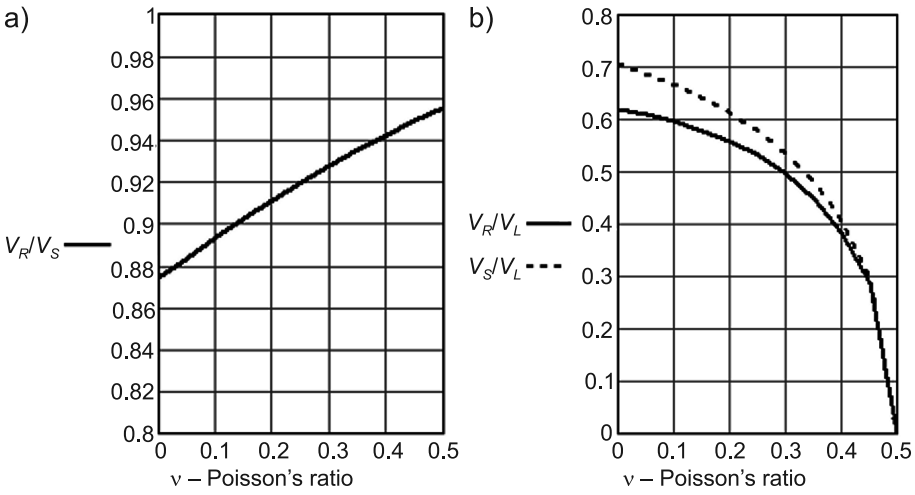

Fig. 2.4. The speed factors depending on Poisson's ratio ν: a) Rayleigh wave speed V_R to the shear wave speed V_s; b) Rayleigh wave speed V_R to the dilatational wave speed V_L and factor V_R to V_L

Table 2.1 shows the value of: ν, $\sqrt{p} = V_R/V_S$, V_L/V_S, β_1, β_2 and C_1/C_2.

Table 2.1

ν	$\sqrt{p} = V_L/V_S$	V_L/V_S	β_1	β_2	C_1/C_2
0.00	0.874032	$\sqrt{2}$	0.786151	0.485868	–1.618034
0.05	0.883695	1.452966	0.793783	0.468063	–1.640578
0.10	0.893106	1.500000	0.803426	0.449846	–1.663393
0.15	0.90222	1.558387	0.815367	0.431276	–1.686343
0.20	0.910996	1.632993	0.829929	0.412415	–1.709276
0.25	0.919402	1.732051	0.847486	0.393319	–1.732053
0.30	0.927413	1.870829	0.868481	0.374039	–1.754534
0.35	0.935013	2.081666	0.893448	0.354613	–1.776591
0.40	0.942195	2.449490	0.923063	0.335065	–1.798123
0.45	0.94896	3.316625	0.958193	0.315396	–1.819054
0.50	0.955313	∞	1.000000	0.295596	–1.839295

3. Rayleigh wave amplitudes on the half-space surface, with $x_3 = 0$ are:

$$\left|u_1(x_1, x_3 = 0)\right| = \left|\frac{p}{2-p}\right| C_2 \tag{2.28a}$$

$$\left|u_3(x_1, x_3 = 0)\right| = \left|\beta_1 + \frac{2-p}{2\beta_2}\right| C_1, \tag{2.28b}$$

where the coefficients $\left|\frac{p}{2-p}\right|$ and $\left|\beta_1 + \frac{2-p}{2\beta_2}\right|$ (according to Table 2.1) are in the range of:

$$0.61803 \le \left|\frac{p}{2-p}\right| \le 0.83929, \quad 2.05817 \le \left|\beta_1 + \frac{2-p}{2\beta_2}\right| \le 2.83929.$$

From equation (2.24b), we obtained $(2-p)C_1 + 2C_2 = 0 \rightarrow |C_1| > |C_2|$. Thus, the displacement amplitude in the vertical direction $\left|u_3(x_1, x_3 = 0)\right|$ is greater than the amplitude of displacement in the horizontal direction.

4. Figure 2.5 shows the motion of material particles (located on the soil surface) during the propagation of Rayleigh waves. The shape of this movement is an ellipse and motion is in the opposite direction to that of wave propagation. The horizontal displacement u_1 disappears at a depth of $0.192 \cdot L$, where $L = 2\pi/k$ is the wavelength, k – wave number (Figure 2.6).

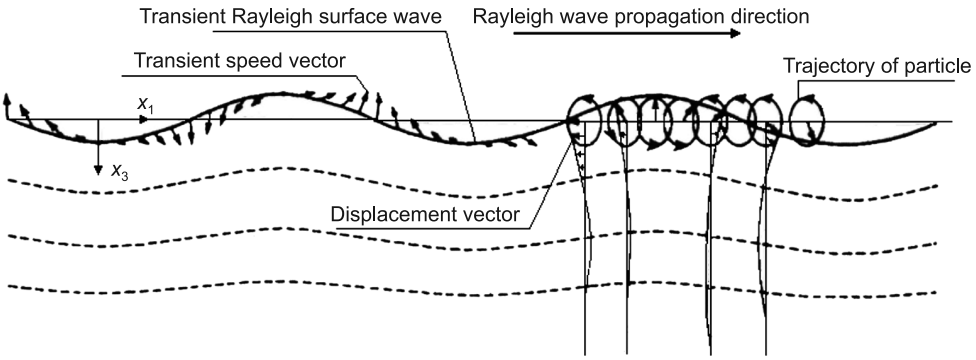

Fig. 2.5. Rayleigh surface wave (Fung, 1965)

Figure 2.7 shows an example record of the vertical component of earthquake acceleration – some typical time periods are shown:

– the first time interval corresponds to the dilatational wave (*P*),

– the second time interval corresponds to the shear wave (*S*),
– the final time interval, with large amplitudes, corresponds to the Rayleigh surface wave.

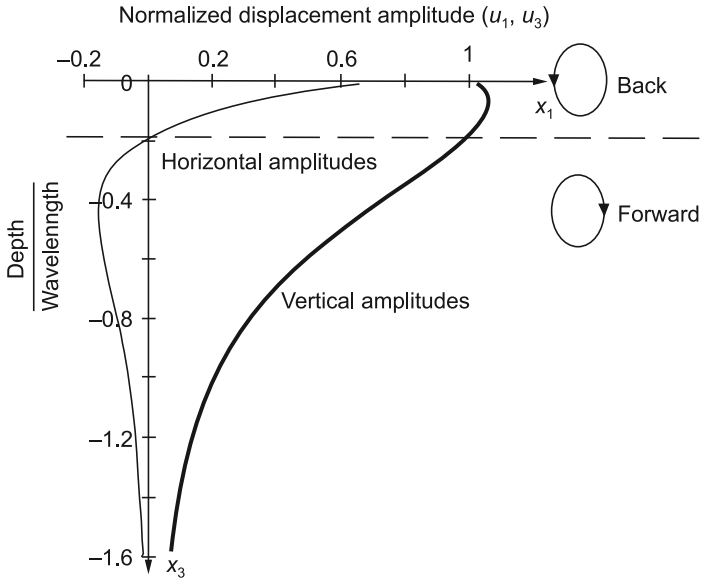

Fig. 2.6. Decreasing the horizontal amplitude u_1 and vertical u_3 with depth (Richard, 1970)

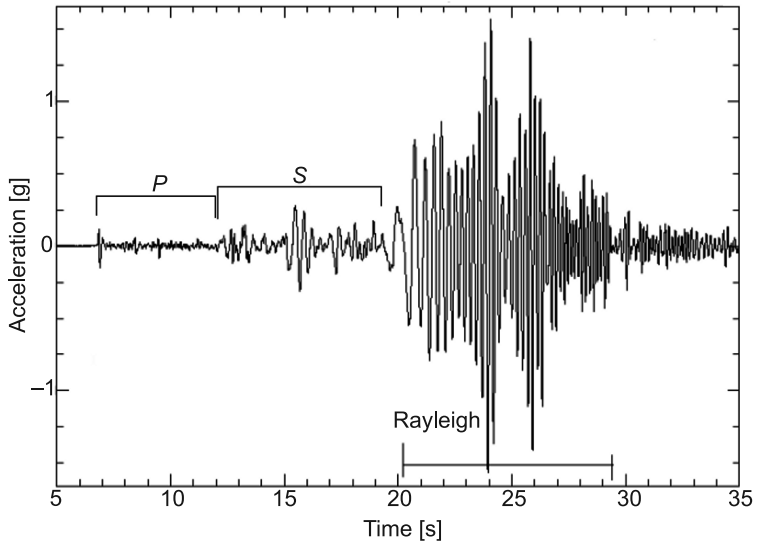

Fig. 2.7. Sample of acceleration during an earthquake

2.9. Love's surface wave

Dilatational waves and shear waves refract in the layered elastic half-space and reflect off its surfaces. In the plane of the layer surface, Love's surface wave also occurs. Love's plane wave propagation is the plane perpendicular to the plane of Rayleigh surface wave propagation. The following is considered the simplest case of Love's wave, propagating in a weak layer with a stronger layer below (Figure 2.8), the case was first considered by Love in 1911.

It is assumed (Figure 2.8) that:

- the upper soil layer ($0 \leq x_3 \leq h$) with parameters (ρ_1, G_1) is different from the lower layer ($x_3 > h$) with parameters (ρ_2, G_2), where ρ is unit density, G is shear modulus and there are no loads on the boundary $x_3 = 0$,
- the wave propagates in the direction of the axis x_1 with the phase velocity c, nonzero displacement is $u_2(x_1, x_3, t)$.

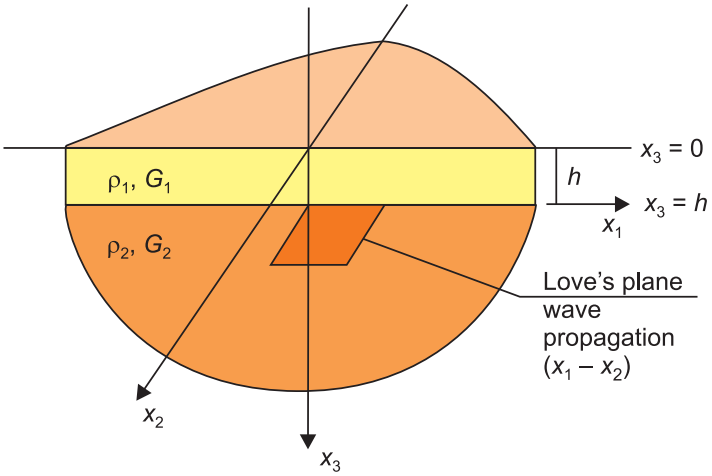

Fig. 2.8. Love's plane ($x_1 - x_2$) wave propagation on the layer surface $x_3 = h$. Rayleigh plane ($x_1 - x_3$) wave propagation near the surface $x_3 = 0$

In the Cartesian coordinate system, the equations of motion (2.1b) have the form:

$$0 \leq x_3 \leq h: \quad G_1\left(\frac{\partial^2 u_2}{\partial x_1^2} + \frac{\partial^2 u_2}{\partial x_3^2}\right) = \rho_1 \frac{\partial^2 u_2}{\partial t^2} \tag{2.29a}$$

$$x_3 > h: \quad G_2\left(\frac{\partial^2 u_2}{\partial x_1^2} + \frac{\partial^2 u_2}{\partial x_3^2}\right) = \rho_2 \frac{\partial^2 u_2}{\partial t^2}, \tag{2.29b}$$

because dilation $\varepsilon_v = u_{k,k} = 0$.

The solution at the base of the exponential functions is proposed in the following form:

$$0 \le x_3 \le h: \quad u_2(A) = [A_1 \exp(\lambda_1 x_3) + A_2 \exp(-\lambda_1 x_3)] \exp[ik(x_2 - ct)] \tag{2.30a}$$

$$x_3 > h: \quad u_2(B) = [B \exp(\lambda_2 x_3)] \exp[ik(x_2 - ct)], \tag{2.30b}$$

where:

k – is the wave number,
ω – angular frequency,
c – unknown wave velocity,
λ_1, λ_2 – unknown parameters.

Substituting (2.30) with (2.29) solution is obtained from the condition $c_1 = \sqrt{G_1 / \rho_1} < c < c_2 = \sqrt{G_2 / \rho_2}$ with the parameters:

$$\lambda_1^2 = k^2\left(1 - \frac{c^2}{c_1^2}\right), \quad \lambda_2^2 = k^2\left(1 - \frac{c^2}{c_2^2}\right) \tag{2.31a, b}$$

obtained from the condition of the disappearance of a wave at infinity, i.e. if $x_3 \to \infty$ then $u_2 \to 0$.

The integration constants A_1, A_2, B are determined:

– from the boundary condition in the plane $x_3 = 0$, where the shear stress $\tau_{23} = 0$

$$G_1 \frac{\partial u_2}{\partial x_3} = 0 \tag{2.32}$$

– from the continuity condition of the displacement in the direction of x_2 and stress in the plane $x_3 = h$

$$u_2(A) = u_2(B), \tag{2.33a}$$

$$G_1 \frac{\partial u_2(A)}{\partial x_3} = G_2 \frac{\partial u_2(B)}{\partial x_3}. \tag{2.33b}$$

Substituting (2.31a) with (2.32), we received

$$A_1 \exp\left(-hk\sqrt{1 - \frac{c^2}{c_1^2}}\right) = A_2 \exp\left(hk\sqrt{1 - \frac{c^2}{c_1^2}}\right). \tag{2.34a}$$

From the (2.33a) condition, we received

$$A_1 + A_2 = B. \tag{2.34b}$$

From the (2.33b) condition and from (2.31), we received

$$G_1(A_1 - A_2)\sqrt{1 - \frac{c^2}{c_1^2}} = G_2 B\sqrt{1 - \frac{c^2}{c_2^2}}. \tag{2.34c}$$

Substituting B from (2.34b) to (2.34c), we obtained:

$$\frac{A_1 - A_2}{A_1 + A_2} = \frac{G_2}{G_1}\sqrt{1-\frac{c^2}{c_2^2}} \Big/ \sqrt{1-\frac{c^2}{c_1^2}} = i\tan\left[ikh\sqrt{1-\frac{c^2}{c_1^2}}\right] \tag{2.35a}$$

or

$$G_2\sqrt{1-\frac{c^2}{c_2^2}} - G_1\tan\left[kh\sqrt{1-\frac{c^2}{c_1^2}}\right]\sqrt{1-\frac{c^2}{c_1^2}} = 0. \tag{2.35b}$$

Equation (2.35b) is the equation depend on c velocity propagation of Love's surface wave. Where $c_1 = \sqrt{G_1/\rho_1} < c_2 = \sqrt{G_2/\rho_2}$ (the upper layer with thickness h is weaker than the lower layer), equation (2.35b) determines the wave surface speed in the range $c_1 < c < c_2$. This case was considered by Love in his work in 1911.

Wave speed c, according to (2.35b), depends on the thickness of the layer h and wave number $k = \omega/c$.

The largest amount of displacement u_2 is at $x_3 = h$, while at $x_3 > h$, displacement value u_2 decreases exponentially with depth x_3.

2.10. References to Chapter 2

Achenbach J.D. (1975): *Wave Propagation in Elastic Solids*, Elsevier, Amsterdam.

Barends F.B.J. (1980): *Dynamics of elastic plate on a flexible subsoil*, LGM-Medelingen, 21, 127-134.

Das B.M. (1993): *Principles of Soil Dynamics*, PWS-Kent, Boston.

De Hoop A.T. (1970): *The surface line source problem in elastodynamics*, De Ingenieur, 82, ET, 19-21.

Fung Y.C. (1965): *Foundation of Solid Mechanics*, Prentice Hall, New Jersey.

Kolsky H. (1963): *Stress Waves in Solids*, Dover, New York.

Kramer S.L. (1996): *Geotechnical Earthquake Engineering*, Printice-Hall.

Lamb H. (1904): *On the propagation of tremors over the surface of an elastic solid*, Philos. Trans. R. Soc., Ser. A, 203, 1-42.

Rayleigh (1885): *On waves propagated along the plane surface of an elastic solid*, Proc. Lond. Math. Soc., 17, 4-11.

Love A.E.H. (1911): *Some problems in geodynamics*, Cambridge.

Pekeris C.L. (1955): *The seismic surface pulse*, Proc. Natl. Acad. Sci., 41, 469-480.

Richart F.E., Hall J.R., Woods R.D. (1970): *Vibrations of Soils and Foundations*, Printice-Hall, Englewood Cliffs.

Westergaard H.M. (1938): *A problem of elasticity suggested by a problem in soil mechanics: soft material reinforced by numerous strong horizontal sheets*. *In Contributions to the Mechanics of Solids*, Stephan Timoshenko 60th Anniversary Volume, Macmillan, New York.

Chapter 3

BIOT THEORY FOR TWO-PHASE MEDIUM – SKELETON AND FLUID

3.1. Notations used in Chapter 3

$\mathbf{A}$ – matrices, tensors,

$\mathbf{a}$ – vectors

$V = \frac{1}{2}\boldsymbol{\varepsilon}^T \mathbf{D}\boldsymbol{\varepsilon}$ – potential energy of two-phase mixture medium

$\boldsymbol{\varepsilon} = \{\varepsilon_{11}, \varepsilon_{22}, \varepsilon_{33}, \varepsilon_{12}, \varepsilon_{13}, \varepsilon_{23}\}^T$ – strain vector of skeleton and fluid mixture medium in Voight's notation

$\boldsymbol{\sigma} = \{\sigma_{11}, \sigma_{22}, \sigma_{33}, \sigma_{12}, \sigma_{13}, \sigma_{23}\}^T$ – vector of total stress of skeleton and fluid mixture medium in Voight's notation

$\boldsymbol{\sigma}' = \{\sigma'_{11}, \sigma'_{22}, \sigma'_{33}, \sigma'_{12}, \sigma'_{13}, \sigma'_{23}\}^T$ – vector of effective stress of skeleton and fluid mixture medium in Voight's notation

$\varepsilon_v = \varepsilon_{11} + \varepsilon_{22} + \varepsilon_{33}$ – dilatation, volumetric strain of skeleton and fluid mixture medium

$q^2 = s_{ij}s_{ij} = \varepsilon_{11}^2 + \varepsilon_{22}^2 + \varepsilon_{33}^2 + \frac{1}{2}(\varepsilon_{12}^2 + \varepsilon_{13}^2 + \varepsilon_{23}^2) - \frac{1}{3}(\varepsilon_v)^2$ – shear invariant, deformation intensity of skeleton and fluid mixture medium

$s_{ij} = \varepsilon_{ij} - \frac{1}{3}\varepsilon_v \delta_{ij}$ – strain deviator of skeleton and fluid mixture medium

n – porosity

ε_v^m – volumetric strain of skeleton

ε_v^f – volumetric strain of fluid

q_m – deformation intensity of skeleton

p – pressure acting on skeleton and fluid mixture medium

p_f – fluid pressure

$\sigma^f = -np_f$ – fluid pressure in pores

σ^m – stress in soil skeleton

$$K_s = -\frac{p_f}{\varepsilon_v^m}$$ – bulk modulus of grains in skeleton

$$K_f = -\frac{p_f}{\varepsilon_v^f}$$ – bulk modulus of fluid in pores

$$K_m = -\frac{p}{\varepsilon_v^m}$$ – bulk modulus of skeleton in soil

P, N, C, R – constants in Biot notation

$$K = P - \frac{4}{3}N = \frac{(1-n)(1-n-K_m/K_s)K_s + nK_sK_m/K_f}{1-n-K_m/K_s + nK_s/K_f}$$

$$C = \frac{(1-n-K_m/K_s)nK_s}{1-n-K_m/K_s + nK_s/K_f}$$

$$R = \frac{n^2K_s}{1-n-K_m/K_s + nK_s/K_f}$$

or

$$K = K_m + Q(\alpha - n)^2$$

$$\alpha = 1 - \frac{K_m}{K_s}$$ – coefficient of Biot effective stress

$$Q = \frac{K_s}{1-n-K_m/K_s + nK_s/K_f}$$

$$\frac{1}{Q} = \frac{\alpha - n}{K_s} + \frac{n}{K_f}$$

$\boldsymbol{\sigma} = \boldsymbol{\sigma}' - \alpha p_f \mathbf{m}$ – total stress equation

$\mathbf{m} = \{1,1,1,0,0,0\}^T$

ρ_s – density of skeleton grains

ρ_f – density of fluid in pores

$\rho = (1-n)\rho_s + n\rho_f = \rho_{11} + 2\rho_{12} + \rho_{22}$ – density of skeleton and fluid mixture medium

Ω_b – macroscopic representative elementary volume

$\Omega_m = (1-n)\Omega_b$ – macroscopic elementary volume of skeleton

$\Omega_f = n\Omega_b$ – macroscopic elementary volume of fluid

$T = \frac{1}{2}\int_{\Omega_m} \rho_s w_i^m w_i^m d\Omega + \frac{1}{2}\int_{\Omega_f} \rho_f w_i^f w_i^f d\Omega$ – kinetic energy of particles at microscopic level

$T = \frac{1}{2}\Omega_b[\rho_{11} v_i^m v_i^m + 2\rho_{12} v_i^m v_i^f + \rho_{22} v_i^f v_i^f]$ – kinetic energy of particles at macroscopic level

w_i^m, w_i^f – skeleton and fluid velocity at microscopic level

$\mathbf{u}^m = \{u_1^m, u_2^m, u_3^m\}^T$ – macroscopic averaged displacement of skeleton

$\mathbf{u}^f = \{u_1^f, u_2^f, u_3^f\}^T$ – macroscopic averaged displacement of fluid

$\mathbf{v}^m = \{v_1^m, v_2^m, v_3^m\}^T$ – macroscopic averaged velocity of skeleton

$\mathbf{v}^f = \{v_1^f, v_2^f, v_3^f\}^T$ – macroscopic averaged velocity of fluid

$\mathbf{D}$ – elasticity coefficient matrix of skeleton and fluid mixture

$\boldsymbol{\Sigma} = \begin{bmatrix} \sigma_{11} & \sigma_{12} & \sigma_{13} \\ \sigma_{21} & \sigma_{22} & \sigma_{23} \\ \sigma_{31} & \sigma_{32} & \sigma_{33} \end{bmatrix}$ – Cauchy stress tensor

$\mathbf{E} = \begin{bmatrix} \varepsilon_{11} & \varepsilon_{12} & \varepsilon_{13} \\ \varepsilon_{21} & \varepsilon_{22} & \varepsilon_{23} \\ \varepsilon_{31} & \varepsilon_{32} & \varepsilon_{33} \end{bmatrix}$ – Euler strain tensor

$v = \frac{\omega}{k}$ – wave phase velocity

k – wave number

ω – angular frequency

3.2. Introduction

Biot theory describes the wave propagation in saturated porous media as a soil skeleton fully saturated with fluid. Biot (1956a, b), assumed that the motion of porous media on the micro level can be described by continuum mechanics of material. He used Lagrange postulate and Hamilton's principle to derive the equations of wave propagation.

The basic assumption of the equations of motion is the homogenisation theory (the literature of the theory is very extensive), for example, the volume averaging method, which is used to describe the micro- and macroscopic relationship, Hassanizadeh and Gray (1979); Burridge and Keller (1985); Pride, Gangi and Morgan (1992), Pride and Berryman (1998). Zwikker and Kosten presented the porous dry medium in 1949 as initial work in which they considered wave propagation using the concept of impedance.

Many books describe Biot theory of wave propagation and deformation theory of the porous medium, inter alia: Rice and Cleary (1976); Johnson (1986); Bourbio at al. (1987); Cristescu (1986); Zimmermann (1991); Allard (1993); Corapcioglu and Tuncay (1996); Mavko at al. (1998); Kubik at al. (2000); Wang (2000); Cederbaum, Li and Schulgasser (2000); Santamarina at al. (2001); Carcione (2001); Coussy (2004).

Biot theory has been extended by several authors on the new soil mechanics problems: to the three-phase medium (skeleton, liquid and gas) was provided by Santos et al. (1990); to the frozen medium Leclaire et al. (1994); to describe the sandstone Carcione et al. (2000); to describe sedimentation of freezing solids and liquid Carcione and Seriani (2001); to describe the filtration with variable porosity Berryman and Wang (2000); to describe the thermal effect of skeleton and fluid expansion McTigue (1986). The dynamic characteristics of the two–phase porous media using wavelet transformation were studied in Cracow University: Wrana and Borowiec (2002 to 2005) and Borowiec (2005). The skeleton spectrum frequency of a two-phase medium was considered by Wrana and Świegoda (2007).

In a porous medium saturated with an electrolyte occurs an acoustic and an electromagnetic wave. The work of Pride (1994) and Pride and Haartsena (1996) is devoted to the extensions of Biot theory which describe these phenomena (electro--seismic wave propagation). Much of the work based on Biot theory was presented at a conference dedicated to the memory of the author in Louvainla Neuve (Thimus et al., 1998).

The main assumptions of Biot theory are as follows:

1. In the porous medium, there is a relationship between the current and reference state. Displacement, velocity and deformations of particles are small. Constitutive

equations, dissipation forces and inertia forces are linear. Thus, the strain energy, dissipation potential and kinetic energy is a square form of variables.
2. The principles of continuum mechanics can be applied to measure the macroscopic value. The size of averaged macroscopic elementary volume is based upon the microscopic structure.
3. The wavelength is large compared to the macroscopic dimensions of the elementary volume. This volume sufficiently and accurately determines properties such as porosity, permeability and the modulus of elasticity.
4. The isothermal state is under consideration.
5. The hydrostatic stress is assumed to fill the pores with viscous fluid.
6. The liquid phase is a continuum. The skeleton is a solid phase with discrete discontinuous areas.

The porous media model for dynamic excitation is based on the kinetic energy equation and dissipation function in soil. The theoretical considerations lead to the equations of motion using Lagrange's postulate.

In the following equations in the introduced indications: "*m*" – refers to the skeleton, "*s*" – refers to the skeleton particles and "*f*" – refers to the liquid phase in the pores (Figure 3.1).

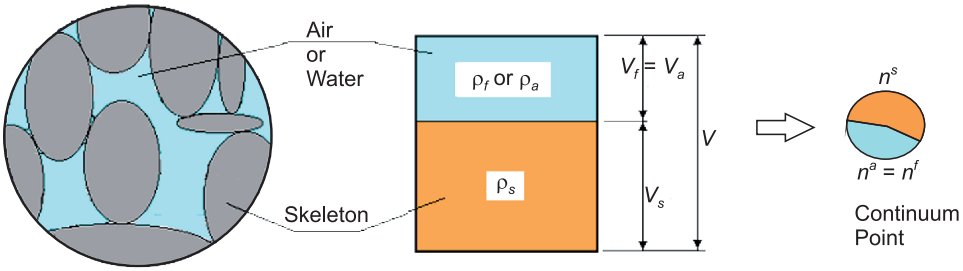

Fig. 3.1. Two-phase soil model, $n^s + n^f = 1$

3.3. Isotropic soil model – Principle of energy conservation – Constitutive Equations

3.3.1. Internal energy of the one-phase soil model

The internal energy of the one–phase soil model (in Voight's notation) is:

$$2V = \boldsymbol{\varepsilon}^T \mathbf{D}\boldsymbol{\varepsilon} \tag{3.1}$$

where:

$$\boldsymbol{\varepsilon} = \{\varepsilon_{11}, \varepsilon_{22}, \varepsilon_{33}, \varepsilon_{12}, \varepsilon_{13}, \varepsilon_{23}\}^T \quad \text{– strain vector,} \tag{3.2}$$

$$\mathbf{D}=\begin{bmatrix} d_{11} & d_{12} & d_{13} & 0 & 0 & 0 \\ d_{21} & d_{22} & d_{23} & 0 & 0 & 0 \\ d_{31} & d_{32} & d_{33} & 0 & 0 & 0 \\ 0 & 0 & 0 & d_{44} & 0 & 0 \\ 0 & 0 & 0 & 0 & d_{55} & 0 \\ 0 & 0 & 0 & 0 & 0 & d_{66} \end{bmatrix} \quad \text{– elastic matrix,} \tag{3.3a}$$

– in the case of deformation symmetry, the following was obtained in three directions: $d_{21} = d_{12}$, $d_{31} = d_{13}$, $d_{32} = d_{23}$,
– in the case of deformation symmetry, the following was obtained in three directions with isotropic material: $d_{11} = d_{22} = d_{33}$, $d_{44} = d_{55} = d_{66}$, $d_{12} = d_{11} - 2d_{66} = d_{13} = d_{23}$, and

$$\mathbf{D}=\begin{bmatrix} d_{11} & d_{11}-2d_{66} & d_{11}-2d_{66} & 0 & 0 & 0 \\ d_{11}-2d_{66} & d_{22} & d_{11}-2d_{66} & 0 & 0 & 0 \\ d_{11}-2d_{66} & d_{11}-2d_{66} & d_{33} & 0 & 0 & 0 \\ 0 & 0 & 0 & d_{66} & 0 & 0 \\ 0 & 0 & 0 & 0 & d_{66} & 0 \\ 0 & 0 & 0 & 0 & 0 & d_{66} \end{bmatrix} \tag{3.3b}$$

The internal energy, taking into account (3.3b):

$$2V = d_{11}(\varepsilon_{11}^2+\varepsilon_{22}^2+\varepsilon_{33}^2)+2(d_{11}-2d_{66})(\varepsilon_{11}\varepsilon_{22}+\varepsilon_{11}\varepsilon_{33}+\varepsilon_{22}\varepsilon_{33})+d_{66}(\varepsilon_{12}^2+\varepsilon_{13}^2+\varepsilon_{23}^2) \tag{3.4}$$

Assuming Lame constant $d_{11} = \lambda + 2G$, $d_{66} = G$, the internal energy of soil skeleton is:

$$2V = \left(\lambda - \frac{4}{3}G\right)\varepsilon_v^2 + 2Gs^2, \tag{3.5}$$

where:

ε_v – the first strain invariant, volumetric strain

$$\varepsilon_v = \varepsilon_{11} + \varepsilon_{22} + {}_{33} \tag{3.6a}$$

q – the second strain invariant, shear strain measure

$$q^2 = s_{ij}s_{ij} = \varepsilon_{11}^2+\varepsilon_{22}^2+\varepsilon_{33}^2+\frac{1}{2}(\varepsilon_{12}^2+\varepsilon_{13}^2+\varepsilon_{23}^2)-\frac{1}{3}\varepsilon_v^2 \tag{3.6b}$$

with

$$s_{ij} = \varepsilon_{ij} - \frac{1}{3}\varepsilon_v\delta_{ij} \tag{3.6c}$$

or

$$\mathbf{s} = \boldsymbol{\varepsilon} - \frac{1}{3}\varepsilon_v \mathbf{m}, \quad \mathbf{m} = \{1,1,1,0,0,0\}^T. \tag{3.6d}$$

3.3.2. Internal energy of two-phase mixture (skeleton and fluid in pores) medium soil model

Because the liquid in the pores does not transfer shear stress, the internal energy of the mixture, assuming the form of (3.5) is:

$$V = A(\varepsilon_v^m)^2 + Bq_m^2 + C\varepsilon_v^m \varepsilon_v^f + D(\varepsilon_v^f)^2, \tag{3.7}$$

where:

A, B, C, D – elasticity coefficients to be determined as a function of material parameters at a microstructure level.

The C coefficient describes the relationship between the skeleton and the fluid parameters. The stress in the skeleton and in the fluid is:

$$\sigma_{ij}^m = \frac{\partial V}{\partial \varepsilon_{ij}^m}, \quad \sigma^f = \frac{\partial V}{\partial \varepsilon^f}. \tag{3.8}$$

After taking into account (3.7), the following is received:

$$\sigma_{ij}^m = 2Bs_{ij}^m + (2A\varepsilon_v^m + C\varepsilon_v^f)\delta_{ij} \tag{3.9}$$

$$\sigma^f = C\varepsilon_v^m + 2D\varepsilon_v^f. \tag{3.10}$$

The coefficients A, B, C, D, determined from the experimental test of mixture medium consist with skeleton and liquid in pores (a description is given below) under static load (Biot and Willis 1957).

The first experiment is a test of the mixture under pure shear of skeleton: $\varepsilon_v^m = \varepsilon_v^f = 0$ and therefore, receives a constant B equal to the shear modulus of the skeleton.

$$B = G_m. \tag{3.11}$$

The second experiment is a compression test of the mixture with undrainage conditions. The material mixture is placed in a sealed rubber shell and subjected to hydrostatic compression p on the outer surface. The liquid pressure inside the shell is maintained at a constant level by an additional hole in the shell (Figure 3.2). The balance of fluid pressure with the external pressure is obtained in the pores in this way, $\sigma^f = 0$. From equations (3.9) and (3.10), the following is obtained:

$$-p = 2A\varepsilon_v^m + C\varepsilon_v^f \tag{3.12}$$

$$0 = 2C\varepsilon_v^m + 2D\varepsilon_v^f. \tag{3.13}$$

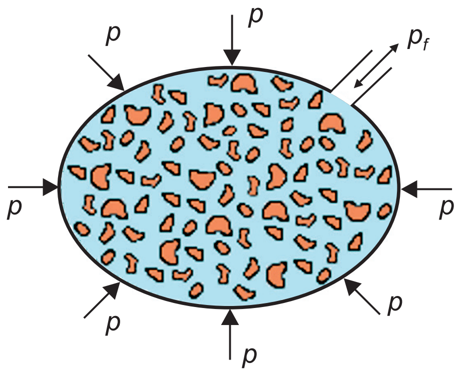

Fig. 3.2. The compression test of a mixture by hydrostatic pressure p in undrained conditions by maintaining the pressure equilibrium between the inside and outside of the sample (Biot and Willis 1957)

In this test, the external pressure p acted on the skeleton, thus:

$$K_m = -\frac{p}{\varepsilon_v^m}, \tag{3.14}$$

where:

K_m – is the bulk modulus of the soil skeleton in undrained condition.

Taking into account (3.14) in equations (3.12) and (3.13), we obtained:

$$2A - \frac{C^2}{2D} = K_m. \tag{3.15}$$

The third experiment is a compression test of the mixture in drainage conditions. The material is immersed in a liquid with equal pressure p_f. The pressure acted both on the skeleton $p_f(1 - n)$ and on the liquid np_f (Figure 3.3).

From equations (3.9), (3.10) we obtained:

$$-(1-n)p_f = 2A\varepsilon_v^m + C\varepsilon_v^f \tag{3.16}$$

$$-np_f = C\varepsilon_v^m + 2D\varepsilon_v^f. \tag{3.17}$$

In the test the constant porosity is kept, therefore the relationship is:

$$K_s = -\frac{p_f}{\varepsilon_v^m}, \quad K_f = -\frac{p_f}{\varepsilon_v^f}, \tag{3.18a, b}$$

where:

K_s – is the bulk modulus of the soil skeleton under drainage conditions,

K_f – bulk modulus of fluid in the pores.

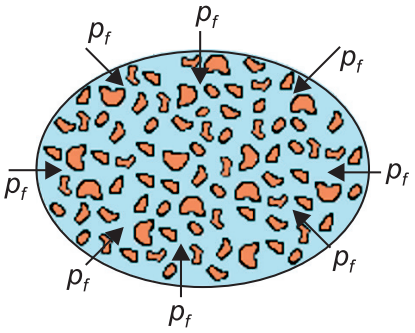

Fig. 3.3. Compression test of the mixture in drainage conditions (Biot and Willis 1957)

Taking into account (3.18) in equations (3.16) and (3.17), the following is obtained:

$$1-n=\frac{2A}{K_s}+\frac{C}{K_f} \tag{3.19}$$

and

$$n=\frac{2D}{K_f}+\frac{C}{K_s}. \tag{3.20}$$

Three coefficient A, B, C can be obtained as the solution result of the system of three equations (3.15), (3.19) and (3.20):

$$K\equiv 2A=\frac{(1-n)(1-n-K_m/K_s)K_s+nK_sK_m/K_f}{1-n-K_m/K_s+nK_s/K_f}=P-\frac{4}{3}N \tag{3.21a}$$

$$C=\frac{(1-n-K_m/K_s)nK_s}{1-n-K_m/K_s+nK_s/K_f}=Q \tag{3.21b}$$

$$2D=\frac{n^2K_s}{1-n-K_m/K_s+nK_s/K_f}=R, \tag{3.21c}$$

where:

P, N, C, R – are constants in Biot notation (Biot 1956a, Biot and Willis 1957).

Substituting to equations (3.9) and (3.10) variables obtained from the three experiments, we receive:

$$\sigma_{ij}^{m} = 2G_m s_{ij}^{m} + (K\varepsilon_v^{m} + C\varepsilon_v^{f})\delta_{ij} \tag{3.22a}$$

or

$$\boldsymbol{\sigma}^{m} = 2G\left(\boldsymbol{\varepsilon}^{m} - \frac{1}{3}\varepsilon_v^{m}\mathbf{m}\right) + K\varepsilon_v^{m}\mathbf{m} + C\varepsilon_v^{f}\mathbf{m} \tag{3.22b}$$

$$\sigma^{f} = C\varepsilon_v^{m} + R\varepsilon_v^{f}. \tag{3.23}$$

In the derivation of equations (3.22) and (3.23), it was assumed that the soil skeleton material is homogeneous. Many authors were considering extending Biot theory to cases of soil skeletons consisting of different grains or different structures, Brown and Korringa (1975) and Carcione et al. (2000).

3.3.3. Concept of effective stress

Terzaghi, in 1936, proposed the distribution of pressure acting on the porous material according to the equation $p_e = p_c - np_f$, where: p_e the pressure acting on the soil skeleton (effective pressure); p_c the pressure acting on the porous medium (total pressure), and p_f is the pressure (hydrostatic) acting on the fluid in the pores. The Terzaghi stress equation is used in Biot theory:

$$\sigma_{ij} = \sigma_{ij}^{m} + \sigma^{f}\delta_{ij} \tag{3.24}$$

and the description of volume changes in the fluid:

$$\varsigma = -\mathrm{div}[n(\mathbf{u}^{f} - \mathbf{u}^{m})] = -n(\varepsilon_v^{f} - \varepsilon_v^{m}), \tag{3.25}$$

where the porosity n is assumed to be constant.

The volume change of the liquid is determined by the difference between the volume of fluid entering and the volume of fluid flowing out of the constant volume porous medium. Equations (3.24) and (3.25) are used to describe the wave propagation and the consolidation problems in mixture theory.

Modulus K in equation (3.21a) can be written as:

$$K = K_m + Q(\alpha - n)^2 \tag{3.26a}$$

where:

$$Q = \frac{K_s}{1 - n - K_m / K_s + nK_s / K_f} \tag{3.26b}$$

$$\alpha = 1 - \frac{K_m}{K_s}. \tag{3.26c}$$

Use of (3.26c) variable Q can be defined as:

$$\frac{1}{Q} = \frac{\alpha - n}{K_s} + \frac{n}{K_f}. \tag{3.26d}$$

Substituting (3.26a) to (3.22) and taking into account the deviatoric strain (3.6c) the following is obtained:

$$\begin{aligned}\sigma_{ij}^m &= 2G_m s_{ij}^m + Ke_m\delta_{ij} + [Q(\alpha - n)^2\varepsilon_v^m + C\varepsilon_v^f]\delta_{ij} = \\ &= d_{ijkl}^m\varepsilon_{kl}^m + [Q(\alpha - n)^2\varepsilon_v^m + C\varepsilon_v^f]\delta_{ij},\end{aligned} \tag{3.27}$$

where:

$$d_{ijkl}^m = \left(K_m - \frac{2}{3}G_m\right)\delta_{ij}\delta_{kl} + G_m(\delta_{ik}\delta_{jl} + \delta_{il}\delta_{jk}) \tag{3.28}$$

is the tensor of elasticity of the porous medium soil skeleton.

Total stress in the equation (3.24) is defined by equation (3.27). The fluid pressure in the pores is determined (3.23). Taking into account that $\alpha - n = C/R$, $Q = R/n^2$, we obtain:

$$\sigma^f = -np_f. \tag{3.29}$$

The equation of total and effective stress is written as:

$$\sigma_{ij} = d_{ijkl}^m\varepsilon_{kl}^m - \alpha p_f\delta_{ij} = 2G_m d_{ij}^m + K_m\varepsilon_v^m\delta_{ij} - \alpha p_f\delta_{ij}. \tag{3.30}$$

Using (3.29) and (3.25) and the relationship $C = nQ(\alpha - n)$, $R = Qn^2$, equation (3.23) can be written as:

$$p_f = Q(\varsigma - \alpha\varepsilon_v^m). \tag{3.31a}$$

The undrained case $\varsigma = 0$:

Eliminating ε_v^m from equations (3.29) and (3.30), the following is obtained:

$$p_f = Bp_e \tag{3.31b}$$

where:

$$B = \frac{\Delta p}{\Delta\sigma} = \frac{\alpha Q}{K_G} \tag{3.32}$$

is Skempton's coefficient (Skempton, 1954), which indicates that the increase in fluid pressure in the pores linearly depends on the effective pressure increase. Parameters α and Q can be defined by coefficient B:

$$\alpha = \frac{1}{B}\left(1 - \frac{K_m}{K_G}\right), \quad Q = \frac{B^2K_G^2}{K_G - K_m}. \tag{3.33}$$

Similarly, having (3.31a) in equation (3.30), we obtain:

$$\sigma_{ij} = 2G_m s_{ij}^m + K_G \varepsilon_v^m \delta_{ij} - \alpha Q \varsigma \delta_{ij}, \tag{3.34a}$$

where:

$$K_G = K_m + \alpha^2 Q = \frac{K_s - K_m + nK_m(K_s / K_f - 1)}{1 - n - K_m / K_s + nK_s / K_f} \tag{3.34b}$$

is the bulk modulus of the mixture in undrained conditions: $\varsigma = 0$.

Equation (3.34) is called Gassmann's equation (Gassmann, 1951). In the case of dry soil, the Gassmann constant is:

$$K_m = \frac{(nK_s / K_f + 1 - n)K_G - K_s}{nK_s / K_f + K_G / K_s - 1 - n}. \tag{3.35}$$

The effective stress, according to (3.30) can be written as:

$$\sigma'_{ij} = d_{ijkl}^m \varepsilon_{kl}^m = \sigma_{ij} + \alpha p_f \delta_{ij}. \tag{3.36}$$

where parameter α given by the equation (3.26c) is called *the Biot effective stress coefficient*.

3.4. Kinetic energy

In the Euler description, the averaged macroscopic skeleton and the fluid velocity introduced:

$v_i^m = \dfrac{\partial u_i^m}{\partial t}$ or $\mathbf{v}^m = \dfrac{\partial}{\partial t}\mathbf{u}^m$ – macroscopic averaged velocity of skeleton,

$v_i^f = \dfrac{\partial u_i^f}{\partial t}$ or $\mathbf{v}^f = \dfrac{\partial}{\partial t}\mathbf{u}^f$ – macroscopic averaged velocity of fluid.

The kinetic energy of the particles at the microscopic level is:

$$T = \frac{1}{2}\int_{\Omega_m} \rho_s w_i^m w_i^m d\Omega + \frac{1}{2}\int_{\Omega_f} \rho_f w_i^f w_i^f d\Omega, \tag{3.37}$$

where:

w_i^m, w_i^f – skeleton and fluid velocity at the microscopic level,
ρ_s – density of skeleton grains,
ρ_f – density of fluid in the pores,
$\Omega_m = (1-n)\Omega_b$, $\Omega_f = n\Omega_b$,
Ω_b – representative elementary macroscopic volume.

Isotropic material and averaged macroscopic velocity in volume Ω_b was assumed. The kinetic energy of the particles at the macroscopic level, similar to form (3.37) is:

$$T = \frac{1}{2}\Omega_b[\rho_{11} v_i^m v_i^m + 2\rho_{12} v_i^m v_i^f + \rho_{22} v_i^f v_i^f], \tag{3.38}$$

where:

ρ_{11} – density of skeleton at macro level,
ρ_{22} – density of fluid at macro level,
ρ_{12} – reciprocal density of skeleton and fluid at macro level.

The considerations below are shown to determine the material constants ρ_{11} and ρ_{12} as a function of the skeleton and fluid parameters.

Assuming a constant fluid and skeleton density in a volume Ω_b, equation (3.37), i.e. the kinetic energy of the particles at the microscopic level, can be written as:

$$T = \frac{1}{2}\rho_s \Omega_m \langle w_i^m w_i^m \rangle_m + \frac{1}{2}\rho_f \Omega_f \langle w_i^f w_i^f \rangle_f, \tag{3.39}$$

where:

$\langle \circ \rangle$ – means averaging in the representative volume.

Assuming balance of kinetic energy on the macroscopic and microscopic level, the density of the mixture medium is obtained:

$$\rho = \rho_{11} v_i^m v_i^m + 2\rho_{12} v_i^m v_i^f + \rho_{22} v_i^f v_i^f = (1-n)\rho_s \langle w_i^m w_i^m \rangle_m + n\rho_f \langle w_i^f w_i^f \rangle_f. \tag{3.40}$$

The momentum of the skeleton and the fluid is

$$\pi_i^m = \frac{\partial T}{\partial v_i^m} = \Omega_b(\rho_{11} v_i^m + \rho_{12} v_i^f) \tag{3.41a}$$

$$\pi_i^f = \frac{\partial T}{\partial v_i^f} = \Omega_b(\rho_{22} v_i^f + \rho_{12} v_i^m). \tag{3.41b}$$

If the relative velocity of the skeleton to the fluid is equal to zero, i.e. $v_i^m = v_i^f$, and the macroscopic velocity is equal to the microscopic velocity, then equation (3.40) can be simplified as:

$$\rho = (1-n)\rho_s + n\rho_f = \rho_{11} + 2\rho_{12} + \rho_{22}. \tag{3.42}$$

The momentum of the skeleton and fluid at the microscopic level determined from the equation (3.39) is:

$$\pi_i^m = \frac{\partial T}{\partial w_i^m} = \Omega_b(1-n)\rho_s w_i^m, \tag{3.43a}$$

$$\pi_i^f = \frac{\partial T}{\partial w_i^f} = \Omega_b n \rho_f w_i^f . \tag{3.43b}$$

Comparing equation (3.41) with (3.43) we obtain:

$$\rho_{11} + \rho_{12} = (1-n)\rho_s \tag{3.44a}$$

$$\rho_{22} + \rho_{12} = n\rho_f . \tag{3.44b}$$

Substituting ρ_{11} and ρ_{22} to (3.40) we obtain the reciprocal density ρ_{12} (Nelson, 1988)

$$\rho_{12} = -\frac{(1-n)\rho_s[\langle w_i^m w_i^m \rangle_m - v_i^m v_i^m] + n\rho_f[\langle w_i^f w_i^f \rangle_f - v_i^f v_i^f]}{(v_i^f - v_i^m)(v_i^f - v_i^m)}. \tag{3.45}$$

The reciprocal density is determined as the difference between the square of the average velocity of the particles at the micro level and the square of the velocity of the particles at the macro level with weights of the skeleton and fluid mass.

Moreover, the reciprocal density can be determined on the basis of tortuosity as a measure of the difference between the velocity of the fluid and the velocity of the skeleton at the micro and macro level.

$$\tau_m = \frac{\langle (w_i^m - v_i^f)(w_i^m - v_i^f) \rangle_m}{(v_i^f - v_i^m)(v_i^f - v_i^m)} \tag{3.46a}$$

$$\tau = \frac{\langle (w_i^f - v_i^m)(w_i^f - v_i^m) \rangle_f}{(v_i^f - v_i^m)(v_i^f - v_i^m)} \tag{3.46b}$$

$$\rho_{12} = -(1-n)\rho_s(\tau_m - 1) - n\rho_f(\tau - 1). \tag{3.46c}$$

In the case of the compatibility of the velocity at the microscopic and the macroscopic levels, with $\tau_m \approx 1$ we obtain:

$$\rho_{12} = -n\rho_f(\tau - 1). \tag{3.47}$$

This case was considered by Biot (1956a).

Assuming that $\frac{w_i^f}{v_i^f} = \frac{l}{L}$, where l is the distance between two points at the micro level, and L is the distance in a straight line (at the macro level), then the tortuosity defined in (3.46b) is:

$$\tau = \left(\frac{l}{L}\right)^2 . \tag{3.48}$$

If ρ_{11} is be considered as a skeleton density moving in fluid, then we obtain:

$$\rho_{11} = (1-n)(\rho_s + r\rho_f) \tag{3.49}$$

where:

rp_f – is the density of fluid associated with the skeleton particles moving in the fluid.

Using (3.44a), (3.47) and (3.49), the tortuosity can be defined as:

$$\tau = 1 + \left(\frac{1-n}{n}\right) r. \tag{3.50}$$

Constant r = 1/2 concerns the case of spherical grains moving in a fluid (Berryman, 1980).

3.5. Dissipation potential

The damping forces (energy dissipation) in the Biot model are proportional to changes of the relative velocity skeleton to fluid $(v_i^m - v_i^f)$, and is assuming as the viscous damping type model:

$$D = \frac{1}{2} b (v_i^m - v_i^f)(v_i^m - v_i^f) \tag{3.51a}$$

or

$$D = \frac{1}{2} b (\mathbf{v}^m - \mathbf{v}^f)^T (\mathbf{v}^m - \mathbf{v}^f), \tag{3.51b}$$

where:

b – is a viscous damping coefficient proportional to the velocity.

It was assumed that the flow of fluid in the pores is laminar, at low Reynold's numbers, and at a low frequency range.

Coefficient b is obtained from a comparison of the resistance of fluid flow described by the Darcy equation to damping forces in the dissipation potential. Damping forces are:

$$F_i = -\frac{\partial D}{\partial v_i^f}, \tag{3.52}$$

hence

$$F_i = b\left|v_i^f - v_i^m\right| \tag{3.53a}$$

or

$$\mathbf{F} = b\left|\mathbf{v}^f - \mathbf{v}^m\right|. \tag{3.53b}$$

Equation (3.53) determines the damping force per unit volume of the liquid in the pores.

Coussy (2004), on the basis of Darcy's law, proposed to adopt:

$$b = n^2 \frac{\eta}{k}, \tag{3.54}$$

where:

η – is the coefficient of viscosity of the fluid, k is a coefficient of permeability.

3.6. Lagrange equation and equation of motion

Lagrangean density of the conservative system is defined as the difference between the kinetic energy (T) and the potential energy (V) with the conservative forces:

$$L = T - V. \tag{3.55}$$

Dynamic of the non-conservative system (taking into account the potential dissipation) is described by the Lagrange equation

$$\frac{d}{dt}\left(\frac{\partial L}{\partial v_i^m}\right) - \frac{\partial L}{\partial u_i^m} - \frac{\partial D}{\partial v_i^m} = 0 \tag{3.56a}$$

$$\frac{d}{dt}\left(\frac{\partial L}{\partial v_i^f}\right) - \frac{\partial L}{\partial u_i^f} - \frac{\partial D}{\partial v_i^f} = 0. \tag{3.56b}$$

The equations above are equivalent to the Biot model:

$$\frac{d}{dt}\left(\frac{\partial T}{\partial v_i^m}\right) + \frac{\partial V}{\partial u_i^m} - \frac{\partial D}{\partial v_i^m} = 0 \tag{3.57a}$$

$$\frac{d}{dt}\left(\frac{\partial T}{\partial v_i^f}\right) + \frac{\partial V}{\partial u_i^f} - \frac{\partial D}{\partial v_i^f} = 0. \tag{3.57b}$$

where T does not depend on $u_i^m \to \partial T / \partial u_i^m = 0,$ and on $u_i^f \to \partial T / \partial u_i^f = 0$ (Biot, 1956b).

Taking into account the stress definition (3.8), we obtain:

$$\sigma_{ij}^{m} = \frac{\partial V}{\partial x_j(u_i^m)} = \frac{\partial V}{\partial \varepsilon_{ij}^{m}}, \quad \sigma_{ij}^{f} = \frac{\partial V}{\partial x_j(u_i^f)} = \frac{\partial V}{\partial \varepsilon^{f}} \tag{3.58a}$$

$$q_i^m = \frac{\partial \sigma_{ij}^{m}}{\partial x_j} = \mathrm{div}\sigma^m, \quad q_i^f = \frac{\partial \sigma_{ij}^{f}}{\partial x_j} = \mathrm{div}\sigma^j. \tag{3.58b}$$

According to equation (3.41), generalised momentum per unit volume acting on the skeleton and the fluid is:

$$\pi_i^m = \frac{\partial T}{\partial v_i^m} = \rho_{11} v_i^m + \rho_{12} v_i^f \tag{3.59a}$$

$$\pi_i^f = \frac{\partial T}{\partial v_i^f} = \rho_{22} v_i^f + \rho_{12} v_i^m. \tag{3.59b}$$

Substituting the Lagrange equations (3.57), we obtained:

$$\frac{\partial \pi_i^m}{\partial t} + F_i^m = \mathrm{div}\sigma^m \tag{3.60a}$$

$$\frac{\partial \pi_i^f}{\partial t} + F_i^f = \mathrm{div}\sigma^f, \tag{3.60b}$$

where damping forces are defined as $F_i^m = \frac{\partial D}{\partial v_i^m}$, $F_i^j = \frac{\partial D}{\partial v_i^j}$.

Taking into account the potential dissipation (3.51), equations of motion of a porous medium fully saturated are defined as:

$$\frac{\partial \sigma_{ij}^{m}}{\partial x_j} = \rho_{11} \frac{\partial^2 u_i^m}{\partial t^2} + \rho_{12} \frac{\partial^2 u_i^f}{\partial t^2} + b(v_i^m - v_i^f) \tag{3.61a}$$

$$-n \frac{\partial p_f}{\partial x_i} = \rho_{12} \frac{\partial^2 u_i^m}{\partial t^2} + \rho_{22} \frac{\partial^2 u_i^f}{\partial t^2} - b(v_i^m - v_i^f). \tag{3.61b}$$

or introducing:

$$Y(t) = m \frac{d\delta(t)}{dt} + \frac{\eta}{\kappa} \delta(t) \tag{3.61c}$$

and $m = \frac{\rho_{22}}{n^2} = \frac{\rho_f \tau}{n}$ to (3.61b), we obtain:

$$-\frac{\partial p_f}{\partial x_i} = \rho_f \frac{\partial^2 u_i^m}{\partial t^2} + Y(t) \cdot \frac{\partial w_i}{\partial t}. \tag{3.61d}$$

In the above equations it is assumed that constant porosity does not depend on time.

3.7. Equations of motion in low frequency range

Adding sides of equation (3.61) and taking into account equation (3.24) and (3.29), we obtain:

$$\frac{\partial \sigma_{ij}}{\partial x_j} = (\rho_{11} + \rho_{12}) \frac{\partial^2 u_i^m}{\partial t^2} + (\rho_{12} + \rho_{22}) \frac{\partial^2 u_i^f}{\partial t^2} \tag{3.62a}$$

or

$$\operatorname{div} \boldsymbol{\Sigma} = (\rho_{11} + \rho_{12}) \frac{\partial^2}{\partial t^2} \mathbf{u}^m + (\rho_{12} + \rho_{22}) \frac{\partial^2}{\partial t^2} \mathbf{u}^f . \tag{3.62b}$$

Assuming the relative displacement of skeleton to fluid:

$$w_i = n(u_i^f - u_i^m) \tag{3.63a}$$

or

$$\mathbf{w} = n(\mathbf{u}^f - \mathbf{u}^m). \tag{3.63b}$$

Taking into account equations (3.44), substituting (3.63) to equations (3.62) and (3.61b) and using the definition of damping coefficient (3.54), equations of motion in the low frequency range can be written as:

$$\frac{\partial \sigma_{ij}}{\partial x_j} = \rho \frac{\partial^2 u_i^m}{\partial t^2} + \rho_f \frac{\partial^2 w_i}{\partial t^2} \tag{3.64a}$$

or

$$\operatorname{div} \boldsymbol{\Sigma} = \rho \frac{\partial^2}{\partial t^2} \mathbf{u}^m + \rho_f \frac{\partial^2}{\partial t^2} \mathbf{w} \tag{3.64b}$$

$$-\frac{\partial p_f}{\partial x_i} = \rho_f \frac{\partial^2 u_i^m}{\partial t^2} + m \frac{\partial^2 w_i}{\partial t^2} + \frac{\eta}{k} \frac{\partial w_i}{\partial t} \tag{3.64c}$$

or

$$-\nabla p_f = \rho_f \frac{\partial^2}{\partial t^2} \mathbf{u}^m + m \frac{\partial^2}{\partial t^2} \mathbf{w} + \frac{\eta}{k} \frac{\partial}{\partial t} \mathbf{w}, \tag{3.64d}$$

where:

$\rho = (1-n)\rho_s + n\rho_f$ – according to (3.42) is the average density of the porous medium fully saturated with liquid,

$m = \dfrac{\rho_{22}}{n^2} = \dfrac{\rho_f \tau}{n}$ – parameter obtained from equations (3.44b) and (3.47).

Equations (3.64) are valid for non-uniform porosity.

3.7.1. Dilatational plane wave

In the isotropic medium, the dilatational plane wave or the shear plane wave can be separated from the equation of motion by the action of the divergence (div) or rotation (rot) operator on the differential equation of motion.

3.7.1.1. Dilatational plane wave without damping

Under consideration is the case of dilatational wave propagation without damping. In the equations of motion (3.61), it is assumed that $b = 0$.

The first step – with the divergence operator applied to (3.61a) with constant parameters of the material (K, G_m, ρ_{11}, ρ_{12}), we obtained:

$$\operatorname{div}(\sigma_{ij}^m) = \rho_{11}\operatorname{div}\left(\frac{\partial^2 u_i^m}{\partial t^2}\right) + \rho_{12}\operatorname{div}\left(\frac{\partial^2 u_i^f}{\partial t^2}\right) \tag{3.65a}$$

or

$$\operatorname{div}\boldsymbol{\Sigma} = \rho_{11}\frac{\partial^2 \varepsilon_v^m}{\partial t^2} + \rho_{12}\frac{\partial^2 \varepsilon_v^f}{\partial t^2}, \tag{3.65b}$$

where:

$\varepsilon_v^m = \partial_i u_i^m = \nabla \mathbf{u}^m$, $\varepsilon_v^f = \partial_i u_i^f = \nabla \mathbf{u}^f$ – is a skeleton and fluid dilatation.

From equation (3.22), taking into account (3.6c), we obtain:

$$\frac{\partial^2 \sigma_{ij}^m}{\partial x_i \partial x_j} = 2G_m \frac{\partial^2 \varepsilon_{ij}^m}{\partial x_i \partial x_j} + \left(K - \frac{2}{3}G_m\right)\frac{\partial^2 \varepsilon_v^m}{\partial x_i \partial x_i} + C\frac{\partial^2 \varepsilon_v^f}{\partial x_i \partial x_i} \tag{3.66a}$$

or

$$\nabla(\operatorname{div}\boldsymbol{\Sigma}) = 2G_m \nabla(\operatorname{div}\mathbf{E}) + \left(K - \frac{2}{3}G_m\right)\Delta\varepsilon_v^m + C\Delta\varepsilon_v^f. \tag{3.66b}$$

Given that: $2\dfrac{\partial^2 \varepsilon_{ij}^m}{\partial x_i \partial x_j} = \dfrac{\partial^2}{\partial x_i \partial x_j}\left(\dfrac{\partial u_j^m}{\partial x_i} + \dfrac{\partial u_i^m}{\partial x_j}\right) = 2\dfrac{\partial^2}{\partial x_i \partial x_i}\left(\dfrac{\partial u_j^m}{\partial x_j}\right) = 2\dfrac{\partial^2 \varepsilon_v^m}{\partial x_i \partial x_i}$, and (3.65) one can obtain:

$$\left(K+\frac{4}{3}G_m\right)\frac{\partial^2\varepsilon_v^m}{\partial x_i\partial x_i}+C\frac{\partial^2\varepsilon_v^f}{\partial x_i\partial x_i}=\rho_{11}\frac{\partial^2\varepsilon_v^m}{\partial t^2}+\rho_{12}\frac{\partial^2\varepsilon_v^f}{\partial t^2} \tag{3.67a}$$

or

$$\left(K+\frac{4}{3}G_m\right)\Delta\varepsilon_v^m+C\Delta\varepsilon_v^f=\rho_{11}\frac{\partial^2\varepsilon_v^m}{\partial t^2}+\rho_{12}\frac{\partial^2\varepsilon_v^f}{\partial t^2}. \tag{3.67b}$$

The second step – with the divergence operator applied to (3.61b) with constant parameters of the material (C, R, ρ_{12}, ρ_{22}) and including (3.10), we obtain:

$$C\frac{\partial^2\varepsilon_v^m}{\partial x_i\partial x_i}+R\frac{\partial^2\varepsilon_v^f}{\partial x_i\partial x_i}=\rho_{12}\frac{\partial^2\varepsilon_v^m}{\partial t^2}+\rho_{22}\frac{\partial^2\varepsilon_v^f}{\partial t^2} \tag{3.68a}$$

or

$$C\Delta\varepsilon_v^m+R\Delta\varepsilon_v^f=\rho_{12}\frac{\partial^2\varepsilon_v^m}{\partial t^2}+\rho_{22}\frac{\partial^2\varepsilon_v^f}{\partial t^2}. \tag{3.68b}$$

In the case of an isotropic material, without loss of generality, a plane wave propagating in the direction of the axis x_1 is considered

$$\varepsilon_v^m=e_1\exp[i(\omega t-kx_1)] \tag{3.69a}$$

$$\varepsilon_v^f=e_2\exp[i(\omega t-kx_1)], \tag{3.69b}$$

where:

k – the real wave number.

Substituting the form of a solution (3.69) to equations (3.67) and (3.68), we obtain:

$$\mathbf{Be}=v_p^2\mathbf{He}, \tag{3.70a}$$

where

$$v_p=\frac{\omega}{k} \quad \text{– phase velocity,} \tag{3.70b}$$

$$\mathbf{B}=\begin{bmatrix}K+\frac{4}{3}G_m & C\\ C & R\end{bmatrix},\quad \mathbf{H}=\begin{bmatrix}\rho_{11} & \rho_{12}\\ \rho_{21} & \rho_{22}\end{bmatrix},\quad \mathbf{e}=\begin{Bmatrix}e_1\\ e_2\end{Bmatrix}. \tag{3.70c}$$

Equation (3.70a) presents a generalized eigenproblem with two arrays **B** and **H**. The eigenproblem solution of (3.70a) consist of two eigenvalues v_{p1}, v_{p2} and two corresponding eigenvectors $\mathbf{e}_1=\begin{Bmatrix}e_{1,1}\\ e_{1,2}\end{Bmatrix}$, $\mathbf{e}_2=\begin{Bmatrix}e_{2,1}\\ e_{2,2}\end{Bmatrix}$ which describe two dilatational plane waves.

From the orthogonality condition of eigenvectors $\mathbf{e}_i^T \mathbf{B} \mathbf{e}_j = \delta_{ij}$, $i, j = 1, 2$ and taking into account (3.70c) following equality is obtained:

$$\left(K + \frac{4}{3} G_m \right) e_{1,1} e_{2,1} + C(e_{1,1} e_{2,2} + e_{1,2} e_{2,1}) + R\, e_{1,2} e_{2,2} = 0. \tag{3.71}$$

From equation (3.71) with the positive material constants K, G_m, C, R, it appears that, if both components of the first eigenvector $\{e_{1,1}, e_{1,2}\}^T$ are of the same sign, the components of the second vector $\{e_{2,1}, e_{2,2}\}^T$ must have opposite signs. This means that in the dilatational wave propagation of saturated soil, either the fluid and skeleton are in a phase, or the fluid and skeleton are in an anti-phase.

Multiplying the left-side equation (3.70a) by $\mathbf{e}_1^T$, we receive $\mathbf{e}_1^T \mathbf{B} \mathbf{e}_1 = v_{p1}^2 \mathbf{e}_1^T \mathbf{R} \mathbf{e}_1$, hence:

$$v_{p1}^2 = \frac{(K + 4G_m / 3) e_{1,1}^2 + 2C e_{1,1} e_{1,2} + R\, e_{1,2}^2}{\rho_{11} e_{1,1}^2 + 2\rho_{12} e_{1,1} e_{1,2} + \rho_{22} e_{1,2}^2}. \tag{3.72}$$

Similar operating may be performed with respect to a pair of v_{p2}, $\mathbf{e}_2$.

In equation (3.72), we take into account the property $\rho_{12} < 0$ according to (3.47). Analysis of the sign of the two eigenvector components $\mathbf{e}_1$ and $\mathbf{e}_2$ leads to the conclusion that:

– if one eigenvector has two components of the same sign, e.g. vector $\mathbf{e}_1$,
– then the second eigenvector has components of the opposite sign, e.g. vector $\mathbf{e}_2$ and in this case there is:

$$v_{p1}^2 > v_{p2}^2. \tag{3.73}$$

It follows that *the second wave velocity* v_{p2} (skeleton and fluid in an anti-phase) is slower than *the first velocity* v_{p1} (skeleton and fluid in a phase). Biot proposed the following names of the waves: 1) the fast wave or wave of the first kind – waves travelling at a higher speed, and 2) the slow wave or waves of the second kind – waves travelling at a slower speed.

3.7.1.2. Dilatational plane wave with damping

Under consideration is the case of dilatational wave propagation with damping realised by the laminar flow of water in the pores. There are considered equations (3.64a, b) and (3.61c, d), taking into account both low and high frequencies.

The first step – the divergence operator is applied to (3.64a, b) including (3.63a, b) with the assumption of constant material parameters (K_G, G_m, M, n, α, ρ, ρ_f)

$$\operatorname{div}\left(\frac{\partial \sigma_{ij}}{\partial x_j}\right) = \rho \operatorname{div}\left(\frac{\partial^2 u_i^m}{\partial t^2}\right) - n\rho_f \operatorname{div}\left(\frac{\partial^2 (u_i^m - u_i^f)}{\partial t^2}\right) \tag{3.74a}$$

or

$$\nabla(\operatorname{div}\boldsymbol{\Sigma}) = \rho \frac{\partial^2 \varepsilon_v^m}{\partial t^2} - n\rho_f \frac{\partial^2 (\varepsilon_v^m - \varepsilon_v^f)}{\partial t^2}. \tag{3.74b}$$

From equation (3.22) taking into account the (3.6c) we obtain:

$$\operatorname{div}\left(\frac{\partial \sigma_{ij}}{\partial x_j}\right) = 2G_m \operatorname{div}\left(\frac{\partial \varepsilon_{ij}^m}{\partial x_j}\right) + \left(K_G - \frac{2}{3}G_m - n\alpha M\right)\operatorname{div}\left(\frac{\partial \varepsilon_v^m}{\partial x_j}\right) + n\alpha M \operatorname{div}\left(\frac{\partial \varepsilon_v^f}{\partial x_j}\right), \tag{3.75a}$$

where K_G is defined in (3.34b).

Because $\operatorname{div}\left(\frac{\partial \varepsilon_{ij}^m}{\partial x_j}\right) = \operatorname{div}\left(\frac{\partial \varepsilon_v^m}{\partial x_i}\right)$ and substituting (3.42) to (3.74) we obtain:

$$\left(K_G + \frac{4}{3}G_m - n\alpha M\right)\operatorname{div}\left(\frac{\partial \varepsilon_v^m}{\partial x_i}\right) + n\alpha M \operatorname{div}\left(\frac{\partial \varepsilon_v^f}{\partial x_i}\right) = (1-n)\rho_s \frac{\partial^2 \varepsilon_v^m}{\partial t^2} + n\rho_f \frac{\partial^2 \varepsilon_v^f}{\partial t^2}. \tag{3.75b}$$

The second step – the divergence operator is applied to (3.61c, d) with constant parameters of the material (K_G, G_m, M, n, α, ρ, ρ_f). Including (3.25) and (3.31a) we receive

$$-\operatorname{div}\left(\frac{\partial p_f}{\partial x_i}\right) = M(\alpha - n)\operatorname{div}\left(\frac{\partial \varepsilon_v^m}{\partial x_i}\right) + Mn \operatorname{div}\left(\frac{\partial \varepsilon_v^f}{\partial x_i}\right) = \rho_f \frac{\partial^2 \varepsilon_v^m}{\partial t^2} - nY \cdot \frac{\partial \varepsilon_v^m}{\partial t} + nY \cdot \frac{\partial \varepsilon_v^f}{\partial t}. \tag{3.76}$$

In the case of an isotropic material, without loss of generality, a plane wave propagating in the direction of the axis x_1 is considered

$$\varepsilon_v^m = e_1 \exp[i(\omega t - k x_1)] \tag{3.77a}$$

$$\varepsilon_v^f = e_2 \exp[i(\omega t - k x_1)], \tag{3.77b}$$

where:

k – is a complex wave number.

Substituting the form of a solution (3.77) to equations (3.75) and (3.76), we obtain:

$$\left[K_G + \frac{4}{3}G_m - n\alpha M - v_c^2(1-n)\rho_s\right]e_1 + n(\alpha M - \rho_f v_c^2)e_2 = 0 \tag{3.78a}$$

$$\left[M(\alpha - n) - v_c^2 \left(\rho_f + i\frac{1}{\omega} n Y_0 \right) \right] e_1 + n \left(M + i\frac{1}{\omega} Y_0 v_c^2 \right) e_2 = 0. \qquad (3.78b)$$

where:

$v_c = \omega/k$ – is a complex dilatational wave velocity.

The non-trivial solution is obtained from the condition of zero determinant of the matrix equation (3.78).

After coefficient manipulation and including (3.34b) the quadratic equation is obtained due to the variable v_c^2:

$$-\left(\rho_f^2 + i\frac{1}{\omega} Y_0 \rho \right) v_c^4 + \left[i\frac{1}{\omega} Y_0 \left(K_G + \frac{4}{3} G_m \right) + M(2\alpha\rho_f - \rho) \right] v_c^2 + M \left(K_m + \frac{4}{3} G_m \right) = 0, \qquad (3.79)$$

The roots are obtained from equation (3.79) corresponding to v_{c-} slow, and v_{c+} fast speed of dilatational wave propagation. The phase velocity v_P is obtained by dividing the angular frequency by the real part of the complex wave number:

$$v_{p\mp} = \frac{\omega}{\mathrm{Re}(k)} = \frac{1}{\mathrm{Re}\left(\dfrac{1}{v_{c\mp}} \right)}. \qquad (3.80)$$

The factor of wave decay is defined as the imaginary part of the complex wave number:

$$\alpha_{\mp} = \mathrm{Im}(k) = \omega\, \mathrm{Im}\left(\frac{1}{v_{c\mp}} \right). \qquad (3.81)$$

The amplitude in the low frequency range is defined by the formula (3.61c) $Y_0 = i\omega m + \eta / \kappa,$ and is equivalent to $\eta = 0$ (viscosity of the fluid is equal to zero), that we consider $i\frac{1}{\omega} Y_0 \to -m,$ In the case of low-frequency we obtain $m = \frac{6}{5}\rho_f,$ and in the case of high-frequency $m = \rho_f$. Thus, in low-frequency equation (3.79) has the form:

$$(m\rho - \rho_f^2) v_\infty^4 - \left[m \left(K_G + \frac{4}{3} G_m \right) - M(2\alpha\rho_f - \rho) \right] v_\infty^2 + M \left(K_m + \frac{4}{3} G_m \right) = 0, \qquad (3.82)$$

where:

v_∞ – is the dilatational wave velocity at low frequencies.

3.7.2. Shear waves

Under consideration is the case of shear wave propagation without damping. In the equations of motion (3.61) it is assumed that $b = 0$.

The first step – the rotation operator is applied to (3.64a) including (3.63)

$$\mathrm{rot}\left(\frac{\partial \sigma_{ij}^{m}}{\partial x_j}\right) = \mathrm{rot}\left[\rho \frac{\partial^2 u_i^m}{\partial t^2} - n\rho_f \left(\frac{\partial^2 u_i^m}{\partial t^2} - \frac{\partial^2 u_i^f}{\partial t^2}\right)\right] \tag{3.83a}$$

or

$$\mathrm{rot}(\mathrm{div}\boldsymbol{\Sigma}) = \rho \frac{\partial^2}{\partial t^2}(\mathrm{rot}\,\mathbf{u}^m) - n\rho_f \left[\left(\frac{\partial^2}{\partial t^2}(\mathrm{rot}\,\mathbf{u}^m) - \frac{\partial^2}{\partial t^2}(\mathrm{rot}\,\mathbf{u}^f)\right)\right] \tag{3.83b}$$

or entering a notation: $\boldsymbol{\Omega}^m = \mathrm{rot}\,\mathbf{u}^m$, $\boldsymbol{\Omega}^f = \mathrm{rot}\,\mathbf{u}^f$

$$\mathrm{rot}(\mathrm{div}\boldsymbol{\Sigma}) = \rho \frac{\partial^2 \boldsymbol{\Omega}^m}{\partial t^2} - n\rho_f \frac{\partial^2 (\boldsymbol{\Omega}^m - \boldsymbol{\Omega}^f)}{\partial t^2}. \tag{3.83c}$$

From equation (3.22), taking into account (3.6c), we obtain:

$$\mathrm{div}\sigma_{ij}^m = 2G_m \mathrm{div}\varepsilon_{ij}^m + \left(K - \frac{2}{3}G_m\right)\mathrm{grad}\,\varepsilon_v^m + C\,\mathrm{grad}\,\varepsilon_v^f. \tag{3.84a}$$

Applying the rotation operator, we obtain:

$$\mathrm{rot}\left(\frac{\partial \sigma_{ij}^m}{\partial x_j}\right) = 2G_m\,\mathrm{rot}\left(\frac{\partial \varepsilon_{ij}^m}{\partial x_j}\right) + \left(K - \frac{2}{3}G_m\right)\mathrm{rot}\,\mathrm{grad}\,\varepsilon_v^m + C\,\mathrm{rot}\,\mathrm{grad}\,\varepsilon_v^f. \tag{3.84b}$$

Including in (3.83a) that $\mathrm{rot}\,\mathrm{grad}\,\varepsilon_v^m = 0$ and $\mathrm{rot}\,\mathrm{grad}\,\varepsilon_v^f = 0$, and taking into account (3.84b) we have the form:

$$2G_m\,\mathrm{rot}\left(\frac{\partial \varepsilon_{ij}^m}{\partial x_j}\right) = \rho\,\mathrm{rot}\left(\frac{\partial^2 u_i^m}{\partial t^2}\right) - n\rho_f\,\mathrm{rot}\left(\frac{\partial^2 u_i^m}{\partial t^2} - \frac{\partial^2 u_i^f}{\partial t^2}\right) \tag{3.85}$$

True equality is:

$$2\mathrm{rot}\left(\frac{\partial \varepsilon_{ij}^m}{\partial x_j}\right) = 2\mathrm{rot}\left[\frac{\partial}{\partial x_j}\left(\frac{\partial u_i^m}{\partial x_j} + \frac{\partial u_j^m}{\partial x_i}\right)\right] = \mathrm{rot}\,\mathrm{grad}\,\varepsilon_v^m + \frac{\partial^2 \mathrm{rot}\,u_i^m}{\partial x_j^2} = \frac{\partial^2 \mathrm{rot}\,u_i^m}{\partial x_j^2}.$$

Equation (3.85) can be written using (3.42):

$$G_m \frac{\partial^2 \boldsymbol{\Omega}^m}{\partial x_j^2} = (1-n)\rho_s \frac{\partial^2 \boldsymbol{\Omega}^m}{\partial t^2} + n\rho_f \frac{\partial^2 \boldsymbol{\Omega}^f}{\partial t^2}. \tag{3.86}$$

The second step – the derivation of equation (3.61d) used:

$$0 = \rho_f \frac{\partial^2 \mathbf{\Omega}^m}{\partial t^2} - nY(t) \cdot \frac{\partial \mathbf{\Omega}^m}{\partial t} + nY(t) \cdot \frac{\partial \mathbf{\Omega}^f}{\partial t}. \tag{3.87}$$

We consider, without loss of generality, a plane wave propagating in the direction of the axis x_1, polarised in the direction x_2. The solution in the vectors form are: $\mathbf{\Omega}^m = \{0,0,S^m\}$, $\mathbf{\Omega}^f = \{0,0,S^f\}$, where $S^m = \frac{\partial u_2^m}{\partial x_1}$, $S^f = \frac{\partial u_2^f}{\partial x_1}$ and

$$S^m = S_1 \exp[i(\omega t - kx_1)] \tag{3.88a}$$

$$S^f = S_2 \exp[i(\omega t - kx_1)] \tag{3.88b}$$

where:

k – complex wave number including the function of damping in equation (3.87).

Substituting the solution (3.88) to (3.86) and (3.87), we obtain:

$$[G_m - v_c^2(1-n)\rho_s]S_1 - n\rho_f v_c^2 S_2 = 0 \tag{3.89a}$$

$$-\left(\rho_f + i\frac{1}{\omega}Y_0 n\right)S_1 + \left(i\frac{1}{\omega}Y_0 n\right)S_2 = 0, \tag{3.89b}$$

where:

$v_c = \omega / k$ – complex shear wave speed.

The solution is:

$$v_c = \sqrt{\frac{G_m}{\rho - i\omega\rho_f^2 Y_0^{-1}}}. \tag{3.90}$$

Phase velocity v_s is obtained through dividing the angular frequency by the real part of the complex wave number:

$$v_{s\mp} = \frac{\omega}{\mathrm{Re}(k)} = \frac{1}{\mathrm{Re}\left(\frac{1}{v_{c\mp}}\right)}. \tag{3.91}$$

The factor of wave decay is defined as the imaginary part of the complex wave number:

$$\alpha = \mathrm{Im}(k) = \omega\,\mathrm{Im}\left(\frac{1}{v_c}\right). \tag{3.92}$$

In the low frequency range, the amplitude defined by formula (3.61c) can be written as $Y_0 = i\omega m + \eta / \kappa,$ which after substituting to (3.90) leads to the formula:

$$v_c = \sqrt{\frac{G_m}{\rho - \rho_f^2 [m - i\eta / (\omega\kappa)]^{-1}}}. \tag{3.93}$$

In the case without damping ($\eta/\kappa = 0$), in (3.93) complex shear wave velocity is given by:

$$v_c = \sqrt{\frac{G_m}{\rho - \rho_f^2 / m}} = \sqrt{\frac{G_m}{\rho - n\rho_f / \tau}}. \tag{3.94}$$

Shear wave amplitude can be obtained from the equation (3.89b)

$$S_2 = \left(1 - \frac{\rho_f}{nm}\right) S_1 = \left(1 - \frac{1}{\tau}\right) S_1. \tag{3.95}$$

In equation (3.95), the expression in brackets is positive, because $\tau \geq 1$; thus, the amplitude of the shear wave of the skeleton and the fluid are of the same sign. From equation (3.89b), we receive $S_1 = S_2$ indicating no relative movement between the skeleton and the fluid in the propagation of shear waves. In the case of zero frequency, $\omega = 0 \rightarrow v_c = \sqrt{G_m / \rho}$ corresponds to the static problem.

Remark

Since $m \geq 0$, the shear wave speed without damping (3.94) is greater than the average speed $\sqrt{G_m / \rho}$.

3.7.3. Example

Gravel as a water-saturated porous medium is considered. The material parameters of soil are: K_s = 35 GPa; ρ_s = 2.65 t/m^3; K_m = 1.7 GPa; G_m = 1.855 GPa; n = 0.3; κ = 1 Darcy; τ = 2; K_f = 2.4 GPa; ρ_f = 1.00 t/m^3 and η = 1 (Carcione, 1998). Substituting the data to the equation of the dilatational wave phase velocity (3.80) v_P and to the shear wave velocity (3.91) $v_{s\mp}$, the results are in frequency-dependent range f [Hz] (Figure 3.4).

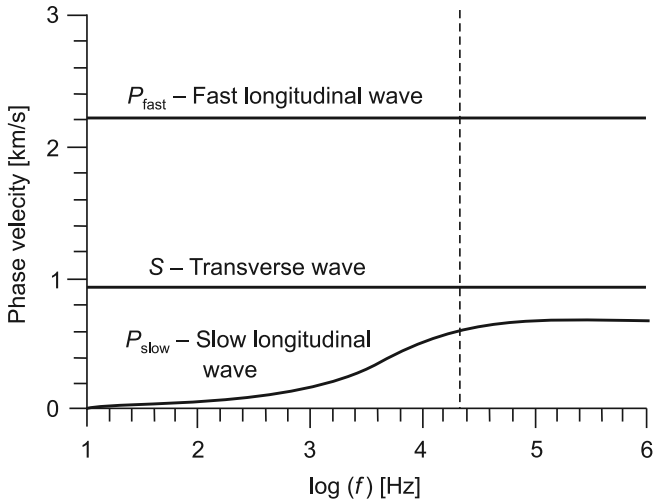

Fig. 3.4. Comparison of the phase velocity of dilatational and shear waves in the fully saturated gravel (Carcione, 1998)

3.8. References to Chapter 3

Allard J.F. (1993): *Propagation of sound in porous media*, Elsevier Science Publ.

Biot M.A. (1956a): *Theory of propagation of elastic waves in a fluid–saturated porous solid. I. Low-frequency range*, J. Acoust. Soc. Am., 28, 168-178.

Biot M.A. (1956b): *Theory of propagation of elastic waves in a fluid-saturated porous solid. II. High-frequency range*, J. Acoust. Soc. Am., 28, 179-191.

Biot M.A., Willis D.G. (1957): *The elastic coefficients of the theory of consolidation*, J. Appl. Mech., 24, 594-601.

Beryman J.G. (1980): *Confirmation of Biot's theory*, Appl. Phys. Lett., 37, 382-384.

Berrman J.G., Wang H.F. (2000): *Elastic wave propagation and attenuation in a doubly-porosity dual-permeability medium*, Internat. J. Rock. Mech. & Min. Sci., 37, 63-78.

Borwiec A. (2005): *The numeric analysis of the wave propagation in two-phase soil medium*, Ph.D. thesis. Cracow University of Technology (in Polish).

Bourbié T., Coussy O., Zinszner B. (1987): *Acoustics of porous media*, Editions Technip.

Brown R., Korringa J. (1975): *On the dependence of the elastic properties of a porous rock on the compressibility of the pore fluid*, Geophysics, 40, 608-616.

Burridge R., Keller J.B. (1985): *Poroelasticity equations derived from micro-structure*, J. Acoust. Soc. Am., 105(2), 626-632.

Carcione J.M. (1998): *Viscoelastic effective rheologies for modeling wave propagation in porous media*, Geophys. Prosp., 46, 249-270.

Carcione J.M., Gurevich B., Cavallini F. (2000): *A generalized Biot-Gassmann model for the acoustic properties of clayey sandstones*, Geophys. Prosp., 48, 539-557.

Carcione J.M., Seriani G. (2001): *Wave simulation in frozen sediments*, J. Comput. Phys., 170, 1-20.

Carcione J.M. (2001): *Wave fields in real media: Wave propagation in anisotropic, an elastic and porous media*, Elsevier Science Ltd.

Cederbaum G., Li L., Schulgasser K. (2000): *Poroelastic structures*, Elsevier Science Ltd.

Corapcioglu M.Y., Tuncay K. (1996): *Propagation of waves in porous media, in Corapcioglu, M. Y., Ed., Advances in Porous Media*, 3, Elsevier Science Pub. Co. Inc., 361-440.

Coussy O. (2004): *Poromechanics*, Chichester, UK: Wiley.

Crisescu N. (1986): *Rock rheology*, Kluwer Academic Publ.

Gasmann F. (1951): *Über die Elastizität poröser Medien*, Vierteljahrsschrift der Naturforschenden, 96, 1-23.

Gurvich B., Schoenberg M. (1999): *Interface boundary conditions for Biot's equations of poroelasticity*, J. Acoust. Soc. Am., 105, 2585-2589.

Hasanizadeh S.M., Gray W.G. (1979*): General conservation equation for multi--phase system: 1. Averaging procedure*, Advances in Water Resources*,* 2, 131--144.

Johnson D.L. (1986): *Recent developments in the acoustic properties of porous media, in D. Sette, Ed*., Frontiers in Physical Acoustics, Proceedings of the International School of Physics "Enrico Fermi", Course 93, 255-290.

Kubk J., Cieszko M., Kaczmarek M. (2000): *Podstawy dynamiki nasyconych ośrodków porowatych*, Biblioteka Mechaniki Stosowanej, Seria A. Monografie.

Leclaire P., Cohen-Tónoudji F., Aguirre-Puente J. (1994): *Extension of Biot's theory of wave propagation to frozen porous media*, J. Acoust. Soc. Am., 96, 3753-3768.

Mavko G., Mukerji T., Dvorkin J. (1998): *The rock physics handbook: tools for seismic analysis in porous media*, Cambridge Univ. Press.

McTigue D.F. (1986): *Thermoelastic response of fluid-saturated porous rock*, J. Geophys. Res., 91(B9), 9533-9542.

Nelson J.T. (1988): *Acoustic emission in a fluid saturated heterogeneous porous layer with application to hydraulic fracture*, Ph.D. thesis, Lawrence Berkeley Laboratory, Univ. of California.

Pride S.R., Gang A.F., Morgan F.D. (1992): *Deriving the equations of motion for porous isotropic media*, J. Acoust. Soc. Am., 92, 3278-3290.

Pride S.R. (1994): *Governing equations for the coupled electromagnetics and acoustics of porous media*, Physical Review, 50, 15678-15696.

Pride S.R., Haartsen M.W. (1996): *Electroseismic wave propagation*, J. Acoust. Soc. Am., 100, 1301-1315.

Pride S.R., Berryman J.G. (1998): *Connecting theory to experiments in poroelasticity*, J. Mech. Phys. Solids, 40, 719-747.

Rice J.R., Cleary M.P. (1976): *Some basic stress diffusion solutions for fluid saturated elastic porous media with compressible coefficients*, Rev. Geophys., 14, 227-241.

Santamarina J.C., Klein K.A., Fam M.A. (2001): *Soils and Waves: particulate materials behavior, characterization and process monitoring*, John Wiley & Sons.

Santos J.E., Douglas Jr. J., Corberó J. (1990): *Static and dynamic behavior of a porous solid saturated by a two-phase fluid*, J. Acoust. Soc. Am., 87, 1428--1438.

Skempton A.W. (1954): *The pore-pressure coefficients A and B*, Geotechnique, 4, 143-152.

Thimus J.F., Abousleiman A., Cheng A.H.D., Coussy O., Detournay E. (1998): Collected papers of M. A. Biot (CD-ROM).

Verruijt A. (2010): *An Introduction to Soil Dynamics*, Springer.

Wang H.F. (2000): *Theory of linear poroelasticity, with applications to geomechanics and hydrogeology*, Princeton University Press.

Wrana B., Borowiec A. (2002): *Drgania przenoszone przez szkielet i przez wodę w warstwie gruntowej*, Zeszyty Naukowe Politechniki Rzeszowskiej, Problemy Dynamiki Konstrukcji, z. 60, 599-603

Wrana B. Borowiec A. (2003): *Dynamic characteristic of saturated porous soil layer used* **u**–*p model*, 15th International Conference on Computer methods in Mechanics CMM-2003, 3–6 June 2003, Gliwice.

Wrana B. (2003): *Saturated porous soil models used in dynamics*, 1st CEACM Conference on computational mechanics, 15th International Conference on Computer methods in Mechanics CMM-2003, 3–6 June 2003, Gliwice.

Wrana B., Borowiec A.(2004): *Zagadnienie modelowania gruntów piaszczystych pod obciążeniem cyklicznym. Przegląd sformułowań oraz analiza czasu osiągnięcia* $p' = 0$, Czasopismo Techniczne Politechniki Krakowskiej, z. 11-B/2004, 147-162.

Wrana B., Borowiec A. (2004): *Rozchodzenie się naprężeń ścinających w dwufazowym ośrodku gruntowym*, Czasopismo Techniczne Politechniki Krakowskiej, z. 5-M/2004, 389-396.

Wrana B., Borowiec A. (2005): *Przegląd wyników obliczeń nasyconych warstw gruntu poddanych obciążeniom dynamicznym*, Mat. XVII Konf. „Metody

Komputerowe w Projektowaniu i Analizie Konstrukcji Hydrotechnicznych", Korbielów, marzec 2005, 173-185.

Wrana B., Świegoda J. (2008): *Współczynnik dynamiczny dla szkieletu gruntu w modelu dwufazowym*, XIII Sympozjum Dynamiki Konstrukcji, Rzeszów, Wydawnictwo Techniczne Politechniki Rzeszowskiej.

Zimmerman R.W. (1991): *Compressibility of sandstones*, Elsevier Science Publ.

Zwikker C., Kosten C.W. (1949): *Sound absorbing materials*, Elsevier Science Publ.

Chapter 4

THREE PHASE MODEL – SKELETON, WATER AND AIR

4.1. Notations used in Chapter 4

According to the convention of continuum mechanics, it is assumed that the normal tensile stress is positive.

$\mathbf{A}$ – matrices, tensors,
a – vectors
$\bar{\chi}$ – function of saturation degree used in formula (4.1), Bishop (1959)
χ – coefficient of volume change defined by formula (4.6)
$\sigma_m = \frac{1}{3}(\sigma_1 + \sigma_2 + \sigma_3)$ – total average stress
$\sigma'_m = \frac{1}{3}(\sigma'_1 + \sigma'_2 + \sigma'_3)$ – effective average stress
p_w – water pressure in pores
p_a – air pressure in pores
$(p_a - p_w)$ – suction
ε_v^s – volumetric strain of skeleton
ε_v^w – volumetric strain of water
ε_v^a – volumetric strain of air
$\mathrm{d}\varepsilon_v^s$ – increment of volumetric strain of skeleton
$\mathrm{d}(\sigma_m + p_a)$ – increment of average total stress
$\mathrm{d}(p_a + p_w)$ – increment of suction
e – void ratio

e_w = (volume of water)/(volume of skeleton) – water ratio
S_r – degree of saturation
θ – volumetric water content
ρ_d – volumetric density of soil skeleton
ρ_w – density of water
ρ_a – density of air
w – water content
n – porosity
n_s – volumetric contents of skeleton phase
n^w – volumetric contents of water phase, $n^w = nS_r$
n^a – volumetric contents of air phase, $n^a = n(1 - S_r)$

$n^s + n^w + n^a = 1$
$\mathrm{d}n^s$ – increment of volumetric contents of skeleton phase
$\mathrm{d}n^w$ – increment of volumetric contents of water phase
$\mathrm{d}n^a$ – increment of volumetric contents of air phase

$$\mathrm{d}n^s = \frac{dV^s}{dV},\ \mathrm{d}n^w = \frac{dV^w}{dV},\ \mathrm{d}n^a = \frac{dV^a}{dV},$$

V^s – volume occupied by skeleton
V^w – volume occupied by water
V^a – volume occupied by air
$V = V^s + V^w + V^a$ – total volume occupied by three phase
m^s – content of skeleton mass per unit volume of soil
m^w – content of water mass per unit volume of soil
m^a – content of air mass per unit volume of soil
$\mathrm{d}m^s$ – increment of skeleton mass per unit volume of soil
$\mathrm{d}m^w$ – increment of water mass per unit volume of soil
G – shear modulus of three phase soil model

ν^s – Poisson ratio of soil skeleton

$m_1^s,\ m_2^s$ – coefficients of volumetric increment of skeleton,

$$m_1^s = \frac{3(1-2\nu^s)}{2(1+\nu^s)G},$$

$m_1^w,\ m_2^w$ – coefficient of volumetric increment of water

$m_1^a,\ m_2^a$ – coefficients of volumetric increment of air

K^s – bulk modulus of skeleton phase in soil

K^w – bulk modulus of water phase in soil

K^a – bulk modulus of air phase in soil

k_w – permeability coefficient of water phase in soil

k_a – permeability coefficient of air phase in soil

g – acceleration due to gravity

$\mathrm{d}\boldsymbol{\sigma} = \{\mathrm{d}\sigma_{11}, \mathrm{d}\sigma_{22}, \mathrm{d}\sigma_{33}, \mathrm{d}\sigma_{12}, \mathrm{d}\sigma_{13}, \mathrm{d}\sigma_{23}\}^T$ – vector of total stress increment

$\mathrm{d}\boldsymbol{\varepsilon} = \{\mathrm{d}\varepsilon_{11}, \mathrm{d}\varepsilon_{22}, \mathrm{d}\varepsilon_{33}, \mathrm{d}\varepsilon_{12}, \mathrm{d}\varepsilon_{13}, \mathrm{d}\varepsilon_{23}\}^T$ – vector of strain increment

$\mathbf{m} = \{1,1,1,0,0,0\}^T$

$\mathbf{D}$ – elasticity coefficient matrix of skeleton, water and air phase as mixture

$\mathbf{u}^s = \{u_1^s, u_2^s, u_3^s\}^T$ – vector of macroscopic averaged displacement of skeleton

$\mathbf{u}^w = \{u_1^w, u_2^w, u_3^w\}^T$ – vector of macroscopic averaged displacement of water

$\mathbf{u}^a = \{u_1^a, u_2^a, u_3^a\}^T$ – vector of macroscopic averaged displacement of air

$[\![\ ]\!]$ – Hadamard jump operator, e.g.

$$[\![\ddot{\mathbf{u}}^s]\!] = \ddot{u}_n^s\mathbf{n} + \ddot{u}_t^s\mathbf{t}$$

4.2. Introduction

The theory of wave propagation in a fully saturated porous medium was formulated by Biot and was subsequently developed by many authors. Partially saturated soil and unsaturated soil are porous media consisting of at least three phases: the skeleton, and two or more fluids (e.g. water and air).

The first proposal of a method to describe unsaturated soil was given by Bishop (1959), he extended the Terzaghi equation to the three phase medium as:

$$\sigma'_m = \sigma_m - p_a + \bar{\chi}(p_a - p_w) \tag{4.1}$$

where:

σ'_m – effective average stress,
σ_m – total average stress,
$\bar{\chi}$ – function of saturation degree S_r,
p_a – air pressure in pores,
p_w – water pressure in pores.

Parameters describing the unsaturated soil

Equation (4.1) allows description of the suction effect $(p_a - p_w)$ on the normal stress, but in this formulation, the increasing humidity on the volumetric strain is not included.

The first study of unsaturated soil in a graphic form as charts of $e - (\sigma_m - p_a) - (p_a - p_w)$ was presented by Bishop and Blight (1963), where e – void ratio, $(\sigma_m - p_a)$ – net stress.

Table 4.1

Pairs of stress state variables used to describe the unsaturated soil

	Variable stress 1	Variable stress 2
Alonso et al. (1990) Wheeler and Sivakumar (1995) Conte et al. (2009)	$(\sigma_m - p_a)$ σ_m – total average stress	$(p_a - p_w)$
Bolzon et al. (1996)	$(\sigma_m - p_a) + \bar{\chi}(p_a - p_w)$ $\bar{\chi} = S_r$	$(p_a - p_w)$
Modaressi and Abou-Bekr (1994)	$(\sigma_m - \pi_c)$ π_c – capillary pressure	π_c
Kohgo et al. (1993a, 1993b)	$(\sigma - p_{eq})$ p_{eq} – equivalent pore pressure	$(p_a - p_w) - s_e$ s_e – initial air suction

Fredlund and Morgenstern (1977) reported that each of the pairs $(\sigma_m - p_a) - (p_a - p_w)$ or $(\sigma_m - p_w) - (p_a - p_w)$ can be used to describe unsaturated soil, but the most commonly used pair is $(\sigma_m - p_a) - (p_a - p_w)$. Table 4.1 shows the currently used pair of stress variables.

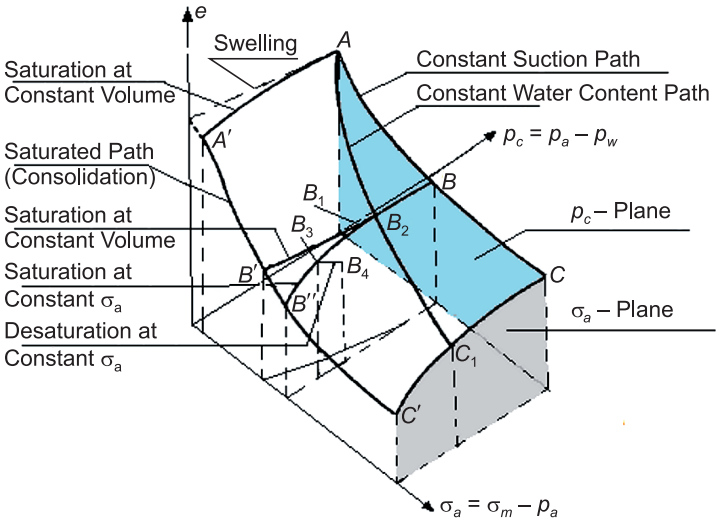

Fig. 4.1a. Chart of unsaturated soil in axis of: $e - (\sigma_m - p_a) - (p_a - p_w)$ (Matyas and Radharkrishna, 1968)

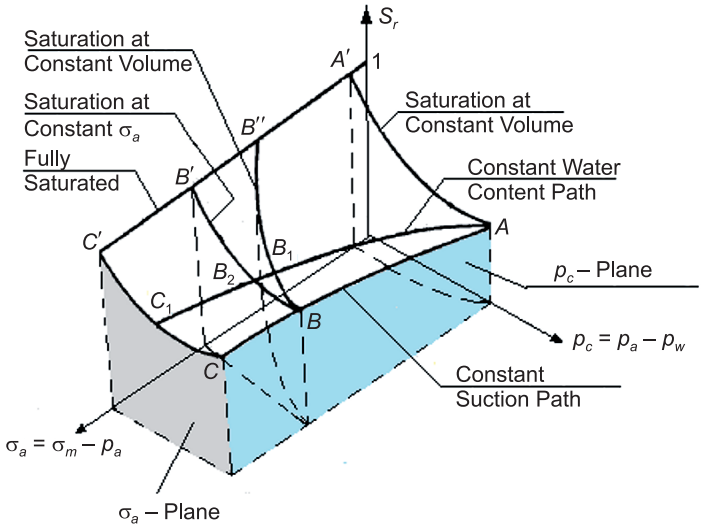

Fig. 4.1b. Chart of unsaturated soil in axis of: $S_r - (\sigma_m - p_a) - (p_a - p_w)$ (Matyas and Radharkrishna, 1968)

Figure 4.1 shows examples of charts of unsaturated soil in axis of $e - (\sigma_m - p_a) - (p_a - p_w)$ (Figure 4.1a) or $S_r - (\sigma_m - p_a) - (p_a - p_w)$ (Figure 4.1b).

Description of volume change

Figure 4.2 shows the chart describing the evolution of the void ratio e and the water ratio e_w = (volume of water)/(volume of skeleton) with respect to the suction increase logarithm $(p_a - p_w)$, Toll (1995). Line A to B is the range of fully saturated water soil. Point B is the point of separation, where line (1) concerns the void ratio e and the line (2) water ratio e_w. The void ratio e slopes gently, and water ratio e_w slopes rapidly. The dashed line shows the average value of the void ratio e.

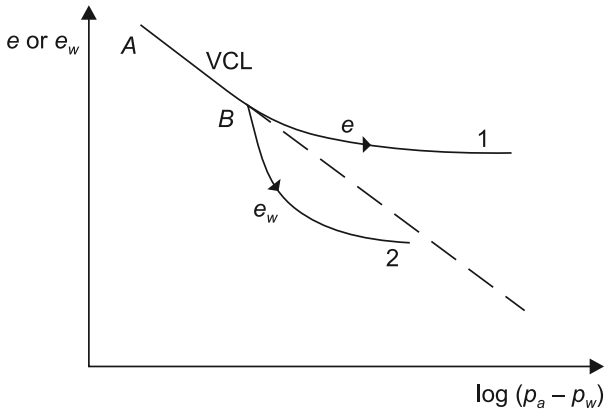

Fig. 4.2. Change of void ratio e and the water ratio e_w with respect to suction $(p_a - p_w)$ (Toll, 1995)

Description of water content

Changing volume of water in pores or increasing humidity can be described by parameter θ – volumetric water content:

$$\theta = \frac{w\rho_d}{\rho_w} \quad \text{or} \quad \theta = \frac{eS_r}{1+e} = nS_r \tag{4.2}$$

Figure 4.3 shows a typical curve of water content depending on the degree of saturation $S_r - (p_a - p_w)$. In this figure, one can identify three areas: the capillary saturation (full saturation), the area of desaturation (drying) and the area that describes the increase in air at a constant pressure of residual saturation.

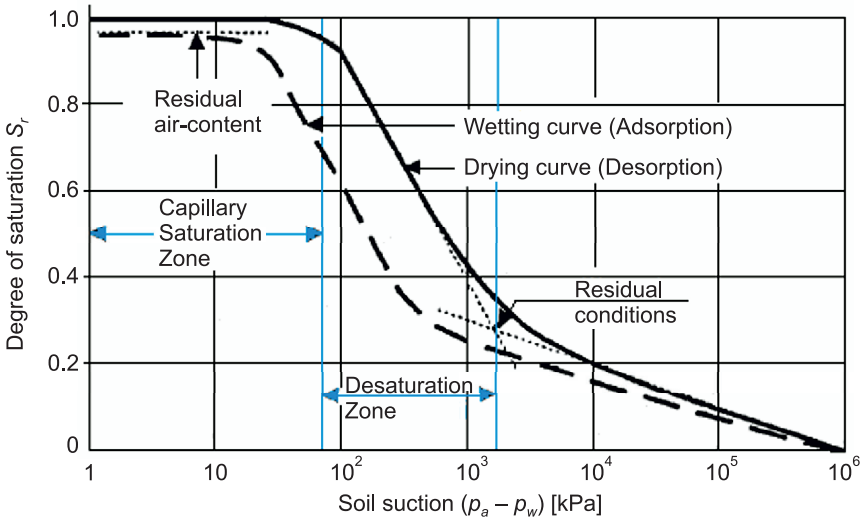

Fig. 4.3. A typical curve of water content in soil (Fredlund, 1998)

Wave propagation

Brutsaert (1964) proposed a model describing the propagation of waves through porous unsaturated soil. This model was then developed by Gray (1983), Berryman et al. (1988), Santos et al. (1990), Lo et al. (2005). Garg & Nayfeh (1986) and Wei & Muraleetharan (2002) used the mixture theory and Tuncay & Corapcioglu (1996) introduced a volume averaging technique. In these works, the authors proved the existence of three different dilatational waves and one shear wave. Wave velocity depends on the frequency; therefore, they are dispersive waves. The dilatational waves depend on the relative motion of fluid to soil skeleton. Especially noteworthy works are those of Foti et al. (2002) and Conte et al. (2009) containing a comparison of computational models to results obtained in situ and laboratory measurements.

This chapter presents the theory of wave propagation in a porous medium consisting of three phases: the soil skeleton, water and air in the pores. Author used constitutive equations proposed by Fredlunda and Morgenstern (1976), describing the change in volume in the unsaturated soil with laminar fluid flow through the soil defined by Darcy's law. In a consideration the variables are used $(\sigma_m - p_a)$, $(p_a - p_w)$.

4.3. Basic assumptions

Unsaturated soil is soil consisting three phases: skeleton, water and air. In the mixtures theory, such soil is a continuous medium, i.e. at the same point of the

medium, there are three phases. In consideration of the wave propagation problem, the following assumptions are used:

a) there is a small deformation,
b) there are incompressible soil grains,
c) the material of skeleton is isotropic and linearly elastic,
d) there is consideration to the laminar flow of water and air in the pores in accordance with the law of Darcy.

The gravity forces, chemical changes and electric fields are omitted. It is also assumed that the soil mixture material is a homogeneous continuous medium in which there are no phenomena of reflection and refraction wave and phase changes.

4.4. Constitutive equations

The following constitutive equation is used to describe the unsaturated soil, proposed by Fredlundem & Morgenstern (1976):

$$\begin{Bmatrix} \mathrm{d}\varepsilon_v^s \\ \mathrm{d}n^w \\ \mathrm{d}n^w \end{Bmatrix} = \begin{bmatrix} m_1^s & m_2^s \\ m_1^w & m_2^w \\ m_1^a & m_2^a \end{bmatrix} \begin{Bmatrix} \mathrm{d}(\sigma_m + p_a) \\ \mathrm{d}(p_a - p_w) \end{Bmatrix}. \tag{4.3}$$

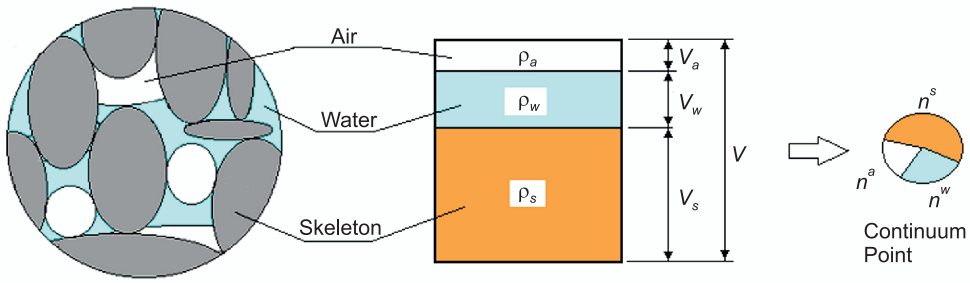

Fig. 4.4. Three phase soil model

The compatibility condition of volume three phases, i.e. $\mathrm{d}\varepsilon_v^s = \mathrm{d}n^w + \mathrm{d}n^a$, leads to the equations:

$$m_1^s = m_1^w + m_1^a \tag{4.4a}$$

$$m_2^s = m_2^w + m_2^a. \tag{4.4b}$$

Special cases:

1) Fully water-saturated soil: $n^a = 0$, $n^w = n$, $p_a = 0$, $-p_w = p$, is equivalent to the two-phase porous soil medium description. In this case, the constitutive equation is $\mathrm{d}\varepsilon_v^s = m_1^s \mathrm{d}\sigma_m + m_2^s \mathrm{d}(-p_w) = m_v \mathrm{d}(\sigma_m + p)$ with one coefficient m_v describes the changes of volume deformation in the total mean stress $\mathrm{d}(\sigma_m + p)$.
2) Dry soil (without water in the pores): $n^a = 0$, $n^w = 0$, $p_a = 0$, $p_w = 0$. In this case, the following equation is obtained: $\mathrm{d}\varepsilon_v = m_v \mathrm{d}\sigma_m$.

The total stress of the three phase soil medium equation is based on the assumption on linear elasticity behaviour of skeleton grains with water and air pressure in the pores (see Fredlund & Rahardjo, 1993), so:

$$\mathrm{d}\boldsymbol{\sigma} = \mathbf{D}\mathrm{d}\varepsilon - \chi dp_w \mathbf{m} - (1-\chi)\mathrm{d}p_a \mathbf{m} \tag{4.5}$$

where:

χ – volume change coefficient defined as:

$$\chi = m_2^s / m_1^s. \tag{4.6}$$

After the substitution of (4.5) to (4.3), we have:

$$\mathrm{d}\varepsilon = \mathbf{D}^{-1}\mathrm{d}\boldsymbol{\sigma} + \frac{\chi}{3K^s}\mathrm{d}p_w \mathbf{m} + \frac{1-\chi}{3K^s}\mathrm{d}p_a \mathbf{m} \tag{4.7a}$$

$$\mathrm{d}n^w = \frac{\psi_w}{3K^s}\mathbf{m}^T \mathrm{d}\boldsymbol{\sigma} + c_{ww}\mathrm{d}p_w + c_{wa}\mathrm{d}p_a \tag{4.7b}$$

$$\mathrm{d}n^a = \frac{\psi_a}{3K^s}\mathbf{m}^T \mathrm{d}\boldsymbol{\sigma} + c_{aw}\mathrm{d}p_w + c_{aa}\mathrm{d}p_a, \tag{4.7c}$$

where:

$$\psi_w = \frac{m_1^w}{m_1^s} \tag{4.8a}$$

$$\psi_a = \frac{m_1^a}{m_1^s} \tag{4.8b}$$

$$c_{ww} = \frac{\chi\psi_w}{K^s} + \frac{m_1^s m_2^w - m_2^s m_1^w}{m_1^s} \tag{4.8c}$$

$$c_{wa} = \frac{(1-\chi)\psi_w}{K^s} + \frac{m_1^s m_2^w - m_2^s m_1^w}{m_1^s} \tag{4.8d}$$

$$c_{aw} = \frac{\chi\psi_a}{K^s} + \frac{m_1^s m_2^a - m_2^s m_1^a}{m_1^s} \tag{4.8e}$$

$$c_{aa} = \frac{(1-\chi)\psi_a}{K^s} + \frac{m_1^s m_2^a - m_2^s m_1^a}{m_1^s}. \tag{4.8f}$$

The effect of temperature and dissipation of energy are omitted. The complementary elastic energy (work of deformation on stress increments) can be submitted, according to Loret and Khalili (2000), and Coussy (2004):

$$\mathrm{d}H_s = \boldsymbol{\varepsilon}^T d\boldsymbol{\sigma} + n^w \mathrm{d}\, p_w + n^a \mathrm{d}\, p_a \tag{4.9}$$

From equation (4.9), we obtain:

$$\varepsilon = \frac{\partial H_s}{\partial \boldsymbol{\sigma}}, \quad n^w = \frac{\partial H_s}{\partial p_w}, \quad n^a = \frac{\partial H_s}{\partial p_a} \tag{4.10}$$

and

$$\mathrm{d}\boldsymbol{\varepsilon} = \frac{\partial^2 H_s}{\partial \boldsymbol{\sigma}\partial \boldsymbol{\sigma}} \mathrm{d}\boldsymbol{\sigma} + \frac{\partial^2 H_s}{\partial \boldsymbol{\sigma}\partial p_w} \mathrm{d}p_w + \frac{\partial^2 H_s}{\partial \boldsymbol{\sigma}\partial p_a} \mathrm{d}p_a \tag{4.11a}$$

$$\mathrm{d}n^w = \left(\frac{\partial^2 H_s}{\partial p_w \partial \boldsymbol{\sigma}} \right)^T \mathrm{d}\boldsymbol{\sigma} + \frac{\partial^2 H_s}{\partial p_w \partial p_w} \mathrm{d}p_w + \frac{\partial^2 H_s}{\partial p_w \partial p_a} \mathrm{d}p_a \tag{4.11b}$$

$$\mathrm{d}n^a = \left(\frac{\partial^2 H_s}{\partial p_a \partial \boldsymbol{\sigma}} \right)^T \mathrm{d}\boldsymbol{\sigma} + \frac{\partial^2 H_s}{\partial p_a \partial p_w} \mathrm{d}p_w + \frac{\partial^2 H_s}{\partial p_a \partial p_a} \mathrm{d}p_a. \tag{4.11c}$$

From the comparison of equations (4.7a, b, c) with equations (4.11a, b, c), we find that the coefficients in equations (4.7a, b, c) depend on the Hessian H_s. Since the Hessian matrix is symmetric, it holds that:

$$m_1^w = m_2^s. \tag{4.12}$$

Using the equality $\mathrm{d}m^w = \mathrm{d}(\rho_w V^w)$ we can obtain:

$$\mathrm{d}n^w = \frac{\mathrm{d}m^w}{\rho_w} - n^w \frac{\mathrm{d}p_w}{K^w}. \tag{4.13a}$$

Similarly, obtained with the air phase is:

$$\mathrm{d}n^a = \frac{\mathrm{d}m^a}{\rho_a} - n^a \frac{\mathrm{d}p_a}{K^a}. \tag{4.13b}$$

Assuming the small displacement amplitude, from mass conservation equations (Coussy, 2004), we can obtain:

$$\frac{\mathrm{d}m^w}{\rho_w} = -n^w \mathrm{div}(\mathbf{u}^w - \mathbf{u}^s) = -n^w(\varepsilon_v^w - \varepsilon_v^s) \tag{4.14a}$$

$$\frac{\mathrm{d}m^a}{\rho_w} = -n^a \mathrm{div}(\mathbf{u}^a - \mathbf{u}^s) = -n^a(\varepsilon_v^a - \varepsilon_v^s) \tag{4.14b}$$

By substituting (4.13a, b) and (4.14a, b) to (4.3b, c) and (4.5), constitutive equations were obtained:

$$\boldsymbol{\sigma} = G\left(\boldsymbol{\varepsilon} - \frac{1}{3}\varepsilon_v^s \mathbf{m}\right) + H\varepsilon_v^s \mathbf{m} + n^w[\chi L + (1-\chi)C]\varepsilon_v^w \mathbf{m} + n^a[\chi C + (1-\chi)N]\varepsilon_v^a \mathbf{m} \tag{4.15a}$$

$$p_w = W\varepsilon_v^s - n^w L\varepsilon_v^w - n^a C\varepsilon_v^a \tag{4.15b}$$

$$p_a = M\varepsilon_v^s - n^w C\varepsilon_v^w - n^a N\varepsilon_v^a, \tag{4.15c}$$

where:

$$H = \frac{2Gv^s}{1-2v^s} - \chi W - (1-\chi)M \tag{4.16a}$$

$$W = -\frac{K^w A}{D} + n^w L + n^a C \tag{4.16b}$$

$$M = -\frac{K^a B}{D} + n^w C + n^a N \tag{4.16c}$$

$$L = \frac{K^w\left[n^a m_1^s + K^a(m_1^s m_2^w - m_2^s m_1^w)\right]}{D} \tag{4.16d}$$

$$N = \frac{K^a\left[n^w m_1^s + K^w(m_1^s m_2^w - m_2^s m_1^w)\right]}{D} \tag{4.16e}$$

$$C = \frac{K^w K^a(m_1^s m_2^w - m_2^s m_1^w)}{D} \tag{4.16f}$$

$$A = n^a m_1^w + K^a(m_1^s m_2^w - m_2^s m_1^w) \tag{4.16g}$$

$$B = n^w m_1^a + K^w(m_1^s m_2^w - m_2^s m_1^w) \tag{4.16h}$$

$$D = (m_1^s m_2^w - m_2^s m_1^w)(n^a K^w + n^w K^a) + n^a n^w m_1^s \tag{4.16i}$$

$$m_1^s = \frac{3(1-2v^s)}{2(1+v^s)G} \tag{4.16j}$$

and with the equations: (4.4), (4.6) and (4.12), we obtained:

$$m_1^a = (1-\chi)m_1^s \tag{4.17a}$$

$$m_2^w = \chi m_1^s - m_2^a \tag{4.17b}$$

$$m_1^w = m_1^s = \chi m_1^s. \tag{4.17c}$$

4.5. Equation of motion

The equation of wave propagation in a porous soil medium consists of the skeleton, water and air per unit volume of soil is considered. Having regarded the inertia forces of the skeleton, water and air, we obtained:

$$\mathrm{div}\boldsymbol{\sigma} = \rho_s(1-n)\ddot{\mathbf{u}}^s + \rho_w n^w \ddot{\mathbf{u}}^w + \rho_a n^a \ddot{\mathbf{u}}^a \tag{4.18}$$

Darcy's law of laminar flow through the soil is applied. In the case of anisotropic material and by omitting gravitational force (Coussy, 2004), we can obtain:

$$n^w(\dot{\mathbf{u}}^w - \dot{\mathbf{u}}^s) = -\frac{k_w}{g\rho_w}(\mathrm{grad}\, p_w + \rho_w \ddot{\mathbf{u}}^w) \tag{4.19a}$$

$$n^a(\dot{\mathbf{u}}^a - \dot{\mathbf{u}}^s) = -\frac{k_a}{g\rho_a}(\mathrm{grad}\, p_a + \rho_a \ddot{\mathbf{u}}^a) \tag{4.19b}$$

Substituting the constitutive equations (4.15) and (4.16) in the equations of motion (4.18) and (4.19), obtained:

$$\begin{aligned}
&(H + 2G + n^w W + n^a M)\mathrm{grad}\varepsilon_v^s - G(\mathrm{grad}\varepsilon_v^s - \nabla^2 \mathbf{u}^s) + \\
&+ n^w[\chi L + (1-\chi)C - n^w L - n^a C]\mathrm{grad}\varepsilon_s^w + \\
&+ n^a[\chi C + (1-\chi)N - n^a N - n^w C]\mathrm{grad}\varepsilon_s^a + \\
&+ \frac{g(n^w)^2\rho_w}{k_w}(\dot{\mathbf{u}}^w - \dot{\mathbf{u}}^s) + \frac{g(n^a)^2\rho_a}{k_a}(\dot{\mathbf{u}}^a - \dot{\mathbf{u}}^s) - (1-n)\rho_s \ddot{\mathbf{u}}^s = 0
\end{aligned} \tag{4.20}$$

$$\begin{aligned}
&n^w W \mathrm{grad}\varepsilon_v^s + (n^w)^2 L \mathrm{grad}\varepsilon_v^s + n^w n^a C \mathrm{grad}\varepsilon_v^a - \\
&- \frac{g(n^w)^2\rho_w}{k_w}(\dot{\mathbf{u}}^w - \dot{\mathbf{u}}^s) - n^w \rho_w \ddot{\mathbf{u}}^w = 0
\end{aligned} \tag{4.21}$$

$$\begin{aligned}
&-n^a M \mathrm{grad}\varepsilon_v^s + n^a n^w C \mathrm{grad}\varepsilon_v^w + (n^a)^2 N \mathrm{grad}\varepsilon_v^a - \\
&- \frac{g(n^a)^2\rho_a}{k_a}(\dot{\mathbf{u}}^a - \dot{\mathbf{u}}^s) - n^a \rho_a \ddot{\mathbf{u}}^a = 0
\end{aligned} \tag{4.22}$$

In the case of a two-phase, fully water-saturated soil model with incompressible grains (Biot model), the relevant parameters are: $S_r = 1$, $m_1^s = m_2^s = m_1^w = m_2^w$. Equations (4.20), (4.21) and (4.22) reduce to two equations:

$$\left[\frac{2G(1-\nu^s)}{1-2\nu^s}+(1-n)^2\frac{K^w}{n}\right]\mathrm{grad}\varepsilon_v^s - G(\mathrm{grad}\varepsilon_v^s-\nabla^2\mathbf{u}^s)+$$

$$+(1-n)K^w\mathrm{grad}\varepsilon_v^w+\frac{n^2\rho_w g}{k_w}(\dot{\mathbf{u}}^w-\dot{\mathbf{u}}^s)-(1-n)\rho_s\ddot{\mathbf{u}}^s=0 \quad (4.23)$$

$$\frac{(1-n)K^w}{n}\mathrm{grad}\varepsilon_v^s+K^w\mathrm{grad}\varepsilon_v^w-\frac{n\rho_w g}{k_w}(\dot{\mathbf{u}}^w-\dot{\mathbf{u}}^s)-\rho_w\ddot{\mathbf{u}}^w=0. \quad (4.24)$$

4.6. Dilatational and shear wave propagation

The theory of discontinuous wave propagation in an unsaturated soil was used (Coussy, 2004). In this theory, displacement and velocity are described by continuous function and acceleration by discontinuous function (skip function). The velocity of wave propagates depends on the soil parameters. There are three cases of phase motion:

a) air and water move independently relative to skeleton;
b) air moves relative to skeleton, water and skeleton move with the same velocity;
c) air, water and skeleton move with the same velocity, the case of undrainage problem of porous material.

Case a)

In this case, the wave propagation problem is described by equations (4.20), (4.21) and (4.22). To solve the wave propagation problem, the jump Hadamard operator is used, marked with double square brackets $[\![\ ]\!]$, where a discontinuity: $[\![\ddot{\mathbf{u}}^s]\!]$, $[\![\ddot{\mathbf{u}}^w]\!]$ and $[\![\ddot{\mathbf{u}}^a]\!]$ means:

$$[\![\ddot{\mathbf{u}}^s]\!]=\ddot{u}_n^s\mathbf{n}+\ddot{u}_t^s\mathbf{t};\quad [\![\ddot{\mathbf{u}}^w]\!]=\ddot{u}_n^w\mathbf{n}+\ddot{u}_t^w\mathbf{t};\quad [\![\ddot{\mathbf{u}}^a]\!]=\ddot{u}_n^a\mathbf{n}+\ddot{u}_t^a\mathbf{t}, \quad (4.25)$$

where:

t – is a unit vector located in a plane tangent to the wave front,
n – is a unit vector normal to the surface of the wave front in the direction of propagation (Kosiński, 1986).

Taking into account $\mathrm{grad}\varepsilon_v^s=[\![\mathbf{n}\cdot\ddot{\mathbf{u}}^s]\!]\mathbf{n}$, $\mathrm{grad}\varepsilon_v^w=[\![\mathbf{n}\cdot\ddot{\mathbf{u}}^w]\!]\mathbf{n}$, $\mathrm{grad}\varepsilon_v^a=[\![\mathbf{n}\cdot\ddot{\mathbf{u}}^a]\!]\mathbf{n}$, from equations (4.20), (4.21) and (4.22) we can obtain:

$$(H+2G+n^wW+n^aM)[\![\mathbf{n}\cdot\ddot{\mathbf{u}}^s]\!]\mathbf{n}+n^w[\chi L+(1-\chi)C-n^wL-n^aC][\![\mathbf{n}\cdot\ddot{\mathbf{u}}^w]\!]\mathbf{n}+$$
$$+n^a[\chi C+(1-\chi)N-n^wC-n^aN][\![\mathbf{n}\cdot\ddot{\mathbf{u}}^a]\!]\mathbf{n}+[G-c^2(1-n)\rho_s][\![\ddot{\mathbf{u}}^s]\!]=0 \quad (4.26)$$

$$-n^w W[\![\mathbf{n}\cdot\ddot{\mathbf{u}}^s]\!]\mathbf{n}+(n^w)^2 L[\![\mathbf{n}\cdot\ddot{\mathbf{u}}^w]\!]\mathbf{n}+n^w n^a C[\![\mathbf{n}\cdot\ddot{\mathbf{u}}^a]\!]\mathbf{n}-c^2 n^w \rho_w[\![\ddot{\mathbf{u}}^w]\!]=0 \quad (4.27)$$

$$-n^a M[\![\mathbf{n}\cdot\ddot{\mathbf{u}}^s]\!]\mathbf{n}+n^a n^w C[\![\mathbf{n}\cdot\ddot{\mathbf{u}}^w]\!]\mathbf{n}+(n^a)^2 N[\![\mathbf{n}\cdot\ddot{\mathbf{u}}^a]\!]\mathbf{n}-c^2 n^a \rho_a[\![\ddot{\mathbf{u}}^a]\!]=0, \quad (4.28)$$

where:

c – is the velocity of wave propagation.

Substituting (4.25) to (4.26), (4.27), and (4.28) and multiplying by the vector **t**, obtained:

$$[G-c^2(1-n)\rho_s]\ddot{u}_t^s=0 \quad (4.29a)$$

$$c^2 n^w \rho_w \ddot{u}_t^w=0 \quad (4.29b)$$

$$c^2 n^a \rho_a \ddot{u}_t^a=0, \quad (4.29c)$$

from which, it follows that:

$$\ddot{u}_t^s\neq 0\rightarrow c^2=V_s^2=\frac{G}{(1-n)\rho_s} \quad (4.30a)$$

$$\ddot{u}_t^w=\ddot{u}_t^a=0. \quad (4.30b)$$

Equation (4.30a) describes a shear wave (S – wave) propagating in a plane tangent to the wave front at a speed of V_s. Substituting (4.25) to (4.26), (4.27), (4.28) and multiplying by the vector **n**, obtained:

$$(\mathbf{K}-c^2\mathbf{M})\begin{Bmatrix}\ddot{u}_n^s\\ \ddot{u}_n^w\\ \ddot{u}_n^a\end{Bmatrix}=0, \quad (4.31a)$$

where:

$$\mathbf{K}=\begin{bmatrix} H+2G+ & n^w(\chi L+(1-\chi)C- & n^a(\chi C+(1-\chi)N-\\ +n^w W+n^a M, & -n^w L-n^a C), & -n^w C-n^a N)\\ -n^w W, & (n^w)^2 L, & n^w n^a C\\ -n^a M, & n^a n^w C & (n^a)^2 N\end{bmatrix} \quad (4.31b)$$

$$\mathbf{M}=\begin{bmatrix}(1-n)\rho_s, & 0, & 0\\ 0, & n^w\rho_w, & 0\\ 0, & 0, & n^a\rho_a\end{bmatrix}. \quad (4.31c)$$

From equality (4.12) we can conclude that **K** is a symmetric matrix. Equation (4.31a) presents three different dilatational waves (P – waves), which propagate

in the normal direction to the wave front. From the condition of zero determinant of matrix $(\mathbf{K} - c^2\mathbf{M})$ we can obtain wave speeds:

$$\det(\mathbf{K} - c^2\mathbf{M}) = 0 \tag{4.32}$$

where:

$c^2 = V_P^2$.

Equation (4.32) leads to the following equation on variable V_P^2:

$$(V_P^2)^3 - (a_{p1}^2 + a_{p2}^2 + a_{p3}^2)(V_P^2)^2 + (a_{p1}^2 a_{p2}^2 + a_{p1}^2 a_{p3}^2 + a_{p2}^2 a_{p3}^2 + A_1 + A_2 - A_3)V_P^2 + \\ - (a_{p1}^2 a_{p2}^2 a_{p3}^2 + A_1 a_{p3}^2 + A_2 a_{p2}^2 - A_3 a_{p1}^2 - A_0) = 0, \tag{4.33a}$$

where:

$$a_{p1}^2 = \frac{H + 2G + n^w W + n^a M}{(1-n)\rho_s} \tag{4.33b}$$

$$a_{p2}^2 = \frac{n^w L}{\rho_w} \tag{4.33c}$$

$$a_{p3}^2 = \frac{n^a N}{\rho_a} \tag{4.33d}$$

$$A_0 = \frac{[\chi L + (1-\chi)C - n^w L - n^a C]n^w n^a MC}{(1-n)\rho_s \rho_w \rho_a} + \frac{[\chi C + (1-\chi)N - n^w C - n^a N]n^w n^a WC}{(1-n)\rho_s \rho_w \rho_a} \tag{4.33e}$$

$$A_1 = \frac{n^w W[\chi L + (1-\chi)C - n^w L - n^a C]}{(1-n)\rho_s \rho_w} \tag{4.33f}$$

$$A_2 = \frac{n^w M[\chi C + (1-\chi)N - n^w C - n^a N]}{(1-n)\rho_s \rho_a} \tag{4.33g}$$

$$A_3 = \frac{n^w n^a C^2}{\rho_w \rho_a}. \tag{4.33h}$$

In equation (4.33a), we have variable V_P^2, hence the solution of this equation is the value of positive and negative V_p. Similar results can be obtained from equation (4.30a) where there is a variable V_s^2.

Case b)

In this case, there is no relative water to skeleton displacement: $\mathbf{u}^w - \mathbf{u}^s = 0$, thus the equation (4.20), (4.21) and (4.22) reduced to the form:

$$[H + 2G + n^w\chi L + n^w(1-\chi)C + n^a(M - n^wC)]\text{grad}\varepsilon_v^s - G(\text{grad}\varepsilon_v^s - \nabla^2\mathbf{u}^s) +$$
$$+ n^a[\chi C + (1-\chi)N - n^aN]\text{grad}\varepsilon_v^a + \frac{(n^a)^2\rho_a g}{k_a}(\dot{\mathbf{u}}^a - \dot{\mathbf{u}}^s) - [(1-n)\rho_s + n^w\rho_w]\ddot{\mathbf{u}}^s = 0 \tag{4.34}$$

$$-n^a(M - n^wC)\text{grad}\varepsilon_v^s + (n^a)^2 N\text{grad}\varepsilon_v^a - \frac{(n^a)^2\rho_a g}{k_a}(\dot{\mathbf{u}}^a - \dot{\mathbf{u}}^s) - n^a\rho_a\ddot{\mathbf{u}}^a = 0. \tag{4.35}$$

As in case 'a)', to solve the wave propagation problem, the Hadamard jump operator $[\![\ ]\!]$ is used – this leads to the determination of one shear wave and two dilatational waves. The velocity of these waves are determined as follows:

$$V_S^2 = \frac{G}{(1-n)\rho_s + n^w\rho_w} \tag{4.36}$$

and

$$V_P^2 = \frac{1}{2}\left[(b_{p1}^2 + b_{p2}^2) \pm \sqrt{(b_{p1}^2 - b_{p2}^2) + 4B_0}\right], \tag{4.37a}$$

where:

$$B_0 = -\frac{n^a[\chi C + (1-\chi)N - n^aN](M - n^wC)}{[(1-n)\rho_s + n^w\rho_w]\rho_a} \tag{4.37b}$$

$$b_{p1}^2 = \frac{H + 2G + n^w\chi L + n^w(1-\chi)C + n^a(M - n^wC)}{(1-n)\rho_s + n^w\rho_w} \tag{4.37c}$$

$$b_{p2}^2 = \frac{n^aN}{\rho_a}. \tag{4.37d}$$

Similarly, when there is a lack of air to skeleton displacement: $\mathbf{u}^a - \mathbf{u}^s = 0$, one shear wave speed V_S and two different dilatational wave speeds V_p are obtained:

$$V_S^2 = \frac{G}{(1-n)\rho_s + n^a\rho_a} \tag{4.38}$$

and

$$V_P^2 = \frac{1}{2}\left[(c_{p1}^2 + c_{p2}^2) \pm \sqrt{(c_{p1}^2 - c_{p2}^2)^2 + 4C_0}\right], \tag{4.39a}$$

where:

$$C_0 = -\frac{n^w[\chi L + (1-\chi)C - n^w L](W - n^a C)}{[(1-n)\rho_s + n^a \rho_a]\rho_w} \tag{4.39b}$$

$$c_{p1}^2 = \frac{H + 2G + n^a \chi C + n^a (1-\chi)N + n^w (W - n^a C)}{(1-n)\rho_s + n^a \rho_a} \tag{4.39c}$$

$$c_{p2}^2 = \frac{n^w L}{\rho_w}. \tag{4.39d}$$

Case c)

In this case, there is no water to skeleton displacement and no air to skeleton displacement, undrained case, $\mathbf{u}^a - \mathbf{u}^w - \mathbf{u}^s = \mathbf{u}$. Equation of motion (4.17) simplifies to the form:

$$\operatorname{div} \boldsymbol{\sigma} = \rho \ddot{\mathbf{u}}, \tag{4.40a}$$

where:

$$\rho = (1-n)\rho_s + S_r n \rho_w + (1-S_r) n \rho_a. \tag{4.40b}$$

Taking into account constitutive equations (4.15) and (4.16) in equation (4.40a), the following was obtained:

$$\left[\frac{2G(1-v^s)}{1-2v^s} + \chi \frac{K^w A}{D} + (1-\chi)\frac{K^a B}{D}\right] \operatorname{grad} \varepsilon_v - G(\operatorname{grad} \varepsilon_v - \nabla^2 \mathbf{u}) - \rho \ddot{\mathbf{u}} = 0 \tag{4.41}$$

In this case, there is one shear wave propagation at the speed of:

$$V_S^2 = \frac{G}{\rho} \tag{4.42}$$

and one dilatational wave propagation at the speed of:

$$V_P^2 = \frac{\left\lfloor 2G(1-v^s)/(1-2v^s) \right\rfloor + (d_{p1}/d_{p2})}{\rho}, \tag{4.43a}$$

where:

$$d_{p1} = K^w K^a (-\chi^2 + m_2^w / m_1^s) + n\left[\chi^2 K^w (1-S_r) + (1-\chi)^2 K^a S_r\right] / m_1^s \tag{4.43b}$$

$$d_{p2} = n\left[S_r K^a + (1-S_r) K^w\right](-\chi^2 + m_2^w / m_1^s) + n^2 S_r (1-S_r) / m_1^s. \tag{4.43c}$$

When the pores are completely filled with air (dry soil, $S_r = 0$) or if the pores are completely filled with water (irrigated soil, $S_r = 1$), the shear wave velocity is defined by formula (4.42) taking account of the volume density ρ:

$$\text{with} \quad S_r = 0, \quad \rho = (1-n)\rho_s + n\rho_a \tag{4.44a}$$

$$\text{with} \quad S_r = 1, \quad \rho = (1-n)\rho_s + n\rho_w. \tag{4.44b}$$

Hence, in accordance with equation (4.43a) the dilatational wave velocity is defining:

$$\text{with} \quad S_r = 0, \quad V_P^2 = \frac{[2G(1-v^s)/(1-2v^s)] + (K^a/n)}{(1-n)\rho_s + n\rho_a} \tag{4.45a}$$

$$\text{with} \quad S_r = 1, \quad V_P^2 = \frac{[2G(1-v^s)/(1-2v^s)] + (K^w/n)}{(1-n)\rho_s + n\rho_w}. \tag{4.45b}$$

Comments

1. The above considerations apply only to the low-frequency range.
2. The above consideration does not include energy dissipation caused by the laminar water motion in the pores. It should be emphasised (Brutsaert, 1964), that in the low-frequency range, relative water to skeleton motion in the pores is negligibly small. In the high-frequency range, water moves freely in the pores and energy dissipation may be omitted.
3. The paper by Miura et al. (2001) shows that the wave speed depends on the frequency for a variety of irrigated soils, from clays to soft rock. The authors showed that the coefficient of permeability is the main parameter of soil which determines the low–frequency bandwidth. A reduction of the permeability coefficient causes the extension frequency bandwidth. In situ geophysical soil measurements accurate to a few hundred kHz carried out by Santamarina et al. (2001) and Miura et al. (2001) show that the largest components of soil response are in the low-frequency range.

4.7. Simplifying the wave velocity calculation of dilatational and shear waves

The simplification in equation (4.43) is used in order to obtain a practical formula. Conversely, equation (4.5) used the formula given by Bishop (1959):

$$\boldsymbol{\sigma} = \boldsymbol{\sigma}' - p_a \mathbf{m} + \overline{\chi}(p_a - p_w)\mathbf{m}, \tag{4.46}$$

where:

- $\boldsymbol{\sigma}'$ – is the effective stress vector in the Voight notation,
- $\overline{\chi}$ – is a parameter in the range of [0,1], which is often converted to S_r as an approximation (Bishop and Blight, 1963).

Using formula (4.16j) on the value m_1^s, dilatational wave velocity, according to (4.43a), is as follows:

$$V_P^2 = \frac{\dfrac{2G(1-v^s)}{(1-2v^s)} + \dfrac{K^a K^w h + nS_r(1-S_r)[K^w S_r + K^a(1-S_r)]}{n[K^a S_r + K^w(1-S_r)]h + n^2 S_r(1-S_r)}}{(1-n)\rho_s + S_r n\rho_w + (1-S_r)n\rho_a}, \tag{4.47a}$$

where:

$$h = m_2^w - \frac{3(1-2v^s)S_r^2}{2(1+v^s)G}. \tag{4.47b}$$

The value of G can be determined from in situ tests, based on measuring the speed of the shear wave V_s. According to (4.42), using (4.40b) one can obtain:

$$G = \rho V_S^2 = [(1-n)\rho_s + S_r n\rho_w + (1-S_r)n\rho_a]V_S^2. \tag{4.47c}$$

Taking the assumption that:

– air density is close to zero: $\rho \cong 0$,
– air bulk modulus can be omitted compared to the water bulk modulus $K^a / K^w \cong 0$, the expression for the dilatational wave velocity (P – wave) takes the form:

$$V_P^2 = \frac{2(1-v^s)}{(1-2v^s)}V_S^2 + \frac{S_r^2}{[(1-n)\rho_s + S_r n\rho_w]m_2^w - \dfrac{3(1-2v^s)S_r^2}{2(1+v^s)V_S^2} + \dfrac{nS_r[(1-n)\rho_s + S_r n\rho_w]}{K^w}}. \tag{4.48}$$

In equation (4.48), there is a constant $m_2^w = \partial n^w / \partial(p_a - p_w)$, which can be determined experimentally (Fredlund and Rahardjo, 1993). Knowing value V_S and V_P from geophysical methods of research, such as *cross-hole or down-hole*, using an inverse formulation, one can obtain:

$$m_2^w = \frac{(1-2v^s)S_r^2}{[(1-n)\rho_s + S_r n\rho_w]} + \left[\frac{3}{2(1+v^s)V_S^2} + \frac{1}{(1-2v^s)V_P^2 - 2(1-v^s)V_S^2}\right] - \frac{nS_r}{K^w}. \tag{4.49}$$

4.8. References to Chapter 4

Alonso E.E., Gens A., Josa A. (1990): *A constitutive model for partially saturated soils*, Géotechnique 40, No. 3, 405-430.

Berryman J.G., Thigpen L, Chin R.C.Y. (1988): *Bulk elastic wave propagation in partially saturated porous solids*, Journal of Acoustic Society of America, 84(1), 360-373.

Bishop A.W. (1959): *The principle of effective stress*, Teknisk Ukeblad, 106(39), 859-863.

Bishop A.W, Blight G.E. (1963): *Some aspects of effective stress in saturated and partly saturated soils*, Géotechnique, 13(3), 177-197.

Bolzon G., Schrefler B.A., Zienkiewicz O.C. (1996): *Elastoplastic soil constitutive laws generalized to partially saturated states*, Géotechnique 46, No. 2, 279-289.

Brutsaert W. (1964): *The propagation of elastic waves in unconsolidated unsaturated granular mediums*, Journal of Geophysical Research, 69(2), 243-257.

Conte E., Cosentini R.M., Troncone A. (2009): *Shear and dilatational wave velocities for unsaturated soils*, Soil Dynamics and Earthquake Engineering, 29, 946-952.

Coussy O. (2004): *Poromechanics*, Chichester, UK: Wiley.

Foti S., Lai G., Lancellotta R. (2002): *Porosity of fluid-saturated porous media from measured seismic wave velocities*, Géotechnique, 52(5), 359-373.

Fredlund D.G., Morgenstern N.R. (1976): *Constitutive relations for volume change in unsaturated soils*, Canadian Geotechnical Journal, 13(3), 261-276.

Fredlund D.G., Morgenstern N.R. (1977): *Stress state variables for unsaturated soils*, J. Geotech. Eng. Div., ASCE 103, GT5, 447-466.

Fredlund D.G., Rahardjo H. (1993): *Soil mechanics for unsaturated soils*, New York: Wiley.

Fredlund D.G. (1998): *Bringing unsaturated soil mechanics into engineering practice*, Proc. 2nd Int. Conf. on Unsaturated soils, Beijing, vol. 2, 1-35.

Garg S.K., Nayfeh A.H. (1986): *Compressional wave propagation in liquid and/or gas saturated elastic porous media*, Journal of Applied Physics, 60(9), 3045-3055.

Gray W.G. (1983): *General conservation equations for multi-phase systems: 4. Constitutive theory including phase change*, Advance in Water Resource, 6, 130-140.

Kohgo Y., Nakano M., Miyazaki T. (1993a): *Theoretical aspects of constitutive modelling for unsaturated soils*, Soils and Foundations 33, No. 4, 49-63.

Kohgo Y., Nakano M., Miyazaki T. (1993b): *Verification of the generalized elastoplastic model for unsaturated soils*, Soils and Foundations 33, No. 4, 64-73.

Kosiński W. (1986): *Field Singularities and Wave Analysis in Continuum Mechanics*, PWN – Polish Scientific Publishers, W-wa, Ellis Horwood Limited, Chichester

Lo W.-C., Majer E, Sposito G. (2005): *Wave propagation through elastic porous media containing two immiscible fluids*, Water Resources Research, 41, 1-20.

Loret B., Khalili N. (2000): *A three-phase model for unsaturated soils*, International Journal for Numerical and Analytical Methods in Geomechanics, 24, 893-927.

Matyas E.L., Radhakrishna H.S. (1968): *Volume change characteristics of partially saturated soils*, Géotechnique 18, 432-448.

Miura K, Yoshida N, Kim Y.-S. (2001): *Frequency dependent property of waves in saturated soil*, Soils and Foundations, 41(2), 1-19.

Modaressi A., Abou-Bekr N. (1994): *A unified approach to model the behaviour of saturated and unsaturated soils*, 8th Int. Conf. Computer Methods & Advances in Geomech., Balkema, 1507-1513.

Santamarina J.C., Klein K.A., Fam M.A. (2001): *Soils and waves*, New York: Wiley.

Santos J.E., Douglas J., Corbero J., Lovera O.M. (1990): *A model for wave propagation in a porous medium saturated by a two-phase fluid*, Journal of Acoustic Society of America, 87(4), 1439-1448.

Toll D.G. (1995): *A conceptual model for the drying and wetting of soil. Unsaturated Soils* (eds. Alonso & Delage), Balkema, Rotterdam, 805-810.

Tuncay K., Corapcioglu M.Y. (1996): *Body waves in poroelastic media saturated by two immiscible fluids*, Journal of Geophysical Research, 101(B11), 25, 149--159.

Wei C., Muraleetharan K.K. (2002): *A continuum theory of porous media saturated by multiple immiscible fluids: I. Linear poroelasticity*, International Journal of Engineering Science, 40, 1807–33.

Wheeler S.J., Sivakumar V. (1995): *An elastoplastic critical state framework for unsaturated soil*, Géotechnique 45, No. 1, 35-53.

Chapter 5

SOIL DEFORMATION BASED ON THE THEORY OF PLASTICITY DESCRIPTION

5.1. Notations used in Chapter 5

$\mathbf{A}$ – matrices, tensors,

$\mathbf{a}$ – vectors

e – void ratio

$\dot{e}$ – void ratio speed

ε_v^s – volumetric strain of skeleton, skeleton dilatation,

$$\varepsilon_v^s = \varepsilon_1^s + \varepsilon_2^s + \varepsilon_3^s$$

ϕ – internal friction angle

ψ – dilation angle

$\boldsymbol{\sigma} = \{\sigma_{11}, \sigma_{22}, \sigma_{33}, \sigma_{12}, \sigma_{13}, \sigma_{23}\}^T$ – stress state vector

$\boldsymbol{\sigma} = \{\sigma_1, \sigma_2, \sigma_3\}^T$ – principal stress vector

$\boldsymbol{\varepsilon} = \{\varepsilon_{11}, \varepsilon_{22}, \varepsilon_{33}, \varepsilon_{12}, \varepsilon_{13}, \varepsilon_{23}\}^T$ – strain state vector

$\boldsymbol{\varepsilon} = \{\varepsilon_1, \varepsilon_2, \varepsilon_3\}^T$ – principal strain vector

I_1, I_2, I_3 – invariants of the stress tensor

$\boldsymbol{\varepsilon} = \boldsymbol{\sigma}' - p\mathbf{m}$ – deviatoric stress

$\boldsymbol{\varsigma} = \boldsymbol{\varepsilon} - \frac{1}{3}\varepsilon_v \mathbf{m}$ – volumetric strain

$p = \frac{1}{3}(\sigma_{11} + \sigma_{22} + \sigma_{33})$ – hydrostatic stress, where, $+p$ determines tensile stress

$q = \sqrt{\frac{3}{2}\boldsymbol{\xi}^T \mathbf{R} \boldsymbol{\xi}}$ – effective deviatoric stress (shear measure)

$\mathbf{m} = \{1,1,1,0,0,0\}^T$, $\mathbf{R} = \mathrm{diag}\{1,1,1,2,2,2\}$, $\mathbf{I}$ – identity matrix

θ – Lode angle, $\cos\theta = -\dfrac{27 J_3}{q^3}$

$J_3 = \xi_{11}\xi_{22}\xi_{33} + \xi_{12}\xi_{23}\xi_{31} - 2(\xi_{11}\xi_{23}^2 + \xi_{22}\xi_{31}^2 + \xi_{33}\xi_{12}^2)$

c – cohesion, expressed in stress

$\dot{\varepsilon}$ – total strain rate

$\dot{\varepsilon}^e$ – elastic strain rate

$\dot{\varepsilon}^p$ – plastic strain rate

$\dot{\varepsilon}^{vp}$ – viscoplastic strain rate

$\dot{\varepsilon}^c$ – creep strain rate

$\dot{\lambda}$ – proportionality factor

$\dot{\varepsilon}_v^p = \dot{\varepsilon}_1^p + \dot{\varepsilon}_2^p + \dot{\varepsilon}_3^p$ – plastic volumetric strain rate

$\dot{\gamma}^p = \dot{\varepsilon}_3^p - \dot{\varepsilon}_1^p$ – plastic shear strain rate

M and p_c – material constants Cam Clay yield surface

$\mathbf{D}^e$ – elastic matrix,

$\mathbf{D}^p$ – matrix plasticity

f_s – static yield surface

f_d – dynamic yield surface

F – overstress function

Symbols in NSFS theory

β – function dependent on time

$\Lambda_1, \Lambda_2, \Lambda_3$ – non-negative coefficients

Different aspects of wave propagation in soil are considered. Many scientists in many research centres have considered this problem and have made significant contributions; therefore, I have tried to limit the number of references. I would like to extend my apologies to all those researchers whose work I have omitted.

Finally, I would to like to express my gratitude to Prof Zbigniew Sikora (Gdańsk University of Technology, Poland) and Prof Roman Lewandowski (Poznań University of Technology, Poland) for their valuable comments in the final editing of this textbook.

5.2. Introduction

To describe the deformation of the soil as an unsaturated porous medium, a few theories are used today, although two main approaches, the theory of plasticity and the theory of hypo-plasticity are widely developed. D.C. Drucker and W. Prager in 1952, as two of the most prominent researchers from the field of both metal and soil, proposed the extended classical form of the Coulomb criterion to the general 3D case of soil analysis. It should be noted that Coulomb set down the first useful yield criterion in 1773. A comprehensive description of the historical background of the theory of plasticity used in soil analysis can be found in Davis R.O. & Selvadurai A.P.S. (2002) or Pietruszczak S. (2010). The beginning of the application of the hypo-elasticity theory is assumed to be Truesdell's work of 1956 in which he showed the ability to describe the material flow. In 1985, Kolymbas provided a description of loading/unloading soil in the range of nonlinear strain rate.

The mechanical response of soils is strongly influenced by their microstructure. General soils have a random structure, but at the macro-level, their behaviour is often described as isotropic material with a typical parameter defined initial porosity. On the other hand, in a number of geomaterials, the microstructure exhibits a strong inherent anisotropy (e.g. deposits of clay and silt sediments) and analysis of the fabric requires some tonsorial, rather than scalar descriptors.

Geomaterial is a porous medium and its response to load strongly affected to the confining pressure. Porous media display an evolution of volume ranging from compaction to dilation that depends on their microstructural arrangement and is described by the dilatation angle (during the shearing of soil, there is a tendency of dense soil to increase in volume). The dilatation angle helps to indicate the direction of the plastic strain rate. Experimental studies by Bauer (1993) identified changes in the internal friction angle and dilatation angle in geomaterials.

Time-dependent engineering problems are related to the constitutive model with the time dependency of the stress-train-strength properties of soils. Viscous effects in the soil skeleton, such as creep, stress relaxation, and strain-rate effects, are taken into account. General stress-strain-time models are often used in an incremental form and are adaptable to numerical implementation in finite element procedures. The following assumption is made: the descriptions are restricted to models concerning the macromechanical properties which use terms such as stress and strain.

Theory includes elastic-viscoplastic effects to description of irreversible deformation of unsaturated porous soil under dynamic loads is proposed in this chapter.

Currently, there are a number of monographs which relate to elastic-viscoplastic theory in the range of static loads and consolidation process: Zaman et al. (2000),

Davis & Selvadurai (2002), Augustesen et al. (2004), Liingaard et al. (2004) and Pietruszczak S. (2010). Today, generalised plasticity, provided by Zienkiewicz & Mróz (1985), is often used in FEM computer calculations.

5.3. Yield criterion

A yield criterion is a mathematical function *f* of stress, strain or both components. There are six independent stress components and *f* can be written as follows:

$$f(\sigma_{11},\sigma_{22},\sigma_{33},\sigma_{12},\sigma_{13},\sigma_{23}) = k \tag{5.1}$$

where *k* represents a constant.

Yielding occurs when this function becomes equal to the constant *k*. There may be functional arguments other than stress, but stress will be the central criterion for yielding in most modern plasticity models. The six stress components in (5.1) can be replaced by the three principal stresses σ_1, σ_2, σ_3, for isotropic bodies, without any loss of generality:

$$f(\sigma_1,\sigma_2,\sigma_3) = k \tag{5.2}$$

where *k* is still a constant, although it may differ from that in (5.1).

Alternatives to the principal stresses are the principal invariants I_1, I_2, I_3:

$$f(I_1,I_2,I_3) = k. \tag{5.3}$$

5.4. Principal stress space

If we know the values of the principal stresses within a deforming body $(\sigma_1,\sigma_2,\sigma_3)$, then we can show this stress *as point* in a Cartesian stress space 3D call the *principal stress space* (Figure 5.1. A point in this space represents the state of stress in the body. The *space diagonal* is a line making equal angles with the three principal stress axes denoted by θ_0. The stress point lies on the space diagonal (all three principal stresses are the same) presents isotropic stress state.

$$\cos\theta_0 = \frac{1}{\sqrt{3}} \tag{5.4}$$

The yield criterion *f* as (5.2) describe stress states in point which exhibits a plastic response. The terms *yield surface* describes the surface *f* = *k* for all points of plastic response and as long as we do not add any more arguments to the function *f*, the surface will be fixed in space.

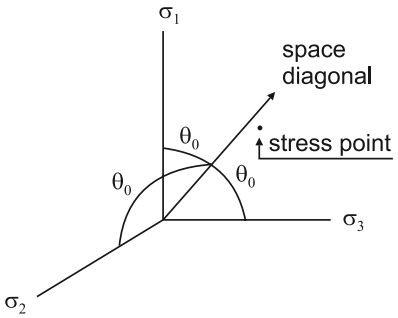

Fig. 5.1. Principal stress space

A planar surface perpendicular to the space diagonal is usually called the π-*plane*, *octahedral plane*, *deviatoric plane* or *Haigh-Westergaard plane* (see Figure 5.2a). If we now look down along the space diagonal towards the origin of the principal stress space, we obtain a view the π-plane.

We can construct a local coordinate system on the π-plane with one direction axis as the projection of σ_1 on the π-plane. We can then define three orthogonal unit vectors denoted $\widehat{\mathbf{n}}_D$, $\widehat{\mathbf{n}}_E$, $\widehat{\mathbf{n}}_F$ (Selvadurai, 2002). Two of these vectors ($\widehat{\mathbf{n}}_E$, $\widehat{\mathbf{n}}_F$) lie in the π-plane and the third ($\widehat{\mathbf{n}}_D$) is the unit vector coinciding with the space diagonal (Figure 5.2b).

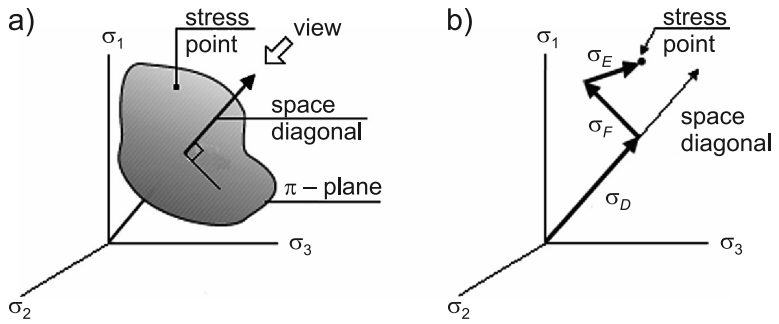

Fig. 5.2. a) schematic view π-plane, b) stress point in $\widehat{\mathbf{n}}_D$, $\widehat{\mathbf{n}}_E$, $\widehat{\mathbf{n}}_F$ directions

The unit vectors denoted by $\widehat{\mathbf{n}}_D$, $\widehat{\mathbf{n}}_E$, $\widehat{\mathbf{n}}_F$ have the following component descriptions in principal stress space:

$$\widehat{\mathbf{n}}_D = \frac{1}{\sqrt{3}}\begin{Bmatrix}1\\1\\1\end{Bmatrix}, \quad \widehat{\mathbf{n}}_E = \frac{1}{\sqrt{3}}\begin{Bmatrix}0\\-1\\1\end{Bmatrix}, \quad \widehat{\mathbf{n}}_F = \frac{1}{\sqrt{3}}\begin{Bmatrix}2\\-1\\-1\end{Bmatrix}. \tag{5.5}$$

A point in principal stresses $\boldsymbol{\sigma} = \{\sigma_1, \sigma_2, \sigma_3\}^T$ can be defined by the components of $\boldsymbol{\sigma} = \{\sigma_D, \sigma_E, \sigma_F\}^T$ as follows:

$$\sigma_D = \frac{1}{\sqrt{3}}(\sigma_1 + \sigma_2 + \sigma_3) = p\sqrt{3},$$

$$\sigma_E = \frac{1}{\sqrt{2}}(-\sigma_2 + \sigma_3),$$

$$\sigma_F = \frac{1}{\sqrt{6}}(2\sigma_1 - \sigma_2 - \sigma_3) \tag{5.6}$$

The radial distance from the space diagonal to the stress point in the π-plane is:

$$\sqrt{\sigma_E^2 + \sigma_F^2} = \sqrt{\frac{2}{3}(\sigma_1^2 + \sigma_2^2 + \sigma_3^2 - \sigma_1\sigma_2 - \sigma_2\sigma_3 - \sigma_3\sigma_1)} = q\sqrt{\frac{2}{3}} \tag{5.7}$$

where:

q – called the *deviatoric stress or stress intensity*:

$$q = \sqrt{(\sigma_1^2 + \sigma_2^2 + \sigma_3^2 - \sigma_1\sigma_2 - \sigma_2\sigma_3 - \sigma_3\sigma_1)} = \sqrt{\frac{1}{2}\left[(\sigma_1 - \sigma_2)^2 + (\sigma_2 - \sigma_3)^2 + (\sigma_3 - \sigma_1)^2\right]} \tag{5.8}$$

The angle between the horizontal (E) direction and the radial dimension to the stress point is (Figure 5.3):

$$\tan\theta = \frac{\sigma_F}{\sigma_E} = \frac{2\sigma_1 - \sigma_2 - \sigma_3}{\sqrt{3}(\sigma_3 - \sigma_2)} \tag{5.9}$$

where:

θ – called the *Lode angle* after the German Engineer W. Lode who first used it in 1926.

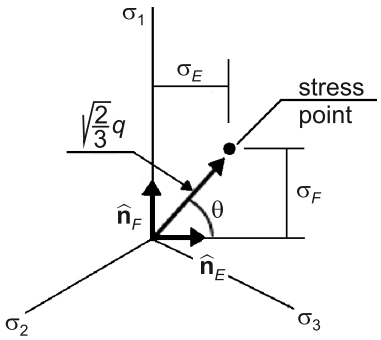

Fig. 5.3. Stress point in π-plane

Remarks:

1. A stress point can be presented in three equivalent axis systems:
   – in Cartesian coordinates by the principal stresses σ_1, σ_2, σ_3,
   – in Cartesian coordinates by the local hydrostatic axis and two orthogonal axes σ_D, σ_E, σ_F,
   – in cylindrical coordinates by the local hydrostatic axis p, orthogonal axis q and angle θ.
2. In the case of an isotropic soil material, the yield criterion is symmetrical, and divides the π – plane into six 60° segments that possess similar properties.
3. In a triaxial compression test, case $\theta = 0$ defines the meridian of conventional triaxial extension (CTE), while $\theta = \pi/3$ denotes the meridian of conventional triaxial compression (CTC).
4. By introducing the projection vector $\mathbf{m} = \{1,1,1,0,0,0\}^T$, one can define the deviatoric stress and strain:

$$\boldsymbol{\xi} = \boldsymbol{\sigma} - p\mathbf{m}, \quad \boldsymbol{\varsigma} = \boldsymbol{\varepsilon} - \frac{1}{3}\varepsilon_v \mathbf{m}.$$

The effective deviatoric stress is defined according to:

$$q = \sqrt{\frac{3}{2}\boldsymbol{\xi}^T \mathbf{R}\boldsymbol{\xi}}, \quad \mathbf{R} = \text{diag}\{1,1,1,2,2,2\}$$

and Lode angle θ as:

$$\cos\theta = -\frac{27J_3}{q^3}, \quad J_3 = \xi_{11}\xi_{22}\xi_{33} + \xi_{12}\xi_{23}\xi_{31} - 2(\xi_{11}\xi_{23}^2 + \xi_{22}\xi_{31}^2 + \xi_{33}\xi_{12}^2).$$

5.5. Yield

5.5.1. The Coulomb yield criterion

In 1773, Coulomb wrote his first scientific paper on soil strength. Coulomb observed that failure is usually associated with a rupture surface within the soil mass. Soil strength depends on cohesion and friction. He wrote his failure criterion as:

$$\tau = \sigma' \tan\phi' + c' \tag{5.10}$$

or

$$f = \tau - \sigma' \tan\phi' - c'$$

where:

τ – represents the shearing stress

σ' – represents normal effective stress on the failure physical plane.

The constant c' is the effective cohesion with dimensions of stress. The quantity $\tan\phi'$ is similar to a coefficient of friction, and ϕ' is the effective angle of internal friction.

Equation (5.10) can be written in the form of (5.2) by using Mohr's circle. The graph of (5.10) is a straight line on the Mohr diagram (see Figure 5.4) with $\sigma_1' \geq \sigma_2' \geq \sigma_3'$.

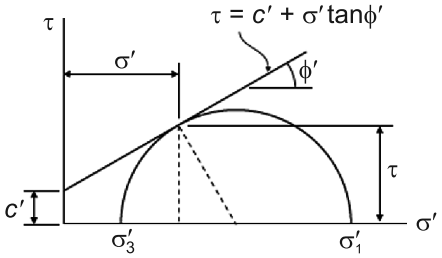

Fig. 5.4. The Coulomb failure criterion

The stress τ and σ' can be expressed by the principal stresses σ_1' and σ_3' by considering the geometry of the dashed triangle in Figure 5.4:

$$\tau = \frac{1}{2}(\sigma_1' - \sigma_3')\cos\phi', \quad \sigma' = \frac{1}{2}(\sigma_1' + \sigma_3') - \frac{1}{2}(\sigma_1' - \sigma_3')\sin\phi'. \tag{5.11}$$

Substituting (5.11) with (5.10) obtains the yield criterion equation:

$$\sigma_1'(1-\sin\phi') - \sigma_3'(1+\sin\phi') = 2c'\cos\phi' \tag{5.12}$$

or

$$\frac{1}{2}(\sigma_3' - \sigma_1') + \frac{1}{2}(\sigma_3' + \sigma_1')\sin\phi' = 2c'\cos\phi' \tag{5.13}$$

Coulomb yield surface can also be submitted by the coordinates σ_D, σ_E, σ_F

$$-\sigma_E\sqrt{3}(1+\sin\phi') + \sigma_F(3-\sin\phi') = 2c'\sqrt{6}\cos\phi' + \sigma_D 2\sqrt{2}\sin\phi' \tag{5.14}$$

where:

σ_D – moved to the right-hand side of this equation as a constant in the π-plane.

The intersection of the Coulomb surface by the π-plane is a closed set of six straight lines broken at 60° (Figure 5.5). Each of the vertices of the hexagon has a particular physical meaning. The uppermost vertex corresponds to the condition

where $\sigma_1 > \sigma_2 = \sigma_3$ (*compression state*), the lowermost vertex is directly opposite and corresponds to $\sigma_1 < \sigma_2 = \sigma_3$ (*extension state*).

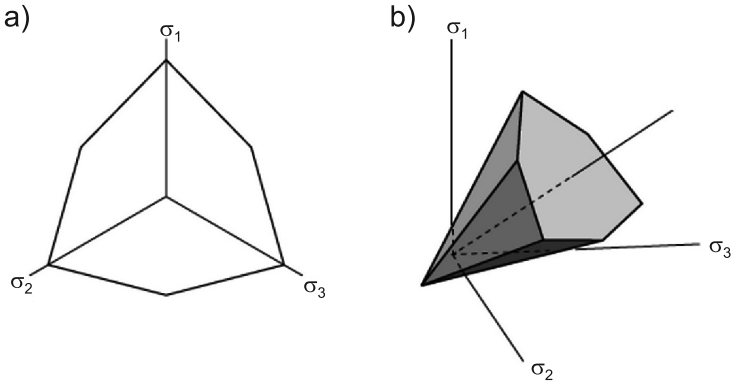

Fig. 5.5. Coulomb yield surface: a) cross-section, b) perspective view

Another cross-sectional area of the Coulomb yield surface is the section in the plane (σ_D, σ_F) along the hydrostatic axis (Figure 5.6). The yield surface is then presented by two straight lines:

– top line, the state of stress $\sigma_1 > \sigma_2 = \sigma_3$ (σ_1 – max, σ_3 – min),
– bottom line, the state of stress $\sigma_1 < \sigma_2 = \sigma_3$ (σ_3–max, σ_1 – min) and setting $\sigma_E = 0$.

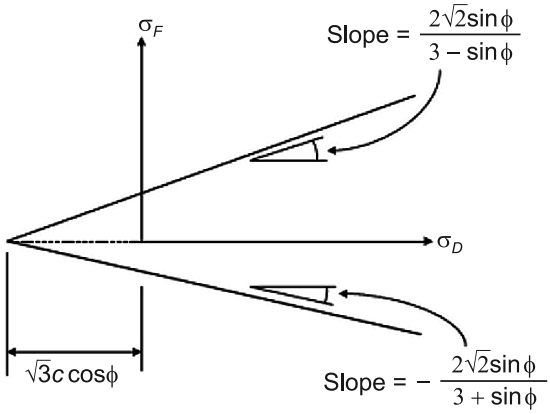

Fig. 5.6. Long section through the Coulomb yield surface

We can ask the question of whether every point of 3D hexagonal Coulomb yield surface is, in fact, realistic. The conventional triaxial test can permits only in plane $\sigma_1 - \sigma_2$ with $\sigma_2 = \sigma_3$. The so-called *cubical true triaxial test* is a much

more specialised test configuration. It appears that the Coulomb hexagon is probably a reasonably good approximation for the true locus of yielding in the π-plane; however, some researchers have suggested slight modifications to Coulomb's criterion that produce smoother surfaces.

5.5.2. Flow rule

One of the main differences between plastic response and elastic response is that plastic flow is irreversible from simple unloading. An important assumption concerning plastic strain relate to Saint–Venant's hypothesis – the normality condition. This assumes that the principal directions of both the stress matrix $\boldsymbol{\sigma}$ and the plastic strain rate matrix $\dot{\varepsilon}^p$ are aligned.

Notation with dot $\dot{\varepsilon}^p$ as the plastic strain rate is using, but it does not involve time dependent, this represents the plastic strain increment within some given parameter increment.

The plastic strain rate $\dot{\varepsilon}^p$ is considered – this can be described in two ways:

– *associated flow rule* by assuming that

$$\dot{\varepsilon}_k^p = \dot{\lambda}\partial f / \partial \sigma_k \quad k = 1,2,3 \tag{5.15}$$

where $\dot{\varepsilon}_k^p$ are the principal plastic strain rate, σ_k denotes the corresponding principal stresses, $\dot{\lambda}$ a proportional positive factor. The adjective *associated* refers to the fact the plastic strain is associated directly with the yield surface *f*.

– *non-associated flow rules*, where the plastic strain rate is obtained by assuming that

$$\dot{\varepsilon}_k^p = \dot{\lambda}\partial g / \partial \sigma_k \quad k = 1,2,3 \tag{5.16}$$

where $\dot{\varepsilon}_k^p$ is derived by differentiating the plastic potential function *g* (different from the yield function *f*) with respect to stress tensor σ_k and multiplied by a proportional positive factor $\dot{\lambda}$

$$g = \frac{1}{2}(\sigma_3 - \sigma_1) + \frac{1}{2}(\sigma_3 + \sigma_1)\sin\psi - \text{const} \tag{5.17}$$

with ψ the angle of dilatancy.

Non-associated flow will generally negate many of the advantages of the normality condition; however, they are desirable for soil materials or more advanced theories.

Experimental studies of soil show that the ψ – dilatancy angle is significantly smaller than the ϕ – internal friction angle ($\psi < \phi$). The angle of dilatancy controls the amount of volumetric plastic strain rate defined as:

$$\dot{\varepsilon}_v^p = \dot{\varepsilon}_1^p + \dot{\varepsilon}_2^p + \dot{\varepsilon}_3^p \tag{5.18}$$

and the rate of plastic shear deformation

$$\dot{\gamma}^p = \dot{\varepsilon}_3^p - \dot{\varepsilon}_1^p \tag{5.19}$$

by substituting (5.17) into (5.16), one can obtain:

$$\dot{\varepsilon}_v^p = \dot{\gamma}^p \sin\psi. \tag{5.20}$$

In the case of non–associated flow rules, the dilatancy angle ψ can take the values:
- $\psi > 0$ while an irreversible increase of volume occurs,
- $\psi < 0$ for when a decrease is predicted (plastic contraction),
- $\psi = 0$ is the special case of a plastically volume-preserving flow (isochoric).

At the destruction of material (collapse) the plastic strain rate is small relative to the total strain rate and can be omitted. Hence, equation (5.20) may change to the total strain rate

$$\dot{\varepsilon}_v = \dot{\gamma} \sin\psi \tag{5.21}$$

with a kinematic constraint on the possible velocity field.

5.5.3. Modifications to Coulomb's criterion

Three modifications to Coulomb's condition are considered:

The first modification of the Coulomb condition was proposed by Drucker and Prager in 1952 – they introduced a modification of von Mises yield criterion, extending this requirement to take into account the average stress p

$$f = q - \xi\, p - k \tag{5.22}$$

Thus, an additional component $\xi\, p$ changes the surface of the von Mises stress from the shape of a cylinder to a cone. Constants ξ and k can be chosen so that the Drucker–Prager cone is in line with the Coulomb cone

$$k = \frac{6c'\cos\phi'}{3 - \sin\phi'}, \quad \xi = \frac{6\sin\phi'}{3 - \sin\phi'}. \tag{5.23a}$$

Graphic interpretation of the Drucker–Prager condition on the π-plane is shown in Figure 5.7.

One can obtain another version of Drucker–Prager's condition through modification of the denominators in (5.23a)

$$k = \frac{6c'\cos\phi'}{3+\sin\phi'}, \quad \xi = \frac{6\sin\phi'}{3+\sin\phi'}. \tag{5.23b}$$

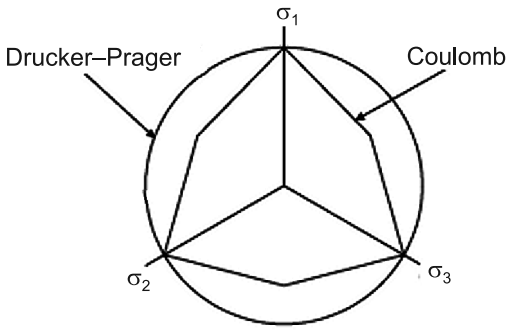

Fig. 5.7. The Drucker–Prager and Coulomb yield surfaces

In the non-associated flow rule, the plastic potential function g is defined as:

$$g = q - \beta p - \text{const}$$

where:

β – dilatancy factor, which can be related to the angle of dilatancy ψ.

The second modification of the Coulomb condition was provided by Lade and Duncan in 1975 in the case of cohesionless soils in the form of equation

$$\sigma_1\sigma_2\sigma_3 = kp^3 \tag{5.24a}$$

where:

k – a constant.

The left side of equation (5.24a) corresponds to the third principal stress invariant. Equation (5.24a) can be represented by stress σ_D, σ_E and σ_F used description (5.6)

$$3\sigma_D(\sigma_E^2+\sigma_F^2) + \sqrt{2}\sigma_F(3\sigma_E^2+\sigma_F^2) = 2(1-k)\sigma_D^3. \tag{5.24b}$$

In the case of cohesionless soils ($c = 0$), we obtain:

$$\sigma_F = \frac{2\sqrt{2}\sigma_D\sin\phi'}{3-\sin\phi'}. \tag{5.25}$$

Taking into account $\sigma_E = 0$ in (5.24b), we obtain:

$$k = 1 - \frac{12\sin^2\phi'}{(3-\sin\phi')^2} + \frac{16\sin^3\phi'}{(3-\sin\phi')^3}. \tag{5.26}$$

Any point in the π-plane, according to (5.24b), is defined by σ_E

$$\sigma_E = \pm\left[\frac{(1-k)\sigma_D^3 + \sqrt{2}\sigma_F^3 - 3\sigma_D\sigma_F^3}{3\sigma_D + 3\sqrt{2}\sigma_F}\right]^{1/2}. \tag{5.27}$$

It can be seen that the Lade–Duncan surface is symmetrical on the π-plane with respect to σ_F. With a constant value of σ_D, the cross-section of the Lade–Duncan surface on the π-plane is shown in Figure 5.8.

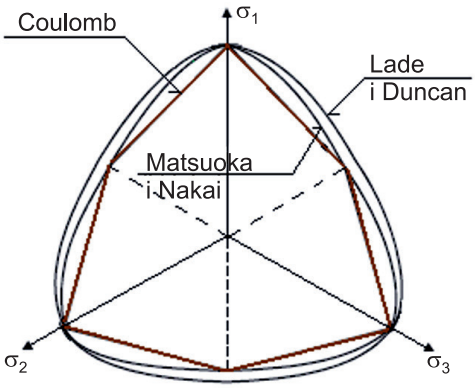

Fig. 5.8. Lade–Duncan and Matsuoka–Nakai yield surfaces compared with the Coulomb yield surface

Third modification of the Coulomb condition was provided by Matsuoka and Nakai in 1974 in the case of cohesionless soils in the form of equation

$$\sigma_1\sigma_2\sigma_3 = \xi p(\sigma_1\sigma_2 + \sigma_2\sigma_3 + \sigma_3\sigma_1) \tag{5.28a}$$

where:

ξ – a constant.

This proposal is consistent with the vertices of the Coulomb surface (both major and minor vertices) if an appropriate value for ξ is used.

Equation (5.28a) can be represented by σ_D, σ_E, σ_F as:

$$2\sigma_F^3 - 6\sigma_E^2\sigma_F + 2\sqrt{2}(1-3\xi)\sigma_D^3 - 3\sqrt{2}(1-\xi)\sigma_D(\sigma_E^2 + \sigma_F^2) = 0. \tag{5.28b}$$

Including (5.14) in equation (5.28b), one can get expression to ξ compatible with vertices of Coulomb surface

$$\xi = \frac{3(1-\sin\phi' - \sin^2\phi' + \sin^3\phi')}{9 - 9\sin\phi' - \sin^2\phi' + \sin^3\phi'}. \tag{5.29}$$

5.5.4. Cam Clay Model

Two cases of Cam Clay surfaces are considered.

– The first plasticity theory for soil as a closed yield surface was devised by K.H. Roscoe together with several co–workers from 1963 to 1968 and is called the Cam Clay model. The yield surface equation written by the invariants p – hydrostatic pressure and q – deviatoric stress is:

$$q + Mp\left(\ln\frac{p}{p_c} - 1\right) = 0 \tag{5.30}$$

where M and p_c are material constants.

The Cam Clay yield surface is a circle on the π-plane. The main difference between the Cam Clay and Coulomb surface is the expression in brackets, which defines the limit stress on the diagonal p (Figure 5.9)

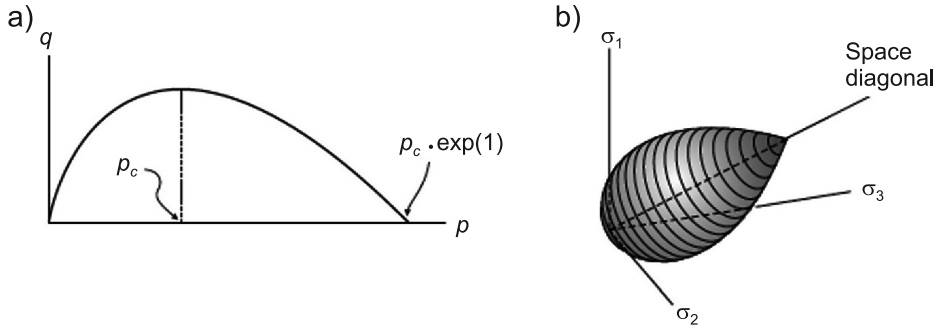

Fig. 5.9. Cam Clay yield surface: a) in (q, p) – space, b) in principal stress space

Parameter p_c is called the *critical state pressure*, it is the ordinate of the maximum deviatoric stress, where equation (5.30) takes the form:

$$q = Mp = Mp_c. \tag{5.31}$$

If we wish the Cam Clay yield surface to agree with the major vertices of the Coulomb hexagon when $p = p_c$, then we make $M = 6\sin\phi(3 - \sin\phi)$, the same as the constant ξ in (5.23).

– The second proposal was based on the discussion of the original Cam Clay model. It was an established model called the Modified Cam Clay, which changed the limit on the p axis by introducing the ellipse surface compressive stress

$$q^2 = M^2 p(2p_c - p) \tag{5.32}$$

where M and p_c play the same roles as in (5.30).

The surfaces of the Cam Clay model and the Modified Cam Clay are shown in Figure 5.10.

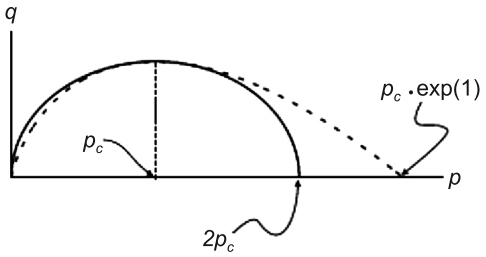

Fig. 5.10. Cam Clay and Modified Cam Clay yield surface

Both surfaces are conforming at the point $p = p_c$, but the Modified Cam Clay surface intersects the stress axis p at point $2p_c$ and the Cam Clay surface at the point $p_c \exp(1) = 2.718 p_c$ (Figure 5.10).

5.5.5. Plane stress problem example

A plane stress problem is considered with the assumption $\sigma_2 = 0$. A Coulomb yield surface and a Drucker–Prager yield surface now will be compared:

a) The Coulomb yield surface area covers six major stress points (Figure 5.11) connected by straight lines, in accordance with equation (5.12)

$$\sigma'_{1,m}(1-\sin\phi') - \sigma'_{3,m}(1+\sin\phi') = 2c'\cos\phi' \tag{5.33}$$

where m refers to indicators points 1 to 6. Figure 5.11a corresponds to $\phi' = 30^o$. For other values of angle ϕ', one can obtain different surfaces, e.g. for $\phi' = 0^o$, one can obtain the Tresca yield surface.

b) The Drucker–Prager yield surface is defined by the equation (5.22). In this case, the cone shape in principal stresses is present with assumption $\sigma_2 = 0$. According to (5.22) and (5.23), one can obtain:

$$(\sigma_1^2 + \sigma_3^2 - \sigma_1\sigma_3)^{1/2} - \frac{2\sin\phi'}{3-\sin\phi'}(\sigma_1+\sigma_2) = \frac{6c'\cos\phi'}{3-\sin\phi'}. \tag{5.34}$$

Figure 5.11b shows the Drucker–Prager yield surface with the Coulomb yield surface with assumption $\sigma_2 = 0,\ \phi' = 30^o$.

Conclusions:

1) As shown in Figure 5.11b, the Drucker–Prager yield area is larger than the Coulomb yield area. The maximum stress points for $\sigma_1 = \sigma_3$ are:

$$\sigma_1 = \sigma_3 = \frac{2c'\cos\phi'}{1-\sin\phi'} \quad \text{– for the Coulomb area} \tag{5.35}$$

$$\sigma_1 = \sigma_3 = \frac{6c'\cos\phi'}{3-\sin\phi'} \quad \text{– for the Druckera–Pragera area} \tag{5.36}$$

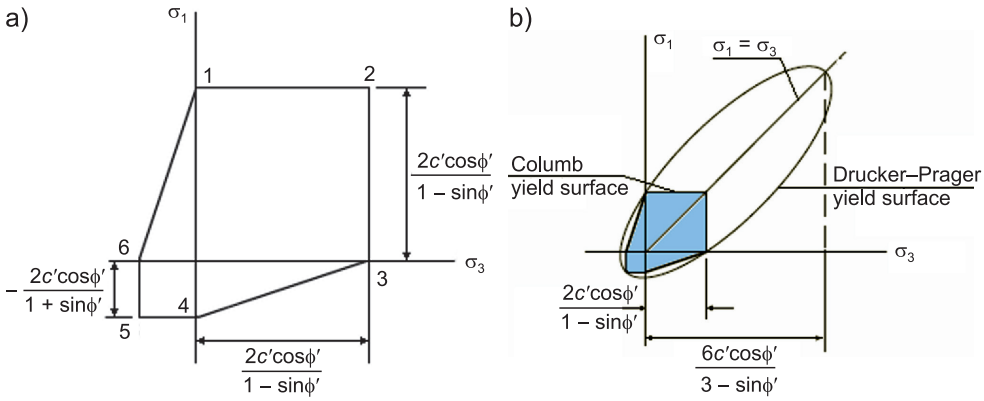

Fig. 5.11. Plane stress problem example: a) Coulomb yield surface, b) Drucker–Prager and Coulomb yield surfaces

2) In the case of $\phi' = 30^{\circ}$, the ratio of the maximum stress value of the Drucker–Prager surface to the Coulomb surface at the point $\sigma_1 = \sigma_3$ is 3. In the case of the Lade–Duncan surface and the Matsuoka–Nakai the ratio of the maximum stress value to the Coulomb surface at the point $\sigma_1 = \sigma_3$ is less.

5.5.6. Plane strain problem example

A plane strain problem is considered with assumption $\varepsilon_1 = 0$ and constant load pressure p_0. We assume isotropic elastic behaviour of cohesionless soil during the application of p_0. The stress state in principal directions is shown in Figure 5.12a. For plane strain condition, stress in third principal direction is $\sigma_3 = \nu(\sigma_1 + \sigma_2)$, where ν is Poisson's ratio and we note that $0 \le \nu \le 1/2$.

The greatest possible values of σ_1 and σ_2 can be obtained from the Coulomb criterion (5.12) with σ_3 as the minor principal stress. The Coulomb criterion (5.12) with $c = 0$ gives

$$\max\sigma_1 = \max\sigma_2 = N\sigma_3 = 2\nu N p_0, \quad N = \frac{(1+\sin\phi')}{(1-\sin\phi')}. \tag{5.37}$$

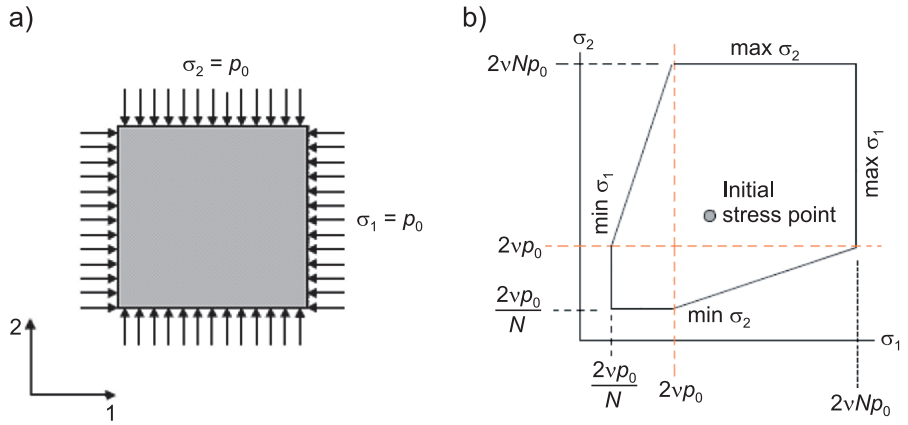

Fig. 5.12. A plane strain problem for cohesionless soil: a) initial stress, b) Coulomb yield surface with initial stress point

The smallest values of σ_1 and σ_2 are found by taking σ_3 to be the major principal stress

$$\min \sigma_1 = \min \sigma_2 = \frac{1}{N}\sigma_3 = \frac{2\nu}{N} p_0. \tag{5.38}$$

These minimum and maximum values for σ_1 and σ_2 define the horizontal and vertical straight-line segments of the two-dimensional yield surface (Figure 5.12b). If σ_1 is equal to its minimum value than σ_2 can be obtain from the yield criterion

$$\sigma_2 = N\sigma_1 = 2\nu p_0. \tag{5.39}$$

Suppose we hold σ_2 constant while reducing σ_1, let

$$\sigma_2 = p_0 \quad \sigma_1 = p_0 - p^* \quad \sigma_3 = 2\nu p_0 - \nu p^* \tag{5.40}$$

The case of stress $\sigma_3 = \sigma_1$ is for $p_* = p_0\left(\frac{1-2\nu}{1-\nu}\right)$. If we take $p_* = p_0\left(1-\frac{1}{N}\right)$, then assuming the Coulomb yield surface in accordance with (5.12), we obtain:

$$\sigma_1 = \frac{(1+\sin\phi')}{(1-\sin\phi')}\sigma_3 = N\sigma_3 = 2N\nu p_0. \tag{5.41}$$

Our problem is to find a strain state ε_1, ε_2 at which the material reaches the plasticity condition with an associated flow law. The elastic stress state changes from point 1 to point 2 until it reaches the Coulomb yield surface (Figure 5.13).

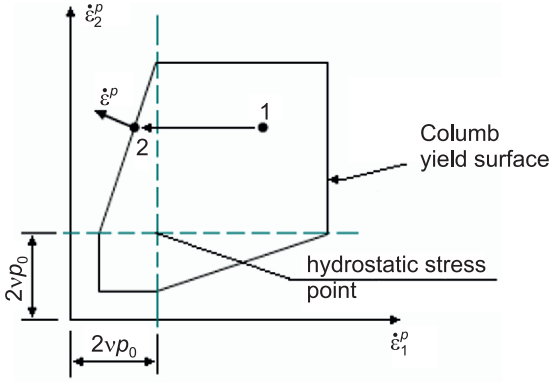

Fig. 5.13. The plastic strain rate $\dot{\varepsilon}^p$ with Coulomb yield surface

Case 1. Associated flow rule

The yield surface equation in point 2 (Figure 5.13), is of the form

$$f = \sigma_2 - N\sigma_1 = 0. \tag{5.42}$$

The principal plastic strain rates $\dot{\varepsilon}_k^p$ are

$$\dot{\varepsilon}_1^p = \dot{\lambda}\frac{\partial f}{\partial \sigma_1} = -\dot{\lambda}Nd \tag{5.43a}$$

$$\dot{\varepsilon}_2^p = \dot{\lambda}\frac{\partial f}{\partial \sigma_2} = -\dot{\lambda} \tag{5.43b}$$

where $\dot{\lambda}$ has dimension (time)$^{-1}$, the value is specified in the case of material with perfect plasticity.

By adding the two equations (5.43), the plastic strain rate equation is obtained:

$$\dot{\varepsilon}^p = \dot{\lambda}(1-N) = \dot{\lambda}\left[1 - \frac{(1+\sin\phi')}{(1-\sin\phi')}\right]. \tag{5.44}$$

In case of $\phi' > 0$ it obtained $\dot{\lambda} < 0$, that indicate the dilatation in plastic deformation (expansion). Such a property always occurs in the case of the Coulomb yield surface, regardless of the load/unload, because it depends on the hydrostatic pressure p. A similar property occurs in the Drucker–Prager, Lade–Duncan and Matsuoka–Nakai yield surfaces.

Case 2. Non-associated flow rule

Yield surface equation in point 2 (Figure 5.13), is defined by function g

$$g = \sigma_2 - M\sigma_1 = 0 \tag{5.45}$$

where:

$$M = \frac{(1+\sin\psi)}{(1-\sin\psi)} \tag{5.46}$$

ψ – the dilatation angle. Similar to (5.43), we obtain:

$$\dot{\varepsilon}_1^p = \dot{\lambda}\frac{\partial g}{\partial \sigma_1} = -\dot{\lambda}M \tag{5.47a}$$

$$\dot{\varepsilon}_2^p = \dot{\lambda}\frac{\partial g}{\partial \sigma_2} = -\dot{\lambda} \tag{5.47b}$$

and

$$\dot{\varepsilon}^p = \dot{\lambda}(1-M) = \dot{\lambda}\left[1 - \frac{(1+\sin\psi)}{(1-\sin\psi)}\right]. \tag{5.48}$$

5.6. Drucker's stability postulate

The constitutive equation of plasticity involves the consideration of plastic energy dissipation in an irreversible process (Drucker, 1958, 1964).

The notion of material stability can be illustrated to the behaviour of a material in uniaxial straining in range of small strain. Let us consider the situation where the specimen is subjected to an arbitrary stress σ_{ij} and $\Delta\sigma_{ij}$ is the increment in stress which produces a corresponding increment in strain $\Delta\varepsilon_{ij}$. The material is said to be *stable* if

$$\Delta\sigma_{ij}\Delta\varepsilon_{ij} > 0. \tag{5.49}$$

The closed path shown in Figure 5.14 (as a closed cycle of loading/unloading) describes the plastic energy dissipation. If the loading that induces a strain increment $\Delta\varepsilon_{ij}$ commences from a reference stress state σ_{ij}^0, the inequality (5.49) can be written as:

$$(\sigma_{ij} - \sigma_{ij}^0)\Delta\varepsilon_{ij}^p > 0. \tag{5.50}$$

Drucker's postulate states that for any stable material, the rate of work done by the stress during plastic deformation at a point in the medium (σ_{ij}^0) over a closed

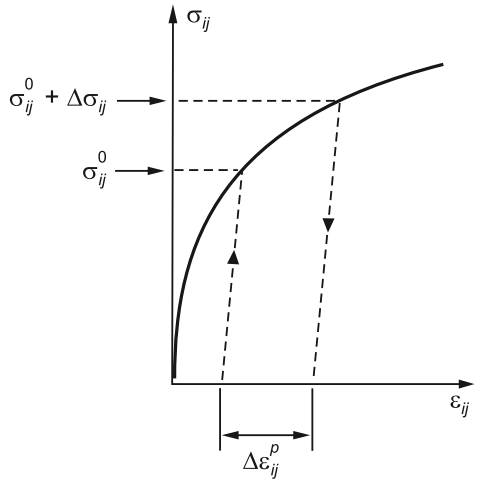

Fig. 5.14. Schematic representation of a loading cycle in stable material

cycle involving loading and unloading is non-negative (see Figure 5.15). If we denote this plastic work rate by W_P, we have:

$$W_p = \int_{t_1}^{t_2} (\sigma_{ij} - \sigma_{ij}^0)\dot{\varepsilon}_{ij}\mathrm{d}t \geq 0 \tag{5.51a}$$

or in principal direction

$$W_p = \int_{t_1}^{t_2} (\sigma_1\dot{\varepsilon}_1 + \sigma_2\dot{\varepsilon}_2 + \sigma_3\dot{\varepsilon}_3)\,\mathrm{d}t \geq 0. \tag{5.51b}$$

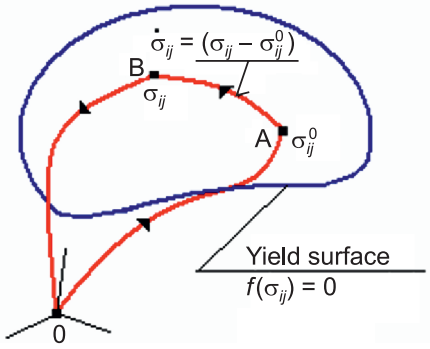

Fig. .15. Closed stress cycle 0–A–B–0 in a principal stress space

A closed stress path cycle is considered (Figure 5.15), starting the cycle at stress σ_{ij}^0 at point A through to points B and O to stress σ_{ij}^0 in relation to the yield surface

$f(\sigma_{ij}) = 0$. The rate of work done by the stress on the elastic strain rate $\dot{\varepsilon}_{ij}^{e}$ is fully recoverable. Therefore, we can focus on the representation of the stability postulate in terms of the total work of the stress done on the plastic strain rate, W_p, over the history of the stress cycle where $t \in (t_1, t_2)$. Let's plastic strain start at $t = t_1$, then W_p can be expand as a Taylor series about the neighbourhood of $\sigma_{ij}^{0}(t_1)$:

$$W_p(t) = (t - t_1)(\sigma_{ij} - \sigma_{ij}^{0})\dot{\varepsilon}_{ij}^{p} + \frac{(t - t_1)^2}{2!}\left[\dot{\sigma}_{ij}\dot{\varepsilon}_{ij}^{p} + (\sigma_{ij} - \sigma_{ij}^{0})\dot{\varepsilon}_{ij}^{p}\right] + \ldots \qquad (5.52)$$

The right side of equation (5.52) is considered. If the plastic work $W_p(t)$ fulfils the Drucker's postulate for $(t - t_1) > 0$, the following inequalities are satisfied:

$$(\sigma_{ij} - \sigma_{ij}^{0})\dot{\varepsilon}_{ij}^{p} \geq 0 \quad \text{for} \quad \sigma_{ij} \neq \sigma_{ij}^{o}$$

$$\dot{\sigma}_{ij}\dot{\varepsilon}_{ij}^{p} \geq 0 \quad \text{for} \quad \sigma_{ij} = \sigma_{ij}^{o}. \qquad (5.53)$$

The first inequality (5.53) is associated with the energy dissipation, while the other corresponds to the condition of a stable material: if $\dot{\varepsilon}_{ij}^{p} \neq 0$ occurs $\dot{\sigma}_{ij}\dot{\varepsilon}_{ij}^{p} \geq 0$.

5.7. Plastic flow rule

The geometric interpretation of inequality (5.53) is a vector of the plastic strain rate $\dot{\varepsilon}^{p}$ normal to the yield surface $f(\sigma_{ij}) = k$ in point stress σ_{ij}. The first inequality (5.53) presents point B in Figure 5.16.

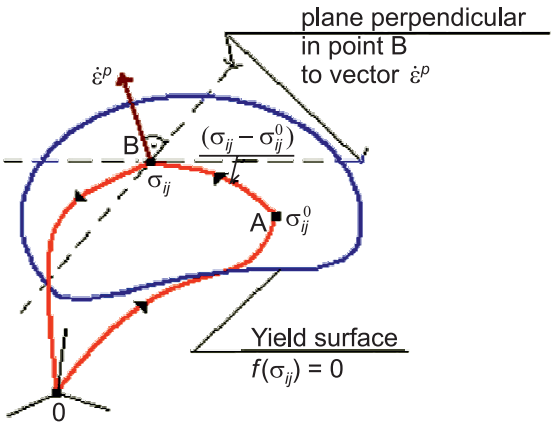

Fig. 5.16. Geometric interpretation of Drucker's stability postulate

Associated flow means that the direction of the plastic flow of the stress point on the surface is a direction normal to the surface plasticity. Non-associated flow means that the direction of the plastic flow of the stress point on the surface is not compatible with a direction normal to the surface plasticity. This property occurs in soil.

It is found that the rate of dilation $\dot{\varepsilon}^p$ suggested by (5.53) is not compatible with data from real soil tests – the rate is often far in excess of realistic values. For many soils, shearing is accompanied by compaction rather than dilation, in other soils, no volumetric strain is evident during shearing. Even for dilating soils, the rate of dilation is usually not as large as that given by (5.53). Thus, the Coulomb criterion should take into account the following phenomena:

a) a reduction of the pressure effect,
b) shrinkage of the yield surface of compacting soils with increasing mean stress,
c) neither growth nor shrinkage of the yield surface for soils that exhibit no volumetric strain,
d) requirement for an expanding yield surface for dilating soils

Almost all of the above types of behaviour can be described with the Cam Clay and Modified Cam Clay yield surfaces.

Case 1. Perfect plasticity

We say that a material is *perfectly plastic* if, on yielding, the plastic strain can grow without bound given that no further change in stress occurs and no outside constraints are present (Figure 5.17a). If the strain is specified, then the stress is known, but not vice versa.

Case 2. Work hardening plasticity

In contrast to perfect plasticity, *work hardening* implies that the yield surface may change in some way once initial yielding has occurred. Usually, the change of yield surface is related to the amount of plastic strain or to the amount of plastic work

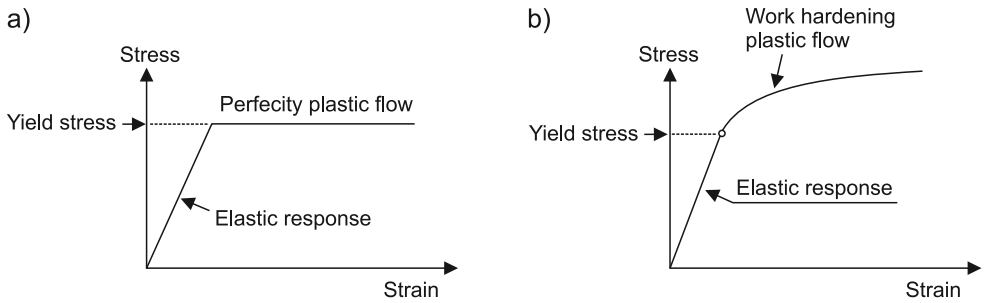

Fig. 5.17. Stress-strain response: a) perfectly plastic material; b) work hardening plastic material

that has accumulated. Here, the stress and strain may have a one-to-one functional relationship both before and after yield (Figure 5.17b).

5.8. Loading criterion

The identifying problem of plastic flow is now considered by specifying the stress state in the two load step conditions. We start from the stress point on the yield surface and consider if the next stress point is in the elastic area or both are on the yield surface. The result will give us a simple criterion for whether or not the plastic response will continue.

The stress increment on the yield surface defined by equation $f(\boldsymbol{\sigma}) = k$ is considered

$$\dot{f} = \frac{\partial f}{\partial \boldsymbol{\sigma}} \dot{\boldsymbol{\sigma}} = \frac{\partial f}{\partial \sigma_1} \dot{\sigma}_1 + \frac{\partial f}{\partial \sigma_2} \dot{\sigma}_2 + \frac{\partial f}{\partial \sigma_3} \dot{\sigma}_3 \tag{5.54}$$

if

$\dot{f} = 0$ – the load increment is carried on the yield surface,

$\dot{f} < 0$ – the next stress point is moving back inside the yield surface in the elastic area,

$\dot{f} > 0$ – the next stress point can go outside the yield surface – this is impossible only with work-hardening materials at the next position of the yield surface.

The criterion for continued plastic loading, called the *consistency condition* is

$$\dot{f} = \frac{\partial f}{\partial \boldsymbol{\sigma}} \dot{\boldsymbol{\sigma}} = 0. \tag{5.55}$$

In the case of the Coulomb yield, criterion $\dot{f}$ is given by:

with $\sigma_1 > \sigma_2 = \sigma_3$

$$\dot{f} = \dot{\sigma}_1 (1 - \sin\phi') - \dot{\sigma}_3 (1 + \sin\phi') - 2c' \cos\phi' \tag{5.56a}$$

with $\sigma_1 < \sigma_2 = \sigma_3$

$$\dot{f} = \dot{\sigma}_3 (1 - \sin\phi') - \dot{\sigma}_1 (1 + \sin\phi') - 2c' \cos\phi'. \tag{5.56b}$$

5.9. Complete stress-strain relationship

The plastic strain rate $\dot{\boldsymbol{\varepsilon}}^p$ in (5.15) depend upon the undetermined multiplier $\dot{\lambda}$. We identify the value of $\dot{\lambda}$ in terms of the rates of change of stress and total strain when plastic loading is occurring. The associated and non-associated flow rules can be considered.

The decomposition of the strain rate into elastic and plastic parts takes the form:

$$\dot{\boldsymbol{\varepsilon}} = \dot{\boldsymbol{\varepsilon}}^e + \dot{\boldsymbol{\varepsilon}}^p \tag{5.57}$$

where vectors $\dot{\boldsymbol{\varepsilon}}^e$ and $\dot{\boldsymbol{\varepsilon}}^p$ have components equal to the elastic and plastic parts of each in principal strain rate.

The vector of elastic stress rates is defined by the equation:

$$\dot{\boldsymbol{\sigma}}^e = \mathbf{D}^e \dot{\boldsymbol{\varepsilon}}^e \tag{5.58}$$

where:

$$\mathbf{D}^e = \begin{bmatrix} \Lambda + 2G & \Lambda & \Lambda \\ \Lambda & \Lambda + 2G & \Lambda \\ \Lambda & \Lambda & \Lambda + 2G \end{bmatrix} \quad - \text{ the elasticity matrix (in case 2D)} \tag{5.59}$$

$$\Lambda = \frac{\nu E}{(1+\nu)(1-2\nu)} = \frac{2G\nu}{(1-2\nu)} \quad - \text{ Lamé constant}$$

or

$$\mathbf{D}^e = \frac{2G}{(1-2\nu)} \begin{bmatrix} (1-\nu) & \nu & \nu \\ \nu & (1-\nu) & \nu \\ \nu & \nu & (1-\nu) \end{bmatrix}$$

Using the non-associated flow rule in (5.16), equation (5.57) takes the form of:

$$\dot{\boldsymbol{\varepsilon}} = \dot{\boldsymbol{\varepsilon}}^e + \dot{\lambda} \frac{\partial g}{\partial \boldsymbol{\sigma}} \tag{5.60}$$

Now, by multiplying both sides of equation (5.60) by $\left(\frac{\partial f}{\partial \boldsymbol{\sigma}} \right)^T \mathbf{D}^e$, then taking into account relationships $\frac{\partial f}{\partial \boldsymbol{\sigma}} \dot{\boldsymbol{\sigma}} = 0$ and $\dot{\boldsymbol{\sigma}}^e = \mathbf{D}^e \dot{\boldsymbol{\varepsilon}}^e$, we obtain:

$$\dot{\boldsymbol{\sigma}} = \mathbf{D}^e \dot{\boldsymbol{\varepsilon}} - \frac{\mathbf{D}^e \left(\frac{\partial g}{\partial \boldsymbol{\sigma}}\right)\left(\frac{\partial f}{\partial \boldsymbol{\sigma}}\right)^T}{\left(\frac{\partial f}{\partial \boldsymbol{\sigma}}\right)\mathbf{D}^e \frac{\partial g}{\partial \boldsymbol{\sigma}}} \mathbf{D}^e \dot{\boldsymbol{\varepsilon}} = \mathbf{D}^{ep} \dot{\boldsymbol{\varepsilon}} \tag{5.61}$$

where:

$$\mathbf{D}^{ep} = \left[\mathbf{I} - \frac{\mathbf{D}^e \left(\frac{\partial g}{\partial \boldsymbol{\sigma}}\right)\left(\frac{\partial f}{\partial \boldsymbol{\sigma}}\right)^T}{\left(\frac{\partial f}{\partial \boldsymbol{\sigma}}\right)^T \mathbf{D}^e \frac{\partial g}{\partial \boldsymbol{\sigma}}} \right] \mathbf{D}^e \quad - \text{ the elastic-plastic matrix (in case 2D).} \tag{5.62}$$

Equation (5.61) specifies the relationship between the stress rates and the total strain rate for a material obeying a non-associated flow rule, provided continued plastic loading occurs.

Remarks:

1. The quantity $\left(\frac{\partial f}{\partial \boldsymbol{\sigma}}\right)\mathbf{D}^e \frac{\partial g}{\partial \boldsymbol{\sigma}}$ in the denominator of the fraction in (5.62) is a scalar, the numerator $\mathbf{D}^e \left(\frac{\partial g}{\partial \boldsymbol{\sigma}}\right)\left(\frac{\partial f}{\partial \boldsymbol{\sigma}}\right)^T$ is a square matrix.
2. Load increment should fulfil the consistency condition. If the loading criterion is not satisfied, then an elastic response occurs according to (5.58) instead of equation (5.61).

Example

Now we consider a plane strain problem example (see point in this book 5.5.6). According to the equation for f (5.42) and g (5.45) one can obtain

$$\frac{\partial f}{\partial \boldsymbol{\sigma}} = \begin{Bmatrix} -N \\ 1 \end{Bmatrix}, \quad \frac{\partial g}{\partial \boldsymbol{\sigma}} = \begin{Bmatrix} -M \\ 1 \end{Bmatrix}. \tag{5.63}$$

We can illustrate the use of (5.61) by considering a simple plane strain example with the assumption $\varepsilon_3 = 0$ (although the elastic and plastic components can be nonzero). In the case of plane strain, $\mathbf{D}^e$ is

$$\mathbf{D}^e = \begin{bmatrix} \Lambda + 2G & \Lambda \\ \Lambda & \Lambda + 2G \end{bmatrix}. \tag{5.64}$$

By substituting (5.63) and (5.64) to (5.62), one can obtain:

$$\mathbf{D}^{ep} = \left[\mathbf{I} - \frac{\mathbf{D}^e \left(\frac{\partial g}{\partial \boldsymbol{\sigma}} \right) \left(\frac{\partial f}{\partial \boldsymbol{\sigma}} \right)^T}{\left(\frac{\partial f}{\partial \boldsymbol{\sigma}} \right)^T \mathbf{D}^e \frac{\partial g}{\partial \boldsymbol{\sigma}}} \right] \mathbf{D}^e = \frac{2G}{(1-\nu)(NM+1)-\nu(M+N)} \begin{bmatrix} 1 & M \\ N & NM \end{bmatrix}. \quad (5.65)$$

Comments:

1. Eigenvalues of $\mathbf{D}^{ep}$ matrix are $\lambda_1 = 0$,

$$\lambda_1 = 0, \quad \lambda_2 = \frac{-2G(1+MN)}{(1-\nu)(NM+1)-\nu(M+N)}.$$

2. Eigenvalue $\lambda_1 = 0$ of $\mathbf{D}^{ep}$ means that in the case of the ideal plasticity, the inverse matrix $(\mathbf{D}^{ep})^{-1}$ cannot be calculated; therefore, at a given stress rate, strain rate cannot be determined.
3. If eigenvalues of matrix $\mathbf{D}^{ep}$ are different from zero, then from equation (5.61), the strain rate can be determined at a given stress rate.

5.10. Work hardening

5.10.1. Work hardening in soil materials

Yield surface and plastic flow is associated with an increase in the strength of the material, this increase in strength is known as hardening. *Strain hardening or work hardening* it is name used for increase of material strength when increases in plastic deformation occur.

The yield stress σ_T can be written as a function of the *plastic work* W_p (see Figure 5.18) as well as a function of the components of stress

$$W_p = \int \dot{W}_p \mathrm{d}t = \int \mathrm{tr}(\boldsymbol{\sigma}\dot{\boldsymbol{\varepsilon}}^p)\,\mathrm{d}t \cong \int (\sigma_1 \mathrm{d}\dot{\varepsilon}_1^p + \sigma_2 \mathrm{d}\dot{\varepsilon}_2^p + \sigma_3 \mathrm{d}\dot{\varepsilon}_3^p). \quad (5.66a)$$

The plastic work is that part of the total stored energy W. Considering the context of a simple one-dimension test (Figure 5.18), the plastic work may be written as:

$$W_p = \int \sigma_1 \mathrm{d}\dot{\varepsilon}_1^p = \int \sigma_1 (\mathrm{d}\dot{\varepsilon}_1 - \mathrm{d}\dot{\varepsilon}_1^e) = W - W_e. \quad (5.66b)$$

Hardening can be described by two parameters, the scalar parameter κ and the vector parameter $\boldsymbol{\omega}$. Plastic potential function can be defined as:

$$g(\boldsymbol{\sigma}', \kappa, \boldsymbol{\omega}) = g(\sigma_1', \sigma_2', \sigma_3', \kappa, \omega_1, \omega_1, \omega_1) = 0 \quad (5.67)$$

where:

$\kappa = \kappa(\dot{\boldsymbol{\varepsilon}}^p)$ – a scalar function of plastic strain rate $\dot{\boldsymbol{\varepsilon}}^p$ called plastic isotropic hardening (Figure 5.19a),

$\boldsymbol{\omega} = \omega(\dot{\boldsymbol{\varepsilon}}^p)$ – a vector function of plastic strain rate $\dot{\boldsymbol{\varepsilon}}^p$ called plastic kinematic hardening (Figure 5.19b).

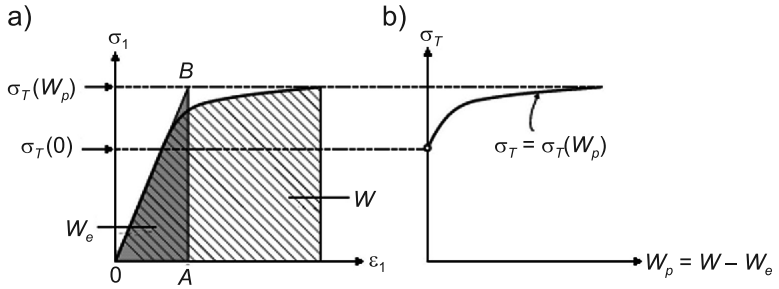

Fig. 5.18. Calculation of plastic work in a work hardening material: a) stress-total strain response; b) yield stress evolves as a function of plastic work

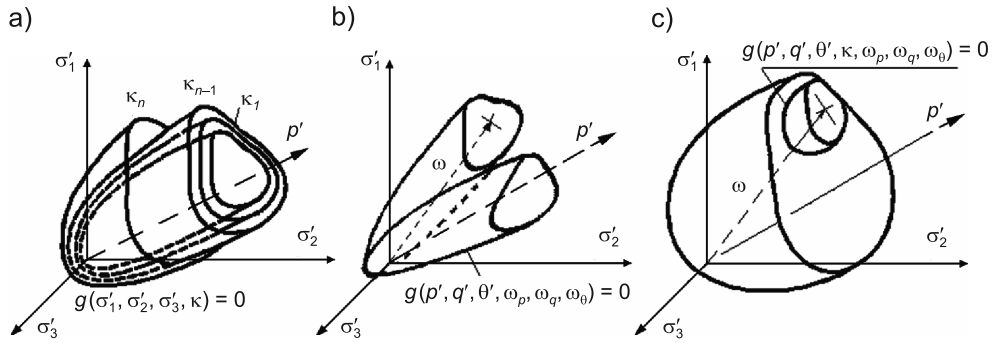

Fig. 5.19. Types of hardening: a) isotropic, b) kinematic, c) isotropic-kinematic assembling

Plastic hardening models used in metals are insufficient to describe the complex behaviour of soils.

This is due to the fact that:

– Irreversible deformation in soil can occur without the participation of shear stress. A typical soil sample test is the odometer test, where a plastic deformation occurs with growth of normal stress.
– Dense soils will dilate and loose soils will compress, both will approach a state at which no further volume change occurs. Typical behaviour of dense and loose sand in a triaxial test is shown in Figure 5.20.

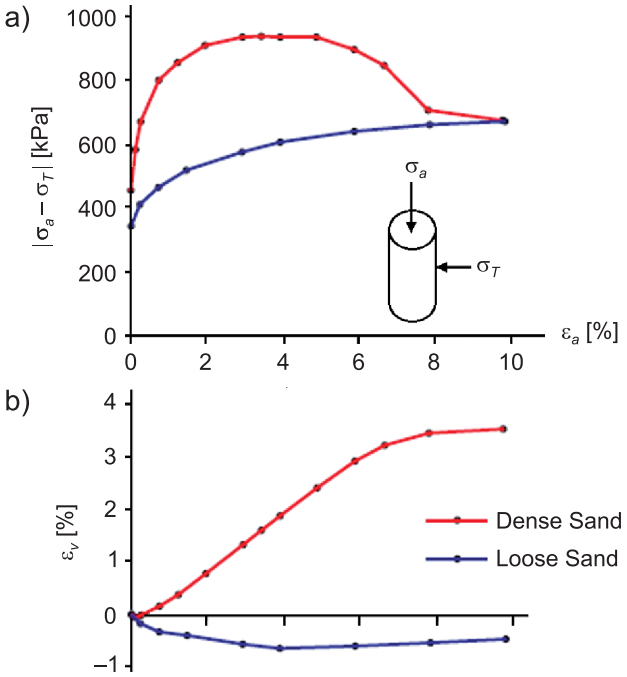

Fig. 5.20. Responses from triaxial compression in dense and loose sands (Cornforth D.H., 1964): a) deviatoric stress versus axial strain; b) volumetric strain versus axial strain

5.10.2. Strain hardening in the Cam Clay model

The problem to be considered is *simple shearing* as illustrated in Figure 5.21. By considering a simple problem, we can avoid a number of minor complications that have no effect on the fundamental model response. A sample of soil is subjected

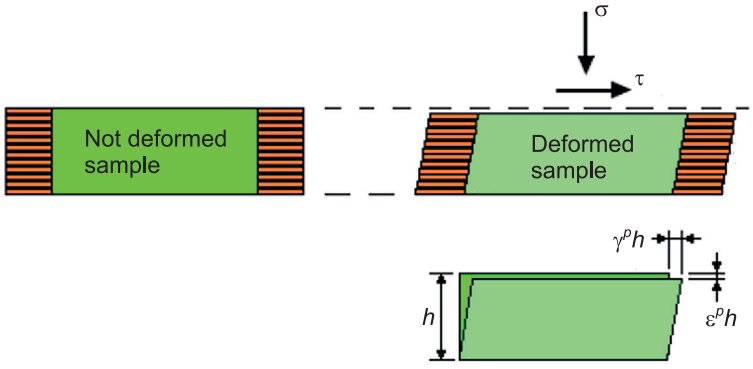

Fig. 5.21. Schematic diagram showing a simple shear test

to applied normal σ and shearing stress τ on its upper surface, no extensional deformation occurs in the horizontal direction. If the sample happens to be saturated, we consider σ as being the effective stress.

A vertical strain denoted by ε^p and a shear strain denoted by γ^p. We denote both strain as plastic.

The Cam Clay model used the triaxial test as the example problem, this also has only two stress and two strain components, but those components are derived from invariants and are slightly more complex than the simple stress and strain considered here.

A yield surface is a function of the stress components as $f(\sigma, \tau)$. The rate of plastic work can be defined as:

$$\dot{W}_p = \sigma\dot{\varepsilon}^p + \tau\dot{\gamma}^p. \tag{5.68}$$

Equation (5.68) with σ = const is called *dissipation function* $\dot{W}_p = \dot{D}$. The Cambridge workers postulated a dissipation function as a homogeneous function of the plastic strain rate multiplied by coefficients that depend upon the stress, with the form:

$$\dot{D} = k\sigma\dot{\gamma}^p \tag{5.69}$$

where:

k – is a material parameter that is constant for any particular soil.

Comparing the right sides of equations (5.68) and (5.69) obtained:

$$\sigma\dot{\varepsilon}^p + \tau\dot{\gamma}^p = k\sigma\dot{\gamma}^p$$

or

$$\dot{\varepsilon}^p = \left(k - \frac{\tau}{\sigma}\right)\dot{\gamma}^p \tag{5.70}$$

where the shear strain rate $\dot{\gamma}^p$ is positive.

According to (5.70), assuming $\dot{\gamma}^p > 0$, we can get three possibilities for the value of strain rate $\dot{\varepsilon}^p$:

– if $\sigma > \frac{\tau}{k} \rightarrow \dot{\varepsilon}^p > 0$ – compression is occurring in loose soil, so-called *weak yielding*, (5.70a)

– if $\sigma < \frac{\tau}{k} \rightarrow \dot{\varepsilon}^p < 0$ – dilation is occurring in dense soil, so-called *strong yielding*, (5.70b)

– if $\sigma = \dfrac{\tau}{k} \rightarrow \dot{\varepsilon}^p = 0$ – the sample volume is not changing, shear strain can grow without any change in volume. (5.70c)

The stress state in which shear strain can grow without any change in volume is known as the *critical state*. Experimental evidence shows that, regardless of the initial state of sample packing, there is always a tendency to move toward the critical state: loose soil compacts; dense soil dilates and moves to the critical packing where no volume change occurs.

Drucker's postulate states that as long as the body remains in equilibrium, the rate of plastic work increment $\delta \dot{W}_p$ should always be equal to or greater than zero. Therefore,

$$\mathrm{d}\dot{W}_p = \delta\sigma\dot{\varepsilon}^p + \delta\tau\dot{\gamma}^p \geq 0. \tag{5.71}$$

In the limiting case, the inequality (5.71) and normal to yield surface condition holds. Equation (5.70) can be written as:

$$\frac{\delta\tau}{\delta\sigma} + \frac{\dot{\varepsilon}^p}{\dot{\gamma}^p} = \frac{\mathrm{d}\tau}{\mathrm{d}\sigma} + k - \frac{\tau}{\sigma} = 0. \tag{5.72}$$

With integration due to stress (5.72), we obtain:

$$\tau = \sigma(C_1 - k\ln\sigma). \tag{5.73}$$

where:

C_1 – is a constant of integration.

According to equation (5.70c), the critical state is for $\sigma = \tau/k$. Suppose we define a critical state stress, $\sigma_c = \tau/k$, then (5.73) can be written as

$$k\sigma_c = \sigma_c(C_1 - k\ln\sigma_c) \tag{5.74}$$

hence $C_1 = k(1 + \ln\sigma_c)$.

By substituting C_1 to (5.73), one can obtain:

$$\tau + k\cdot\sigma\left[\ln\left(\frac{\sigma}{\sigma_c}\right) - 1\right] = 0. \tag{5.75}$$

Equation (5.75) presents the Cam Clay yield surface model in a simple shear test. A graph of (6.75) is shown in Figure 5.22. Using invariants, the p and q equation (5.75) takes the form (5.30):

$$q + Mp\left[\ln\left(\frac{p}{p_c}\right) - 1\right] = 0.$$

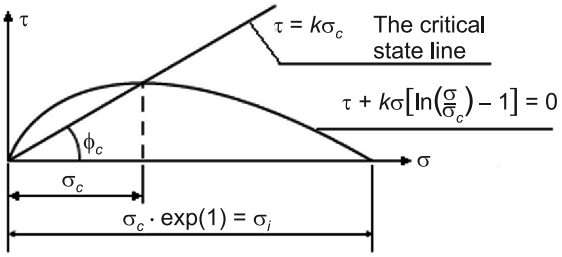

Fig. 5.22. The Cam Clay yield surface model in a simple shear tes

Soil testing demonstrated the possibility of increasing the normal stress over $\sigma_c \exp(1) = \sigma_i$ (Figure 5.22). Thus, existing soil hardening depends on the amount of plastic strain ε^p. We will define this process by $\sigma_c = \sigma_c(\varepsilon^p)$ as the *hardening parameter*.

Increased stress σ at $\tau = 0$ is present in odometer test soil, where the results are presented in the axes $h - \log\sigma$ or $e - \log\sigma$. The hardening process in the Cam Clay model can be shown in axis $\varepsilon^p - \ln\sigma$ or $\varepsilon^p - \ln(\sigma_i / \sigma_i^0)$ to give equation:

$$\varepsilon^p = m \cdot \ln(\sigma_i / \sigma_i^0) \tag{5.76}$$

where:

m – is a material constant representing the slope of $\varepsilon^p - \ln(\sigma_i / \sigma_i^0)$,

σ_i^0 – is the initial value of σ_i and corresponds to the upper point of the virgin compression curve, the so-called pre-consolidation stress.

Therefore, yield surface changes with plastic deformation ε^p, equation (5.76) can be written as:

$$\varepsilon^p = m \cdot \ln(\sigma_c / \sigma_c^0) \tag{5.77}$$

where:

$\sigma_c^0 = \sigma_i^0 \cdot \exp(-1)$ – the initial value of σ_c.

Equations (5.75), (5.77) and the associated flow rule describe the plastic behaviour of our sample. Three material constants have been used, k, m and σ_c^0. The constant m and σ_c^0 are determined directly from odometer test data, where σ_c^0 defines the initial shape and the position of the yield surface. The constant k represents the ratio $k = \tau / \sigma_c$ for $\varepsilon^p = 0$. ϕ_c is used to denote the critical state friction angle for soil, i.e. $\phi_c = \arctan(\tau/\sigma)$ at failure, thus $k = \tan\phi_c$.

The strain rate was obtained from the associated plastic flow law according to the relationships:

$$\dot{\gamma}^p = \dot{\lambda}\frac{\partial f}{\partial \tau} = \dot{\lambda}, \tag{5.78}$$

$$\dot{\varepsilon}^p = \dot{\lambda}\frac{\partial f}{\partial \sigma} = \dot{\lambda} k \ln\left(\frac{\sigma}{\sigma_c}\right) \tag{5.79}$$

where:

f – the yield surface defined by (5.75).

By differentiating (5.77), one can obtain:

$$\dot{\varepsilon}^p = m\frac{\dot{\sigma}_c}{\sigma_c}. \tag{5.80}$$

Comparing (5.79) and (5.80) gives:

$$\dot{\sigma}_c = \frac{k}{m}\sigma_c \ln\left(\frac{\sigma}{\sigma_c}\right)\dot{\gamma}^p \quad \text{or} \quad \frac{1}{\sigma_c \ln\left(\frac{\sigma}{\sigma_c}\right)} = \frac{k}{m}\frac{\dot{\gamma}^p}{\dot{\sigma}_c} \quad \text{where} \quad \frac{\dot{\gamma}^p}{\dot{\sigma}_c} = \frac{d\gamma^p}{d\sigma_c}. \tag{5.81}$$

Assuming σ = cons, after integration, one can obtain:

$$\ln\left[\ln\left(\frac{\sigma}{\sigma_c}\right)\right] = -\frac{k}{m}\gamma^p + C_2 \tag{5.82a}$$

or

$$\ln\left(\frac{\sigma}{\sigma_c}\right) = \exp\left(-\frac{k}{m}\gamma^p + C_2\right) = \exp\left(-\frac{k}{m}\gamma^p\right)\exp(C_2) \tag{5.82b}$$

where:

C_2 – the constant obtained from condition $\sigma_c = \sigma_c^0$, when $\gamma^p = 0$

$$\ln\left(\frac{\sigma}{\sigma_c}\right) = \exp\left(-\frac{k}{m}\gamma^p\right)\exp(C_2) \rightarrow \ln\left(\frac{\sigma}{\sigma_c^0}\right) = \exp(C_2). \tag{5.83}$$

After the substitution of (5.83) for (5.82b), one can obtain:

$$\ln\left(\frac{\sigma}{\sigma_c}\right) = \ln\left(\frac{\sigma}{\sigma_c^0}\right)\exp\left(-\frac{k}{m}\gamma^p\right). \tag{5.84}$$

Finally, substituting (5.84) to (5.75), the Cam Clay yield surface is of the form:

$$\tau = k \cdot \sigma \left[1 - \ln\left(\frac{\sigma}{\sigma_c^0} \right) \exp\left(-\frac{k}{m} \gamma^p \right) \right]. \tag{5.85}$$

Equation (5.85) defines the shear stress $\tau - \gamma^p$ plastic shear strain of the Cam Clay model in simple shear. An example of shear stress response is shown in Figure 5.23 for parameter values of k = 1.0 and m = 0.025. Two cases are considered: a) compacted soil under stress $\sigma = 1.4\sigma_c^0$, b) loose soil under stress $\sigma = 0.6\sigma_c^0$ (Davis, 2002).

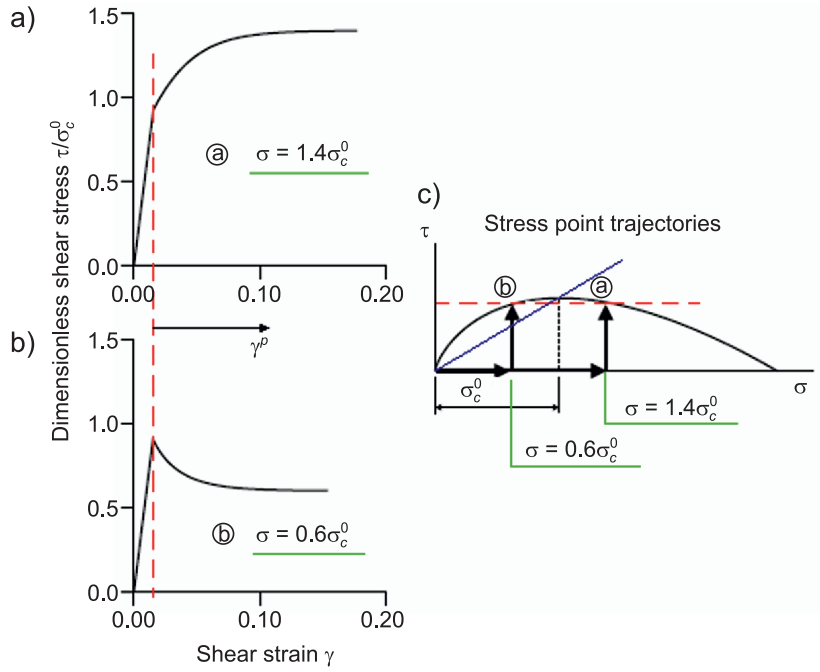

Fig. 5.23. Cam Clay stress–strain response: a) compacted soil under stress $\sigma = 1.4\sigma_c^0$, b) loose soil under stress $\sigma = 0.6\sigma_c^0$, c) cases comparison σ–τ (Davis, 2002)

In the equation (5.85) coefficient σ / σ_c^0 plays an important role:

– if $\sigma / \sigma_c^0 > 1$, then $\ln\left(\frac{\sigma}{\sigma_c^0} \right) > 0$ – an increase of the plastic shear strain $\gamma^p > 0$ causes an increase in the shear stress $\tau > 0$ (Figure 5.23a),

– if $\sigma / \sigma_c^0 < 1$, then $\ln\left(\frac{\sigma}{\sigma_c^0}\right) < 0$ – an increase of the plastic shear strain $\gamma^p > 0$ causes a decrease in the shear stress, $\tau < 0$ (Figure 5.23b).

Relationship $\gamma^p - \varepsilon^p$ is based on equations (5.79) and (5.84) gives the form:

$$\varepsilon^p = \gamma^p \cdot k \cdot \ln\left(\frac{\sigma}{\sigma_c^0}\right) \exp\left(-\frac{k}{m}\gamma^p\right). \tag{5.86}$$

Figure 5.24 shows plots of $\gamma^p - \varepsilon^p$ (5.86) for the two situations in Figure 5.23. You can notice that:

– if $\sigma / \sigma_c^0 > 1$, then $\ln\left(\frac{\sigma}{\sigma_c^0}\right) > 0$ – in this case $\varepsilon^p > 0$, the sample compresses (yield surface enlargement, soil is hardening),

– if $\sigma / \sigma_c^0 < 1$, then $\ln\left(\frac{\sigma}{\sigma_c^0}\right) < 0$ – in this case $\varepsilon^p < 0$, indicating dilation occurrence (yield surface decreases, soil is softening).

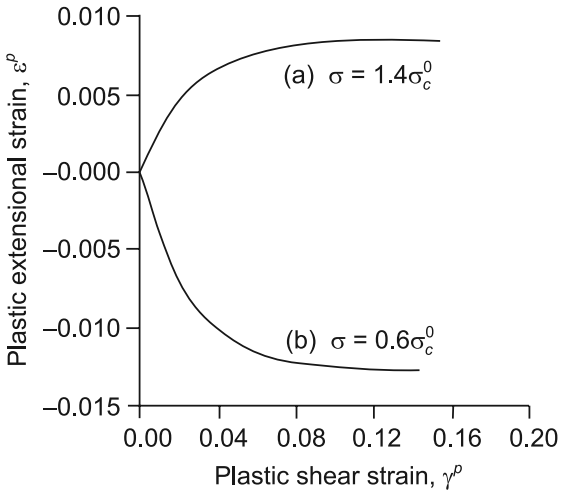

Fig. 5.24. Strain response for Cam Clay in a simple shear (Davis, 2002)

In both the hardening and softening cases, the sample is being attracted towards the critical state (Figure 5.25):

a) for softening yield surface moves downward towards the critical state (Figure 5.25a),

b) for hardening yield surface moves up towards the critical state (Figure 5.25b), $\sigma = \sigma_c^0$ corresponds to the initial yield surface, and $\sigma = 2\sigma_c^0$ corresponds to the critical yield surface.

Normal vector to the initial yield surface in a stress point (as strain rate vector) is inclined from the vertical direction, and on subsequent yield surfaces change this direction. This stress point reaches the critical state (on critical yield surface) if the normal vector in this point is the vertical direction (Figure 5.25).

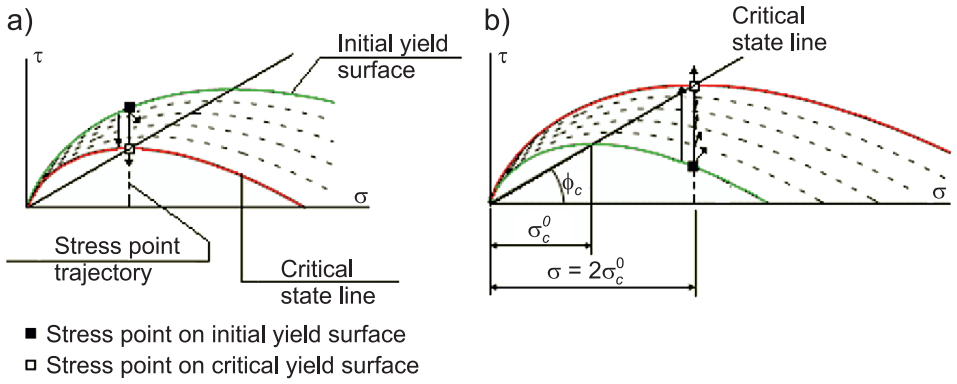

Fig. 5.25. Evolution of the Cam Clay yield surface in a simple shear: a) for softening; b) for hardening

Finally, the size of the yield surface depends directly on ε^p through (5.77). If the stress point σ on the initial yield surface is greater than σ_c^0 (Figure 5.25b), then the next plastic deformation leads to an increase σ_c, and to an increase of the yield surface. If the stress point σ on the initial yield surface is less than σ_c^0 (Figure 5.25a), then strain rate vector is directed downward, indicating to dilatation and the yield surface is reduced.

The above description of the Cam Clay model is based on simple shear apparatus. A description of the Cam Clay model based on the triaxial apparatus is shown below.

The rate of plastic work, instead of being defined by equation (5.68), can be defined by the relationship:

$$\dot{W}_p = p\dot{\varepsilon}^p + q\dot{\gamma}^p \tag{5.87}$$

where q and p are the deviatoric and mean stress, which, in the context of the triaxial test, are given by:

$$p = \frac{1}{3}(\sigma_1 + 2\sigma_3), \quad q = \sigma_1 - \sigma_3 \tag{5.88}$$

where σ_1 is the axial stress and $\sigma_2 = \sigma_3$ is the radial stress. The plastic strain rate is:

$$\dot{p}^p = \dot{\varepsilon}_1^p + 2\dot{\varepsilon}_3^p, \quad \dot{\xi}^p = \frac{2}{3}(\dot{\varepsilon}_1^p - \dot{\varepsilon}_3^p). \tag{5.89}$$

The dissipation function is written as:

$$\dot{D} = Mp\dot{\xi}^p \tag{5.90}$$

where:

M – a material constant that plays the same role as k in (5.69).

The yield surface equation is defined by (5.30). However, equation (5.77) is replaced by the relationship:

$$\varepsilon^p = \mu \cdot \ln(p_c / p_c^0) \tag{5.91}$$

where:

p_c – the critical state mean stress,

μ – a constant similar to m.

The above equations defined for triaxial test apparatus can be extended to the three-dimensional stress state where the invariants are defined as:

$$p = \frac{1}{3}(\sigma_1 + \sigma_2 + \sigma_3)$$

$$q = \frac{1}{\sqrt{2}}\left[(\sigma_1 - \sigma_2)^2 + (\sigma_2 - \sigma_3)^2 + (\sigma_3 - \sigma_1)^2\right]^{1/2}. \tag{5.92}$$

The plastic strain rate is obtained by:

$$\dot{\varepsilon}_k^p = \dot{\lambda}\frac{\partial f}{\partial \sigma_k} = \dot{\lambda}\left[\frac{3}{2}\frac{\sigma_k - p}{q} + \frac{M}{3}\ln\left(\frac{p}{p_c}\right)\right] \quad k = 1,2,3. \tag{5.93}$$

The volumetric plastic strain rate $\dot{\varepsilon}_v^p$ and the plastic shear rate deformation $\dot{\xi}^p$ are defined as:

$$\dot{\varepsilon}^p = \dot{\varepsilon}_1^p + \dot{\varepsilon}_2^p + \dot{\varepsilon}_3^p, \tag{5.94a}$$

$$\dot{\xi}^p = \frac{\sqrt{2}}{3}\left[(\dot{\varepsilon}_1^p - \dot{\varepsilon}_2^p)^2 + (\dot{\varepsilon}_2^p - \dot{\varepsilon}_3^p)^2 + (\dot{\varepsilon}_3^p - \dot{\varepsilon}_1^p)^2\right]^{1/2} \tag{5.94b}$$

where in the Cam Clay model, one can obtain:

$$\dot{\varepsilon}_v^p = \dot{\lambda}\frac{\partial f}{\partial p} = \dot{\lambda}M\ln\left(\frac{p}{p_c}\right) \tag{5.95a}$$

$$\dot{\xi}^p = \dot{\lambda}\frac{\partial f}{\partial q} = \dot{\lambda}. \tag{5.95b}$$

5.11. Time dependent models

5.11.1. Introduction

Description of soil behaviour in dynamics is associated with the use of constitutive equations taking into account the stress-strain relationship over time. The main parameter of the soil, variability over time, in the theory of plasticity is the soil skeleton viscosity, which define damping forces. In dynamic analysis, the inertia forces which are proportional to mass and acceleration should also be included.

Time dependent models can be generally divided into:

– simple models, one-dimensional, described by analytical equations confirmed by experience;
– general stress-strain models describing changes over time, they are often given in an incremental form. They are readily adaptable to the numerical implementation of finite element procedures. Such a procedure on general models require calibration parameters according to soil tests.

In these models, the following assumptions are used:

1) material models of macromechanics are employed with parameters such as stress and strain variable at the time,
2) equations determined within the mechanics of continuum material.

Readers can also find reviews of models which take into account the time factor in Augustesen et al. (2004) and Lingaard et al. (2004).

5.11.2. Empirical models

Experimental models apply only to selected creep and relaxation problems of specific boundary conditions. These are categorised as follows:

1) *Primary models* – empirical relationships are obtained by directly fitting the observed test data with simple mathematical functions. These are, for example: models describing the change in the soil compressibility over the time – Yin (1999); change over time the deviator stress q – Lacerda & Houston (1973); change over time $q - p$ relation for saturated clays under drained and undrained conditions – Prevost (1976). In the primary models, two types of hardening are used: time-hardening models defined by $\dot{\varepsilon}^c = f(\sigma)g(t)$ and strain-hardening models written as $\dot{\varepsilon}^c = f(\sigma)g(\varepsilon^c)$,
2) *Secondary models* – semi-empirical models are classified as models obtained by combining one or more of the primary models. Such models include, for example: changes over time in the volumetric strain $\dot{\varepsilon}_v$ in the constitutive equation –

Kavazanjian & Mitchell (1977); the concept of *equivalent time*, which is used to model the creep behaviour of normally consolidated and over-consolidated clays – Yin and Graham (1994).

5.11.3. Rheological models

The term *rheological models* is often used when describing linear elastic--viscoplastic in soil behaviour. These models are usually divided into three categories:

– The differential approach – this often refers to mechanical rheological models taking into account the elementary material models, such as *Hookean, Saint-Vernant's*, and *Newtonian* materials. Three well-known models used in geomechanics are: 1) the Maxwell model, 2) the Kelvin–Voigt model, and 3) the Bingham model. The importance of the Bingham model should be emphasized because the concept coincides with the *overstress model* used in FEM.
– Engineering theories of creep – these are widely applied in mechanics of concrete and metal. The mathematical structures of empirical models are varieties of this approach.
– The hereditary approach – this is also known as the method of integral representation. In this approach, the time-dependent creep strain or stress is defined by function, this is a hereditary (memory) function describing the historic dependence of strain or stress.

A. Bingham model

The Bingham model is a three–parameter model that consists of a parallel unit composed of a viscous dashpot with a plastic slider and a linear spring connected in series, Meschyan (1995), as shown in Figure 5.26. The model shows a pure elastic response below the yield stress σ_y.

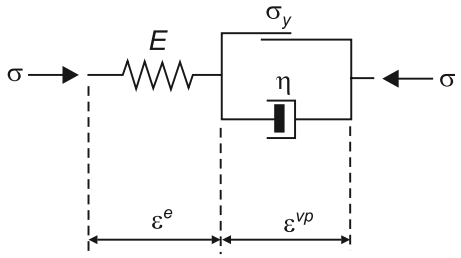

Fig. 5.26. Structure of the Bingham model with ε^e – elastic strain, and ε^{vp} – viscoplastic strain

Two parts of the model are connected in series: the elastic part represented by the spring constant E independent of time; the viscoplastic part, time dependent

and consisting of a viscous damper of the parameter η and a plastic slider with the parameter σ^y. The total deformation is the sum of elastic ε^e and viscoplastic strain ε^{vp}. The plastic slider is active if $\sigma > \sigma_y$, and difference $\sigma - \sigma_y$ is called the overstress. The Bingham model is described by the equation:

$$\dot{\varepsilon} = \begin{cases} \dot{\varepsilon}^e + \dot{\varepsilon}^{vp} = \dfrac{\dot{\sigma}}{E} + \dfrac{(\sigma - \sigma_y)}{\eta} & \text{dla} \quad \sigma > \sigma_y \\ \dot{\varepsilon}^e = \dfrac{\dot{\sigma}}{E} & \text{dla} \quad \sigma \le \sigma_y, \end{cases} \tag{5.96}$$

where:

$\dot{\varepsilon}$ – the total strain rate,

$\dot{\varepsilon}^e$, $\dot{\varepsilon}^{vp}$ – strain rate in the elastic and viscoplastic elements, respectively.

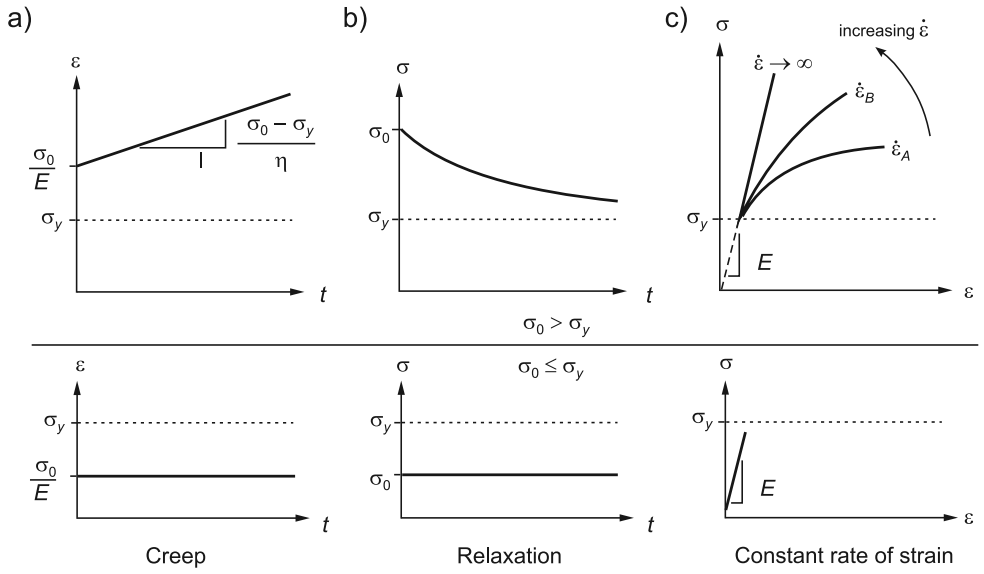

Fig. 5.27. Response of a Bingham model. The upper curves correspond to viscoplastic conditions where the stress state is above ($\sigma_0 > \sigma_y$). The lower curves show the response in the elastic region below ($\sigma_0 \le \sigma_y$): a) response for creep; b) response for relaxation; and c) response for constant rate of strain. ε_A and ε_B are different constant strain rate where $\varepsilon_B > \varepsilon_A$

Figure 5.27 shows the curves of changes in stress and strain over the time according to the Bingham model.

Comments

In the case of viscoelastic material, the Maxwell model describes the relaxation phenomenon and Kelvin–Voigt model describes the creep phenomenon. In the case where plastic behaviour is present, the Maxwell, Kelvin–Voigt and Bingham models are not appropriate for the following reasons:

– The constitutive material relations are too simple. The spring, the dashpot, and the slider are assumed to describe linear constitutive relationships. It is well known that soils show highly nonlinear elastic and plastic behaviour. The linear viscous assumption is also inadequate.
– The constitutive relationships for the rheological models are formulated for uniaxial compression conditions. The generalisation of rheological models from one into three dimensions is possible, but practical calibration and application seems to be difficult (Singh & Mitchell, 1968).

For references about the use of the differential approach in soil mechanics, see, for example, Murayama & Shibata (1961), Barden (1965), and Murayama et al. (1984).

B. Engineering theories of creep

Engineering models of creep include the phenomenological approaches based on observation and material testing and are a group of methods similar to empirical models. Most of the work within the engineering theories of creep has been concentrated in the fields of metals, concrete, and ice, where the loading is below the initial yield stress. For a comprehensive review of the engineering theories of creep applied to steels and other metals, see Rabotnov (1969), and Skrzypek (1993). In the case of soil creep, the description is based on the model of plastic consolidation. The engineering theories of creep are represented by Skrzypek (1993):

– The total strain model, $\varepsilon^c = f(\sigma)g(t)$, where f, g are functions, Rabotnow (1969),
– The time-hardening model, $\dot{\varepsilon}^c = f(\sigma)g(t)$, where f, g are functions,
– The strain-hardening model, $\dot{\varepsilon}^c = f(\sigma)g(\varepsilon^c)$, where f, g are functions.

Comments

The time-hardening models or the strain-hardening models are Maxwell models with non-linear creep components, where the dashpot element is dependent upon time or dependent upon deformation. The non-linear Maxwell model can be written as

$$\dot{\varepsilon} = \dot{\varepsilon}^e + \dot{\varepsilon}^c = \frac{\sigma}{E} + \frac{\sigma}{\eta(\sigma,t)}$$ – in the case of the time-hardening model,

$$\dot{\varepsilon} = \dot{\varepsilon}^e + \dot{\varepsilon}^c = \frac{\sigma}{E} + \frac{\sigma}{\eta(\sigma, \varepsilon^c)} \quad - \text{ in the case of the strain-hardening model.} \qquad (5.97)$$

where the viscosity parameter η is no longer constant but hardens with either stress and time or stress and strain.

C. Hereditary approach

The principle of the hereditary approach is that the current strain $\varepsilon(t)$ is obtained by integration over the entire loading history until the current time t; hence, the name the hereditary approach. The theory is developed for two cases. The simplest case is the hereditary approach based on linear viscoelasticity and the second case is based on nonlinear material behaviour corresponding to the engineering theories of creep. In the case of soil mechanics, the general opinion is that the hereditary approach is too complex due to the fact that the approach needs a great number of experiments for calibration. For further studies of the hereditary approach, see Feda (1992) and Mechyan (1995).

5.11.4. General stress-strain-time models

The general constitutive laws describe not only viscous effects but also the rate--dependent behaviour of soils under any possible loading change over time. Special approaches are the elastic-viscoplastic models which combine elastic and time--dependent plastic behaviour. Elastic-viscoplastic models can be general divided into two classes, Sekiguchi (1985):

A) elastic-viscoplastic models based on the concept of *overstress theory*,
B) elastic-viscoplastic models based on the concept of a *nonstationary flow surface* (NSFS).

A. Overstress theory

The concept of overstress theory was introduced and developed by Ludwick (1922), Prandtl (1928), Hohenemser & Prager (1932), Sokolovsky (1948), and Malvern (1951) as reported by Satake (1989). Perzyna's overstress theory is a three--dimensional version of Malvern's (1951) one–dimensional constitutive model. The following description of Perzyna's overstress theory is based on Perzyna (1963a, b, c, 1966), Olszak & Perzyna (1970), Sekiguchi (1985) and Lade at al. (2004).

The assumptions of the overstress Perzyna's theory are:

– in an elastic range the viscous effects are ignored, i.e. the deformation is independent over time,
– in a plastic range the viscous effects are considered, i.e. the deformation is dependent over time.

The total strain rate $\dot{\varepsilon}_{ij}$ is additively composed of the $\dot{\varepsilon}^{e}_{ij}$ elastic and viscoplastic $\dot{\varepsilon}^{vp}_{ij}$ strain rate:

$$\dot{\varepsilon}_{ij} = \dot{\varepsilon}^{e}_{ij} + \dot{\varepsilon}^{vp}_{ij}. \tag{5.98}$$

In the theory of elastic-viscoplasticity, the inelastic strain rate represents combined viscous and plastic effects, while $\dot{\varepsilon}^{vp}_{ij}$ is assumed to obey the nonassociated flow rules:

$$\dot{\varepsilon}^{vp}_{ij} = \gamma \Phi(F) \frac{\partial g}{\partial \sigma'_{ij}} \tag{5.99}$$

where:

γ – fluidity parameter,
Φ – viscous nucleus,
F – *overstress* function,
g – potential function,
σ'_{ij} – effective stress state.

The overstress function can be written as:

$$F(\sigma'_{ij}, W^{vp}) = \frac{f_d(\sigma'_{ij}, W^{vp})}{\kappa_s(W^{vp})} - 1 \tag{5.100}$$

where:

$\kappa_s = \kappa_s\left(\int_0^{\varepsilon^{vp}_{ij}} \sigma'_{ij} \varepsilon^{vp}_{ij} \right)$ – the hardening parameter

f_d – the dynamic loading surface function (dependent on time) on which the current stress state P is located, as shown in Figure 5.28, dependent on the current stress state and the viscoplastic work W^{vp}.

The overstress F is defined as the distance in stress space between the current stress state P and the static yield Surface f_s. In the case of $F = 0$, $f_d(\sigma'_{ij}, W^{vp}) = \kappa_s(W^{vp})$ corresponds to the static yield surface f_s.

The overstress theory differs from general elastic-plasticity in the sense that the consistency rule (5.55) is not used in this theory, the stress state is allowed to be on, within or outside the static yield surface. The inelastic strain in the overstress model are not related to the stress history but to the current stress point only. Inelastic strain is related to the stress rate. According to the assumption and the flow rule, the following constraints apply to the *viscous nucleus* Φ:

$$\langle \Phi(F) \rangle = \begin{cases} 0 & \text{dla} \quad F \le 0 \\ \Phi(F) & \text{dla} \quad F > 0 \end{cases} \quad \text{for} \tag{5.101}$$

Equation (5.101) can be considered as the loading criterion for inelastic deformations.

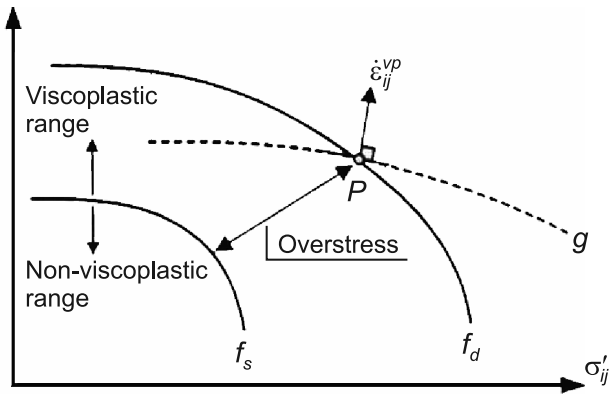

Fig. 5.28. Stress state in point P is part of the dynamic yield surface f_d and overstress F is defined as the distance between P and the static yield surface f_s. The viscoplastic strain rate vector $\dot{\varepsilon}^{vp}$ is perpendicular to the plastic potential surface g

Definitions of the function $\Phi(F)$ were proposed by Phillips & Wu (1973), Adachi & Oka (1982), di Prisco & Imposimato (1996). Two commonly used forms of this function are:

$$\Phi(F) = aF^b \quad \text{and} \quad \Phi(F) = c\exp(jK^k) - 1 \tag{5.102}$$

where:

a, b, c, j, k – are constants.

Yen (1981), Wood (1990), and Eisenberg, Hinchberger & Rowe (1998) claim that the static yield surface can be obtained by performing extremely slow tests. A method to determine an appropriate strain rate can be found in Sheahan (1995).

Consequences of the overstress theory

– *Creep* – Different cases that initiate creep can be considered.
  – Creep is initiated at a point which lies outside the area of static f_s. If $F > 0$, viscoplastic flow will occur. In the case of *non-hardening perfectly plastic yield surface*, a constant rate appears and the distance between the static and dynamic surface remains constant (Figure 5.29a).
  – Creep initiated at the point lies outside the area of static f_s. In the case of *hardening yield surface,* the magnitude of overstress ***F***

decreases $F(t=0) > F_1(t=t_1) > F_2(t=t_2)$ in the following time steps $t = 0 < t_1 < t_2 < t = \infty$. This implies that $\Phi(F)$ is a monotonically increasing function where $\dot{\delta}\varepsilon_{ij}^{vp}$ (Figure 29b). A new static surface stabilises when $\dot{\varepsilon}_{ij}^{vp} = 0$.

When static surface f_s change in time interval $0 < t < t_k$ the viscoplastic strain increment changing with the value of $\dot{\delta}\varepsilon_{ij}^{vp}$ according to the equation:

$$\int_0^{t_k} \delta\varepsilon_{ij}^{vp}(t)\,\mathrm{d}t = \delta\dot{\varepsilon}_{ij}^{vp}. \tag{5.103}$$

– Creep initiated at the point lies outside the area of static f_s. In this case, overstress $F < 0$. According to equations (5.99) and (5.101), viscoplastic strain does not occur – this is contrary to experimental results. The nature of creep strains is similar to that of plastic strain as postulated by Lade & Liu (1998). Adachi et al. (1987) have shown that – due to its theoretical structure – the overstress-type model cannot describe the acceleration creep process.

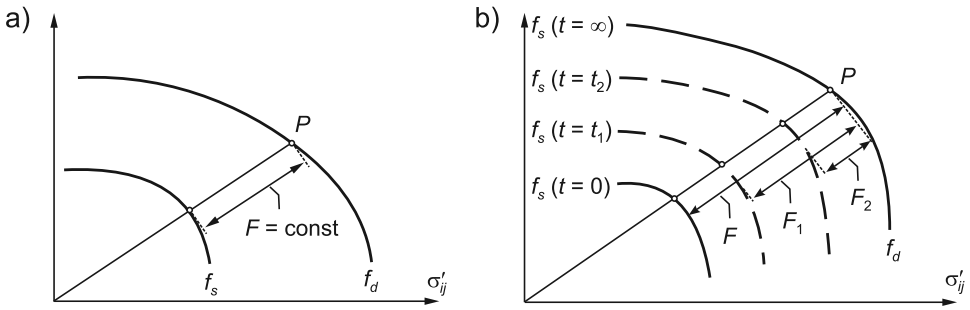

Fig. 5.29. Creep is initiated at a point which lies outside the area of the static surface f_s: a) creep process for a non-hardening material; b) creep for a hardening material

– Relaxation – similar comments can be applied to the phenomenon of relaxation.
  – Consider now a stress state that lies outside the current static yield surface f_s (the overstress $F > 0$) with a total strain rate of zero $\dot{\varepsilon}_{ij} = 0$, which corresponds to the relaxation process. According to (5.98), stress decreases.
  – Now consider a stress state that lies inside the current static yield surface f_s. In this case, the viscoplastic strain is zero because the overstress $F < 0$. This implies, according to equation (5.98), that elastic strain must be zero too, and this is impossible during a stress relaxation process characterised by a stress decrease.

Remark – in the overstress theory, it is possible to model stress relaxation only in the case where the process is initiated from a stress state that lies outside the current static yield surface f_s.

– *Constant Rate of Strain*.

In a constant rate of strain test, the total strain rate must be constant, i.e. the sum of the elastic and viscoplastic strain must be constant according to Equation (5.98) $\dot{\varepsilon}_{ij} = \dot{\varepsilon}_{ij}^{e} + \dot{\varepsilon}_{ij}^{vp} = \text{const.}$ Now consider loading from a stress state inside the static yield surface f_s, in this case, the total strain rate is equal to the elastic strain rate. The amount of overstress F must be updated and adjusted all the time in the numerical algorithms in such a way that the total strain rate is constant. By contrast, when an unloading process takes place from a stress point outside the static yield surface, elastic–viscoplastic strain is generated until the static yield surface is reached.

Remark – in the overstress theory, it is possible to model a constant rate of strain tests.

– *Static yield surface versus classical yield surface*.

Many authors have established that the static yield surface f_s may be understood as the classical yield surface in rate independent plasticity. This analogy has been suggested by, for example, Zienkiewicz & Cormeau (1974), Katona & Mulert (1984), and di Prisco & Imposimato (1996). They postulated that the integration of the viscoplastic strain over time eventually gives the elastic-plastic solution.

Hashiguchi & Okayasu (2000) report that the viscoplastic overstress model is fundamentally different from elastic-plasticity. This is due to the fact that plastic straining in the overstress model is not related to the stress rate but to stress.

Theory	Relation
Overstress theory	Plastic strain = stress function
Classical elastic–plasticity theory	Plastic strain = stress rate function

B. Nonstationary flow surface theory – NSFS

The concept of the NSFS theory was introduced and developed by Naghdi & Murch (1963) and Olszak & Perzyna (1966b, 1970) as reported by Matsui & Abe (1985a, b) and Satake (1989). NSFS theory was developed by Matsui & Abe (1985a, b) in the application for consolidation of clays.

The NSFS theory is based on the basic concepts of inviscid elastic-plasticity. The major difference between the NSFS theory and classical elastic-plasticity lies in the definition of the yield condition:

$f(\sigma'_{ij}, \varepsilon_{ij}^{p}) = 0$ in the case of classical elastic-plasticity, (5.104a)

$f(\sigma'_{ij}, \varepsilon^{vp}_{ij}, \beta) = 0$ in the case of the NSFS theory, this depends on time (Figure 5.30), (5.104b)

where:

σ'_{ij} – effective stress state,

ε^{p}_{ij} – plastic strain,

ε^{vp}_{ij} – viscoplastic strain,

β – time-dependent function.

According to equation (5.104a), classical elastic–plastic is *stationary*, not dependent on time. It can be concluded from equation (5.104b) that the yield surface is time-dependent (through parameter β), and changes every moment – even the viscoplastic strain is held constant $\varepsilon^{vp}_{ij} = 0$. In that sense, the flow surface can be denoted as *nonstationary*.

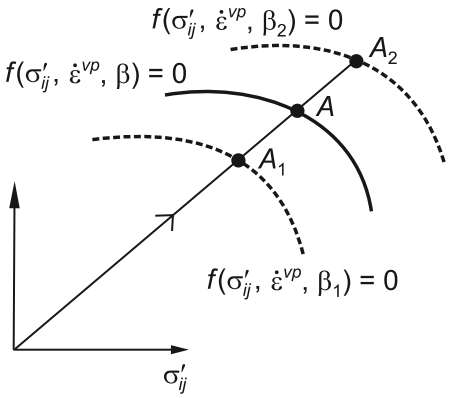

Fig. 5.30. Loading path and yield surfaces of the NSFS theory depends on time β

In the case of an elastic-viscoplastic material, the yield surface corresponding to a given viscoplastic strain is reached at different points (A, A_1 or A_2) dependent on time β (Figure 5.30). By contrast, for an elastic-plastic material, the yield surface corresponding to a given viscoplastic strain is reached at the same point ($A = A_1 = A_2$) independently of time β.

In the case of $f = 0$ and a loading condition is considered, the soil is said to be in an elastic-viscoplastic state (both elastic and viscoplastic strain occur). When $f < 0$, the current stress state lies inside the flow surface and the soil is therefore in the elastic state and only elastic strain occur.

Similar to the overstress theory, the total strain rate in the NSFS is:

$$\dot{\varepsilon}_{ij} = \dot{\varepsilon}_{ij}^{e} + \dot{\varepsilon}_{ij}^{vp} \tag{5.105}$$

where the viscoplastic strain rate $\dot{\varepsilon}_{ij}^{vp}$ is defined according to the flow rule:

$$\dot{\varepsilon}_{ij}^{vp} = \langle \Lambda \rangle \frac{\partial g}{\partial \sigma'_{ij}} \tag{5.106}$$

where:

Λ – non-negative multiplier,
g – viscoplastic potential,
$\langle\ \rangle$ – MacCauley's brackets.

MacCauley's brackets ensure that the viscoplastic deformation arises as a result of the plastic load state, in all other cases, the viscoplastic strain is zero. Multiplier Λ is determined by using the consistency rule, which says that loading from a stress state lying on the current yield surface must again lead to a stress state lying on another yield surface. The expression for Λ is:

$$\Lambda = -\frac{\dfrac{\partial f}{\partial \sigma'_{ij}}\sigma'_{ij} + \dfrac{\partial f}{\partial \beta}\dot{\beta}}{\dfrac{\partial f}{\partial \varepsilon_{ij}^{vp}}\dfrac{\partial g}{\partial \sigma'_{ij}}} \tag{5.107}$$

where Λ, is the sum of two parameters, Λ_1 and Λ_2:

$$\Lambda_1 = -\frac{\left(\dfrac{\partial f}{\partial \sigma'_{ij}}\sigma'_{ij}\right)}{\left(\dfrac{\partial f}{\partial \varepsilon_{ij}^{vp}}\dfrac{\partial g}{\partial \sigma'_{ij}}\right)}, \quad \Lambda_2 = -\frac{\left(\dfrac{\partial f}{\partial \beta}\dot{\beta}\right)}{\left(\dfrac{\partial f}{\partial \varepsilon_{ij}^{vp}}\dfrac{\partial g}{\partial \sigma'_{ij}}\right)} \tag{5.108}$$

Parameter Λ_1 corresponds to the plastic multiplier λ defined in classical elastic--plasticity depends on $\dot{\sigma}'_{ij}$. Factor Λ_2 includes an additional term $\dot{\beta}(\partial f / \partial \beta)$, this implies that elastic-viscoplastic strain occur even though the stress holds constant – this corresponds to a creep process.

The constitutive equations of the NSFS theory can, by use of equations (5.105) to (5.107) and including Hooke's generalised law, can be described as:

$$\dot{\varepsilon} = \frac{\sigma'}{E} + \left\langle \frac{\dfrac{\partial f}{\partial \sigma'_{ij}} \dot{\sigma}'_{ij} + \dfrac{\partial f}{\partial \beta} \dot{\beta}}{\dfrac{\partial f}{\partial \varepsilon^{vp}_{ij}} \dfrac{\partial g}{\partial \sigma'_{ij}}} \right\rangle \frac{\partial g}{\partial \sigma'_{ij}} \tag{5.109}$$

According to Naghdi & Murch (1963) and Perzyna (1996), criteria for unloading, neutral loading, and loading can be described as:

$$\begin{aligned} f = 0 \quad L(\dot{\sigma}'_{ij}, \dot{\beta}) < 0 \quad \text{(unloading)} \\ f = 0 \quad L(\dot{\sigma}'_{ij}, \dot{\beta}) = 0 \quad \text{(neutral loading)} \\ f = 0 \quad L(\dot{\sigma}'_{ij}, \dot{\beta}) > 0 \quad \text{(loading)} \end{aligned} \tag{5.110}$$

where the operator $L(\dot{\sigma}'_{ij}, \dot{\beta})$ is in the form:

$$L(\dot{\sigma}'_{ij}, \dot{\beta}) = \frac{\partial f}{\partial \sigma'_{ij}} \frac{\partial \sigma'_{ij}}{\partial t} + \frac{\partial f}{\partial \beta} \frac{\partial \beta}{\partial t} \tag{5.111}$$

It can be note that loading at one rate may be unloading for another, non-tangent directions to the yield surface may also result in neutral loading. This can be illustrated by use of a geometrical interpretation of the loading conditions. Now we consider the yield condition for an isotropic hardening material, equation (5.104b) can be expressed as:

$$\begin{aligned} f(\sigma'_{ij}, \varepsilon^{vp}_{ij}, \beta) = f'(\sigma'_{ij}, \varepsilon^{vp}_{ij}) - \kappa(\varepsilon^{vp}_{ij}, \beta) = 0 \\ \Rightarrow f'(\sigma'_{ij}, \varepsilon^{vp}_{ij}) = \kappa(\varepsilon^{vp}_{ij}, \beta), \end{aligned} \tag{5.112}$$

where κ = hardening function.

By differentiating equation (5.112) and introducing it into equations (5.110) and (5.111), one can obtain an equation for the case of neutral loading:

$$\begin{aligned} \frac{\partial f}{\partial \sigma'_{ij}} \frac{\partial \sigma'_{ij}}{\partial t} - \frac{\partial \kappa}{\partial \beta} \frac{\partial \beta}{\partial t} = 0 \\ \Rightarrow \theta = \arccos\left(\frac{\dfrac{\partial \kappa}{\partial \beta} \dfrac{\partial \beta}{\partial t}}{\left| \dfrac{\partial f}{\partial \sigma'_{ij}} \right| \left| \dot{\sigma}'_{ij} \right|} \right) \end{aligned} \tag{5.113}$$

where:

θ – the angle between the stress rate $\dot{\sigma}'_{ij}$ and the normal to the yield surface $\partial f / \partial \sigma'_{ij}$ in the case of neutral loading. Neutral loading can geometrically be shown as a cone in stress space with the opening angle θ as illustrated in Figure 5.31.

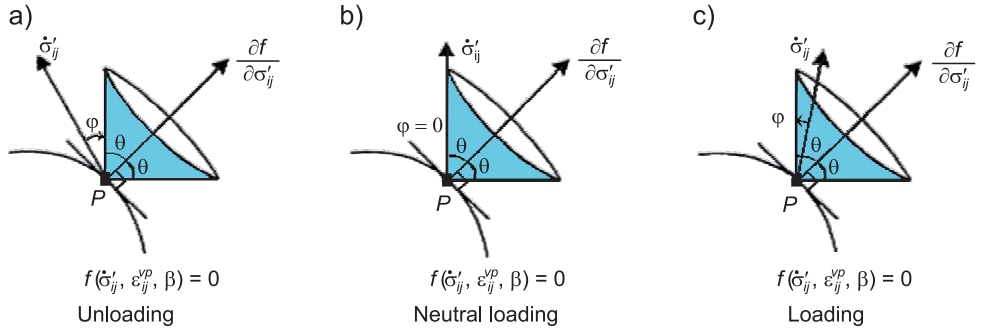

Fig. 5.31. Loading criteria for an elastic–viscoplastic material based on the concept of NSFS theory

The *loading criteria* can be defined on the basis of φ angle (angle between the $\dot{\sigma}'_{ij}$ and the vector normal to the current yield surface $\partial f / \partial \sigma'_{ij}$) as:

$$\begin{aligned} \varphi > 0 \quad & \text{(unloading)} \\ \varphi = 0 \quad & \text{(neutral loading)} \\ \varphi < 0 \quad & \text{(loading)} \end{aligned} \tag{5.114}$$

Consequences of the nonstationary flow surface theory

– *Creep* – different cases which initiate creep are considered.
  – Creep initiates at the stress point located within the yield surface. In this case, the NSFS theory does not predict any inelastic strain and cannot describe a creep process inside the yield surface.
  – The NSFS theory can describe the creep process initiated at point *Q* lying on the current yield surface *f* at a given time *t* as illustrated in Figure 5.32. Viscoplastic strain ε^{vp}_{ij} occur according to equations (5.106) and (5.107), however, the term that includes the stress rate $\dot{\sigma}'_{ij}$ vanishes. The yield surface expands in the stress space as indicated in equation (5.104b) and at a subsequent time t_1 the imposed constant stress state *Q* is inside the new current yield surface f_1 as illustrated in Figure 5.32. However, in association with the NSFS

theory, a viscoplastic deformation process is triggered in connection with a creep process initiated at point Q on the yield surface f. The creep process will then continue even though the stress state Q at a subsequent time t_1 will be inside the new current yield surface f_1.

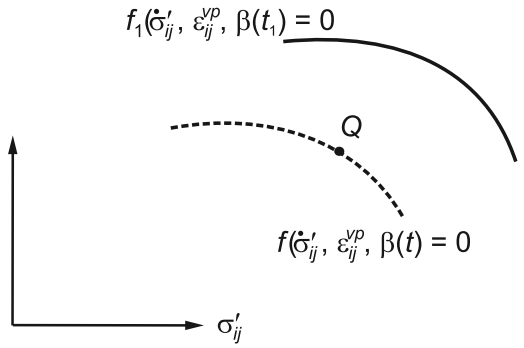

Fig. 5.32. If a creep process is initiated at stress state Q lying on the current yield surface, viscoplastic strain occur and the yield surface expands with time even though stress state Q is held constant

– Now we consider normally consolidated clay under the assumption that the primary consolidation is instantaneous. The clay is subjected to the stress path *origin* → A → B → C → D (Figure 5.33). From the origin to A, only elastic strain occurs because the stress state is inside the current yield surface f. Point A lies on the yield surface f and a creep process is initiated. Over a short time period, the stress state remains constant – this implies that A and B coincide. Next, viscoplastic strain develop during a creep process initiated from a stress state lying on the current yield surface f. The flow surface expands with time in such a way that $f_1 = 0$ constitutes the new current yield surface and point C is located on f_1. When loading from B to C occurs, elastic stiffness occurs until point C is reached and the response is instantaneous. From C to D, the stress state is always on the current yield surface and the

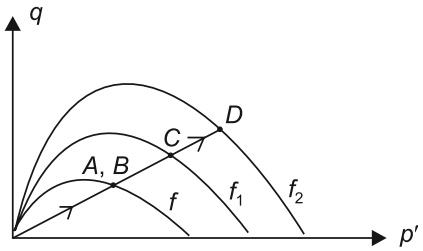

Fig. 5.33. Normally consolidated clay subjected to the stress path *origin* → A → B → C → D

response is elastic-viscoplastic. The above example shows that during the creep process, the flow surface expands.

– *Relaxation* – Consider a relaxation process initiated at a point which lies inside the flow surface. The total strain rate $\dot{\varepsilon}_{ij} = 0$, according to (5.105) $\dot{\varepsilon}^{e}_{ij} = -\dot{\varepsilon}^{vp}_{ij}$. The effective stress can predict the elastic strain and no viscoplastic strain is assumed to occur. Therefore, the NSFS theory is not able to describe such a case.

Note – in the NSFS theory, it is possible to model stress relaxation only in cases where the process is initiated from a stress state which lies on the flow surface.

C. Comparison of properties of overstress and nonstationary flow surface theories

The application domain of both theories is shown in Figure 5.34 where q is the deviator stress, ε_1 is the principal strain, and $\dot{\varepsilon}$ is the strain rate. The instant time line and the limit state line were defined by Yin & Graham (1994), i.e.:

– *The instant time line* defines the instant response at an infinitely high rate.
– *The limit state line* defines the transition from the non-viscous region to the viscoplastic domain.

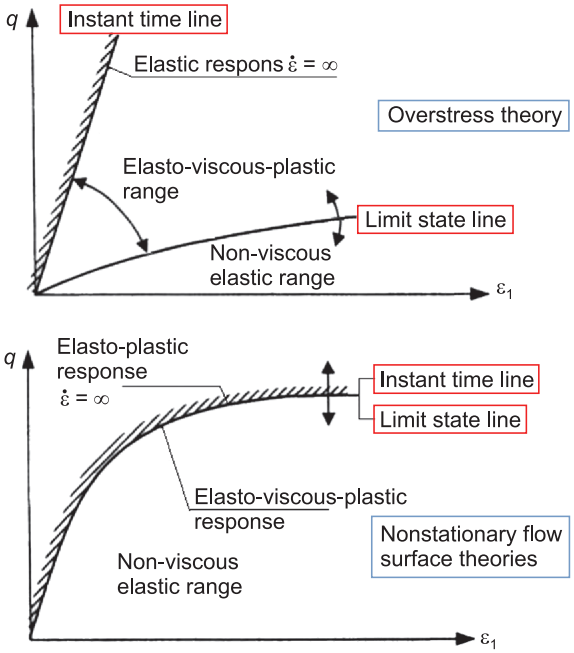

Fig. 5.34. Domains and reference lines showing the comparison of overstress and nonstationary flow surface theory

Comparison of the two theories in relation to the application of a very high rate of load:

– Response determined according to the overstress theory, equation (5.98) is elastic.
– Response determined by NSFS theory, according to (5.109) is elastic-plastic (time-independent) since the duration of the load is very small (parameter β is close to zero).

Comments

1. It should be noted that both methods (overstress and NSFS) have been tested with regard to the consolidation of clays while to the sands there is currently no similar experiences.
2. There is still open problem to determine a general formulation of constitutive equations usable in numerical analysis to properly modelled both creep and relaxation (at a constant speed load).

5.12. References to Chapter 5

Adachi T., Oka F. (1982): *Constitutive equations for normally consolidated clay based on elastic-viscoplasticity*, *Soil Found.*, 22(4), 57-70.

Augustesen A., Liingaard M., Lade P.V. (2004): *Evaluation of time-dependent behaviour of soils*, Int. J. Geomech., 4(3), 137-156.

Bauer E., Wu W. (1993): *A hypoplastic model for barotropy and pyknotropy of granular soils* (ed. D. Kolymbas), Proceedings of International Workshop on Modern Approaches to Plasticity for Granular Materials, Horton, Greece, 225-245.

Coulomb C.A. (1776): *Essai sur une application des r`egles des maximis et minimis `a quelques problemes de statique relatifs `a l'architecture*, Mem. Acad. Roy. Pres. divers Sav., 5, 7.

Coussy O. (2004): *Poromechanics*, Chichester, UK: Wiley.

Cornforth D.H. (1964): *Some experiments on the influence of strain conditions on the strength of sand*, Géotechnique, 14:143-167, 1964.

Davis R.O., Selvadurai A.P.S. (2002): *Plasticity and geomechanics*, Cambridge University Press., UK.

di Prisco C. Imposimato S. (1996): *Time dependent mechanical behaviour of loose sands*, Mech. Cohesive-Frict. Mater., 1(1), 45-73.

Drucker D.C., Prager W. (1952): *Soil mechanics and plastic analysis of limit design*, Quart. Appl. Math., 10, 157-165.

Drucker D.C. (1958): *The definition of a stable inelastic material*, J. Appl. Mech., Trans ASME, 26, 101-106.

Drucker D.C. (1964): *On the postulate of stability of material in the mechanics of continua*, J. Mecanique, 3, 235–249.

Feda J. (1992): *Creep of soils and related phenomena, developments in geotechnical engineering*, Elsevier Science, North-Holland, Amsterdam, The Netherlands, Vol. 68.

Hohenemser K., Prager W. (1932): *Über die Ansatze der Mechanik isotroper Kontinuum*, Z. Angew. Math. Mech., 12, 216-226.

Katona M.G., Mulert M.A. (1984): *A viscoplastic cap model for soils and rock*, Mechanics of engineering materials, C.S. Desai, R.H. Gallagher, eds., Wiley, New York, 335-350.

Kavazanjian E., Mitchell J.K. (1977): *A general stress-strain-time formulation for soils*, Proc, 9th ICSMFE, 113-120.

Kolymbas D. (1985): *A generalized hypoelastic law*, In Proc. XI Int. Conf. Soil Mechanics and Foundation Engineering, Volume 5, San Francisco, Balkema.

Kolymbas D. (ed.) (2000): *Constitutive Modelling of Granular Materials*, Springer.

Lacerda W.A., Houston W.N. (1973): *Stress relaxation in soils*, Proc, 8th ICSMFE, 1/34, 221-227.

Lade P.V., Duncan J.M. (1975): *Elastoplastic stress strain theory for cohesionless soil*, J. Geotech. Eng. Div. ASCE, 101, 1037.

Lade P.V., Liu C. T. (1998): *Experimental study of drained creep behaviour of sand*, J. Eng. Mech., 124(8), 912-920.

Liingaard M., Augustesen A., Lade P.V. (2004): *Characterization of Models for Time–Dependent Behaviour of Soils*, Intern. Journ. of Geomechanics, ASCE/Sept., 157-177.

Ludwick P. (1922): *Über den Einfluss der Deformationsgeschwindigkeit bei bleibenden Deformationen mit besonderer Berücksichtigung der Nach Wirkungserscheinungen*, Phys. Z., 10(12), 411-417.

Malvern L.E. (1951): *The propagation of longitudinal waves of plastic deformation in a bar of metal exhibiting a strain rate effect*, J. Appl. Mech., 18, 203-208.

Matsui T., Abe N. (1985a): *Elastic/viscoplastic constitutive equation of normally consolidated clays based on flow surface theory*, 5th Int. Conf. on Numerical Methods in Geomechanics, Nagoya, Japan, 407-413.

Matsui T., Abe N. (1985b): *Undrained creep characteristics of normally consolidated clay based on the flow surface model*, Proc,11th ICSMFE,140-143.

Matsuoka T., Nakai K. (1974): *Stress-deformation and strength characteristics of soil under three different principal stresses*, Proc. Japan. Soc. Civil Engineers, 232, 59.

Meschyan S.R. (1995): *Experimental rheology of clayey soils*, *geotechnics 13* (selected translation of Russian geotechnical literature), A.A. Balkema, Rotterdam/Brookfield.

Murayama S. (1983): *Formulation of stress–strain–time behaviour of soils under deviatoric stress conditio*, Soils Found., 23(2), 43-57.

Murayama S., Michihiro K., Sakagami T. (1984): *Creep characteristics of sands*, Soils Found., 24(2), 1-15.

Naghdi P.M., Murch S.A. (1963): *On the mechanical behaviour of viscoelastic/plastic solids*, J. Appl. Meteorol, 30, 321-328.

Nova R. (1982): *A viscoplastic constitutive model for normally consolidated clay*, Int. Union of Theoretical and Applied Mechanics Conf. on Deformation and Failure of Granular Materials, Delft, The Netherlands, 287-295.

Oka F. (1985): *Elastic-viscoplastic constitutive equations with memory and internal variables*, Comput. Mech., 1, 59-69.

Olszak W., Perzyna P. (1966): *On elastic-viscoplastic soils, rheology and soil mechanics*, *Int. Union of Theoretical and Applied Mechanics Symp*., Grenoble, Springer, Berlin.

Olszak W., Perzyna P. (1970): *Stationary and nonstationary viscoplasticity*, McGraw-Hill, New York.

Pamin J. (2004): *Gradient-Enhanced Continuum Models: Formulation, Discretisation and Applications*, Monograph 301, Series Civil Engineering, Wydawnictwo Politechniki Krakowskiej, Kraków

Perzyna P. (1963a): *The constitutive equations for work-hardening and rate sensitive plastic materials*, Proc, Vib. Probl, 3(4), 281-290.

Perzyna P. (1963b): *The constitutive equations for rate sensitive plastic materials*, Q. Appl. Math., 20(4), 321-332.

Perzyna P. (1963c): *The study of the dynamical behaviour of rate sensitive plastic materials*, Arch. Mech. Stos., 1(15), 113-130.

Perzyna P. (1966): *Fundamental problems in viscoplasticity*, Adv. Appl. Mech., 9, 244-377.

Phillips A., Wu H.C. (1973): *A theory of viscoplasticity*, Int. J. Solids Struct., 9, 15-30.

Prandt L. (1928): *Ein Gedanken model zur kinetischen Theorie der festen Korper*, Z. Angew. Math. Mech., 8, 85-106.

Pietruszczak S. (2010): *Fundamentals of Plasticity in geomechanics*, CRC Press Taylor & Francis Group.

Prevost, J.-H. (1976): *Undrained stress-strain-time behaviour of clays*, J. Geotech. Eng., 102(12), 1245-1259.

Rabotnov Y.N. (1969): *Creep problems in structural members*, North–Holland, Amsterdam, The Netherlands.

Roscoe K.H., Schofield A.N., Thurairajah A. (1963): *Yielding of clays in states wetter than critical*, Geotechnique, 13, 211.

Roscoe K.H., Burland J.B. (1968): *On the generalised stress-strain behaviour of 'wet clay*, *in Engineering Plasticity* (ed. J. Heyman, F.A. Leckie), Cambridge University Press, Cambridge.

Satake M. (1989): *Mechanics of granular materials*, Rep., Int. Society of Soil Mechanics and Foundation Engineering, technical committee on mechanics of granular materials, 12th, ICSMFE, 62-79.

Sekiguchi H. (1985): *Macrometric Approaches-Static-Intrinsically Time Dependent Constitutive Laws of Soils*, Rep., ISSMFE Subcommittee on Constitutive Laws of Soils and Proc. of Discussion Session 1A, Int. Society of Soil Mechanics and Foundation Engineering, Subcommittee on Constitutive Laws of Soils, 11th ICFMFE, San Francisco, 66-98.

Sheahan T.C. (1995): *Interpretation of undrained creep tests in terms of effective stress*, Can. Geotech. J., 32, 373-379.

Sikora Z. (1992): *Hypoplastic flow of granular materials. A numerical approach*, Zeszyty Naukowe Instytutu Mechaniki Gruntów i Mechaniki Skał, Uniwersytet W Karlsruhe, z. 123.

Sikora Z. (2006): *Cone Penetration Test. Methods and Application in Geotechnics*, Wydawnictwo Naukowo-Techniczne, Warszawa (in Polish).

Singh A., Mitchell J.K. (1968): *General stress-strain-time function for soils*, J. Soil Mech. Found. Div., 94(1), 21-46.

Skrzypek J. (1993): *Plasticity and creep-Theory, examples, and problems (English edition)*, B.H. Richard, ed., CRC Press, London.

Sokolovsky V.V. (1948): *Propagation of elastic-viscoplastic waves in bar*, Dokl. Akad. Nauk SSSR, 60, 775-778 (in Russian).

Truesdell C. (1956): *Hypo-elastic shear*, Journ. Appl. Phys., 27, 441-447.

Winnicki A. (2009): *Viscoplastic and internal discontinuity models in analysis of structural concrete*, Monograph, Politechnika Krakowska, Kraków 2009.

Wrana B. (2001*): Soil Dynamics Formulation*, 13th Conf. on Numerical Methods in Hydrotechnics Structures, Korbielow, Poland (in Polish).

Wrana B. (2002): *Two-Phase Soil Models in Dynamics*, 14th Conf. on Numerical Methods in Hydrotechnics Structures, Korbielow, Poland (in Polish).

Wrana B. (2003): *Saturated Porous Soil Models Used in Dynamics*, 15th Int. Confer. on Computer methods in Mechanics CMM-2003, Gliwice, Poland.

Wrana B. (2007): *Identification of Damping by Means of Wavelet and Half Bandwidth Method*, 16th Int. Confer. on Computer methods in Mechanics CMM-2007, Łódź–Spała, Poland.

Yin J.H. (1999): *Nonlinear creep of soils in odometer tests*, Geotechnique, 49(2), 699-707.

Yin J.H., Graham J. (1994): *Equivalent times and one-dimensional elastic viscoplastic modelling of time-dependent stress-strain behaviour of clays*, Can. Geotech. J., 31, 45-52.

Zaman M., Gioda G., Booker J. (2000): *Modelling in geomechanics*, John Wiley & Sons, LTD.

Zienkiewicz O.C., Cormeau I. C. (1974): *Viscoplasticity and creep in elastic solids – A unified numerical solution approach*, Int. J. Numer. Methods Eng., 8, 821-845.

Zienkiewicz O.C., Mróz Z. (1985): *Generalized Plasticity formulation and application to Geomechanics*, Mech. Eng. Mater., Desai C.S., Gallagher R.H. (eds.), Ch. 33, 655-680, John Wiley and Sons.

Chapter 6

SOIL DYNAMICS IN THE FINITE ELEMENT METHOD

6.1. Notations used in Chapter 6

m^s – mass of skeleton phase
m^w – mass of water phase
n^s – volumetric contents of skeleton phase, $n^s = V^s / V$
n^w – volumetric contents of water phase, $n^w = V^w / V$
n^a – volumetric contents of air phase, $n^a = V^a / V$
ρ^s – skeleton density
ρ^w – water density
ρ^a – air density
n – porosity of unsaturated soil
REV – *Representative Elementary Volume*
$\mathbf{x}$ – material point coordination
$\boldsymbol{\sigma}$ – total stress vector in Voight's notation
$\mathbf{b}$ – body force per unit
$\mathbf{k}^w$ – matrix of water phase permeability
$\mathbf{k}^a$ – matrix of air phase permeability
$\mathbf{u}^s$ – displacement vector of skeleton phase
$\mathbf{u}^w$ – displacement vector of water phase
$\mathbf{u}^a$ – displacement vector of air phase
$\varepsilon_v^s = \mathrm{div}(\mathbf{u}^s)$ – volumetric strain of skeleton phase
$\varepsilon_v^w = \mathrm{div}(\mathbf{u}^w)$ – volumetric strain of water phase
$\varepsilon_v^a = \mathrm{div}(\mathbf{u}^a)$ – volumetric strain of air phase
$\mathbf{v}^s$ – velocity vector of skeleton phase
$\mathbf{v}^w$ – velocity vector of water phase

$\mathbf{v}^s$	–	velocity vector of air phase
$\dot{\varepsilon}_v^s = \mathrm{div}(\mathbf{v}^s)$	–	volumetric strain rate of skeleton phase
$\dot{\varepsilon}_v^w = \mathrm{div}(\mathbf{v}^w)$	–	volumetric strain rate of water phase
$\dot{\varepsilon}_v^a = \mathrm{div}(\mathbf{v}^a)$	–	volumetric strain rate of air phase
p_w	–	pore-water pressure
p_a	–	pore-air pressure
$\dot{p}_w$	–	pore-water pressure rate
$\dot{p}_a$	–	pore-air pressure rate
$S = p_a - p_w$	–	suction
K^w	–	bulk modulus of water phase
K^a	–	bulk modulus of air phase
$\mathbf{N}^s(\mathbf{x})$, $\mathbf{N}^w(\mathbf{x})$, $\mathbf{N}^a(\mathbf{x})$	–	shape function of skeleton, water and air displacement respectively
$\mathbf{x}$	–	vector of point coordinates
$\overline{\mathbf{u}}^s$, $\overline{\mathbf{u}}^w$, $\overline{\mathbf{u}}^a$	–	displacement vector of FEM nodes of skeleton, water and air respectively
$\mathbf{M}(t)$, $\mathbf{C}(t)$, $\mathbf{K}(t)$	–	global matrix of mass, damping and stiffness respectively
$\mathbf{p}(t)$	–	internal forces vector in FEM nodes from initial strain at t-time
$\mathbf{f}(t)$	–	external forces vector in FEM nodes at t-time
θ	–	volumetric water content
w	–	water content
B	–	Skempton's constant

6.2. Dynamics of unsaturated soils using finite element formulations

6.2.1. Introduction

The soil model as unsaturated porous material consists of three volumetric phases: the solid skeleton, water and air. In the model, there are also three interface connectors and interaction forces between phases: skeleton to water, skeleton to air and water to air. The use of the water to air function leads to the model taking into account changes in the volume of water in the pore and water pressure in the pore,

it also creates a complex model in comparison to the fully saturated soil or dry soil model.

The equations governing the behaviour of the unsaturated soil material can be derived based on physical laws such as the balance of mass, linear momentum, and the first and second laws of thermodynamics. The microscopy technique was used in determining the volume by averaging macroscopic parameters such as density and water content, Hassanizadeh & Gray (1979) and Wei & Muraleetharan (2002a, 2002b). In the case of the finite element modelling of unsaturated soils, the relative displacement of water and air with respect to the solid skeleton are typically neglected in the solution procedure, Schrefler et al. (1990), Ravichandran & Muraleetharan (2009). In the most common form of the finite element solution for unsaturated soils, simplified governing equations are solved considering: $\mathbf{u}^s$ – skeleton displacement, p_w – water pressure and p_a – air pressure with respect to S_r – degree of saturation, as the primary nodal unknowns $(\mathbf{u}^s - p_w - p_a$ formulation), as proposed by Xikui & Zienkiewicz (1992). The use of continuous bilinear interpolation for both displacement and pressure fields in the finite element formulation violates the Brezzi-Babuska (Brezzi & Fortin, 1991) or the much simpler Zienkiewicz-Taylor patch test (Zienkiewicz & Taylor, 2000) for solvability and convergence.

6.2.2. Governing equations

The soil dynamic problem of unsaturated porous material is considered at the macro level of continuum mechanics. Continuous macroscopic field parameters are introduced by using the concept of a representative elementary volume (REV). The volume spanned by the solid phase is considered as a REV and its motion is given by the function $n^S(\mathbf{x},t)$ – volumetric contents of skeleton phase where $n^S = V_s / V$, $\mathbf{x}$ is the material coordinate and t is the time.

Water and air occupying the voids in the reference configuration may move out of the REV and occupy a volume spanned by a different current configuration (Figure 6.1). Therefore, there is a net flow across the closed REV, which has to be accounted for in deriving the mass balance equations for the unsaturated soils.

The amount of water is directly related to the matric suction $(S = p_a - p_w)$; therefore, the volume fraction of the water phase $n^w = f(s, \varepsilon_v^s)$ is assumed to be a function of matric suction S and volumetric strain of the solid skeleton ε_v^s.

For an isothermal problem, the energy balance is satisfied. All equations written below refer to the current configuration.

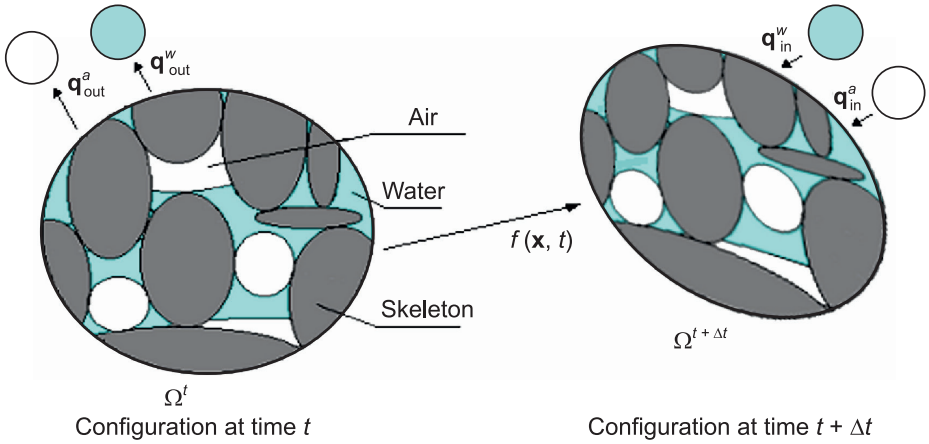

Fig. 6.1. Motion in an unsaturated soil model

– *Mass balance equations*

Mass balance for a bulk phase is given by the following equation:

$$m^{\alpha}(\Omega) = \int_{\Omega} (n^{\alpha}\rho^{\alpha})\mathrm{d}\Omega \tag{6.1}$$

where α is skeleton ($\alpha = s$), water ($\alpha = w$) or air ($\alpha = a$) phase indicator.

– *Mass balance for the solid phase*

It is assumed that skeleton grains are incompressible; therefore, we can use the following equation:

$$-\dot{n} + (1-n)\,\mathrm{div}(\mathbf{v}^s) = 0 \tag{6.2a}$$

or

$$-\dot{n} + (1-n)\,\dot{\varepsilon}^s_v = 0 \tag{6.2b}$$

– *Mass balance for the water phase*

The mass balance for the water phase can be received considering the three--phase mass balance equation and taking into account the mass balance equation for the skeleton phase:

$$\frac{\partial n^w}{\partial \varepsilon^s_v}\dot{\varepsilon}^s_v + n^w\dot{\varepsilon}^w_v + \left(\frac{n^w}{K^w} - \frac{\partial n^w}{\partial S}\right)\dot{p}_w + \left(\frac{\partial n^w}{\partial S}\right)\dot{p}_a = 0 \tag{6.3}$$

– *Mass balance for the air phase*

As in the case for the water phase, the mass balance equation for the air phase can be written as:

$$\left(1-n-\frac{\partial n^w}{\partial \varepsilon_v^s}\right)\dot{\varepsilon}_v^s + n^a\dot{\varepsilon}_v^a + \left(\frac{n^a}{K^a}-\frac{\partial n^w}{\partial S}\right)\dot{p}_a + \left(\frac{\partial n^w}{\partial S}\right)\dot{p}_w = 0 \tag{6.4}$$

– *Momentum balance equations*

Momentum balance equations for the three-phase soil are considered as mixture model (unsaturated soil model) consist of the water, air and skeleton phase. The flows of the water and air phase within the unsaturated soil pore system is important to include this to the overall behaviour. Generalised Darcy's flow equations are used as the laminar flow. The major resistance to the flow of fluids in the unsaturated soil model is the drag forces from the solid skeleton and the driving force is the fluid pressure gradient.

– *Linear momentum balance for the mixture*

$$\mathrm{div}\boldsymbol{\sigma} + \rho\mathbf{b} - n^s\rho^s\ddot{\mathbf{u}}^s - n^w\rho^w\ddot{\mathbf{u}}^w - n^a\rho^a\ddot{\mathbf{u}}^a = 0. \tag{6.5}$$

– *Linear momentum balance for the water phase*

$$\rho^w\ddot{\mathbf{u}}^w + n^w(\mathbf{k}^w)^{-1}(\dot{\mathbf{u}}^w - \dot{\mathbf{u}}^s) + \mathrm{grad}p_w - \rho_w\mathbf{b} = 0. \tag{6.6}$$

– *Linear momentum balance for the air phase*

$$\rho^a\ddot{\mathbf{u}}^a + n^a(\mathbf{k}^a)^{-1}(\dot{\mathbf{u}}^a - \dot{\mathbf{u}}^s) + \mathrm{grad}p_a - \rho_a\mathbf{b} = 0. \tag{6.7}$$

– *Stress state variables for unsaturated soils*

Two independent stress state variables, net stress $\boldsymbol{\sigma} - \rho^a\mathbf{m}$ and the matric suction $S = p_a - p_w$, are typically used to describe the stress–strain behaviour of the solid skeleton, Fredlund & Rahardjo (1993). Other stress state variables can also be used to describe the stress-strain behaviour of the solid skeleton, see Muraleetharan et al. (2006).

6.2.3. Set of governing equations

Differential equations of motion of the unsaturated porous soil model consist of a set of five equations: 1) linear momentum balance for the mixture; 2) linear momentum balance for water phase, and 3) linear momentum balance for the air phase; 4) mass balance for the water phase and 5) mass balance for the air phase. There are five unknown variables: 1) skeleton displacement; 2) water displacement; 3) air displacement; 4) water pore pressure and 5) air pore pressure. The set of equations of motion of the unsaturated soil model are given below:

$$\mathrm{div}\boldsymbol{\sigma} + \rho\mathbf{b} - n^s\rho^s\ddot{\mathbf{u}}^s - n^w\rho^w\ddot{\mathbf{u}}^w - n^a\rho^a\ddot{\mathbf{u}}^a = 0 \tag{6.8a}$$

$$\rho^w\ddot{\mathbf{u}}^w + n^w(\mathbf{k}^w)^{-1}(\dot{\mathbf{u}}^w - \dot{\mathbf{u}}^s) + \mathrm{grad}p_w - \rho^w\mathbf{b} = 0 \tag{6.8b}$$

$$\rho^a \ddot{\mathbf{u}}^a + n^a (\mathbf{k}^a)^{-1} (\dot{\mathbf{u}}^a - \dot{\mathbf{u}}^s) + \operatorname{grad} p_a - \rho^a \mathbf{b} = 0 \tag{6.8c}$$

$$\frac{\partial n^w}{\partial \varepsilon_v^s} \dot{\varepsilon}_v^s + n^w \dot{\varepsilon}_v^w + \left(\frac{n^w}{K^w} - \frac{\partial n^w}{\partial S} \right) \dot{p}_w + \left(\frac{\partial n^w}{\partial S} \right) \dot{p}_a = 0 \tag{6.8d}$$

$$\left(1 - n - \frac{\partial n^w}{\partial \varepsilon_v^s} \right) \dot{\varepsilon}_v^s + n^a \dot{\varepsilon}_v^a + \left(\frac{n^a}{K^a} - \frac{\partial n^w}{\partial S} \right) \dot{p}_a + \left(\frac{\partial n^w}{\partial S} \right) \dot{p}_w = 0. \tag{6.8e}$$

This set of equations can be simplified further without any loss of accuracy by eliminating the water and air pressures in the momentum balance equations using the mass balance equations. The final set of equations contains the displacement, velocity and acceleration of the skeleton, water and air – this is called a *complete formulation of the three-phase displacement model* $(\mathbf{u}^s - \mathbf{u}^w - \mathbf{u}^a)$ and is summarised below:

$$\operatorname{div} \boldsymbol{\sigma} + \rho \mathbf{b} - n^s \rho^s \ddot{\mathbf{u}}^s - n^w \rho^w \ddot{\mathbf{u}}^w - n^a \rho^a \ddot{\mathbf{u}}^a = 0 \tag{6.9a}$$

$$\rho^w \ddot{\mathbf{u}}^w + n^w (\mathbf{k}^w)^{-1} (\dot{\mathbf{u}}^w - \dot{\mathbf{u}}^s) + \operatorname{grad} p_w - \rho^w \mathbf{b} = 0 \tag{6.9b}$$

$$\rho^a \ddot{\mathbf{u}}^a + n^a (\mathbf{k}^a)^{-1} (\dot{\mathbf{u}}^a - \dot{\mathbf{u}}^s) + \operatorname{grad} p_a - \rho^a \mathbf{b} = 0 \tag{6.9c}$$

For the new variables proposed by Ravichandran & Muraleetharan (2009):

$$\mu_{11} = \left(\frac{a_{12} b_{21} - a_{22} b_{11}}{a_{22} a_{11} - a_{12} a_{21}} \right), \quad \mu_{12} = -\left(\frac{a_{22} b_{12}}{a_{22} a_{11} - a_{12} a_{21}} \right), \quad \mu_{13} = \left(\frac{a_{12} b_{22}}{a_{22} a_{11} - a_{12} a_{21}} \right),$$

$$\mu_{21} = \left(\frac{a_{21} b_{11} - a_{11} b_{21}}{a_{22} a_{11} - a_{12} a_{21}} \right), \quad \mu_{22} = \left(\frac{a_{21} b_{12}}{a_{22} a_{11} - a_{12} a_{21}} \right), \quad \mu_{23} = -\left(\frac{a_{11} b_{22}}{a_{22} a_{11} - a_{12} a_{21}} \right),$$

$$a_{11} = \left(\frac{n^w}{K^w} - \frac{\partial n^w}{\partial S} \right), \quad a_{12} = \left(\frac{\partial n^w}{\partial S} \right), \quad b_{11} = \left(\frac{\partial n^w}{\partial \varepsilon_v^s} \right), \quad b_{12} = n^w,$$

$$a_{21} = a_{12}, \quad a_{22} = \left(\frac{n^a}{K^a} - \frac{\partial n^w}{\partial S} \right), \quad b_{21} = \left(1 - n - \frac{\partial n^w}{\partial \varepsilon_v^s} \right), \quad b_{22} = n^a, \tag{6.9d}$$

one can receive water pore pressure and air pore pressure as follows:

$$p_w = \mu_{11} \varepsilon_v^s + \mu_{12} \varepsilon_v^w + \mu_{13} \varepsilon_v^a \tag{6.9e}$$

$$p_a = \mu_{21} \varepsilon_v^s + \mu_{22} \varepsilon_v^w + \mu_{23} \varepsilon_v^a. \tag{6.9f}$$

The system of equations simplified by neglecting the relative accelerations and velocities of the pore water and pore air is called the *reduced formulation* $(\mathbf{u}^s - p_w - p_a)$

$$\operatorname{div}\boldsymbol{\sigma} + \rho\mathbf{b} - \rho^s\ddot{\mathbf{u}} = 0 \tag{6.10a}$$

$$\left(n^w + \frac{\partial n^w}{\partial \varepsilon_v^s}\right)\dot{\varepsilon}_v^s + \left(\frac{n^w}{K^w} - \frac{\partial n^w}{\partial S}\right)\dot{p}_w + \left(\frac{\partial n^w}{\partial S}\right)\dot{p}_a = 0 \tag{6.10b}$$

$$\left(1 - n^w - \frac{\partial n^w}{\partial \varepsilon_v^s}\right)\dot{\varepsilon}_v^s + \left(\frac{\partial n^w}{\partial S}\right)\dot{p}_w + \left(\frac{n^a}{K^a} - \frac{\partial n^w}{\partial S}\right)\dot{p}_a = \mathbf{0}. \tag{6.10c}$$

The FEM formulation used the displacement approximation by an element shape functions defined as:

$$\mathbf{u}^s(\mathbf{x}) = \mathbf{N}^s(\mathbf{x})\bar{\mathbf{u}}^s, \quad \mathbf{u}^w(\mathbf{x}) = \mathbf{N}^w(\mathbf{x})\bar{\mathbf{u}}^w, \quad \mathbf{u}^a(\mathbf{x}) = \mathbf{N}^a(\mathbf{x})\bar{\mathbf{u}}^a \tag{6.11a}$$

Through introducing approximation (6.11a) to equations (6.9) and (6.10), we can obtain the final matrix equation of motion:

$$\mathbf{M}(t)\ddot{\bar{\mathbf{u}}}(t) + \mathbf{C}(t)\dot{\bar{\mathbf{u}}}(t) + \mathbf{K}(t)\bar{\mathbf{u}}(t) + \mathbf{p}(t) = \mathbf{f}(t) \tag{6.11b}$$

6.3. Two-phase, fully-saturated soil dynamic, u^s–w–p formulation

Equation of motion of the fully saturated porous soil model include a set of three equations: 1) linear momentum balance for the mixture (soil-water model); 2) linear momentum balance for the water phase and 3) water mass balance with the deformable skeleton. There are three unknown variables: 1) skeleton displacement; 2) water displacement and 3) water pore pressure. The equations presented below are in accordance with Zienkiewicz (1984, 2000).

6.3.1. Linear momentum balance for the soil-water mixture

$$\sigma'_{ij,j} - \rho\ddot{u}_i^s + \rho^w(\dot{w}_i + w_j w_{i,j}) + \rho b_i = 0 \tag{6.12a}$$

or

$$\mathbf{L}^T\boldsymbol{\sigma}' - \rho\ddot{\mathbf{u}}^s + \rho^w(\dot{\mathbf{w}} + \mathbf{w}\nabla^T\mathbf{w}) + \rho\mathbf{b} = 0 \tag{6.12b}$$

where

$$\mathbf{L}^T = \begin{bmatrix} \dfrac{\partial}{\partial x_1} & 0 & 0 & \dfrac{\partial}{\partial x_2} & 0 & \dfrac{\partial}{\partial x_3} \\ 0 & \dfrac{\partial}{\partial x_2} & 0 & \dfrac{\partial}{\partial x_1} & \dfrac{\partial}{\partial x_3} & 0 \\ 0 & 0 & \dfrac{\partial}{\partial x_3} & 0 & \dfrac{\partial}{\partial x_2} & \dfrac{\partial}{\partial x_1} \end{bmatrix}, \tag{6.13}$$

$$\mathbf{w}\nabla^T\mathbf{w} = \begin{Bmatrix} w_1 w_{1,1} + w_2 w_{1,2} + w_3 w_{1,3} \\ w_1 w_{2,1} + w_2 w_{2,2} + w_3 w_{2,3} \\ w_1 w_{3,1} + w_2 w_{3,2} + w_3 w_{3,3} \end{Bmatrix} \quad - \text{ convective vector}$$

$\mathbf{w} = \dot{\mathbf{u}}^w - \dot{\mathbf{u}}^s$ – vector of relative velocity of pore water with respect to velocity of skeleton

$\dot{\mathbf{w}}$ – vector of relative acceleration of pore water with respect to acceleration of skeleton

Equation (6.12) is an extension of the linear momentum balance for the soil--water mixture (6.8a) including the convective vector. Overall density of the soil--water mixture is

$$\rho = n\ \rho^w + (1-n)\ \rho^s \tag{6.14}$$

6.3.2. Linear momentum balance for the water

$$-p_{,i} - R_i - \rho^w \ddot{u}_i^s - \rho^w (\dot{w}_i + w_j w_{i,j}) / n + \rho^w b_i = 0 \tag{6.15a}$$

or

$$-\nabla p - \mathbf{R} - \rho^w \ddot{\mathbf{u}}^s - \rho^w (\dot{\mathbf{w}} + \mathbf{w}\nabla^T\mathbf{w}) / n + \rho^w \mathbf{b} = 0, \tag{6.15b}$$

where **R** represents the viscous drag forces, which assuming the Darcy seepage law, can be written as:

$$k_{ij} R_j = w_j \quad \text{or} \quad \mathbf{kR} = w. \tag{6.16}$$

Equation (6.15) is an extension of the linear momentum balance for the pore water (6.8b) including convective component $\rho^w w_j w_{i,j}$. The other components are: $(-p_{,i})$ – the gradient pore water pressure, $\rho^w \ddot{u}_i^s$ – the inertia force of skeleton, $\rho^w \dot{w}_i$ – the inertia force of pore water, $\rho^w b_i$ – the water body force, and R_i – the viscous drag force.

In equation (6.16), the permeability coefficient k_{ij} is used with dimensions of [length]^3 [time]/[mass] which is different from the usual soil mechanics convention k' which has the dimension of velocity, i.e. [length]/[time]. Their values are related by $k = k'/(\rho^w g)$ where ρ^w and g are the water density and acceleration due to gravity at which the permeability is measured, for this unit a vector **R** has a dimension of force.

6.3.3. Water mass balance with deformable skeleton

Water mass balance with deformable skeleton describe equilibrium in the soil--water mixture during the flow divergence $w_{i,j}$, which occurs during the pore change over time dt. This storage change may cause by several components; these are provided below in order of importance:

- the increased volume due to a change in strain i.e.: $\mathrm{d}\varepsilon_{ii} = \delta_{ij}\mathrm{d}\varepsilon_{ij} = \mathbf{m}^T\boldsymbol{\varepsilon}$,
- the additional volume stored by compression of void due to water pressure increase: $n\mathrm{d}\rho / K^w$,
- the additional volume stored by the compression of grains by the water pressure increase:

$$(1-n)\,\mathrm{d}\,p / K^s$$

where:
K^s – bulk modulus of skeleton,

- the change in volume of the solid phase due to a change in the intergranular effective contact stress $\sigma' = \sigma + \delta_{ij}\,p$:

$$(1/3)\delta_{ij}\mathrm{d}\sigma'_{ij} / K_s = (K_T / K_s)(\mathrm{d}\varepsilon_v + \mathrm{d}p / K_s),$$

where:
K_T – the average bulk modulus of the solid-water mixture,
ε_v – the total volumetric strain.

Adding all the above contributions together with a source term $\dot{s}_o$ and a second--order term due to the change in fluid density in the process $n\dot{\rho}^w / \rho^w$, we can finally write the flow conservation equation:

$$w_{i,i} + \dot{\varepsilon}_v + \frac{n\dot{p}}{K_w} + \frac{(1-n)\,\dot{p}}{K^s} - \frac{K_T}{K^s}\left(\dot{\varepsilon}_v + \frac{\dot{p}}{K^s}\right) + \frac{n\dot{\rho}^w}{\rho^w} + \dot{s}_o = 0 \tag{6.17a}$$

or

$$w_{i,i} + \left(1 - \frac{K_T}{K^s}\right)\dot{\varepsilon}_v + \left(\frac{n}{K_w} + \frac{1-n}{K^s} - \frac{K_T}{K^s K^s}\right)\dot{p} + \frac{n\dot{\rho}^w}{\rho^w} + \dot{s}_o = 0. \tag{6.17b}$$

For simplified description one can use new variables:

$$\frac{1}{Q} = \frac{n}{K_w} + \frac{1-n}{K^s} - \frac{K_T}{K^s K^s} = \frac{n}{K^w} + \frac{\alpha - n}{K^s} \tag{6.18a}$$

$$\alpha = 1 - \frac{K_T}{K^s}$$

with α=1, we can get

$$\frac{1}{Q} = \frac{n}{K^w} + \frac{1-n}{K^s}. \tag{6.18b}$$

Given the above notation, equation (6.17) can be written as:

$$w_{i,i} + \alpha \dot{\varepsilon}_v + \frac{1}{Q}\dot{p} + \frac{n\dot{\rho}^w}{\rho^w} + \dot{s}_o = 0 \tag{6.19a}$$

or

$$\nabla^T \mathbf{w} + \alpha \mathbf{m} \dot{\boldsymbol{\varepsilon}}_v + \frac{1}{Q}\dot{p} + \frac{n\dot{\rho}^w}{\rho^w} + \dot{s}_o = 0. \tag{6.19b}$$

6.3.4. Constitutive equations

1) The effective stress equation

$$\sigma'_{ij} = \sigma'_{ij} + \alpha \delta_{ij} p \tag{6.20}$$

in practical calculations often is assumed $\alpha = 1$.

2) Constitutive equations of the soil skeleton in incremental forms are as follows:
   – in the case of small deformations

$$\mathrm{d}\sigma'_{ij} = D_{ijkl}(\mathrm{d}\varepsilon_{ij} - \mathrm{d}\varepsilon^0_{ij}) \tag{6.21a}$$

   – in the case of large deformations

$$\mathrm{d}\sigma'_{ij} = D_{ijkl}(\mathrm{d}\varepsilon_{kl} - \mathrm{d}\varepsilon^0_{kl}) + \sigma'_{ik}\mathrm{d}\omega_{kj} + \sigma'_{jk}\mathrm{d}\omega_{ki}, \tag{6.21b}$$

where:

$\mathrm{d}\varepsilon_{ij} = \frac{1}{2}(\mathrm{d}u_{i,j} + \mathrm{d}u_{j,i})$ – increment of strain,

$\mathrm{d}\omega_{ij} = \frac{1}{2}(\mathrm{d}u_{i,j} - \mathrm{d}u_{j,i})$ – increment of rotation.

6.3.5. Boundary and initial conditions

The behaviour of the two-phase medium (e.g. skeleton and the water in the pores) in dynamic analysis is described by equations: (6.12) – linear momentum balance for the soil-water mixture; (6.15) – linear momentum balance for the water; (6.19) – water mass balance with deformable skeleton; (6.20) – constitutive equations. Unknowns in these equations are:

$P = p_w$ – pore water pressure;
$\mathbf{w} = \{w_1, w_2, w_3\}^T$ – average velocity vector of water flow inside the pore with respect to the skeleton;
$\mathbf{u}^s = \{u_1^s, u_2^s, u_3^s\}^T$ – displacement vector of soil skeleton.

Boundary conditions

1) The boundary conditions for the soil skeleton are the following known values:
   – the displacement $\bar{\mathbf{u}}^s$ on the boundary Γ_u,
   – the normal stress $\mathbf{n}\boldsymbol{\sigma} = \bar{\mathbf{t}}$ on the boundary Γ_t, where $\Gamma = \Gamma_t \cup \Gamma_u$.
2) The boundary conditions for the pore water are the following known values:
   – the relative flow velocity with respect to skeleton $\bar{\mathbf{w}}$ through the boundary Γ_w,
   – the pore water pressure $p = q$ on boundary Γ_p, where $\Gamma = \Gamma_p \cup \Gamma_w$.

Boundary condition of the two-phase soil model (Figure 6.2):

Skeleton phase	Pore water phase
$\Gamma = \Gamma_t \cup \Gamma_u$	$\Gamma = \Gamma_p \cup \Gamma_w$
$\mathbf{t} = \mathbf{n}\boldsymbol{\sigma} = \bar{\mathbf{t}}$ on Γ_t	$p = q$ on Γ_p
$\mathbf{u}^s = \bar{\mathbf{u}}^s$ on Γ_u	$\mathbf{w} = \bar{\mathbf{w}}$ on Γ_w

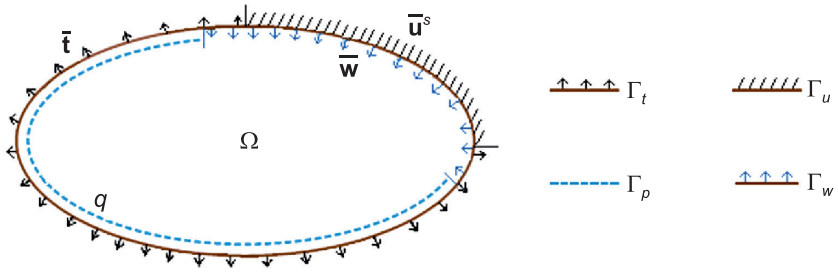

Fig. 6.2. Boundary condition of two-phase, fully-saturated soil model

Initial conditions

1) The initial conditions for the soil skeleton are the following known values:
   – the displacement at time t_o, $\mathbf{u}^s(t = t_o) = \mathbf{u}_o^s$,
   – the velocity at time t_o, $\dot{\mathbf{u}}^s(t = t_o) = \dot{\mathbf{u}}_o^s$.
2) The initial conditions for the pore water are the following known values:
   – the relative flow velocity with respect to skeleton at time t_o, $\mathbf{w}(t = t_o) = \mathbf{w}_o$,
   – the pore water pressure at time t_o, $p(t = t_o) = p_o$.

6.4. Two-phase, fully-saturated soil dynamic for undrained behaviour – Skempton's constant

Some typical soil behaviours are implied in the undrained behaviour. In this case, $w_i = 0$, i.e. with no net outflow of water. Substituting $w_i = 0$ into equation (6.19) and omitting the last two terms $(\dot{\rho}^w = 0,\ \dot{s}_o = 0)$ obtained the following equation which is expressed in velocity:

$$\alpha \mathrm{d}\dot{\varepsilon}_v + \frac{\mathrm{d}\dot{p}}{Q} = 0. \tag{6.22}$$

With integration with respect to time, the following equation is obtained:

$$\mathrm{d}p = -Q\alpha \mathrm{d}\varepsilon_v. \tag{6.23}$$

The total stress equation becomes:

$$\mathrm{d}\boldsymbol{\sigma} = \mathrm{d}\boldsymbol{\sigma}' + \alpha \mathbf{m}\mathrm{d}p = \mathbf{D}\mathrm{d}\varepsilon + \alpha \mathbf{m}\,(-Q\alpha \mathbf{m}^T \mathrm{d}\varepsilon)$$

or

$$\mathrm{d}\boldsymbol{\sigma} = (\mathbf{D} + \alpha^2 Q \mathbf{m}\mathbf{m}^T)\mathrm{d}\varepsilon. \tag{6.24}$$

If the pressure change dp is considered as a fraction of the mean total stress change $\mathbf{m}^T \mathrm{d}\sigma / 3$, we obtain the so-called B soil parameter, Skempton (1954), as the relationship between dp and $\mathrm{d}\sigma_{ii}$

$$\mathrm{d}p = -Q\alpha \mathrm{d}\varepsilon_{ii} = -\frac{B}{3} d\sigma_{ii} \tag{6.25}$$

where:

$$B = \frac{3\mathrm{d}p}{\mathbf{m}^T \mathrm{d}\boldsymbol{\sigma}} = \frac{3Q\alpha \mathbf{m}^T \mathrm{d}\boldsymbol{\varepsilon}}{\mathbf{m}^T (\mathbf{D} + \alpha^2 Q \mathbf{m}\mathbf{m}^T)\mathrm{d}\boldsymbol{\varepsilon}} \quad - \text{ Skempton's constant}$$

or multiplying by $\mathbf{m}$

$$B = \frac{3Q\alpha \mathbf{m}^T \mathbf{m}}{\mathbf{m}^T (\mathbf{D} + \alpha^2 Q \mathbf{m}\mathbf{m}^T)\mathbf{m}} = \frac{9Q\alpha}{\mathbf{m}^T \mathbf{D}\mathbf{m} + 9\alpha^2 Q}. \tag{6.26}$$

In the case of isotropic material, we have $\mathbf{m}^T \mathbf{D}\mathbf{m} = 9K_T$

$$B = \frac{9\alpha}{9K_T / Q + 9\alpha^2}. \tag{6.27}$$

The Skempton's constant B by Terzaghi (1925), Craig (1992) is: $B \approx 1$ in the case of fully-saturated soil, and $B < 1$ in the case of unsaturated soil.

6.5. Two-phase, fully-saturated soil dynamic, u^s–U formulation

Now one can consider simplified set of equations (6.12), (6.15) and (6.19) eliminating the members with pore water pressure p.

The following simplifications are used in the equations:

- member $\dot{\mathbf{w}} + \mathbf{w}\nabla^T\mathbf{w} = 0,$ omitted in equations (6.12) and (6.15),
- the water density changes over time $\dot{\rho}^w = 0,$ were omitted,
- the effects of temperature changes over time $\dot{s}_o = 0,$ were omitted.

After entering the unknown $\mathbf{U}^R$ – water displacement relative to the skeleton,

$$\dot{\mathbf{U}}^R = \mathbf{w} / n \tag{6.28}$$

and

$$\ddot{\mathbf{U}}^R = \dot{\mathbf{w}} / n.$$

equation (6.19b) can be written in the form:

$$\nabla^T(n\dot{\mathbf{U}}^R) + \alpha\mathbf{m}\dot{\varepsilon}_v + \frac{1}{Q}\dot{p} = 0. \tag{6.29}$$

Then, integration with respect to time obtained:

$$p = -Q(\alpha\mathbf{m}\varepsilon + n\nabla^T\mathbf{U}^R). \tag{6.30}$$

The total displacement of the water is defined as:

$$\mathbf{U} = \mathbf{U}^R + \mathbf{u}^s \tag{6.31}$$

where $\mathbf{u}^s$ is the displacement of the skeleton, hence $\mathbf{w} = n\dot{\mathbf{U}}^R = n(\dot{\mathbf{U}} - \dot{\mathbf{u}}^s)$ and $\dot{\mathbf{w}} = n(\ddot{\mathbf{U}} - \ddot{\mathbf{u}}^s).$

The pore water pressure in accordance with equation (6.30) is currently

$$p = -Q[\alpha\nabla^T\mathbf{u}^s + n\nabla^T(\mathbf{U} - \mathbf{u}^s)] = -Q[(\alpha - n)\nabla^T\mathbf{u}^s + n\nabla^T\mathbf{U}]. \tag{6.32}$$

Equation (6.20) on the total stress $\boldsymbol{\sigma}$, can be written in the form:

$$\boldsymbol{\sigma} = \boldsymbol{\sigma}' + \alpha\mathbf{m}p = \boldsymbol{\sigma}' + \alpha\mathbf{m}Q[(\alpha - n)\nabla^T\mathbf{u}^s + n\nabla^T\mathbf{U}]. \tag{6.33}$$

Equation (6.12) can now be written as:

$$\mathbf{L}^T\boldsymbol{\sigma}' + \alpha Q\nabla[(\alpha - n)\nabla^T\mathbf{u}^s + n\nabla^T\mathbf{U}] - \rho\ddot{\mathbf{u}}^s - \rho^w n(\ddot{\mathbf{U}} - \ddot{\mathbf{u}}^s) + \rho\mathbf{b} = 0 \tag{6.34}$$

and equation (6.15) can be written as:

$$Q\nabla[(\alpha - n)\nabla^T\mathbf{u}^s + n\nabla^T\mathbf{U}] - \mathbf{k}^{-1}n(\dot{\mathbf{U}} - \dot{\mathbf{u}}^s) - \rho^w\ddot{\mathbf{u}}^s - \rho^w(\ddot{\mathbf{U}} - \ddot{\mathbf{u}}^s) + \rho^w\mathbf{b} = 0. \tag{6.35}$$

6.6. Two-phase, fully-saturated soil dynamic, $\mathbf{u}^s$–p formulation

6.6.1. The basic equations

Now one can consider simplified set of equations (6.12), (6.15) and (6.19) eliminating the members with relative pore water velocity **w** with respect to skeleton.

The following simplifications were used in the equations:

– omitted in equations (6.12) and (6.15) member $\dot{\mathbf{w}} + \mathbf{w}\nabla^T\mathbf{w} = 0,$ as small with respect to $\mathbf{u}^s$ – displacement of skeleton and with respect to p – pore water pressure,
– the linear Darcy seepage law $\mathbf{kR} = \mathbf{w}$ was assumed,
– the water density changes over time $\dot{\rho}^w = 0,$ were omitted,
– the effects of temperature changes over time $\dot{s}_o = 0$ were omitted.

Equation (6.12) takes the form:

$$\mathbf{L}^T\boldsymbol{\sigma}' - \rho\ddot{\mathbf{u}}^s + \rho\mathbf{b} = 0. \tag{6.36}$$

From equation (6.15), the force $\mathbf{R} = -\nabla p - \rho^w\ddot{\mathbf{u}}^s + \rho^w\mathbf{b} = 0$ is determined, hence Darcy seepage law can be written as $\mathbf{kR} = \mathbf{k}(-\nabla p - \rho^w\ddot{\mathbf{u}}^s + \rho^w\mathbf{b}) = \mathbf{w}.$ Next, substituting **kR** to (6.19) received

$$\nabla^T\mathbf{k}(-\nabla p - \rho^w\ddot{\mathbf{u}}^s + \rho^w\mathbf{b}) + \alpha\mathbf{m}\dot{\boldsymbol{\varepsilon}} + \frac{1}{Q}\dot{p} + \dot{s}_o = 0. \tag{6.37}$$

Comments:

1) Equations (6.36) and (6.37) are dynamic consolidation equations which take into account the inertia forces $\rho\ddot{\mathbf{u}}^s$ and $\rho^w\ddot{\mathbf{u}}^s$.
2) Omitting members of inertia forces, we can have obtained the two-phase soil equations for static consolidation problem

$$\mathbf{L}^T\boldsymbol{\sigma} + p\mathbf{b} = 0$$

$$\nabla^T\mathbf{k}(-\nabla p + p^w\mathbf{b}) = 0. \tag{6.38}$$

Initial conditions

1) The initial conditions for the soil skeleton are the following known values:
   – displacement at time t_o, $\mathbf{u}^s(t = t_o) = \mathbf{u}_o^s$,
   – velocity at time t_o, $\dot{\mathbf{u}}^s(t = t_o) = \dot{\mathbf{u}}_o^s$.

2) The initial condition for the pore water is the known value for the pore water pressure at time t_o, $p(t=t_o)=p_o$. (6.39)

Boundary conditions

1) The boundary conditions for the soil skeleton are the following known values:
   – the displacement $\bar{\mathbf{u}}^s$ on the boundary Γ_u,
   – the normal stress $\mathbf{n}\boldsymbol{\sigma}=\bar{\mathbf{t}}$ on the boundary Γ_t, where $\Gamma=\Gamma_u\cup\Gamma_t$.
2) The boundary conditions for the pore water are the following known values:
   – the pore water pressure $p=q$ on the boundary Γ_p,
   – the water flow q^w through the boundary Γ_p^q, where $\Gamma=\Gamma_p\cup\Gamma_p^q$.

Equation boundary conditions:

– displacement of skeleton $\mathbf{u}^s=\bar{\mathbf{u}}^s, \quad \text{on} \quad \Gamma_u,$ (6.40a)

– normal stress $\mathbf{N}^T\boldsymbol{\sigma}=\mathbf{t}, \quad \text{on} \quad \Gamma_t,$ (6.40b)

– pore water pressure $p=\bar{p}, \quad \text{on} \quad \Gamma_p,$ (6.41)

where:

$$\mathbf{N}=\begin{bmatrix} n_1 & 0 & 0 & n_2 & 0 & n_3 \\ 0 & n_2 & 0 & n_1 & n_3 & 0 \\ 0 & 0 & n_3 & 0 & n_2 & n_1 \end{bmatrix}$$

– water flow condition

$$\frac{\rho^w}{\mu^w}\mathbf{k}(-\text{grad}p_w+\rho^w\mathbf{b}-\rho^w\ddot{\mathbf{u}}^s)^T\mathbf{n}=q^w \quad \text{on} \quad \Gamma_p^q, \tag{6.42}$$

where:

q^w – the known value of the external water flow normal to the boundary,

$\mathbf{n}=\{n_1,n_2,n_3\}^T$.

6.6.2. Weak formulation

The momentum equation, called *a strong form* (6.36), (6.37), to *a weak form*, (often called *a variational form or the principle of virtual work or virtual power*), will be developed. The weak form will be used to approximate the strong form by finite elements; solutions obtained by finite elements are approximate solutions to the strong form.

A weak form is now developed for the momentum equation and the traction boundary conditions. For this purpose, we define trial functions $(\mathbf{u}^s, p_w)$ which satisfy any displacement boundary conditions and are smooth enough so that all derivatives in the momentum equation are well defined. The weight function $(\mathbf{w}, p)$ is assumed to be smooth enough so that all of the following steps are well defined and will vanish on the prescribed displacement boundary. The weak form is obtained by taking the product of the momentum equation expressed in terms of the trial function with the test function. This gives

$$\int_\Omega \mathbf{w}^T (\mathbf{L}^T \boldsymbol{\sigma}' - \rho \ddot{\mathbf{u}}^s + \rho \mathbf{b}) \, \mathrm{d}\Omega + \int_\Gamma \mathbf{w}^T (\mathbf{N}^T \boldsymbol{\sigma}' - \bar{\mathbf{t}}) \, \mathrm{d}\Gamma_u = 0, \tag{6.43}$$

where:

- $\mathbf{u}^s$ – displacement of skeleton, trial function (which was once differentiable) is adopted so as to satisfy boundary condition (6.40) on Γ_u,
- $\mathbf{w}$ – weight function satisfy vanish and prescribed condition on boundary (6.44) are used:

$$\begin{aligned} &\mathbf{w} = 0 \qquad \text{on} \quad \Gamma_u \\ &\bar{\mathbf{w}} = -\mathbf{w} \qquad \text{on} \quad \Gamma_u^q. \end{aligned} \tag{6.44}$$

Through use of the Green theorem $\int_\Omega \varphi \frac{\partial \psi}{\partial x} \mathrm{d}\Omega = -\int_\Omega \frac{\partial \varphi}{\partial x} \psi \mathrm{d}\Omega + \int_\Gamma \varphi \psi \, n_x \mathrm{d}\Gamma$ with respect to equation (6.43), one can obtain:

$$-\int_\Omega (\mathbf{Lw})^T \boldsymbol{\sigma} \mathrm{d}\Omega + \int_\Gamma \mathbf{w}^T \mathbf{N}^T \boldsymbol{\sigma} \mathrm{d}\Gamma - \int_\Omega \mathbf{w}^T \rho \ddot{\mathbf{u}}^s \mathrm{d}\Omega + \int_\Omega \mathbf{w}^T \rho \mathbf{b} \mathrm{d}\Omega + \int_{\Gamma_u^q} \bar{\mathbf{w}}^T (\mathbf{N}^T \boldsymbol{\sigma} - \bar{\mathbf{t}}) \mathrm{d}\Gamma = 0$$

and after taking into account (6.44), we finally obtain:

$$\int_\Omega (\mathbf{Lw})^T \boldsymbol{\sigma} \mathrm{d}\Omega = \int_\Omega \mathbf{w}^T \rho \mathbf{b} \mathrm{d}\Omega - \int_\Omega \mathbf{w}^T \rho \ddot{\mathbf{u}}^s \mathrm{d}\Omega + \int_{\Gamma_u^q} \bar{\mathbf{w}}^T \bar{\mathbf{t}} \mathrm{d}\Gamma = 0. \tag{6.45}$$

The weak formulation for the soil-water mixture mass balance equation (6.37) with the boundary condition (6.42) is now used, we finally obtain:

$$\int_\Omega \mathbf{w}^{*T} \left\{ \nabla^T \left[\frac{\mathbf{k}}{\mu^w} (-\nabla p - \rho^w \ddot{\mathbf{u}}^s + \rho^w \mathbf{b}) \right] + \alpha \mathbf{m}^T \mathbf{L} \dot{\mathbf{u}}^s + \left(\frac{\alpha - n}{K^s} + \frac{n}{K^w} \right) \frac{\partial p}{\partial t} \right\} \mathrm{d}\Omega +$$

$$+ \int_\Gamma w^{*T} \left[\frac{\mathbf{k}}{\mu^w} (-\nabla p - \rho^w \ddot{\mathbf{u}}^s + \rho^w \mathbf{b})^T \mathbf{n} - \frac{q^w}{\rho^w} \right] \mathrm{d}\Gamma = 0, \tag{6.46}$$

where for pore pressure, trial function p, twice differentiable with satisfy boundary condition (6.41) on Γ_p is adopted, and weight function $\mathbf{w}^*$ satisfy prescribed condition on boundary (6.47) is now used:

$$\mathbf{w}^* = 0 \qquad \text{on} \quad \Gamma_p,$$
$$\bar{\mathbf{w}}^* = -\mathbf{w}^* \quad \text{on} \quad \Gamma_p^q. \tag{6.47}$$

Use of the Green theorem to equation (6.46) finally obtained:

$$\int_\Omega \left[-(\nabla \mathbf{w}^*)^T \left(-\frac{\mathbf{k}}{\mu^w} \nabla p - \frac{\mathbf{k}}{\mu^w} \rho^w \ddot{\mathbf{u}}^s + \frac{\mathbf{k}}{\mu^w} \rho^w \mathbf{b} \right) + \mathbf{w}^{*T} \alpha \mathbf{m}^T \mathbf{L} \dot{\mathbf{u}}^s + \right.$$
$$\left. + \mathbf{w}^{*T} \left(\frac{\alpha - n}{K^s} + \frac{n}{K^w} \right) \frac{\partial p}{\partial t} \right] \mathrm{d}\Omega + \int_{\Gamma_p^q} \mathbf{w}^{*T} \frac{q^w}{\rho^w} \mathrm{d}\Gamma = 0. \tag{6.48}$$

6.6.3. FEM discretization

FEM discretization is used, for the skeleton displacement, the following approximation is introduced:

$$\mathbf{u}^s = \mathbf{N}_u \bar{\mathbf{u}} \tag{6.49a}$$

and for pore water pressure:

$$p_w = \mathbf{N}_p \bar{\mathbf{p}}, \tag{6.49b}$$

where shape function $\mathbf{N}_u$ and $\mathbf{N}_p$ should fulfil the Brezzi–Babuska condition for the mixed field formulation, Brezzi and Fortin (1991).

Similarly, in the place of the weight function $\mathbf{w}$, the shape function $\mathbf{N}_u$ is used, and in the place of the weight function $\mathbf{w}^*$, the shape function $\mathbf{N}_w$ is introduced. After introduction into (6.45) and including $\boldsymbol{\sigma} = \boldsymbol{\sigma}' + \alpha \mathbf{m} p$, the following is then obtained:

$$\int_\Omega \mathbf{N}_u^T \rho \mathbf{N}_u \mathrm{d}\Omega \ddot{\bar{\mathbf{u}}} + \int_\Omega \mathbf{B}^T \boldsymbol{\sigma}' \mathrm{d}\Omega - \int_\Omega \mathbf{B}^T S_w \mathbf{m} \mathbf{N}_w \mathrm{d}\Omega \bar{\mathbf{p}}^w = \int_\Omega \mathbf{N}_u^T \rho \mathbf{b} \mathrm{d}\Omega + \int_{\Gamma_u^q} \mathbf{N}_u^T \bar{\mathbf{t}} \mathrm{d}\Gamma +$$
$$+ \int_\Omega \mathbf{B}^T (S_g p_{gw} - p_{atm}) \mathbf{m} \mathbf{N}_w \mathrm{d}\Omega, \tag{6.50}$$

where:

$$p = S_w p_w + S_g p_{gw} - p_{atm}, \quad \rho = \rho^s (1 - n) + n \rho^w S_w.$$

By transforming equation (6.48) in a similar manner, one can obtain:

$$\int_\Omega \mathbf{N}_w^T S_w \mathbf{m}^T \dot{\bar{\mathbf{u}}} + \mathbf{B} \mathrm{d}\Omega \int_\Omega \mathbf{N}_w^T S_g \frac{\rho^{gw}}{\rho^w} \mathbf{m}^T \mathbf{B} \mathrm{d}\Omega \dot{\bar{\mathbf{u}}} + \int_\Omega (\nabla \mathbf{N}_w)^T \mathbf{k}_w \nabla \mathbf{N}_w \mathrm{d}\Omega \bar{\mathbf{p}} +$$
$$+ \int_\Omega (\nabla \mathbf{N}_w)^T \mathbf{k}_g \frac{\rho^{gw}}{\rho^w} \frac{\partial p_{gw}}{\partial p_w} \nabla \mathbf{N}_w \mathrm{d}\Omega \bar{\mathbf{p}} + \int_\Omega \mathbf{N}_w^T \frac{1}{Q_w} \mathbf{N}_w \mathrm{d}\Omega \dot{\bar{\mathbf{p}}} +$$

$$+\int_{\Omega}\mathbf{N}_w^T\frac{\rho^{gw}}{\rho^w}\frac{1}{Q_w}\mathbf{N}_w\mathrm{d}\Omega\dot{\overline{\mathbf{p}}}=\int_{\Omega}(\nabla\mathbf{N}_w)^T\mathbf{k}_w\rho^w\mathbf{b}\mathrm{d}\Omega-\int_{\Gamma_p^q}\mathbf{N}_p^T\frac{q^w}{\rho^w}\mathrm{d}\Gamma. \tag{6.51}$$

where in equation (6.51), inertia force $\rho^w\ddot{\mathbf{u}}^s$ is omitted.

The set of equations (6.50) and (6.51) is written in matrix form for the arbitrary $(n+1)$ time step, $t=t_{n+1}$:

$$\begin{aligned}\mathbf{M}_{n+1}\ddot{\overline{\mathbf{u}}}+\overline{\mathbf{P}}_{n+1}-\mathbf{Q}_{n+1}^w\overline{\mathbf{P}}_{n+1}&=\mathbf{f}_{n+1}^u\\(\mathbf{Q}_{n+1}^w+\mathbf{Q}_{n+1}^{gw})^T\dot{\overline{\mathbf{u}}}+(\mathbf{H}_{n+1}^w+\mathbf{H}_{n+1}^{gw})\overline{\mathbf{p}}_{n+1}+(\mathbf{S}_{n+1}^w+\mathbf{S}_{n+1}^{gw})\dot{\overline{\mathbf{p}}}_{n+1}&=\mathbf{f}_{n+1}^p,\end{aligned} \tag{6.52}$$

where:

$\mathbf{B}=\mathbf{L}\mathbf{N}_u$ – strain differential operator (6.53a)

$\int_{\Omega}\mathbf{N}_u^T[\rho^s(1-n)+n\rho^wS_w]\mathbf{N}_u\mathrm{d}\Omega$ – mass matrix (6.53b)

$\mathbf{Q}^w=\int_{\Omega}\mathbf{B}^TS_w\mathbf{m}\mathbf{N}_u\mathrm{d}\Omega$ – water coupling matrix (6.53c)

$\mathbf{Q}^{gw}=\int_{\Omega}\mathbf{B}^T\frac{\rho^{gw}}{\rho^w}S_g\mathbf{m}\mathbf{N}_u\mathrm{d}\Omega$ – steam coupling matrix (6.53d)

$\mathbf{H}^w=\int_{\Omega}(\nabla\mathbf{N}_w)^T\mathbf{k}_w\nabla\mathbf{N}_w\mathrm{d}\Omega$ – water permeability matrix (6.53e)

$\mathbf{H}^{gw}=\int_{\Omega}(\nabla\mathbf{N}_w)^T\mathbf{k}_g\frac{\rho^{gw}}{\rho^w}\frac{\partial p_{gw}}{\partial p_w}\nabla\mathbf{N}_w\mathrm{d}\Omega$ – steam permeability matrix (6.53f)

$\mathbf{S}^w=\int_{\Omega}\mathbf{N}_w^T\frac{1}{Q_w}\mathbf{N}_w\mathrm{d}\Omega$ – water compressibility matrix (6.53g)

$\mathbf{S}^{gw}=\int_{\Omega}\mathbf{N}_w^T\frac{\rho^{gw}}{\rho^w}\frac{1}{Q}\mathbf{N}_w\mathrm{d}\Omega$ – steam compressibility matrix (6.53h)

$\overline{\mathbf{P}}=\int_{\Omega}\mathbf{B}^T\boldsymbol{\sigma}'\mathrm{d}\Omega$ – internal forces vector of effective stress (6.53i)

$\mathbf{f}^u=\int_{\Omega}\mathbf{N}_u^T[\rho^s(1-n)+n\rho^wS_w]g\mathrm{d}\Omega+\int_{\Gamma_u^q}\mathbf{N}_u^T\overline{\mathbf{t}}\mathrm{d}\Gamma+\int_{\Omega}\mathbf{B}^T(S_gp_{gw}-p_{atm})\mathbf{m}\mathbf{N}_w\mathrm{d}\Omega$ – external node forces vector acting on skeleton (6.53j)

$$\mathbf{f}^{p} = \int_{\Omega} (\nabla \mathbf{N}_{w})^{T} \mathbf{k}_{w} \rho^{w} \mathbf{b} \mathrm{d}\Omega - \int_{\Gamma_{p}^{q}} \mathbf{N}_{p}^{T} \frac{q^{w}}{\rho^{w}} \mathrm{d}\Gamma \quad - \text{ external node forces vector acting on pore water (6.53k)}$$

and

$$\frac{1}{Q_{w}} = C_{s} + \frac{nS_{w}}{K^{w}} + \frac{(\alpha - n)}{K^{s}} S_{w}^{2} \left(1 + \frac{C_{s}}{nS_{w}} p_{w} + \frac{S_{g}}{S_{w}} \frac{\partial p_{gw}}{\partial p_{w}} \right) \tag{6.53l}$$

$$C_{s} = n \frac{\partial S_{w}}{\partial p_{w}} \tag{6.53m}$$

$$\frac{1}{Q} = -C_{s} + \frac{nS_{g}}{K^{g}} \frac{\partial p_{gw}}{\partial p_{w}} + \frac{(\alpha - n)}{K^{w}} S_{w} S_{g} \left(1 + \frac{C_{s}}{nS_{w}} p_{w} + \frac{S_{g}}{S_{w}} \frac{\partial p_{gw}}{\partial p_{w}} \right) \tag{6.53n}$$

in the case of fully saturated soil, we have $S_{w} = 1$ and $C_{s} = 0$.

6.7. Numerical approximation of unbounded soil domain

6.7.1. Introduction

Computational problems with an unbounded soil domain need to introducing special boundary condition. Frequently in engineering problems, the following computational methods are used: finite element method – FEM; boundary (integral) element method – BEM; finite difference method – FDM; discrete element method – DEM and meshless method. Problems in an unbounded domain can often be solved using the boundary element method in terms of both static and dynamic analysis.

In terms of the finite element method the unbounded domain is truncating to the domain around the region of interest (referred to as the interior), applying so calling absorbing boundary conditions – ABC. On this artificial boundary, the special boundary conditions, different for statics and dynamics problems are proposed. In the case of static problems, the condition is to fulfil the disappearance of displacement towards unlimited (disappearance of the potential energy). In the case of dynamic problems, apart from the disappearance of displacement, the disappearance of acceleration should be fulfilling (disappearance of kinetic energy). Many researchers have proposed several ABCs since the 1970s, which can be classified into two broad classes: direct method (based on differential equation) and sub-structure method (based on sub-domain approached).

6.7.2. Conditions of disappearing of kinetic energy

An absorbing boundary condition on FEM mesh in dynamics problem is considered.

Considerations start for a one–dimensional dilatation wave propagation problem in an infinite area. Pressure p is known on the surface dA at the initial time. A dilatational wave propagates at the speed of c_p, and after dt time cover pdtdA area. The momentum in this area is $\rho c_p \mathrm{d}t A\dot{u}$, where ρ is the medium density and $\dot{u}$ is the wave propagation speed in a direction normal to the artificial boundary. In accordance with the principle of conservation of momentum, one can obtain the condition

$$p\mathrm{d}A\mathrm{d}t = \rho c_p \mathrm{d}t\mathrm{d}A\dot{u} \tag{6.54}$$

hence

$$p = \rho c_p \dot{u}. \tag{6.55}$$

Equation (6.55) gives information that the dilatational incident wave pressure p is balanced with the viscous damper $\rho c_p \dot{u}$ (damping force) located on the artificial boundary.

Similar consideration is used for the transverse wave, to give the damping force $\rho c_s \dot{v}$, where $\dot{v}$ is the wave propagation speed in direction tangential to the artificial boundary.

In the angular frequency range ω, the theoretical radiation condition was given by Sommerfield (1949) in the case of the scalar wave equation in the form of:

$$\lim_{r\to\infty} r^{\frac{s-1}{2}} \left[u(\omega)_{,r} + \frac{i\omega}{c} u(\omega) \right] = 0, \tag{6.56}$$

where:

$u(\omega)$ – displacement amplitude according to wave direction
c – wave propagation speed
s – space dimension, $s = 2$ or $s = 3$.

Note: Part of equation (6.56) written in square brackets is equivalent to equation (6.55) with notation $c = c_p = \sqrt{(\lambda + 2G)/\rho}$, $p(\omega) = -(\lambda + 2G)u(\omega)_{,r}$ and λ, G – Lame's constants.

6.7.3. Sub-structure and direct method

A structure staying on soil (with finite shape) can be cover by FEM mesh with a finite number of degrees of freedom. A similar FEM mesh cannot be applied to the unbounded soil domain. Thus, in the soil structure interaction analysis in FEM computation, there are two main approaches explained below.

Sub-structure method – (Figure 6.3a) proposes use of a finite element mesh on the area of the structure itself and the surrounding soil area (in which the nonlinear deformation occurs) up to the artificial boundary. It is assumed that outside of the artificial boundary, a linear deformations occur and there is no need to analyse this area. Thus, FEM elements on the artificial boundary should approximate the elastic infinite area in space and in time domain.

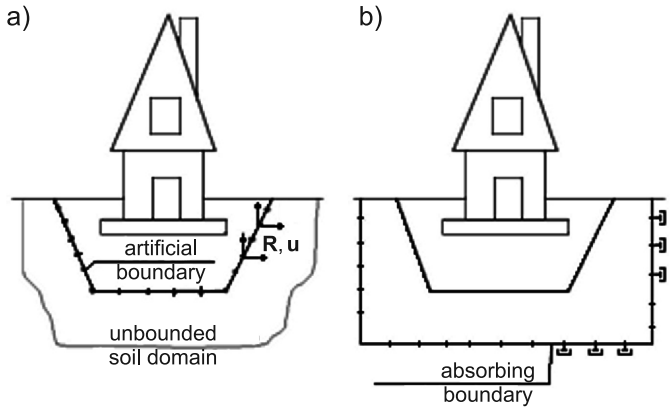

Fig. 6.3. Numerical approximation of unbounded soil domain: a) sub-structure method, b) direct method

Relationship between global forces **R** and global displacement **u** in space and time domain on an artificial boundary is formulated (Figure 6.3a). The interaction forces **R** in the given degree of freedom in the considering time depends on displacement in all degrees of freedom on the absorbing boundary and all previous time. This is due to the fact that the forced displacement of a unit pulse in the degree of freedom causes forces in all degrees of freedom at the boundary of the currently considered time and subsequent times. Thus, force vector (interaction) $\mathbf{R}(t)$ in all degrees of freedom at the artificial boundary of a given time t is equal to the convolution integral of the response matrix per unit pulse displacement $\mathbf{S}^{\infty}(t)$ and displacement vector $\mathbf{u}(t)$ in the form:

$$\mathbf{R}(t) = \int_0^t \mathbf{S}^{\infty}(t-\tau)\,\mathbf{u}(\tau)\,\mathrm{d}\tau \tag{6.57}$$

where:

$\mathbf{S}^{\infty}(t)$ – the dynamic stiffness matrix in the time domain,

∞ – indicator refers to the infinite outside area.

In the angular frequency range ω

$$\mathbf{R}(\omega) = S^{\infty}(\omega)\,\mathbf{u}(\omega) \tag{6.58}$$

where:

$\mathbf{S}^{\infty}(\omega)$ – the dynamic stiffness matrix in the frequency domain ω.

The system equations of motion of the soil-structure interaction problem are sum of the interaction forces $\mathrm{R}(t)$ according to (6.57) and the equations of motion of the structure itself.

In the sub-structure method, the interaction forces can be defined by equation (6.57) in time domain or by (6.58) in frequency domain. Modification of the substructure method is the similarity method. This method in the case of 2D is shown in Figure 6.4, where centre point O is the reference point – the distance of any point from the origin O is indicated by '*r*'.

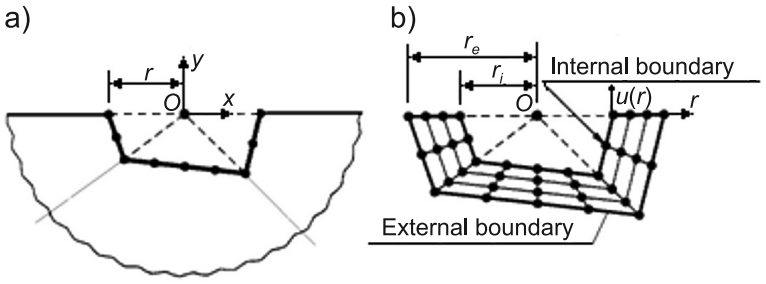

Fig. 6.4. Similarity method: a) sub-structure method, b) direct method

In the sub-structure similarity method (Figure 6.4a), coefficients of the dynamic stiffness matrix $\mathrm{S}^{\infty}(t)$ or $\mathrm{S}^{\infty}(\omega)$ are calculated on the basis of the response unit function (Green function) depend on distance *r*.

Direct method – (Figure 6.3b) proposes use of a one area with a structure staying on soil and some domain of the surrounding soil. In the finite elements discretization, the artificial boundary is defined as the absorbing boundary area. The absorbing boundary is designed to absorb the dynamics of oncoming waves without the possibility of reflection or refraction. The direct method proposes the determination of the absorbing forces $\mathbf{R}(t)$ on the boundary in a simplified manner.

The direct method also uses the central point *O*, with radial lines of finite elements (Figure 6.4b). In this case, the shape function of elements relate to a central point *O* and decay condition at infinity is satisfied without the use of an analytical solution.

In the pioneering work of Dasgupta (1982), this approach was called 'cloning' and given an average dynamic stiffness matrix.

The response matrix of the unit impulse can be determined in two ways:

– **prediction method** – this method assumes the presence of two or three layers of elements at the boundary (Figure 6.4b), which arranged radially with respect to point *O* between the internal and external areas. The response matrix of the unit impulse of the external boundary is determined by the response matrix of the unit impulse of the internal boundary and the transit time by the layers,
– **method of infinitesimal finite element** – this method assumes the existence of one element layer at the boundary relative to point *O*.

6.7.4. Approximate methods

Approximate methods are used in the direct methods (Figure 6.3b) with acceptable solution error. The absorbing boundary should be here at a sufficient distance from a structure and the potential and kinetic radiation energy condition should have satisfied in an approximate way.

Many approximate methods have been proposed, most of them are based on the theory of wave propagation:

– the most commonly used in computer programs is *the absorbing viscous dampers* (viscous boundary) consisting of the wave propagation of absorbing dampers in a direction perpendicular to the boundary (see equation [6.55]),
– another approach is *the averaging solution boundary* (superposition boundary) – this averages the two boundary solutions: symmetric (with fixed boundary) and anti-symmetric (with free boundary) eliminating the reflected wave,
– the next approach is *the enhanced absorption boundary* (paraxial boundary) in which the differential equation is introduced to strengthen the outgoing wave,
– another approach is *the boundary with double approximation* (double-asymptotic boundary). This boundary consists of the viscous dampers and the springs asymptotically exact in the high and low frequencies for the incident wave perpendicular to the boundary,
– next is *the extrapolation boundary*, this is the estimated wave propagation velocity on the basis of information collected from the nodes close to the boundary.

Another popular proposition is to use the infinite element. In this case, the shape function should ensure the disappearance of wave propagation in the direction of the infinite element in the frequency domain. Such an element in the sense of FEM is inaccurate, because if the element size tends to infinity, the solution error does not tend to zero.

6.8. The experience of the research program VELACS

6.8.1. Program VELACS

The computer programs use single–phase and multiphase models with different plasticity hypotheses. Verification of these proposals is based on the comparison of calculation results with the results of full-scale soil research.

In the natural scale researches there are following problems:

– definition of the research area compared to the real infinite soil domain,
– setting track measuring sensors, their scope and signal analysis measurement,
– build a proper force dynamic excitation,
– economic analysis of studies.

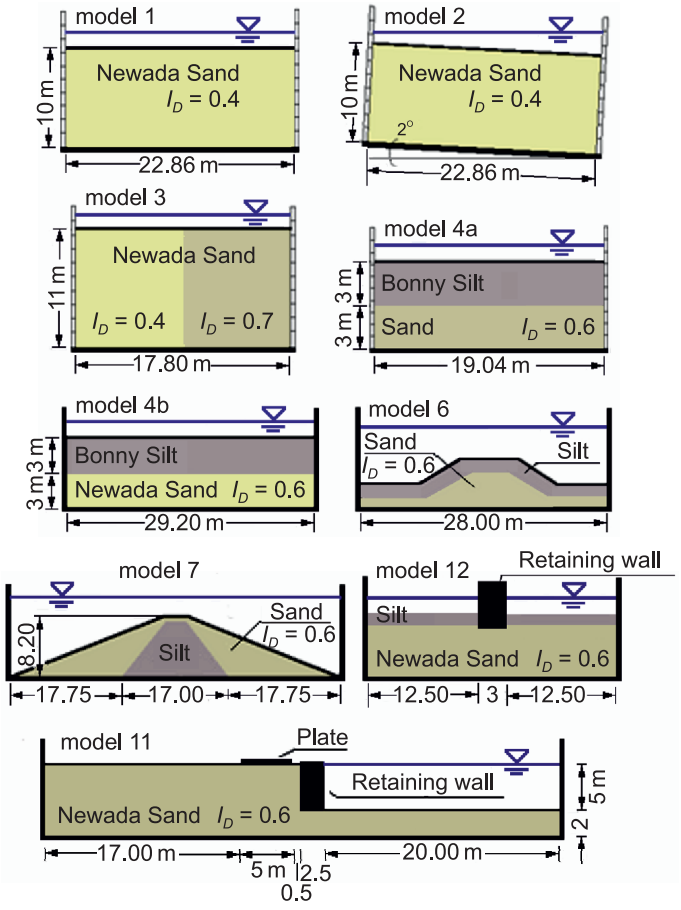

Fig. 6.5. Summary of research models in the VELACS program

Due to these difficulties of research in the natural scale, today it is possible to perform tests in the geotechnical centrifuge, which allows the soil deformation simulation under dynamic loading. The results of these tests are used to verify the numerical models, especially verification of soil liquefaction models.

Centrifuge equipment was already being used in the 1960s to simulate the stress of gravity, Roscoe (1968). Currently, in the geotechnical centrifuge, it is possible to test for any time-varying loads, such as seismograph records.

In 1993, the research program called VELACS was conducted (*Verification of Liquefaction Analysis by Centrifuge Studies*, 1992, *Technical report*, *Earth Technology Project No. 90-0562*), the aim of which was to verify the numerical models describing the phenomenon of soil liquefaction on seismic excitation. The VELACS program included testing nine selected models of geotechnical centrifuges and comparing them with the numerical calculations. A summary of test models is shown in Figure 6.5.

6.8.2. Estimation of results from centrifuge tests

Many research centres dealing with the soil dynamics joined the VELACS program. The aim of this program was verification of numerical models the following variables: pore water pressure; displacement, and acceleration of soil skeleton. The verification procedure was divided into two steps:

- Step A – numerical calculation for proposed samples (shown above) at a given time-load excitation, based on own research centre models. The research centre received soil samples (Newada sand and Bonny silt) with the possibility to execute their own laboratory testing. At this stage, research centres did not know the results of the centrifuge tests.
- Step B – comparison of the results obtained in step A with the results of the centrifuge tests.

Verification of numerical models were based on comparing measurement results from centrifuge with numerical results.

The results of geotechnical centrifuge tests carried out in different centres are not compatible, therefore, there was a problem determining set of correct results. The reasons for the incompatibility of the measurement results was both the low number of tests (insufficient) and the different measuring apparatus used in various centres. Under these conditions, it was necessary to adopt criteria for the selection of results and the averaged measurement error.

The calculation results obtained in research centres differ from each other and were different from the results of the centrifuge; therefore, direct comparison of results was difficult. The causes of incompatibility calculation results, besides the use of different models in different centres, were as follows:

– error of scale between the laboratory model and the numerical model;
– errors of boundary conditions;
– errors of sample measuring, soil layers and measuring equipment;
– inaccurate representation of the seismic excitation;
– inaccuracies of pressure sensors, displacement sensors and acceleration, and inaccuracies of the measuring equipment.

Table 6.1 presents a list of research centres that performed centrifuge tests. In laboratory tests, the same soil models were tested (see Figure 6.5) as those in the geotechnical centrifuge. However, the individual laboratories were using the following different types of centrifuges:

– Centre for Geotechnical Modelling at the University of California at Davis (Figure 6.6), opened in 1988. The centrifuge was made by UC Davis and NASA. Basic technical specifications are: radius arm 9.1 m, dimensions of the test area 2.14 × 1.88 × 1.88 m, acceleration × mass = 240 g × t, maximum acceleration – 53 g, maximum mass of samples 4.5 t.

Fig. 6.6. Centre for Geotechnical Modelling at the University of California at Davis

– Geotechnical Centrifuge Laboratory of the University of Colorado AT Boulder (Figure 6.7), opened in 1988. Basic technical specifications are: radius arm 5.5 m, dimensions of the test area 1.22 × 1.22 × 0.91 m, acceleration × mass = = 400 g × t, maximum mass of samples 1.78 t.

Fig. 6.7. Geotechnical Centrifuge Laboratory of the University of Colorado AT Boulder

– Geotechnical Centrifuge Centre, Rensselaer Polytechnic Institute (Figure 6.8), opened in 1989. The centrifuge was made by Acutronic Machines (France). Basic technical specifications are: radius arm 3.0 m, dimensions of the test area 1.00 × 1.00 × 0.80 m, acceleration × mass = 150 g × t, maximum acceleration 200 g, maximum mass of samples 1.00 t.

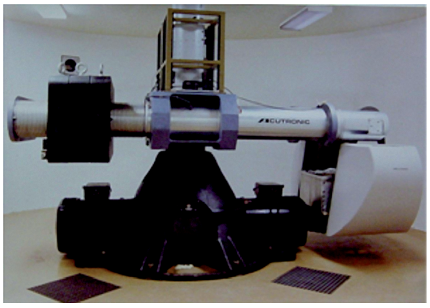

Fig. 6.8. Geotechnical Centrifuge Centre, Rensselaer Polytechnic Institute

Table 6.1

List of research centres that performed centrifuge tests

Model No	Test type	Laboratory	Number of tests
1	Primary Repeated Repeated	RPI UC Davis CU Boulder	3
2	Primary Repeated Repeated	RPI UC Davis Caltech	3
3	Primary Repeated Repeated	Caltech RPI UC Davis	2
4a	Primary Repeated Repeated	UC Davis RPI Caltech	3
4b	Primary Repeated Repeated	UC Davis RPI CU Boulder	3
6	Primary	UC Davis	1
7	Primary Repeated Repeated	CU Boulder RPI UC Davis	3

cd. tab. 6.1

11	Primary	Cambridge	1
12	Primary Repeated Repeated	PU (4 tests) RPI UC Davis (2 tests)	7

Abbreviations research centres:
RPI – Rensselaer Polytechnic Institute,
UC Davis – University of California, Davis,
CU Boulder – Colorado Univ. AT Boulder,
Caltech – California Institute of Technology,
PU – Princeton University,
Cambridge – Cambridge University (UK).

Table 6.2

Summary of the results of numerical calculations performed in step A

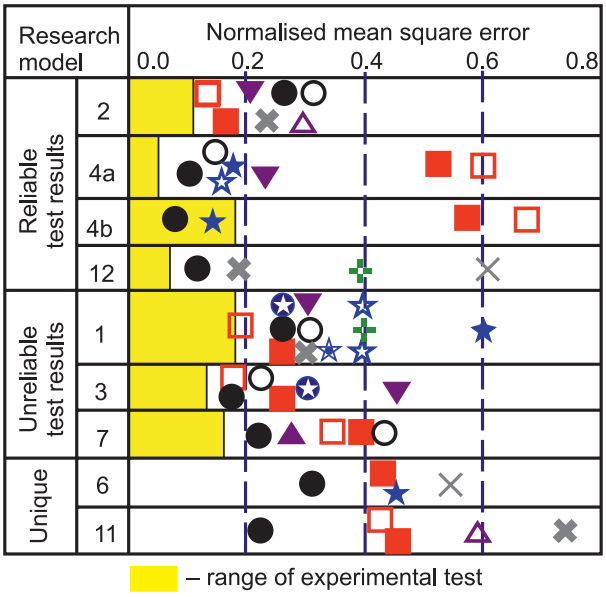

The VELACS research program has contributed to the verification of the various numerical models used to simulate soil liquefaction. Results of soil displacements and accelerations were divergent and no attempt was made to compare them. Only the results of the pore pressure were verified. The work of Pepescu and Prevost (1995) shows how to estimate the validity of the results of pore pressure.

Table 6.2 summarizes the results of calculations performed in step A by the various research centres and the comparison of the normalised mean square error.

Estimation of the constitutive model used in calculation

Dafalias (1994) tried to estimate constitutive models based on the results of calculations of pore pressure in the VELACS. A summary of results obtained using different constitutive equations is provided in Table 6.3. The calculation results are related to the average results of the measurements of pore pressure in the centrifuge. Constitutive models used to describe of soil skeleton non-linear deformation can be divided into three groups:

– multi-yield surface or recessed yield surface (indicated by a circle);
– generalized plasticity (as squares),
– bounding surface (indicated by a star).

Table 6.3

Names of research centres, computer programs and constitutive models

Research centre	Computer program name	Symbol	Constitutive model
Princeton University	DYNAFLOW	●	Multi-yield
Tufts University	DYNAFLOW	○	plasticity
University Collage Swansea	SWANDYNE4	■	Generalized plasticity
Glasgow University	DIANA–SWANDYNE	□	Generalized plasticity
Leighton & Assoc.	DYSA C2	★	Bounding surface
ETC	DYSA C2	☆	Bounding surface
U. South. Calif.	LINOS	✪	Bounding surface
UC Davis	SUMDES	★	Bounding surface
University Tokyo		★	Bounding surface
CU Boulder	LIQCA	×	Classical plasticity
Takeneka Copr.		✖	Classical plasticity
University Nevada Reno	TARA–2	▼	Direct
Damek & Moore	FLAC	▲	Direct
University Tokyo (Towhata)	Exact solution	△	Empirical
Brigham Young University	QUAD4	✣	Total stress

From Table 6.2, which presents comparison of the results performed in step A, it follows that:

– for test models 1 and 2, the results of numerical simulation of all the constitutive equations are close to the results of the experiment. In the case of model 2, the results obtained from the model of generalized plasticity were close to results

of the experiment, while the numerical results from the multi-yield surface model and the bounding surface model were greater than those obtained in the experiment,
– in the case of vertical layers of sand (model 3), the results of numerical simulation obtained from the experiment were close to both the generalized plasticity model as well as multi–yield surface plasticity,
– in the case of two horizontal layers of sand (model 4a and 4b), the results of numerical simulation were close to both the multi-yield surface plasticity model and the bounding surface model, while for the generalized plasticity model, results were lower than those obtained in the experiment,
– for models with an embankment (models 6 and 7), and models with a retaining wall (models 11 and 12), the results of numerical simulation and experiment were close to both the generalized plasticity model and those of multi-yield surface plasticity.

6.9. References to Chapter 6

Brezzi F., Fortin M. (1991): *Mixed and Hybrid Finite Element Methods*, Springer: Berlin, Heidelberg, New York.

Chan A.H.C. (1988): *A Unified Finite Element Solution to Static and Dynamic Geomechanics Problems*, Ph.D. Dissertation, University College of Swansea, Wales.

Chen W.F., Mizuno E. (1990): *Nonlinear analysis in soil mechanics. Theory and Implementation*, Developments in Geotechnical Engineering, Vol. 53, Elsevier.

Dafalias Y.F. (1994): *Overview of constitutive models used in VELACS*, [in:] Proc. Int. Conf. on Verif. Numerical Proc. For the Analysis of Soil Liq. Problems, Vol. 2, Balkema, Rotterdam, 1293-1303.

Dasgupta G. (1982): *A finite element formulation for unbounded homogeneous continua*, Journal of Applied Mechanics, ASME, Vol. 49, 136-140.

Drucker D.C., Prager W. (1952): *Soil mechanics and plastic analysis of limit design*, Quart. Appl. Math., 10, 157-165.

Fredlund D.G., Rahardjo H. (1993): *Soil Mechanics for Unsaturated Soils*, Wiley: New York.

Griffiths D.V., Smith I.M. (1998): *Programming the Finite Element Method*, John Willey & Sons.

Hassanizadeh S.M., Gray W.G. (1979): *General conservation equation for multi--phase system: 1. Averaging procedure*, Advances in Water Resources, 2, 131--144.

Lewis R.W., Schrefler B.A. (1998): *The Finite Element Method in Static and Dynamic Deformation and Consolidation of Porous Media*, 2nd ed., John Wiley & Sons, Chichester.

Muraleetharan K.K., Wei C.F, Liu C. (2006): *A comprehensive approach to modelling the behaviour of unsaturated soils using an elastoplastic framework*, [in:] *Geomechanics II: Testing, Modelling, and Simulation*, Lade PV, Naki T. (eds). GSP No. 156, Geo-Institute, ASCE, *Proceedings of the Second Japan–U.S. Workshop on Testing*, *Modelling*, *and Simulation in Geomechanics*, Kyoto, Japan, 515-527.

Popescu R., Prevost J.H. (1995): *Comparison between VELACS numerical 'class A' predictions and centrifuge experimental soil test results*, Soil Dynamics and Earthquake Engineering, 14, 79-92.

Ravichandran N. (2009): *Fully coupled finite element model for dynamics of partially saturated soils*, Soil Dynamics and Earthquake Engineering, 29, 1294-1304.

Ravichandran N., Muraleetharan K.K. (2009): *Dynamics of unsaturated soils using various finite element formulations*, Int. J. Numer. Anal. Meth. Geomech, 33, 611-631.

Roscoe K.H. (1968): *Soils and model tests*, J. Strain Analysis, 1968, 3(1), 57-64.

Schrefler B.A., Simoni L, Xikui L, Zienkiewicz O.C. (1990): *Mechanics of partially saturated porous media*, [in:] *Numerical Methods and Constitutive Modelling in Geomechanics*, Desai CS, Gioda G (eds). CISM Lecture Notes. Springer: Wein, 169-209.

Sikora Z. (2006): *Sondowanie statyczne. Metody i zastosowanie w geoinżynierii*, Wydawnictwo Naukowo-Techniczne, Warszawa.

Sommerfield A. (1949): *Partial Differential Equations in Physics*, Chapter 28, Academic Press, New York.

Toll D.G. (1995): *A conceptual model for the drying and wetting of soil*, Unsaturated Soils (eds. Alonso & Delage), Balkema, Rotterdam, 805-810.

The Earth Technology Corporation, VELACS laboratory testing program soil data report (1992), Technical report, Earth Technology Project No. 90-0562.

Truesdell C. (1955): *Hypo-elasticity*, Journ. Rational Mech. Anal., 4, 83-133, 1019--1020.

Truesdell C. (1956): *Hypo-elastic shear*, Journ. Appl. Phys., 27, 441-447.

Wei C.F., Muraleetharan K.K. (2002a): *A continuum theory of porous media saturated by multiphase fluids: I. Linear poroelasticity*, International Journal of Engineering Science, 40, 1807-1833.

Wei C.F., Muraleetharan K.K. (2002b): *A continuum theory of porous media saturated by multiphase fluids: II. Lagrangian description and variational structure*, International Journal of Engineering Science, 40, 1835-1854.

Wolf J. P., Song Chongmin (1966): *Finite-element modelling of unbounded media*, John Wiley & Sons.

Wolf J.F. (1988): *Soil-Structure-Interaction Analysis in Time Domain*, Prentice–Hill, Englewood Cliffs.

Xikui L., Zienkiewicz O.C. (1992): *Multiphase flow in deforming porous media and finite element solution*, Computers and Structures, 45(2), 211-227.

Zienkiewicz O.C., Shiomi T. (1984): *Dynamic behaviour of saturated porous media; The generalized Biot formulation and its numerical solution*, International Journal for Numerical Methods in Geomechanics, 8, 71-96.

Zienkiewicz O.C., Chan A.H.C., Pastor M., Schrefler B.A., Shiomit T. (2000): *Computational Geomechanics with reference to Earthquake Engineering*, John Wiley & Sons.

Zienkiewicz O.C., Taylor R.L. (2000): *The Finite Element Method-Solid Mechanics (5th edn)*, Butterworth-Heinemann Publication: Oxford, 2000; 459. ISBN 0 7506 5055 9, 2.

Chapter 7

NUMERICAL INTEGRATION OF FINITE ELEMENT EQUATIONS OF MOTION

7.1. Notations used in Chapter 7

$\mathbf{M}$	–	mass matrix
$\mathbf{C}$	–	matrix of viscous damping
$\mathbf{K}$	–	stiffness matrix
$\mathbf{f}(t)$, $\mathbf{f}_t$	–	vector of nodal load at t time
$\ddot{\mathbf{d}}(t)$, $\ddot{\mathbf{d}}_t$	–	vector of acceleration in nodes at t time
$\dot{\mathbf{d}}(t)$, $\dot{\mathbf{d}}_t$, $\mathbf{v}(t)$, $\mathbf{v}(t)$	–	vector of velocity in nodes at t time
$\mathbf{d}(t)$, $\mathbf{d}_t$	–	vector of displacement in nodes at t time
$\mathbf{\Phi}$	–	matrix of eigenvectors
$\mathbf{\Psi} = \mathrm{diag}\{2\xi_1\omega_1, 2\xi_2\omega_2, \ldots\}$	–	diagonal matrix of viscous damping
ω_i	–	angular frequency of i-th eigenvector [rad/s]
ξ_i	–	critical damping coefficient of i-th eigenvector
$\mathbf{A}$	–	iteration matrix, amplification matrix, transition matrix in numerical integration of equation of motion
$\rho(\mathbf{A}) = \max(\lvert\lambda_1\rvert, \lvert\lambda_2\rvert, \ldots)$	–	spectral radius of iteration matrix $\mathbf{A}$
λ_i	–	i-th eigenvalue of iteration matrix $\mathbf{A}$
$\tilde{\delta}$	–	logarithmic decrement of *parasite damping* of numerical integration of equation of motion
$RE(\tilde{\Omega})$	–	relative period error of numerical integration of equation of motion
$f_m \geq \dfrac{1}{2\Delta t}$	–	Nyquist frequency

$f_p = \dfrac{1}{\Delta t}$ – sampling frequency

k_m – wave number

λ_m – wavelength

c – wave phase velocity

$L_{\text{ele}} = \lambda_m / 2$ – dimension of element for analysis of wave propagation

$\ddot{\mathbf{u}}$ – nodal acceleration of finite element method mesh

$\dot{\mathbf{u}}$ – nodal velocity of finite element method mesh

$\mathbf{u}$ – nodal displacement of finite element method mesh

$\mathbf{p}$ – nodal pore pressure of finite element method mesh

n_u – number of degrees of freedom of nodal displacement

n_p – number of degrees of freedom of nodal pore pressure

7.2. Introduction

The finite element equations of motion are considered

$$\mathbf{M}\ddot{\mathbf{d}}(t) + \mathbf{C}\dot{\mathbf{d}}(t) + \mathbf{K}\mathbf{d}(t) = \mathbf{f}(t), \tag{7.1}$$

where:

$\mathbf{M}$, $\mathbf{C}$, $\mathbf{K}$ – mass, damping and stiffness matrix respectively,

$\mathbf{f}(t)$ – vector of nodal load at t time,

$\ddot{\mathbf{d}}(t)$, $\dot{\mathbf{d}}(t)$, $\mathbf{d}(t)$ – vector of acceleration, velocity and displacement in FEM mesh nodes at t time respectively,

$\mathbf{M}\ddot{\mathbf{d}}(t)$ – presents the inertial forces,

$\mathbf{C}\dot{\mathbf{d}}(t)$ – presents the damping forces,

$\mathbf{K}\mathbf{d}(t)$ – presents the stiffness forces.

Equation (7.1) is a system of differential equations of the second order. If the parameters of a system (mass, damping and stiffness) are constant, independent of the deformation and time-invariant, then equation (7.1) presents a system of second-order differential equations with constant coefficients.

In terms of the finite element method to solve equation (7.1), two main methods are used:

1. modal superposition method, especially for linear problems and problems with low non-linearity;
2. direct numerical integration of (7.1) over time, both to the linear and non-linear problems.

7.3. Modal superposition method

The modal superposition method leads to uncoupling system (7.1) with n degrees of freedom on set of n independent equations with one degree of freedom. For this purpose, the transformation is used from the initial Cartesian coordinate system to the eigenvectors system. Orthogonal transformation is introduced using eigenvectors:

$$\ddot{\mathbf{d}}(t) = \mathbf{\Phi}\ddot{\mathbf{u}}(t), \quad \dot{\mathbf{d}}(t) = \mathbf{\Phi}\dot{\mathbf{u}}(t), \quad \mathbf{d}(t) = \mathbf{\Phi}\mathbf{u}(t), \tag{7.2}$$

where:

$\mathbf{\Phi}$ – the matrix of eigenvectors.

Substituting (7.2) to (7.1) and left-multiplying by $\mathbf{\Phi}^T$, obtained:

$$\mathbf{\Phi}^T\mathbf{M}\mathbf{\Phi}\ddot{\mathbf{u}}(t) + \mathbf{\Phi}^T\mathbf{C}\mathbf{\Phi}\dot{\mathbf{u}}(t) + \mathbf{\Phi}^T\mathbf{K}\mathbf{\Phi}\mathbf{u}(t) = \mathbf{\Phi}^T\mathbf{f}(t). \tag{7.3}$$

In terms of the finite element method, a generalized eigenproblem is determined by the equation:

$$\mathbf{K}\mathbf{\Phi} = \mathbf{M}\mathbf{\Phi}\mathbf{\Omega}^2 \tag{7.4}$$

where:

$\mathbf{\Omega}^2 = \text{diag}\{\omega_1^2, \omega_2^2, \ldots\}$ – diagonal matrix of angular frequency ω.

Eigenvectors satisfy the following properties (Bathe, 1996):

$$\mathbf{\Phi}^T\mathbf{M}\mathbf{\Phi} = \mathbf{I} \tag{7.5}$$

i.e. they are orthogonal with respect to $\mathbf{M}$, and

$$\mathbf{\Phi}^T\mathbf{K}\mathbf{\Phi} = \mathbf{\Omega}^2. \tag{7.6}$$

If the viscous damping model is used as the damping model, then it is also takes the following property:

$$\mathbf{\Phi}^T\mathbf{C}\mathbf{\Phi} = \mathbf{\Psi} \tag{7.7}$$

where:

$\mathbf{\Psi} = \text{diag}\{2\xi_1\omega_1, 2\xi_2\omega_2, \ldots\}$ – diagonal matrix of viscous damping model,

ξ_i – critical damping coefficient of i-th eigenvector.

Including equations from (7.4) to (7.7) in the equation (7.3) one can obtain relation:

$$\begin{Bmatrix} \ddot{u}_1(t) \\ \ddot{u}_2(t) \\ \vdots \\ \ddot{u}_n(t) \end{Bmatrix} + 2\xi_i\omega_i \begin{Bmatrix} \dot{u}_1(t) \\ \dot{u}_2(t) \\ \vdots \\ \dot{u}_n(t) \end{Bmatrix} + \omega_i^2 \begin{Bmatrix} u_1(t) \\ u_2(t) \\ \vdots \\ u_n(t) \end{Bmatrix} = \mathbf{\Phi}_i^{\mathrm{T}} \mathbf{f}(t) \tag{7.8}$$

for subsequent angular frequency ω_i and corresponding eigenvector $\mathbf{\Phi}_i$, $i = 1, 2, \ldots, n$.

Matrix equation (7.8) is a set of n independent equations of motion with one degree of freedom. Each of these separate equations can be solved using the Duhamel integral (see equation (C.31) in Appendix C).

After determining the acceleration $\ddot{\mathbf{u}}(t)$, velocity $\dot{\mathbf{u}}(t)$ and displacement vector $\mathbf{u}(t)$ at time points t, the solution in the initial coordinate system is achieved by using an orthogonal projection of eigenvectors, in accordance with (7.2).

7.4. Numerical integration methods of finite element equations of motion

Direct numerical integration of the equations of motion (7.1) over the time is perform by the step-by-step integration method in a discrete time steps, where the word „*direct*" means that there is no transformation of equation (7.1). Direct integration is based on two assumptions:

– integration of equation (7.1) is performed only in discrete time steps,
– the so-called *integration scheme* is proposed as the formula for displacement, velocity and acceleration of the transition from time step t to time step $t + \Delta t$, where Δt is the time increment (time step).

Each of the proposed integration schemes is analysed for stability and accuracy in order to determine a convergence error level.

It is assumed that the solution of equation (7.1) at time $t = 0$ is known by the initial condition in the form of displacement vector $\mathbf{d}(0)$ and velocity vector $\dot{\mathbf{d}}(0)$.

Usually the constant time step $\Delta t = T/n$, where T is the final time of dynamic analysis and n is the number of time steps is used in an integration scheme over the time interval (0, T].

In the case of the linear dynamic problem, the results obtained by the modal superposition and direct integration methods is the same. The solution for both methods, in this case, are based on this same equation of motion (built on the same matrices – **K**, **M**, **C**), and this same orthogonal eigenvectors $\mathbf{\Phi}$ and eigenvalues $\mathbf{\Omega}^2$. Thus, in the analysis of the convergence and accuracy of the integration scheme, instead of considering the system of equations of motion (7.1), one can consider a set

of independent equations with one degree of freedom (7.8). Time step Δt will apply to all n equations representing various eigenfrequencies $\omega_i = 2\pi / T_i$.

It is sufficient to consider the typical equation of motion (see equation (C.1b) in Appendix C):

$$\ddot{u} + 2\xi\omega\dot{u} + \omega^2 u = r \tag{7.9}$$

and analyse the effect of the $\Delta t/T$ on the convergence and accuracy of the proposed integration scheme.

Analysis of convergence of an iterative process

Knowing the solution at time t, $\{q(t_n), \dot{q}(t_n)\}$ and the solution in the next time step $t + \Delta t$, $\{q(t_{n+1}), \dot{q}(t_{n+1})\}$, according to the formula (C.37), one can obtain:

$$\begin{Bmatrix} q(t_{n+1}) \\ \dot{q}(t_{n+1}) \end{Bmatrix} = \mathbf{A} \begin{Bmatrix} q(t_n) \\ \dot{q}(t_n) \end{Bmatrix} + \mathbf{L}_n^{n+1}. \tag{7.10}$$

In time interval $(0, T]$ at a constant time step, $\Delta t = T/n$ is performed calculation:

$$\begin{Bmatrix} q(t_{n+1}) \\ \dot{q}(t_{n+1}) \end{Bmatrix} = \mathbf{A} \left\{ \mathbf{A} \left\{ \mathbf{A} \begin{Bmatrix} q(t_{n-2}) \\ \dot{q}(t_{n-2}) \end{Bmatrix} \cdots \right\} + \mathbf{L}_{n-2}^{n-1} \right\} + \mathbf{L}_{n-1}^{n} \Bigg\} + \mathbf{L}_n^{n+1} \tag{7.11a}$$

or

$$\begin{Bmatrix} q(t_{n+1}) \\ \dot{q}(t_{n+1}) \end{Bmatrix} = \mathbf{A}^n \begin{Bmatrix} q(t_0) \\ \dot{q}(t_0) \end{Bmatrix} + \mathbf{A}^{n-1}\mathbf{L}_{n-1}^{n} + \mathbf{A}^{n-2}\mathbf{L}_{n-2}^{n-1} + \cdots + \mathbf{L}_n^{n+1}. \tag{7.11b}$$

The iterative convergence process described by equation (7.11b) depends on the transition matrix $\mathbf{A}^n$, in particular, the spectral radius $\rho(\mathbf{A}) = \max(|\lambda_1|, |\lambda_2|)$, where λ_1, λ_2 are eigenvalues of matrix $\mathbf{A}$.

The exact analytical transition matrix $\mathbf{A}$ is of the form (see Equation C.37c Appendix C):

$$\mathbf{A} = \begin{bmatrix} \cos\omega\Delta t & \dfrac{1}{\omega}\sin\omega\Delta t \\ -\omega\sin\omega\Delta t & \cos\omega\Delta t \end{bmatrix}, \tag{7.12}$$

where $\lambda_1 = \lambda_2 = 1$.

This means that calculation defined by (7.11) with matrix $\mathbf{A}$ according to (7.12), do not introduce numerical error to displacement $q(t_{n+1})$ and velocity $\dot{q}(t_{n+1})$ in the following time steps $(n + 1)\Delta t$.

The condition for convergence is:

$$\rho(\mathbf{A}) \leq 1. \tag{7.13}$$

Analysis of accuracy: error of amplitude and error of period

The test problem of damped free vibration is considered

$$\ddot{d}(t) + 2\xi\omega\dot{d}(t) + \omega^2 d(t) = 0 \tag{7.14}$$

with initial conditions: $d(0) = 1$, $\dot{d}(0) = 0$, where the solution for $\xi = 0$ is $d(t) = \cos(\omega t)$.

The accuracy analysis determines the error between the analytical solution $d(t) = \cos(\omega t)$ and the numerical solution proposed by integration scheme $\tilde{d}(t) = (1 - \Delta D)\cos(\tilde{\omega} t)$. Now we consider (Figure 7.1):

1) Amplitude error ΔD – measured by logarithmic decrement, called *parasite damping*.
2) Period error $\Delta T / T$ – measured by the ratio of the difference between the numerical solutions period $\tilde{T}$ and the analytical solutions period $\Delta T = \tilde{T} - T$ to analytical solution period T.

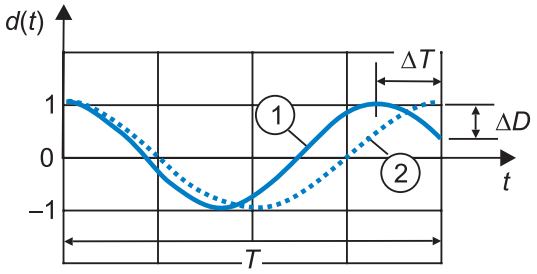

Fig. 7.1. Measurement accuracy of the integration scheme: ΔD – amplitude error; ΔT – period error; 1 – numerical solution $\tilde{d}(t) = (1 - \Delta D)\cos(\tilde{\omega} t)$, 2 – analytical solution $d(t) = \cos(\omega t)$

Amplitude error

The numerical integration scheme introduces the approximate transition matrix $\tilde{\mathbf{A}}$ instead of exact matrix $\mathbf{A}$ defined in (7.12):

$$\tilde{A} = \begin{bmatrix} \tilde{A}_{11} & \tilde{A}_{12} \\ \tilde{A}_{21} & \tilde{A}_{22} \end{bmatrix}. \tag{7.15}$$

The analytical solution of displacement $q(t)$ after time $t = T$ with initial conditions: $q_o = 1,\ \dot{q}_o = 0$ is:

$$q(t = T) = \cos \omega T = \cos 2\pi = 1. \tag{7.16}$$

Assuming that the parasitic damping is of a small size, then $\sqrt{1 - \tilde{\xi}^2} \cong 1 \rightarrow$ $\rightarrow \tilde{\omega} \approx 2\pi / \Delta t,$ hence $\tilde{\omega} \Delta t = 2\pi.$

For the case of damped free vibration (with no load), the numerical solution of displacement $q(T)$ according to (C.35a), is:

$$q(t_{t+\Delta t}) = e^{-\xi 2\pi}(\cos 2\pi + \tilde{\xi} \sin 2\pi) = e^{-\xi 2\pi} \approx 1 - 2\pi\tilde{\xi} + \frac{(2\pi\tilde{\xi})^2}{2} - \frac{(2\pi\tilde{\xi})^3}{6} + \ldots \tag{7.17}$$

Taking into account the two components of power series function $e^{-\xi 2\pi}$, the following estimate of the parasitic damping AD is obtained:

$$AD \approx e^{-2\pi\tilde{\xi}} = 1 - 2\pi\tilde{\xi}. \tag{7.18}$$

The eigenvalues λ_i of $\tilde{\mathbf{A}}$ matrix can be written as:

$$\det(\tilde{\mathbf{A}} - \lambda \mathbf{I}) = \lambda^2 - \lambda \mathrm{tr}\tilde{\mathbf{A}} + \det \tilde{\mathbf{A}} \tag{7.19}$$

and are

$$\lambda_{1,2} = \lambda \mathrm{tr}\tilde{\mathbf{A}} \pm \mathrm{i}\sqrt{\det \tilde{\mathbf{A}} - (\mathrm{tr}\tilde{\mathbf{A}})^2} = a \pm \mathrm{i}b. \tag{7.20}$$

The module of the complex eigenvalue of $\tilde{\mathbf{A}}$ matrix is

$$\left|\tilde{\mathbf{A}}\right| = |\lambda| = \sqrt{a^2 + b^2}. \tag{7.21}$$

Assuming parasitic numerical damping as viscous damping, one can obtain:

$$e^{-\xi\omega\Delta t} = \left|\tilde{\mathbf{A}}\right|. \tag{7.22}$$

The logarithm of both sides of equation (7.22), taking into account the definition of the measure of parasitic damping AD according to (7.18) with $\tilde{\xi} = \tilde{\delta} / \pi,$ where $\tilde{\delta}$ – logarithmic decrement of parasite damping, finally obtained:

$$\tilde{\delta} = -\frac{\pi}{\omega \Delta t} \ln \left|\tilde{\mathbf{A}}\right|. \tag{7.23}$$

Period error

The theory of digital signal processing, in particular, the digital filters theory, is used to estimate the period error. Numerical integration schemes may be represented in the frequency domain as the digital filter:

$$\mathbf{d}(\tilde{\Omega})_{t+\Delta t} = \mathbf{H}(\tilde{\Omega})\mathbf{d}(\tilde{\Omega})_t = \tilde{\mathbf{A}}(\tilde{\Omega})\mathbf{d}(\tilde{\Omega})_t, \tag{7.24}$$

where:

$\tilde{\Omega} = \tilde{\omega}\Delta t$, $\mathbf{d}(\tilde{\Omega})_t$ and $\mathbf{d}(\tilde{\Omega})_{t+\Delta t}$ – the Fourier spectra of solutions in time t and $t + \Delta t$,

$\tilde{\mathbf{A}}(\tilde{\Omega})$ – the Fourier spectra of numerical integration scheme,

$\mathbf{H}(\tilde{\Omega})$ – the transmittance matrix.

Each frequency $\tilde{\Omega}$ of matrix $\tilde{\mathbf{A}}(\tilde{\Omega})$ is represented by a complex number; therefore, the modulus and phase angle of the numerical integration scheme matrix $\tilde{\mathbf{A}}(\tilde{\Omega})$ is:

$$\left|\tilde{\mathbf{A}}(\tilde{\Omega})\right| = \sqrt{a(\tilde{\Omega})^2 + b(\tilde{\Omega})^2} \text{ – modulus,} \tag{7.25}$$

$$\varphi(\tilde{\Omega}) = \operatorname{arctg}\left(\frac{b(\tilde{\Omega})}{a(\tilde{\Omega})}\right) = \tilde{\Omega} \text{ – phase angle.} \tag{7.26}$$

The period error as the ratio of the difference between the numerical solutions period and the analytical solutions period to the analytical solution period is calculated as:

$$RE(\tilde{\Omega}) = \frac{\Delta T}{T} = \frac{\tilde{T} - T}{T} = \frac{\Omega - \tilde{\Omega}}{\tilde{\Omega}} \tag{7.27}$$

where:

$T = 2\pi / \omega$ – the period of differential equation (7.14),

$\tilde{T} = 2\pi / \tilde{\omega}$ – the period of the numerical integration scheme (see Figure 7.1).

7.5. Direct integration methods of equations of motion

7.5.1. Central difference method

The central difference method, Bathe (1996), used a finite difference method to approximate solutions of differential equations of motion. Figure 7.2 shows a schematic of the multipliers in the approximation of acceleration and velocity.

The central difference approximation used in time is defined as:

for acceleration $$\ddot{d}_t = \frac{1}{\Delta t^2}(d_{t+\Delta t} - 2d_t + d_{t-\Delta t}), \tag{7.28}$$

for velocity $$\dot{d}_t = \frac{1}{2\Delta t}(d_{t+\Delta t} - d_{t-\Delta t}). \tag{7.29}$$

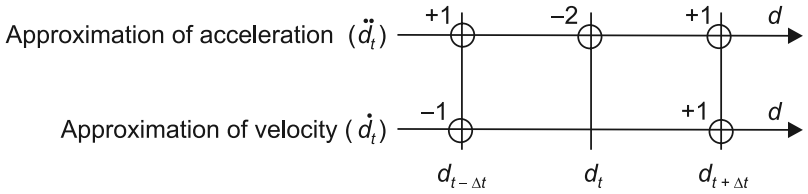

Fig. 7.2. Approximation of derivative with respect to time by the central difference

The equation of motion at time t is considered to be:

$$m\ddot{d}_t + c\dot{d}_t + kd_t = f_t. \tag{7.30}$$

By substituting the equation of motion, the acceleration approximation (7.28) and the velocity (7.29) obtained:

$$m\left[\frac{1}{\Delta t^2}\left(d_{t+\Delta t} - 2d_t + d_{t-\Delta t}\right)\right] + c\left[\frac{1}{2\Delta t}\left(d_{t+\Delta t} - d_{t-\Delta t}\right)\right] + kd_t = f_t \tag{7.31}$$

or

$$\left(\frac{1}{\Delta t^2}m + \frac{1}{2\Delta t}c\right)d_{t+\Delta t} = f_t + \left(\frac{2}{\Delta t^2}m - k\right)d_t - \left(\frac{1}{\Delta t^2}m - \frac{1}{2\Delta t}c\right)d_{t-\Delta t} \tag{7.32}$$

in the case of the matrix equation of motion with n degrees of freedom

$$\left(\frac{1}{\Delta t^2}\mathbf{M} + \frac{1}{2\Delta t}\mathbf{C}\right)\mathbf{d}_{t+\Delta t} = \mathbf{f}_t + \left(\frac{2}{\Delta t^2}\mathbf{M} - \mathbf{K}\right)\mathbf{d}_t - \left(\frac{1}{\Delta t^2}\mathbf{M} - \frac{1}{2\Delta t}\mathbf{C}\right)\mathbf{d}_{t-\Delta t}. \tag{7.33}$$

If matrices **M** and **C** are diagonal matrices, the transition of time step t to time step $t + \Delta t$ is mainly based on the performance of matrix multiplication operations by the vector. The right side of equation (7.33) presented in the form of a vector $\bar{\mathbf{f}}_t$ is:

$$\bar{\mathbf{f}}_t = \mathbf{f}_t + \left(\frac{2}{\Delta t^2}\mathbf{M} - \mathbf{K}\right)\mathbf{d}_t - \left(\frac{1}{\Delta t^2}\mathbf{M} - \frac{1}{2\Delta t}\mathbf{C}\right)\mathbf{d}_{t-\Delta t}. \tag{7.34}$$

The solution at time step $t + \Delta t$, is obtained by calculation on the elements of the vector $\bar{\mathbf{f}}_t$ used elements of diagonal mass matrix **M** and elements of diagonal damping matrix **C**, and does not require solving the system of equations:

$$d_{i,t+\Delta t} = \bar{f}_{i,t} \Big/ \left(\frac{m_i}{\Delta t^2} + \frac{c_i}{2\Delta t}\right) \tag{7.35}$$

where:

$d_{i,t+\Delta t}$ – i-th element of displacement vector $\mathbf{d}_{t+\Delta t}$,

$\bar{f}_{i,t}$ – i-th element of nodal load vector $\bar{\mathbf{f}}_t$,

m_i – i-th element of diagonal mass matrix **M**,
c_i – i-th element of diagonal damping matrix **C**.

Analysis of convergence of an iterative process

The convergence test is carried out on the equation of motion with one degree of freedom $m\ddot{d}_t + c\dot{d}_t + kd_t = f_t$. Using the approximation of acceleration (7.28) and velocity (7.29) gives the recursive formula (i.e. the formula of transition from the time step t to the next time step $t + \Delta t$):

$$\begin{Bmatrix} d_{t+\Delta t} \\ d_t \end{Bmatrix} = \begin{bmatrix} \dfrac{2-\omega^2\Delta t^2}{1+\xi\omega\Delta t} & -\dfrac{1-\xi\omega\Delta t}{1+\xi\omega\Delta t} \\ 1 & 0 \end{bmatrix} \begin{Bmatrix} d_t \\ d_{t-\Delta t} \end{Bmatrix} + \begin{Bmatrix} \dfrac{\Delta t^2}{1-\xi\omega\Delta t} \\ 0 \end{Bmatrix} r_t \tag{7.36a}$$

or

$$\begin{Bmatrix} d_{t+\Delta t} \\ d_t \end{Bmatrix} = \mathbf{A}_{rc} \begin{Bmatrix} d_t \\ d_{t-\Delta t} \end{Bmatrix} + \mathbf{L}_{rc} \cdot r_t. \tag{7.36b}$$

Convergence analysis is the study of the spectral radius of the transition matrix $\mathbf{A}_{rc}$. Omitting the damping ($\xi = 0$), eigenvalues of the transition matrix $\mathbf{A}_{rc}$ are:

$$\lambda_{1,2} = \frac{(2-\omega^2\Delta t^2) \pm \sqrt{(2-\omega^2\Delta t^2)^2 - 4}}{2}. \tag{7.37}$$

From the condition $\rho(\mathbf{A}_{rc}) \leq 1$, a condition on the value of the time step was obtained:

$$\omega\Delta t = \frac{2\pi\Delta t}{T} \leq \frac{1}{2\pi^2} \quad \rightarrow \quad \frac{\Delta t}{T} \leq \frac{1}{\pi}. \tag{7.38}$$

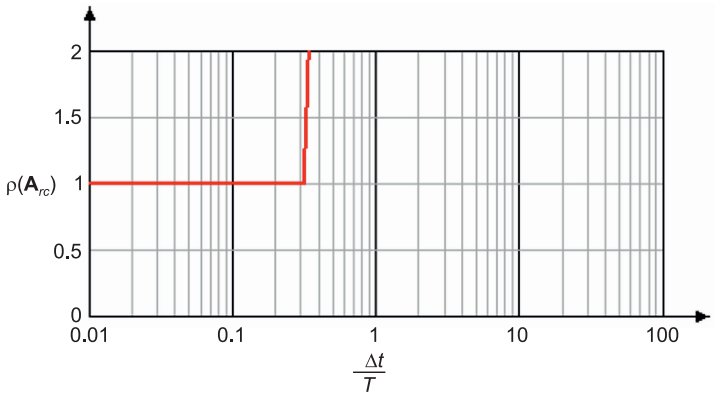

Fig. 7.3. Spectral radius of finite difference method

The central difference method is the method of the conditionally convergent. The convergence depends on the length of the time step Δt in relation to the period T/π of equation of motion with one degree of freedom. Figure 7.3 indicates that if the time step Δt is greater than the period T/π, the amplitudes of displacement d dramatically increase in each time step in the absence of damping ($\xi = 0$) and no-load dynamic ($\mathbf{L} = \mathbf{0}$).

7.5.2. Wilson method

Wilson, in 1973, proposed the use of linear approximation of acceleration in the time interval $t + \theta\Delta t$, with $\theta \geq 1$, where the value of the spectral radius $\rho(\mathbf{A}_W)$ is closest to unity, i.e. it is the smallest numerical error. Figure 7.4 shows the acceleration in time t, $t + \Delta t$ and $t + \theta\Delta t$.

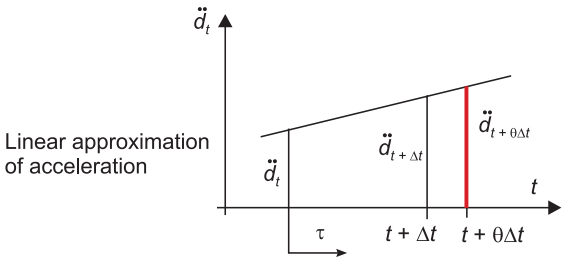

Fig. 7.4. Approximation of accelerations by Wilson

Approximation at time τ:

for acceleration:
$$\ddot{d}_{t+\tau} = \ddot{d}_t + \frac{\tau}{\theta\Delta t}(\ddot{d}_{t+\theta\Delta t} - \ddot{d}_t) \tag{7.39}$$

for velocity:
$$\dot{d}_{t+\tau} = \dot{d}_t + \tau\ddot{d}_t + \frac{\tau^2}{2\theta\Delta t}(\ddot{d}_{t+\theta\Delta t} - \ddot{d}_t) \tag{7.40}$$

for displacement:
$$d_{t+\tau} = d_t + \tau\dot{d}_t + \frac{1}{2}\tau^2\ddot{d}_t + \frac{\tau^3}{6\theta\Delta t}(\ddot{d}_{t+\theta\Delta t} - \ddot{d}_t) \tag{7.41}$$

where $0 \leq \tau \leq \theta\Delta t$.

At time τ the displacement and the velocity are:

$$\dot{d}_{t+\theta\Delta t} = \dot{d}_t + \frac{\theta\Delta t}{2}(\ddot{d}_{t+\theta\Delta t} - \ddot{d}_t) \tag{7.42}$$

$$d_{t+\theta\Delta t} = d_t + \theta\Delta t\dot{d}_t + \frac{\theta^2\Delta t^2}{6}(\ddot{d}_{t+\theta\Delta t} - \ddot{d}_t). \tag{7.43}$$

The equation of motion at the time $t + \theta\Delta t$ is considered:

$$m\ddot{d}_{t+\theta\Delta t} + c\dot{d}_{t+\theta\Delta t} + kd_{t+\theta\Delta t} = f_{t+\theta\Delta t}, \tag{7.44}$$

where the approximation of load in time $f_{t+\theta\Delta t}$ is in the form:

$$f_{t+\theta\Delta t} = f_t + \theta(f_{t+\Delta t} - f_t). \tag{7.45}$$

By substituting in the equation of motion (7.44), the acceleration approximation (7.42) and velocity approximation (7.43) obtained:

$$\left(k + \frac{6}{\theta^2\Delta t^2}m + \frac{3}{\theta\Delta t}c\right)d_{t+\theta\Delta t} = f_{t+\theta\Delta t} + m\left(\frac{6}{\theta^2\Delta t^2}d_t + \frac{6}{\theta\Delta t}\dot{d}_t + 2\ddot{d}_t\right) + \\ + c\left(\frac{3}{\theta\Delta t}d_t + 2\dot{d}_t + \frac{\theta\Delta t}{2}\ddot{d}_t\right) \tag{7.46}$$

in the case of the matrix equation of motion with n degrees of freedom

$$\left(\mathbf{K} + \frac{6}{\theta^2\Delta t^2}\mathbf{M} + \frac{3}{\theta\Delta t}\mathbf{C}\right)\mathbf{d}_{t+\theta\Delta t} = \mathbf{f}_{t+\theta\Delta t} + \mathbf{M}\left(\frac{6}{\theta^2\Delta t^2}\mathbf{d}_t + \frac{6}{\theta\Delta t}\dot{\mathbf{d}}_t + 2\ddot{\mathbf{d}}_t\right) + \\ + \mathbf{C}\left(\frac{3}{\theta\Delta t}\mathbf{d}_t + 2\dot{\mathbf{d}}_t + \frac{\theta\Delta t}{2}\ddot{\mathbf{d}}_t\right) \tag{7.47}$$

Equation (7.47) presents a solution at time $t + \theta\Delta t$ with a known solution at time t: $(\mathbf{d}_t, \dot{\mathbf{d}}_t, \ddot{\mathbf{d}}_t)$. For displacement $\mathbf{d}_{t+\theta\Delta t}$, one should solve the matrix equation:

$$\bar{\mathbf{K}}\mathbf{d}_{t+\theta\Delta t} = \bar{\mathbf{f}}_{t+\theta\Delta t} \tag{7.48}$$

where:

$$\bar{\mathbf{K}} = \left(\mathbf{K} + \frac{6}{\theta^2\Delta t^2}\mathbf{M} + \frac{3}{\theta\Delta t}\mathbf{C}\right) \tag{7.49a}$$

$$\bar{\mathbf{f}} = \mathbf{f}_{t+\theta\Delta t} + \mathbf{M}\left(\frac{6}{\theta^2\Delta t^2}\mathbf{d}_t + \frac{6}{\theta\Delta t}\dot{\mathbf{d}}_t + 2\ddot{\mathbf{d}}_t\right) + \mathbf{C}\left(\frac{3}{\theta\Delta t}\mathbf{d}_t + 2\dot{\mathbf{d}}_t + \frac{\theta\Delta t}{2}\ddot{\mathbf{d}}_t\right) \tag{7.49b}$$

Therefore, the transition from time step t to time step $t + \theta\Delta t$ requires solving a system of n equations. This increases the calculation time by the Wilson method in relation to the time of calculation by the central difference method.

Analysis of convergence of an iterative process

The convergence test is carried out on the equation of motion with one degree of freedom $m\ddot{d}_{t+\theta\Delta t} + c\dot{d}_{t+\theta\Delta t} + kd_{t+\theta\Delta t} = f_{t+\theta\Delta t}$. Using the approximation of velocity (7.42) and displacement (7.43), obtained the recursive formula:

$$\begin{Bmatrix} \ddot{d}_{t+\Delta t} \\ \dot{d}_{t+\Delta t} \\ d_{t+\Delta t} \end{Bmatrix} = \begin{bmatrix} \left(1-\frac{\beta\theta^2}{3}-\frac{1}{\theta}-\kappa\theta\right) & \frac{1}{\Delta t}(-\beta\theta-2\kappa) & \frac{1}{\Delta t^2}(-\beta) \\ \Delta t\left(1-\frac{1}{2\theta}-\frac{\beta\theta^2}{6}-\frac{\kappa\theta}{2}\right) & \left(1-\frac{\beta\theta}{2}-\kappa\right) & \frac{1}{\Delta t}\left(-\frac{\beta}{2}\right) \\ \Delta t^2\left(\frac{1}{2}-\frac{1}{6\theta}-\frac{\beta\theta^2}{18}-\frac{\theta^3}{6}\right) & \Delta t\left(1-\frac{\beta\theta}{6}-\frac{\kappa}{3}\right) & \left(1-\frac{\beta}{6}\right) \end{bmatrix} \begin{Bmatrix} \ddot{d}_t \\ \dot{d}_t \\ d_t \end{Bmatrix} + \begin{Bmatrix} \frac{\beta}{\omega^2\Delta t^2} \\ \frac{\beta}{2\omega^2\Delta t} \\ \frac{\beta}{6\omega^2} \end{Bmatrix} r_{t+\Delta t} \tag{7.50a}$$

or

$$\begin{Bmatrix} \ddot{d}_{t+\Delta t} \\ \dot{d}_{t+\Delta t} \\ d_{t+\Delta t} \end{Bmatrix} = \mathbf{A}_W \begin{Bmatrix} \ddot{d}_t \\ \dot{d}_t \\ d_t \end{Bmatrix} + \mathbf{L}_W \cdot r_{t+\Delta t} \tag{7.50b}$$

where:

$$\beta = \left(\frac{\theta}{\omega^2\Delta t^2}+\frac{\xi\theta^2}{\omega\Delta t}+\frac{\theta^3}{6}\right)^{-1}, \quad \kappa = \frac{\xi\beta}{\omega\Delta t}. \tag{7.50c}$$

Convergence analysis is the study of the spectral radius of the transition matrix $\mathbf{A}_W$.

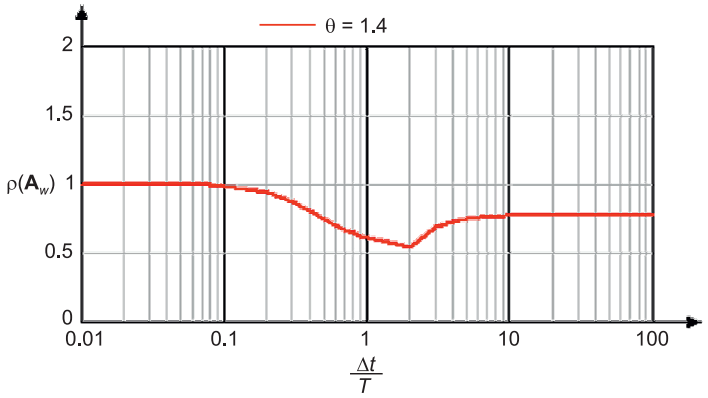

Fig. 7.5. Spectral radius of the Wilson method with θ = 1.4

Wilson's method is an unconditionally convergent method, i.e. the convergence does not depend on the length of the time step Δt in relation to the period T of the equation of motion with one degree of freedom in the absence of damping and no-load dynamic. Figure 7.5 shows that if $\Delta t/T > 0.1$, the calculation from

the time t to the time step $t + \Delta t$ according to (7.50), an artificial, numerical decrease of amplitudes occurs. With $\Delta t/T = 2$, the reduce in amplitude is almost 50%, and if $\Delta t/T > 10$ this reduction is approximately 20%. Thus, in a system of n degrees of freedom, the amplitudes in the high frequency range are numerically dampened.

7.5.3. Newmark method

Newmark, in 1959, proposed the use of linear approximation of acceleration in the time interval $(t, t + \Delta t)$, where the value of the spectral radius $\rho(\mathbf{A}_N)$ is closest to unity. Figure 7.6 shows the acceleration in time $t + \Delta t$ and $t + \gamma\Delta t$.

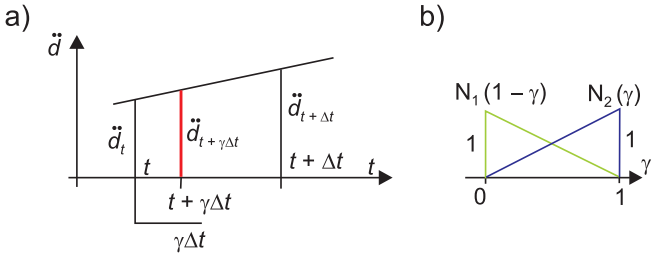

Fig. 7.6. Approximation in Newmark method: a) Linear approximation of acceleration, b) Linear shape functions

Approximation at time $t + \gamma\Delta t$ is as follows:
acceleration:

$$\ddot{d}_{t+\gamma\Delta t} \approx (1-\gamma)\ddot{d}_t + \gamma\ddot{d}_{t+\Delta t} \tag{7.51}$$

velocity:

$$\dot{d}_{t+\gamma\Delta t} \approx \dot{d}_t + \Delta t\ddot{d}_{t+\gamma\Delta t} = \dot{d}_t + \Delta t[(1-\gamma)\ddot{d}_t + \gamma\ddot{d}_{t+\Delta t}] \tag{7.52}$$

displacement:

$$d_{t+\gamma\Delta t} \approx d_t + \Delta t\dot{d}_t + \frac{1}{2}\Delta t^2\ddot{d}_{t+\gamma\Delta t} = d_t + \Delta t\dot{d}_t + \Delta t^2\left[\left(\frac{1}{2}-\beta\right)\ddot{d}_t + \beta\ddot{d}_{t+\Delta t}\right]. \tag{7.53}$$

with $\beta = \dfrac{\gamma}{2}$.

The equation of motion at time $t + \gamma\Delta t$ is considered:

$$m\ddot{d}_{t+\gamma\Delta t} + c\dot{d}_{t+\gamma\Delta t} + kd_{t+\gamma\Delta t} = f_{t+\gamma\Delta t}. \tag{7.54}$$

Substituting in the equation of motion (7.54), the velocity approximation (7.52) and the displacement approximation (7.53) received the following equation in time step $t + \Delta t$:

$$\left(k + \frac{1}{\beta \Delta t^2} m + \frac{\gamma}{\beta \Delta t} c\right) d_{t+\Delta t} = f_{t+\Delta t} + m\left[\frac{1}{\beta \Delta t^2} d_t + \frac{1}{\beta \Delta t} \dot{d}_t + \left(\frac{1}{2} - \beta\right) \ddot{d}_t\right] + \\ + c\left[\frac{\gamma}{\beta \Delta t} d_t + \left(\frac{\gamma}{\beta} - 1\right) \dot{d}_t + \frac{\Delta t}{2}\left(\frac{\gamma}{\beta} - 2\right) \ddot{d}_t\right] \tag{7.55}$$

in the case of the matrix equation of motion with n degrees of freedom

$$\left(\mathbf{K} + \frac{1}{\beta \Delta t^2} \mathbf{M} + \frac{\gamma}{\beta \Delta t} \mathbf{C}\right) \mathbf{d}_{t+\Delta t} = \mathbf{f}_{t+\Delta t} + \mathbf{M}\left[\frac{1}{\beta \Delta t^2} \mathbf{d}_t + \frac{1}{\beta \Delta t} \dot{\mathbf{d}}_t + \left(\frac{1}{2} - \beta\right) \ddot{\mathbf{d}}_t\right] + \\ + \mathbf{C}\left[\frac{\gamma}{\beta \Delta t} \mathbf{d}_t + \left(\frac{\gamma}{\beta} - 1\right) \dot{\mathbf{d}}_t + \frac{\Delta t}{2}\left(\frac{\gamma}{\beta} - 2\right) \ddot{\mathbf{d}}_t\right] \tag{7.56}$$

Equation (7.56) presents a solution at time $t + \Delta t$ with a known solution at time t: $(\mathbf{d}_t, \dot{\mathbf{d}}_t, \ddot{\mathbf{d}}_t)$ For displacement $\mathbf{d}_{t+\Delta t}$, one should solve the matrix equation:

$$\bar{\mathbf{K}} \mathbf{d}_{t+\Delta t} = \bar{\mathbf{f}}_{t+\Delta t}, \tag{7.57}$$

where:

$$\bar{\mathbf{K}} = \left(\mathbf{K} + \frac{1}{\beta \Delta t^2} \mathbf{M} + \frac{\gamma}{\beta \Delta t} \mathbf{C}\right) \tag{7.58a}$$

$$\bar{\mathbf{f}}_{t+\Delta t} = \mathbf{f}_{t+\Delta t} + \mathbf{M}\left[\frac{1}{\beta \Delta t^2} \mathbf{d}_t + \frac{1}{\beta \Delta t} \dot{\mathbf{d}}_t + \left(\frac{1}{2} - \beta\right) \ddot{\mathbf{d}}_t\right] + \\ + \mathbf{C}\left[\frac{\gamma}{\beta \Delta t} \mathbf{d}_t + \left(\frac{\gamma}{\beta} - 1\right) \dot{\mathbf{d}}_t + \frac{\Delta t}{2}\left(\frac{\gamma}{\beta} - 2\right) \ddot{\mathbf{d}}_t\right] \tag{7.58b}$$

Therefore, the transition from time step t to time step $t + \Delta t$ requires solving a system of n equations. This increases the calculation time by the Newmark method in relation to the time of calculation by the central difference method.

Analysis of convergence of an iterative process

The convergence test is carried out on the equation of motion with one degree of freedom $m\ddot{d}_{t+\gamma\Delta t} + c\,\dot{d}_{t+\gamma\Delta t} + k d_{t+\gamma\Delta t} = f_{t+\gamma\Delta t}$. Using the approximation of velocity (7.52) and displacement (7.53), obtained the recursive formula:

$$\begin{Bmatrix} \ddot{d}_{t+\Delta t} \\ \dot{d}_{t+\Delta t} \\ d_{t+\Delta t} \end{Bmatrix} = \begin{bmatrix} \left(-\left(\frac{1}{2}-\beta\right)\varphi-(1-\gamma)\kappa\right) & \frac{1}{\Delta t}(-\varphi-2\kappa) & \frac{1}{\Delta t^2}(-\varphi) \\ \Delta t\left(1-\gamma-\left(\frac{1}{2}-\beta\right)\varphi\gamma-2(1-\gamma)\gamma\kappa\right) & (1-\varphi\gamma-2\gamma\kappa) & \frac{1}{\Delta t}(-\varphi\gamma) \\ \Delta t^2\left(\frac{1}{2}-\beta-\left(\frac{1}{2}-\beta\right)\varphi\beta-2(1-\gamma)\beta\kappa\right) & \Delta t(1-\varphi\beta-2\beta\kappa) & (1-\varphi\beta) \end{bmatrix} \begin{Bmatrix} \ddot{d}_t \\ \dot{d}_t \\ d_t \end{Bmatrix} + \\ + \begin{Bmatrix} \frac{\varphi}{\omega^2\Delta t^2} \\ \frac{\varphi}{\omega^2\Delta t} \\ \frac{\beta\varphi}{\omega^2} \end{Bmatrix} r_{t+\Delta t}, \tag{7.59a}$$

or

$$\begin{Bmatrix} \ddot{d}_{t+\Delta t} \\ \dot{d}_{t+\Delta t} \\ d_{t+\Delta t} \end{Bmatrix} = \mathbf{A}_N \begin{Bmatrix} \ddot{d}_t \\ \dot{d}_t \\ d_t \end{Bmatrix} + \mathbf{L}_W \cdot r_{t+\Delta t} \tag{7.59b}$$

where:

$$\varphi = \left(\frac{1}{\omega^2\Delta t^2} + \frac{2\xi\gamma}{\omega\Delta t} + \beta\right)^{-1}, \quad \kappa = \frac{\xi\varphi}{\omega\Delta t}. \tag{7.59c}$$

Convergence analysis is the study of the spectral radius of the transition matrix $\mathbf{A}_N$.

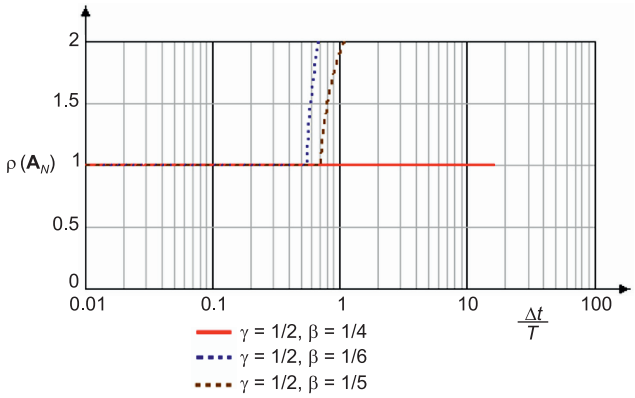

Fig. 7.7. Spectral radius of the Newmark method

The convergence of the Newmark method depends on the choice of parameters γ and β. According to Figure 7.7, the method is conditionally or unconditionally convergent (in the absence of damping and dynamic load) in the following cases:

– with $\gamma = 1/2$, $\beta = 1/4$ – this method is unconditionally convergent, and the spectral radius $\rho(\mathbf{A}_N) = 1$, independently from the value $\Delta t/T$ i.e. the amplitude of the displacement, velocity and acceleration do not change for any frequencies of the system (no numerical amplitude distortion),
– with $\gamma = 1/2$, $\beta = 1/5$ and with $\gamma = 1/2$, $\beta = 1/6$ – this method is conditionally convergent, because the spectral radius $\rho(\mathbf{A}_N)$ increases beyond a certain value $\Delta t/T$.

7.5.4. HHT-α method

The HHT-α method proposed by Hilbert, Hughes and Taylor in 1977 introduces approximation of displacement and velocity according to the Newmark method and proposes the addition of parameter α to the equation of motion in order to dampen the upper part of frequency spectrum

$$\mathbf{M}\ddot{\mathbf{d}}_{t+\Delta t} + (1+\alpha)\mathbf{C}\dot{\mathbf{d}}_{t+\Delta t} - \alpha\mathbf{C}\dot{\mathbf{d}}_t + (1+\alpha)\mathbf{K}\mathbf{d}_{t+\Delta t} - \alpha\mathbf{K}\mathbf{d}_t = (1+\alpha)\mathbf{f}_{t+\Delta t} - \alpha\mathbf{f}_t, \quad (7.60)$$

where according to (7.52) and (7.53)

$$\dot{\mathbf{d}}_{t+\Delta t} = \dot{\mathbf{d}}_t + \Delta t[(1-\gamma)\ddot{\mathbf{d}}_t + \gamma\ddot{\mathbf{d}}_{t+\Delta t}] \quad (7.61)$$

$$\mathbf{d}_{t+\Delta t} = \mathbf{d}_t + \Delta t\dot{\mathbf{d}}_t + \Delta t^2\left[\left(\frac{1}{2}-\beta\right)\ddot{\mathbf{d}}_t + \beta\ddot{\mathbf{d}}_{t+\Delta t}\right]. \quad (7.62)$$

Taking into account the approximations of velocity and displacement in the equation of motion (7.60), one can obtain the following matrix equation for the acceleration at the time of $t + \Delta t$:

$$\bar{\mathbf{M}}\ddot{\mathbf{d}}_{t+\Delta t} = \bar{\mathbf{f}}_{t+\Delta t}, \quad (7.63)$$

where:

$$\bar{\mathbf{M}} = \mathbf{M} + [(1+\alpha)\beta\Delta t^2]\mathbf{K} + [(1+\alpha)\gamma\Delta t]\mathbf{C}, \quad (7.64a)$$

$$\bar{\mathbf{f}}_{t+\Delta t} = (1+\alpha)\mathbf{f}_{t+\Delta t} - \alpha\mathbf{f}_t - (1+\alpha)\Delta t\left[\Delta t\left(\frac{1}{2}-\beta\right)\mathbf{K} + (1-\gamma)\mathbf{C}\right]\ddot{\mathbf{d}}_t -$$
$$-[(1+\alpha)]\Delta t\mathbf{K} + \mathbf{C}]\dot{\mathbf{d}}_t - \mathbf{K}\mathbf{d}_t \quad (7.64b)$$

The transition from time step t to time step $t + \Delta t$ requires solving the matrix equation for acceleration. For this reason, the calculation time when using the HHT-α method is comparable to the calculation time of the Newmark method.

Analysis of convergence of an iterative process

Using the approximation of velocity (7.61) and displacement (7.62) with equation of motion (7.60) with $\gamma = 1/2$ and $\beta = 1/4$, obtained the recursive formula:

$$\begin{Bmatrix} d_{t+\Delta t} \\ \dot{d}_{t+\Delta t} \\ \ddot{d}_{t+\Delta t} \end{Bmatrix} = \mathbf{A}_{\mathrm{HHT}} \begin{Bmatrix} d_t \\ \dot{d}_t \\ \ddot{d}_t \end{Bmatrix} + \mathbf{L}_{\mathrm{HHT}} \begin{Bmatrix} r_t \\ r_{t+\Delta t} \end{Bmatrix} \tag{7.65}$$

where:

$$\mathbf{A}_{\mathrm{HHT}} = \frac{1}{d} \begin{bmatrix} (4 + \Omega^2\alpha - & 4\Delta t & -\Delta t^2(-1-2\alpha+\alpha^2) \\ -2\Omega^2\alpha^2 + \Omega^2\alpha^3) & & \\ \dfrac{2\Omega^2}{\Delta t}(-1+2\alpha) & (4 - \Omega^2 + \Omega^2\alpha + & \Delta t(2 + 4\alpha + \\ & +3\Omega^2\alpha^2 + \Omega^2\alpha^3) & +\Omega^2\alpha^2 + \Omega^2\alpha^3) \\ \dfrac{-4\Omega^2}{\Delta t^2} & \dfrac{-4}{\Delta t}(1+\alpha)\Omega^2 & \Omega^2(1+\alpha)(-1-2\alpha+\alpha^2) \end{bmatrix}$$

$$\mathbf{L}_{\mathrm{HHT}} = \frac{1}{d} \begin{bmatrix} -\Delta t^2(-1+\alpha)^2\alpha & \Delta t^2(-1+\alpha)^2(1+\alpha) \\ 2\Delta t\alpha(-1+2\alpha) & -2\Delta t(1+\alpha)(-1+2\alpha) \\ 4\alpha & 4(1+\alpha) \end{bmatrix} \tag{7.66}$$

$$d = (4 + \Omega^2 - \Omega^2\alpha - \Omega^2\alpha^2 + \Omega^2\alpha^3), \quad \Omega = \omega\Delta t,$$

with $-1/3 \leq \alpha \leq 0$, the HHT-α method is unconditionally convergent.

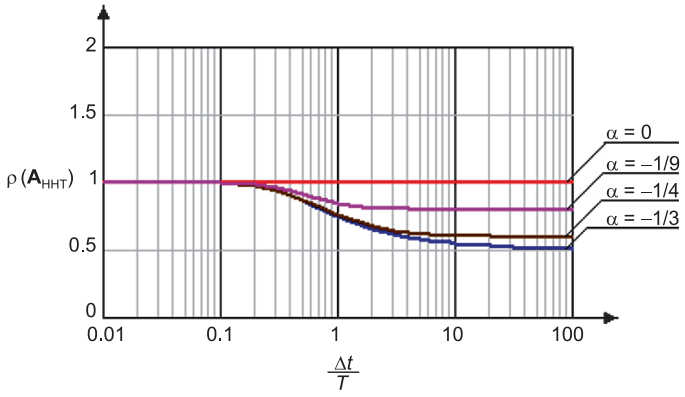

Fig. 7.8. Spectral radius of the HHT-α method

Reducing the amplitude, measured by the spectral radius, depends on the value of the parameter α (see Figure 7.8):

- with $\alpha = 0$, the HHT–α method is equivalent to the Newmark method ($\gamma = 1/2$, $\beta = 1/4$), and is unconditionally convergent without reducing the amplitude, in this case, $\rho(\mathbf{A}_{HHT}) = 1$,
- with $-1/3 \leq \alpha \leq 0$, the HHT–α method introduces a reduction in the amplitude in the upper part of the frequency spectrum with $\Delta t/T > 0.2$:
  - with $\alpha = -1/3$, $\rho(\mathbf{A}_{HHT}) \to 0.5$ for $(\Delta t/T \to \infty)$, method introduce the greatest decrease in amplitude.
  - with $\alpha = -1/4$, $\rho(\mathbf{A}_{HHT}) \to 0.6$ for $(\Delta t/T \to \infty)$,
  - with $\alpha = -1/5$, $\rho(\mathbf{A}_{HHT}) \to 0.6666$ for $(\Delta t/T \to \infty)$,
  - with $\alpha = -1/9$, $\rho(\mathbf{A}_{HHT}) \to 0.8$ for $(\Delta t/T \to \infty)$,
  - with $\alpha = -1/20$, $\rho(\mathbf{A}_{HHT}) \to 0.9$ for $(\Delta t/T \to \infty)$.

7.5.5. TDG method

The general equation of dynamics is considered:

$$\mathbf{M}\ddot{\mathbf{d}}(t) + \mathbf{C}\dot{\mathbf{d}}(t) + \mathbf{K}\mathbf{d}(t) = \mathbf{f}(t). \tag{7.67}$$

To solve equation (7.67), the Hamilton's principle was applied using the continuous functions in space and the discontinuous functions in time, using the so-called *Time–Discontinuous Galerkin* (*TDG*) *Method*. Hughes and Hulbert in 1988, proposed using the TDG method to solve dynamic problems.

The TDG version with piecewise linear approximation of displacement and velocity (marked by P1–P1) is considered.

Let $0 = t < \ldots < t + n\Delta t < t + (n+1)\Delta t < \ldots < t + N\Delta t = T$ is a sequence in time $t + n\Delta t$. Let the space of test functions are defined as:

$$\mathbf{V}_{\Delta t}^{h} \subset \{\mathbf{u} \in \mathbf{H}^1(S_{\Delta t}), \mathbf{u} = \bar{\mathbf{u}} \quad \text{on} \quad \Gamma_1 \times \Delta t\} \tag{7.68}$$

and the space of weight functions are defined as:

$$\mathbf{W}_{\Delta t}^{h} \subset \{\mathbf{w} \in \mathbf{H}^1(S_{\Delta t}), \mathbf{w} = 0 \quad \text{on} \quad \Gamma_1 \times \Delta t\} \tag{7.69}$$

and are determined in every point of the space-time step $S_{\Delta t} = \Omega \times \Delta t$.

It is assumed that in both spaces $\mathbf{V}_{\Delta t}^{h}$ and $\mathbf{W}_{\Delta t}^{h}$ the tensor product of bi-linear functions of variables $\mathbf{x}$ and t was realized in space-time $\Gamma_1 \times \Delta t$. The variables of displacement and velocity are discretized both in space and in time.

The following denotation of a discrete function in time t used:

$$\mathbf{w}_t^{+} = \lim_{\varepsilon \to 0^+} \mathbf{w}(t + \varepsilon) \tag{7.70a}$$

$$\mathbf{w}_t^{-} = \lim_{\varepsilon \to 0^-} \mathbf{w}(t - \varepsilon) \tag{7.70b}$$

where functions are continuous in the interior of each time step Δt, and allow for a description of the jump in discrete time $t + n\Delta t$ (see Figure 7.9).

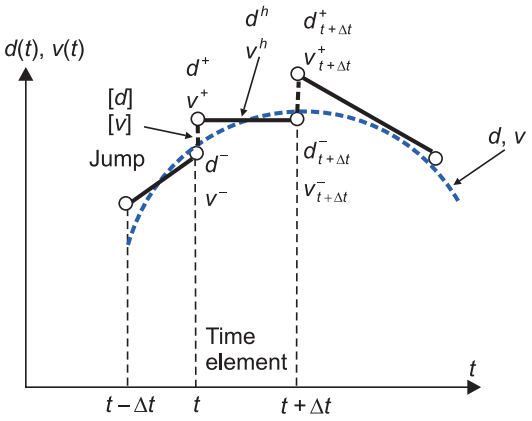

Fig. 7.9. Approximation in time with piecewise linear function during time step Δt and jump in discrete time point $t + n\Delta t$

Let $\mathbf{d}_1$ and $\mathbf{v}_1$ be the nodal displacement and velocity in time $(t)^+$; next, let $\mathbf{d}_2$ and $\mathbf{v}_2$ be the nodal displacement and velocity in time $(t + \Delta t)^-$. Moreover, let $\mathbf{d}_1^-$ and $\mathbf{v}_1^-$ be the nodal displacement and velocity in time $(t)^-$, which are either known in the previous time step, or at $t = 0$ as initial values. The displacement and velocity of any material point $\mathbf{x}$ in space and at any point of time $\tau \in (t, t + \Delta t)$ are defined by the equation:

$$\mathbf{d}^h(\mathbf{x},\tau) = \mathbf{N}(\mathbf{x})\phi_1(\tau)\mathbf{d}_1 + \mathbf{N}(\mathbf{x})\phi_2(\tau_2)\mathbf{d}_2 \tag{7.71a}$$

where:

$$\phi_1(\tau) = \frac{(t+\Delta t)-\tau}{\Delta t} \tag{7.71b}$$

$$\phi_2(\tau) = \frac{\tau - t}{\Delta t} \tag{7.71c}$$

are the linear shape functions.

The velocity vector at any point of time $\tau \in (t, t + \Delta t)$ is approximated by using linear shape functions

$$\mathbf{v}^h(\mathbf{x},\tau) = \mathbf{N}(\mathbf{x})\phi_1(\tau)\mathbf{v}_1 + \mathbf{N}(\mathbf{x})\phi_2(\tau)\mathbf{v}_2. \tag{7.72}$$

Nodal displacement vector $\mathbf{d}$ and nodal velocity vector $\mathbf{v}$ are the independent variables in the equation of motion at each time step Δt.

In this approach, equation (7.67) takes the form

$$\mathbf{M}\dot{\mathbf{v}} + \mathbf{C}\mathbf{v} + \mathbf{K}\mathbf{d} = \mathbf{f}^e \tag{7.73}$$

with the compliance condition

$$\dot{\mathbf{d}} - \mathbf{v} = 0. \tag{7.74}$$

The weak form (7.73) with compliance condition (7.74) and lack of continuity of vectors **d** and **v** at each time step Δt leads to a generalized Hamilton equation

$$\int_{\Delta t} \delta\mathbf{v}^T(\mathbf{M}\dot{\mathbf{v}} + \mathbf{C}\mathbf{v} + \mathbf{K}\mathbf{d} - \mathbf{f}^e)\,\mathrm{d}t + \int_{\Delta t} \delta\mathbf{d}^T\mathbf{K}(\dot{\mathbf{d}} - \mathbf{v})\,\mathrm{d}t + \delta\mathbf{d}_n^T\mathbf{K}[\![\mathbf{d}_n]\!] + \delta\mathbf{v}_n^T\mathbf{M}[\![\mathbf{v}_n]\!] = 0 \tag{7.75}$$

By substituting approximations (7.71) and (7.72) into equation (7.75), the matrix equation is obtained for the variable vectors $\mathbf{d}_t$, $\mathbf{d}_{t+\Delta t}$, $\mathbf{v}_t$, $\mathbf{v}_{t+\Delta t}$:

$$\begin{bmatrix} \frac{1}{2}\mathbf{K} & \frac{1}{2}\mathbf{K} & -\frac{\Delta t}{3}\mathbf{K} & -\frac{\Delta t}{6}\mathbf{K} \\ -\frac{1}{2}\mathbf{K} & \frac{1}{2}\mathbf{K} & -\frac{\Delta t}{6}\mathbf{K} & -\frac{\Delta t}{3}\mathbf{K} \\ \frac{\Delta t}{3}\mathbf{K} & \frac{\Delta t}{6}\mathbf{K} & \frac{1}{2}\mathbf{M} + \frac{\Delta t}{3}\mathbf{C} & \frac{1}{2}\mathbf{M} + \frac{\Delta t}{6}\mathbf{C} - \frac{\Delta t^2}{12}\mathbf{K} \\ \frac{\Delta t}{6}\mathbf{K} & \frac{\Delta t}{3}\mathbf{K} & -\frac{1}{2}\mathbf{M} + \frac{\Delta t}{6}\mathbf{C} - \frac{\Delta t^2}{12}\mathbf{K} & \frac{1}{2}\mathbf{M} + \frac{\Delta t}{3}\mathbf{C} \end{bmatrix} \begin{Bmatrix} \mathbf{d}_t \\ \mathbf{d}_{t+\Delta t} \\ \mathbf{v}_t \\ \mathbf{v}_{t+\Delta t} \end{Bmatrix} =$$

$$= \begin{Bmatrix} \mathbf{K}\mathbf{d}_t^- \\ \mathbf{0} \\ \mathbf{F}_1 + \mathbf{M}\mathbf{v}_t^- \\ \mathbf{F}_2 \end{Bmatrix} \tag{7.76}$$

where:

$$\mathbf{F}_1 = \int_{\Delta t} \phi_1(\tau)\mathbf{F}\,\mathrm{d}\tau \tag{7.77a}$$

$$\mathbf{F}_2 = \int_{\Delta t} \phi_2(\tau)\mathbf{F}\,\mathrm{d}\tau. \tag{7.77b}$$

Nodal displacement $\mathbf{d}_t$, $\mathbf{d}_{t+\Delta t}$ are independent of the nodal velocity $\mathbf{v}_t$, $\mathbf{v}_{t+\Delta t}$. It was assumed that the load node vector within the time interval is determined by linear shape functions ϕ_1 and ϕ_2 as

$$\mathbf{F}(\tau) = \mathbf{f}(t)\phi_1 + \mathbf{f}(t+\Delta t)\phi_2 = \mathbf{f}_t\phi_1 + \mathbf{f}_{t+\Delta t}\phi_2 \tag{7.78}$$

where $\mathbf{f}_t$, $\mathbf{f}_{t+\Delta t}$ are nodal external forces at times t, $t + \Delta t$, respectively.

By substituting (7.71b, c) to (7.77), we obtain:

$$\mathbf{F}_1 = \frac{\Delta t}{3}\mathbf{f}_t + \frac{\Delta t}{6}\mathbf{f}_{t+\Delta t} \tag{7.79a}$$

$$\mathbf{F}_2 = \frac{\Delta t}{6}\mathbf{f}_t + \frac{\Delta t}{3}\mathbf{f}_{t+\Delta t}. \tag{7.79b}$$

Equation (7.76) can be written as:

$$\begin{bmatrix} \frac{1}{2}\mathbf{K} & \frac{1}{2}\mathbf{K} & -\frac{\Delta t}{3}\mathbf{K} & -\frac{\Delta t}{6}\mathbf{K} \\ -\frac{1}{2}\mathbf{K} & \frac{1}{2}\mathbf{K} & -\frac{\Delta t}{6}\mathbf{K} & -\frac{\Delta t}{3}\mathbf{K} \\ \frac{\Delta t}{3}\mathbf{K} & \frac{\Delta t}{6}\mathbf{K} & \frac{1}{2}\mathbf{M}+\frac{\Delta t}{3}\mathbf{C} & \frac{1}{2}\mathbf{M}+\frac{\Delta t}{6}\mathbf{C}-\frac{\Delta t^2}{12}\mathbf{K} \\ \frac{\Delta t}{6}\mathbf{K} & \frac{\Delta t}{3}\mathbf{K} & -\frac{1}{2}\mathbf{M}+\frac{\Delta t}{6}\mathbf{C}-\frac{\Delta t^2}{12}\mathbf{K} & \frac{1}{2}\mathbf{M}+\frac{\Delta t}{3}\mathbf{C} \end{bmatrix} \begin{Bmatrix} \mathbf{d}_t \\ \mathbf{d}_{t+\Delta t} \\ \mathbf{v}_t \\ \mathbf{v}_{t+\Delta t} \end{Bmatrix} =$$

$$= \begin{Bmatrix} \mathbf{K}\mathbf{d}_t^- \\ 0 \\ \mathbf{F}_1 - \mathbf{F}_2 + \mathbf{M}\mathbf{v}_t^- \\ \mathbf{F}_1 + \mathbf{F}_2 + \mathbf{M}\mathbf{v}_t^- - \Delta t\mathbf{K}\mathbf{d}_t^- \end{Bmatrix}. \tag{7.80}$$

Static condensation was used to the equation (7.80), this obtained:

$$\mathbf{d}_t = \mathbf{d}_t^- \quad \text{with} \quad \mathbf{d}_t^+ = \mathbf{d}_t^- \tag{7.81}$$

$$\begin{bmatrix} \mathbf{M}+\frac{\Delta t}{6}\mathbf{C}-\frac{\Delta t^2}{12}\mathbf{K} & -\frac{\Delta t}{6}\mathbf{C}-\frac{\Delta t^2}{12}\mathbf{K} \\ \frac{\Delta t}{2}\mathbf{C}+\frac{\Delta t^2}{3}\mathbf{K} & \mathbf{M}+\frac{\Delta t}{2}\mathbf{C}+\frac{\Delta t^2}{6}\mathbf{K} \end{bmatrix} \begin{Bmatrix} \mathbf{v}_t \\ \mathbf{v}_{t+\Delta t} \end{Bmatrix} = \begin{Bmatrix} \mathbf{F}_1 - \mathbf{F}_2 + \mathbf{M}\mathbf{v}_t^- \\ \mathbf{F}_1 + \mathbf{F}_2 + \mathbf{M}\mathbf{v}_t^- - \Delta t\mathbf{K}\mathbf{d}_t^- \end{Bmatrix} \tag{7.82}$$

$$\mathbf{d}_{t+\Delta t} = \mathbf{d}_1^- + \frac{1}{2}\Delta t(\mathbf{v}_t + \mathbf{v}_{t+\Delta t}). \tag{7.83}$$

In the considered formulation, the continuity of the nodal vector displacement $\mathbf{d}_t$ at each point time t in time interval $t = (0, T)$ is automatically provided with discontinuities of the nodal vector velocity. This is particularly important in the dynamic analysis with nonlinear materials (such as soil) with quick-changing excitations in time, e.g. shock loads.

Analysis of convergence of an iterative process

The discontinuity of the velocity in time approximation is considered with the TDG method (*Time Discontinuous Galerkin Method*), which provides a reduction in the degree of differentiation using the equation of motion in the form:

$$\dot{v}(t) + 2\xi\omega v(t) + \omega^2 d(t) = r(t) \quad t \in (0, t_f] \tag{7.84}$$

$$\dot{d}(t) - v(t) = 0 \quad t \in (0, t_f] \tag{7.85}$$

$$d(0) = d_0, \qquad v(0) = v_0. \tag{7.86}$$

For simplicity, we considered the case with $\xi = 0$. Assuming that the load at the time $r(t)$ is a stationary signal and can be presented by the sum of harmonic excitation at a constant frequency η. The solution of the equations of motion can be represented as the sum of

$$d(t) = d_h(t) + d_p(t) \tag{7.87}$$

where:

$$d_h(t) = d_0 \cos(\omega t) + \frac{v_0}{\omega} \sin(\omega t) \tag{7.88}$$

$$d_p(t) = \frac{-\omega\cos(\eta t) + \omega\cos(\omega t) - i\omega\sin(\eta t) + i\omega\sin(\omega t)}{\omega(\eta^2 - \omega^2)} \tag{7.89}$$

$d_h(t)$ – a solution to the homogeneous equation,
$d_p(t)$ – a particular solution to the non-homogeneous equation.

The transition matrix with linear shape functions is:

$$\begin{Bmatrix} d_{t+\Delta t} \\ \dot{d}_{t+\Delta t} \end{Bmatrix} = \mathbf{A}_{\mathrm{TDG}} \begin{Bmatrix} d_t \\ \dot{d}_t \end{Bmatrix} + \mathbf{L}_{\mathrm{TDG}} \begin{Bmatrix} r_t \\ r_{t+\Delta t/2} \\ r_{t+\Delta t} \end{Bmatrix}, \tag{7.90a}$$

where:

$$\mathbf{A}_{\mathrm{TDG}} = \frac{1}{d} \begin{bmatrix} (36 - 14\Omega^2) & \Delta t(36 - 2\Omega^2) \\ 2\Omega^2(\Omega^2 - 18)/\Delta t & (36 - 14\Omega^2) \end{bmatrix} \tag{7.90b}$$

$$\mathbf{L}_{\mathrm{TDG}} = \frac{\Delta t}{3d} \begin{bmatrix} -\Delta t(\Omega^2 - 18) & 2\Delta t(7\Omega^2 + 18) & 2\Omega^2 \Delta t \\ -(7\Omega^2 - 18) & -4(\Omega^2 - 18) & (5\Omega^2 + 18) \end{bmatrix} \tag{7.90c}$$

$$d = (\Omega^4 + 4\Omega^2 + 36), \quad \Omega = \omega\Delta t. \tag{7.90d}$$

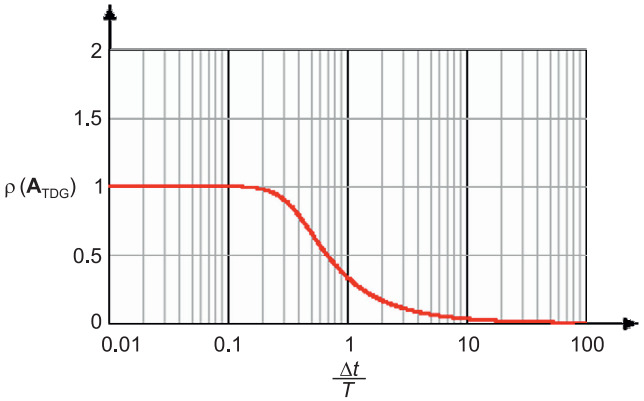

Fig. 7.10. Spectral radius of the TDG method

Figure 7.10 shows the value of the spectral radius TDG method $\rho(\mathbf{A}_{\mathrm{TDG}})$, depending on the length of time step $\Delta t/T$. Full amplitude damping in the upper part of the spectrum with $\Delta t/T \to \infty$ occurs here.

7.6. Analysis of the accuracy: error of amplitude and error of period – comparison of methods

According to equation (7.4), in a set of n equations of motion are n eigenperiods of a structure $T_i = \dfrac{2\pi}{\omega_i}$, $i = 1, 2, \ldots n$, or the ordering $\{T_1, T_2, \ldots, T_n\}$, where $T_1 > T_2, \ldots, T_i > T_{i+1}$. For a constant time step Δt, $\Delta t/T_1$ is the smallest value, and $\Delta t/T_n$ is the highest value. Thus, with the constant Δt, for an increasing value of $\Delta t/T \to \infty$ Figure 7.11 shows the effect of Δt in smaller periods T, i.e. the influence of Δt on the upper part of the eigenspectrum of structure (to the high frequency of the structure).

Amplitude error

Figure 7.11 shows the amplitude error, measured by logarithmic decrement of parasitic damping (numerical damping), according to (7.23) $\tilde{\delta} = -\dfrac{\pi}{\omega \Delta t} \ln |\mathbf{A}|$, for considering the above direct integration methods. According to Figure 7.11, the error of amplitude is the largest with the Wilson method with $\theta = 1.4$, but in the Newmark method with $\gamma = 1/2$, $\beta = 1/4$ and in the HHT-α method with $\alpha = 0$, there is no error of amplitude.

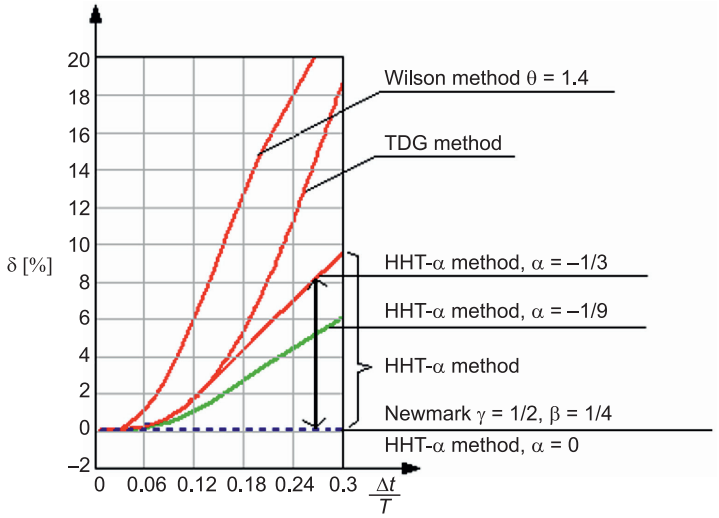

Fig. 7.11. Amplitude error of direct integration methods of equation of motion

Period error

Figure 7.12 shows the period error according to (7.27), $RE(\tilde{\Omega}) = \dfrac{\Delta T}{T} = \dfrac{\tilde{T} - T}{T}$, for considering the above direct integration methods.

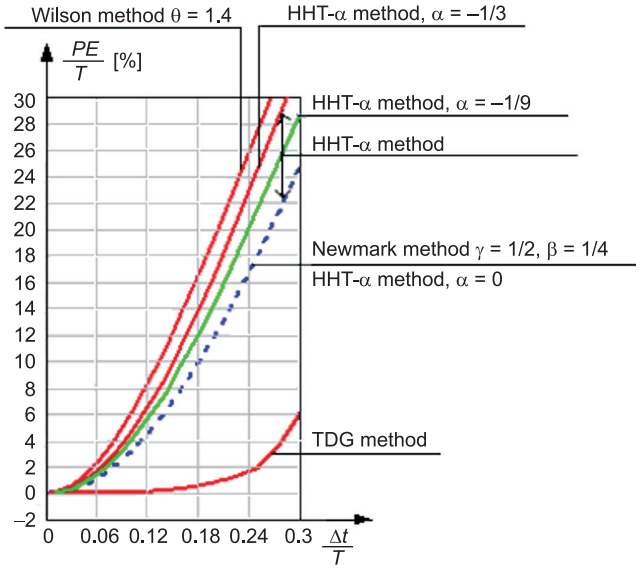

Fig. 7.12. Error of period of direct integration methods of equation of motion

As shown in Figure 7.12, all methods which are under consideration cause the error of period. This is a phenomenon known in digital signal analysis, called *aliasing*, which involves a shift of frequency greater than the Nyquist frequency to a lower frequency. According to Figure 7.12, the error of period is the largest in the Wilson method with $\theta = 1.4$, and the lowest in the TDG method.

7.7. FEM mesh in problems of wave propagation

Dynamic analysis of engineering structures (including a soil area) can be divided into two classes of problems:

1. Dynamic analysis of structure with loads in the low frequency range – this category of problem is associated with dynamic structures with long-term load excitation. To solve these tasks, there are two methods:
   a) the modal method, where the solution is the sum of motion in eigenforms without the need to include information about the phase angle between the frequencies,
   b) the method of numerical integration of the equations of motion over time.
2. Dynamic analysis of structure with loads at high frequencies – this category of problem is associated with wave propagation problems in short-term load excitation, e.g. shock or impact. To solve these problems, the integration methods over time are used, here it is necessary to take into account information about the phase angle between the frequencies.

The limit of low and high frequencies depends on material parameters of the structure including the soil area – it is generally accepted that low frequencies are in the tens of Hz, and high frequencies are of several hundred Hz or more.

Currently, FEM is most commonly used to solve problems of wave propagation. In this method, the high frequencies (with a small wavelength) determine the size of the finite elements mesh. To obtain reliable answers, you need to use a mesh of elements with very small dimensions. In the wave propagation problem the element length should be less than half the wave length. The error of numerical solution occurs for the large–sized element compared to the wave length.

The solution to the problem of wave propagation is the sum of the components of the wave propagation at various frequencies. The theoretical solution includes the infinitely large number of wave components. The numerical solution is limited to a finite number of components depending on the number of mesh nodes. If the FE mesh nodes are equally spaced, the problem of wave propagation can be compared with the digital signal sampling problem.

The sampling process (digitization) for continuum signal $x(t)$ involves on reading $x(t)$ at a time with constant increment Δt (Figure 7.13).

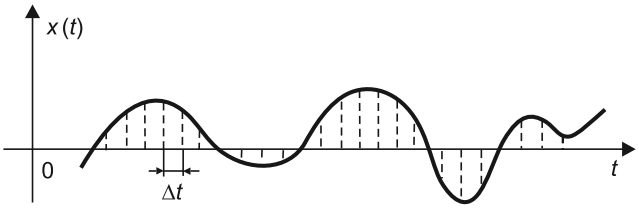

Fig. 7.13. The sampling process of continuum signal $x(t)$

The sampling theorem is used, to define error between the continuous function $x(t)$ and the sequence of the discrete values $\{x_k\}$. The assumption of theory are:

1) signal $x(t)$ is defined by $-\infty < t < +\infty$,
2) power spectral density $G_x(f)$ has a finite value of signal $x(t)$,
3) the spectrum has the value $G_x(f) = 0$ for frequency $|f| > f_m$, where f_m – is the maximum frequency in signal $x(t)$.

Sampling theorem

If a sampling step Δt *in time of signal* $x(t)$*, is shorter than the* $1/2f_m$*, then signal can be reproduced almost anywhere from the samples* $\{x_k\}$; $k = -\infty, \ldots, -1, 0, 1, \ldots, +\infty$.

From the sampling theorem one can get, for the signal with the frequency band $(0, f_m)$, the minimum sampling time Δt enabled to reproduce the signal from the samples set:

$$\Delta t \le \frac{1}{2 f_m}, \tag{7.91}$$

where:

f_m – a *Nyquist frequency*, maximum frequency value in signal.

Thus, the sampling frequency $f_p = \dfrac{1}{\Delta t}$ must be greater than the maximum frequency value of the signal f_m to satisfy the requirement specified in the sampling theorem. Comparing f_m and f_p we can get

$$f_p = \frac{1}{\Delta t} \ge 2 f_m. \tag{7.92}$$

It follows, that for the period of maximum frequency f_m occurring in the signal $x(t)$, there must be at least two samples.

If sampling is performed at intervals Δt that are too long, then there is the effect of a shift of components at high frequencies (higher than the Nyquist frequency f_N) to the low-frequency range $0 - f_N$ (see Figure 7.14 and Figure 7.15).

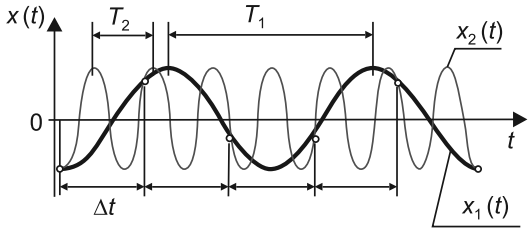

Fig. 7.14. Effects of sampling intervals Δt. Case 1 – sampling of signal $x_1(t)$ with period T_1, here $T_1/\Delta t > 2$ – fulfilling sampling theorem. Case 2 – sampling of signal $x_2(t)$ with period T_2, here $T_2/\Delta t < 2$ – not fulfilling sampling theorem

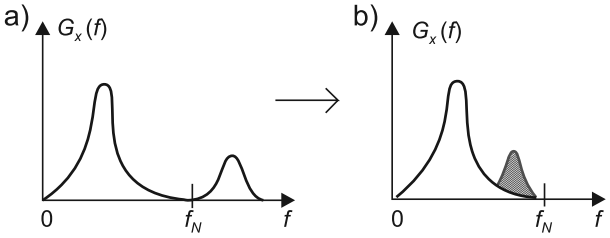

Fig. 7.15. Power spectral density: a) $x(t)$ signal before sampling, b) after sampling the signal at intervals $\Delta t > 1/2 f_N$

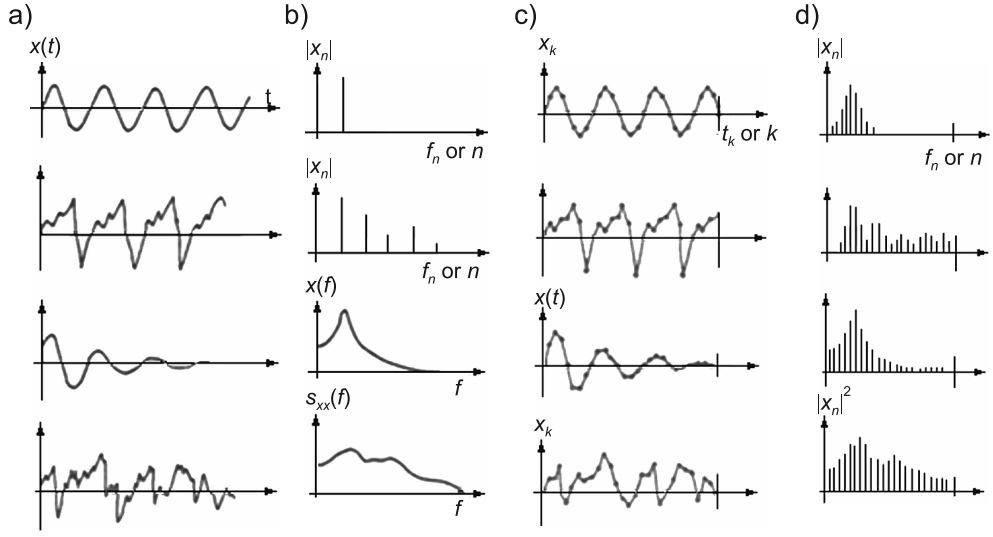

Fig. 7.16. Examples of the influence of the signal sampling on the amplitudę-frequency spectrum: a) continuum signal; b) spectrum of continuum signal; c) sampling signal; d) spectrum after sampling signal

This phenomenon can be seen on the graph of power spectral density (Figure 7.15), where the higher frequency components of f_N are shifted to lower frequencies.

As a result of discrete signal sampling, the following errors can occur (see Figure 7.16):

- ***aliasing*** – when the signal frequency is greater than the Nyquist frequency;
- if the sampling time of signal is too short, the frequencies are ***smearing***;
- the effect of multiplying the signal by a window function in the time domain is ***windowing***;
- the effect of multiplying the signal by a window function in the frequency domain is ***filtration***.

Aliasing

Aliasing – distortion of the upper part of the frequency spectrum. According to Figure 7.17, all frequencies present in the continuous signal $\omega > \omega_p/2 = \pi f_p$, located above $\omega_p/2$, shift and occur under $\omega_p/2$ with "*mirror reflection*".

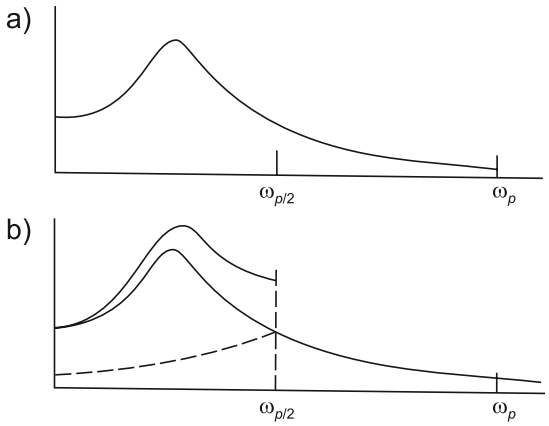

Fig. 7.17. Aliasing problem: a) spectrum before sampling, b) spectrum after sampling with aliasing error

The problem of plane wave propagation with a frequency f_m given by the following equation is considered:

$$\mathbf{d}(f) = \mathbf{A}\sin(2\pi f_m t - k_m \mathbf{x}) \tag{7.93}$$

where:

- $\mathbf{A}$ – the amplitude of the wave,
- k_m – the wavenumber,
- $\mathbf{x}$ – the space coordinate.

Where wavenumber k_m, wavelength λ_m and the corresponding frequency f_m are interrelated:

$$k_m = \frac{2\pi}{\lambda_m} \tag{7.94a}$$

$$\lambda_m = \frac{c}{f_m}, \tag{7.94b}$$

where:

c – the wave phase velocity.

The wavelength is inversely proportional to the frequency of the wave. The proportionality coefficient is the phase velocity of waves c in the soil (depends upon the physical properties of the soil medium and can have different values in different areas). Moreover, the wave velocity can also vary depending on its frequency (*dispersion*). The wavelength may vary with speed.

By substituting $f_m = c / \lambda_m$, the condition on the time step (7.91) obtained:

$$\Delta t \le \frac{\lambda_m}{2c}. \tag{7.95}$$

If a wavelength λ_m is coner at least by a two finite elements, i.e. $L_{\text{ele}} \le \lambda_m / 2$, then dimension of this element (with the linear shape function) can be defined as:

$$L_{\text{ele}} \le c\Delta t. \tag{7.96}$$

In problems of the propagation of elastic waves, the finite element mesh nodes should be at equal intervals. In such cases, the *h*-type adaptive mesh elements or *p*-type mesh elements of a Lagrange are used. The spacing between nodes, according to (7.96) depends on the speed of the wave c, which depends on the physical parameters of the soil E_{dyn} and ν.

In the case of an inelastic domain (with locally changing the physical parameters of the soil, plasticity area), decrease the value of wave speed c occur. In these areas, mesh elements density should be adapted to fulfil condition (7.96).

7.8. Nonlinear problems

7.8.1. Introduction

Practical problems of the dynamics of structure with the water flow and the change of water pressure in the deformable soil skeleton are often considered. An example might be the analysis of slopes or dam reservoirs while passing seismic waves or para-seismic waves derived from mining or transport vibration (Figure 7.18).

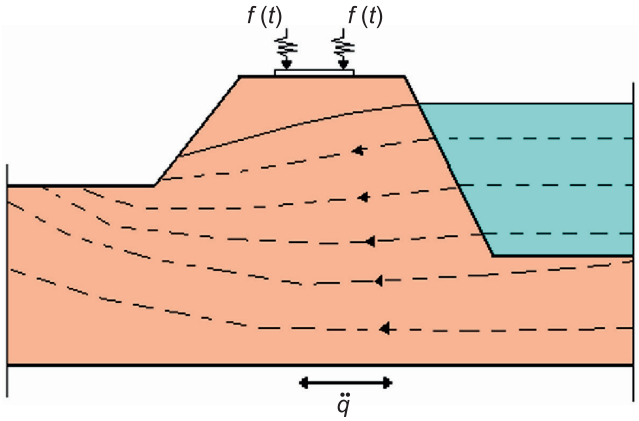

Fig. 7.18. Example of the dynamics of a coupled multiphase problem

The problem of solving the equation of motion of a nonlinear structure in discrete time t is considered

$$\mathbf{M}_t\ddot{\mathbf{d}}_t + \mathbf{C}_t\dot{\mathbf{d}}_t + \mathbf{K}_t\mathbf{d}_t = \mathbf{f}_t. \tag{7.97}$$

The method of numerical integration of equations of motion in the FEM is used. The main difference between the integration of linear and nonlinear dynamics is that in the non-linear dynamics, the iteratively solving of nonlinear equations is needed in each time step at the transition from time t to time $t + \Delta t$.

7.8.2. Integration over time in the formulation of $\mathbf{u}^s$–p

To solve the system of equations (7.97), the Newmark integration scheme is used to calculate displacements $\bar{\mathbf{u}}$, velocity $\dot{\bar{\mathbf{u}}}$ and acceleration $\ddot{\bar{\mathbf{u}}}$ and the scheme of a first order to determine pore pressure $\bar{\mathbf{p}}$. At time $t = t_{n+1}$ adopted approximations

$$\begin{gathered}
\ddot{\bar{\mathbf{u}}}_{n+1} = \ddot{\bar{\mathbf{u}}}_n + \Delta\ddot{\bar{\mathbf{u}}}_n \\
\dot{\bar{\mathbf{u}}}_{n+1} = \dot{\bar{\mathbf{u}}}_n + \ddot{\bar{\mathbf{u}}}_n\Delta t + \beta_1\Delta\ddot{\bar{\mathbf{u}}}_n\Delta t = \dot{\bar{\mathbf{u}}}^p_{n+1} + \beta_1\Delta\ddot{\bar{\mathbf{u}}}_n\Delta t \\
\bar{\mathbf{u}}_{n+1} = \bar{\mathbf{u}}_n + \dot{\bar{\mathbf{u}}}_n\Delta t + (\Delta\ddot{\bar{\mathbf{u}}}_n\Delta t^2)/2 + \beta_2\Delta\ddot{\bar{\mathbf{u}}}_n\Delta t^2 = \bar{\mathbf{u}}^p_{n+1} + \beta_2\Delta\ddot{\bar{\mathbf{u}}}_n\Delta t^2 \\
\dot{\bar{\mathbf{p}}}_{n+1} = \dot{\bar{\mathbf{p}}}_n + \Delta\dot{\bar{\mathbf{p}}}_n \\
\bar{\mathbf{p}}_{n+1} = \bar{\mathbf{p}}_n + \dot{\bar{\mathbf{p}}}_n\Delta t + \theta\Delta\dot{\bar{\mathbf{p}}}_n\Delta t = \bar{\mathbf{p}}^p_{n+1} + \theta\Delta\dot{\bar{\mathbf{p}}}_n\Delta t,
\end{gathered} \tag{7.98}$$

where $\dot{\bar{\mathbf{u}}}^p_{n+1}$, $\bar{\mathbf{u}}^p_{n+1}$ oraz $\bar{\mathbf{p}}^p_{n+1}$ are predictors of the known values of the previous time t_n, and β_1, β_2, θ are Newmark parameters.

Substituting (7.98) to (7.97) obtained:

$$\mathbf{M}_{n+1}(\ddot{\bar{\mathbf{u}}}_n + \Delta\ddot{\bar{\mathbf{u}}}_n) + \bar{\mathbf{P}}_{n+1} - \mathbf{Q}^w_{n+1}(\bar{\mathbf{p}}_n + \dot{\bar{\mathbf{p}}}_n\Delta t + \theta\Delta\dot{\bar{\mathbf{p}}}_n\Delta t) = \mathbf{f}^u_{n+1}$$

$$(\mathbf{Q}^w_{n+1} + \mathbf{Q}^{gw}_{n+1})^T(\dot{\bar{\mathbf{u}}}_n + \ddot{\bar{\mathbf{u}}}_n\Delta t + \beta_1\Delta\ddot{\bar{\mathbf{u}}}_n\Delta t) + (\mathbf{H}^w_{n+1} + \mathbf{H}^{gw}_{n+1})^T(\bar{\mathbf{p}}_n + \dot{\bar{\mathbf{p}}}_n\Delta t + \theta\Delta\dot{\bar{\mathbf{p}}}_n\Delta t) +$$

$$+ (\mathbf{S}^w_{n+1} + \mathbf{S}^{gw}_{n+1})^T(\dot{\bar{\mathbf{p}}}_n + \Delta\dot{\bar{\mathbf{p}}}_n) = \mathbf{f}^p_{n+1} \tag{7.99a}$$

or

$$\boldsymbol{\Psi}^u_{n+1} = \mathbf{M}_{n+1}\Delta\ddot{\bar{\mathbf{u}}}_n + \bar{\mathbf{P}}_{n+1} - \mathbf{Q}^w_{n+1}\theta\Delta\dot{\bar{\mathbf{p}}}\Delta t - \mathbf{F}^u_{n+1} = 0$$

$$\boldsymbol{\Psi}^p_{n+1} = (\mathbf{Q}^w_{n+1} + \mathbf{Q}^{gw}_{n+1})^T\beta_1\Delta\ddot{\bar{\mathbf{u}}}_n\Delta t + (\mathbf{H}^w_{n+1} + \mathbf{H}^{gw}_{n+1})^T\theta\Delta\dot{\bar{\mathbf{p}}}_n\Delta t +$$

$$+ (\mathbf{S}^w_{n+1} + \mathbf{S}^{gw}_{n+1})^T\Delta\dot{\bar{\mathbf{p}}}_n - \mathbf{F}^p_{n+1} = 0, \tag{7.99b}$$

where:

$$\mathbf{F}^u_{n+1} = \mathbf{f}^u_{n+1} - \mathbf{M}_{n+1}\ddot{\bar{\mathbf{u}}}_n + \mathbf{Q}^w_{n+1}(\bar{\mathbf{p}}_n + \dot{\bar{\mathbf{p}}}_n\Delta t)$$

$$\mathbf{F}^p_{n+1} = \mathbf{f}^p_{n+1} - (\mathbf{Q}^w_{n+1} + \mathbf{Q}^{gw}_{n+1})^T(\dot{\bar{\mathbf{u}}}_n + \ddot{\bar{\mathbf{u}}}_n\Delta t) - (\mathbf{H}^w_{n+1} + \mathbf{H}^{gw}_{n+1})^T(\bar{\mathbf{p}}_n + \dot{\bar{\mathbf{p}}}_n\Delta t) -$$

$$- (\mathbf{S}^w_{n+1} + \mathbf{S}^{gw}_{n+1})^T\dot{\bar{p}}_n \tag{7.99c}$$

Detailing description of each matrix is presented in Chapter 6.6 – two-phase fully-saturated soil dynamic, $\mathbf{u}^s$–p formulation. At any time point t_{n+1} should specify the components of vector $\bar{\mathbf{P}}_{n+1}$, which are obtaine by integration of the constitutive equations of the elastic-viscoplastic strain with the known distribution of the previous time point. In addition, the water vapour pressure p_{gw} and density ρ^{sw} should be determined at each time step.

Set of equations (7.99) is a system of non-linear equations which include the non-linear constitutive equation and the degree of saturation of the pore. To solve non-linear equations, a procedure of Newton–Raphson iteration is proposed

$$\boldsymbol{\Psi}^\pi_i + \left.\frac{\partial\boldsymbol{\Psi}^\pi_i}{\partial\mathbf{x}}\right|_{\mathbf{x}=\mathbf{x}_i}\Delta\mathbf{x}_i = 0, \tag{7.100}$$

where the Jacobian matrix is defined as

$$\mathbf{J} = \left.\frac{\partial\boldsymbol{\Psi}^\pi_i}{\partial\mathbf{x}}\right|_{\mathbf{x}=\mathbf{x}_i} = \begin{bmatrix} \dfrac{\partial\boldsymbol{\Psi}^u_i}{\partial\Delta\ddot{\bar{\mathbf{u}}}} & \dfrac{\partial\boldsymbol{\Psi}^u_i}{\partial\Delta\dot{\bar{\mathbf{p}}}} \\ \dfrac{\partial\boldsymbol{\Psi}^p_i}{\partial\Delta\ddot{\bar{\mathbf{u}}}} & \dfrac{\partial\boldsymbol{\Psi}^p_i}{\partial\Delta\dot{\bar{\mathbf{p}}}} \end{bmatrix} =$$

$$= \begin{bmatrix} \mathbf{M} + \mathbf{K}_T\beta_2\Delta t^2 & -\mathbf{Q}^w\theta\Delta t \\ (\mathbf{Q}^w + \mathbf{Q}^{gw})^T\beta_1\Delta t & (\mathbf{H}^w + \mathbf{H}^{gw})^T\theta\Delta t + (\mathbf{S}^w + \mathbf{S}^{gw})^T \end{bmatrix} \tag{7.101}$$

where:

$\mathbf{K}_T$ – a tangential elastic-viscoplastic matrix.

The second equation (7.99) was modified: a) multiplied by $-\frac{\theta}{\beta_1}$ and b) the coupling steam matrix $(\mathbf{Q}^{gw})^T$ was transferred on the right side. Then substituting (7.101) to (7.100) finally obtained:

$$\begin{bmatrix} \mathbf{M}+\mathbf{K}_T\beta_2\Delta t^2 & -\mathbf{Q}^w\theta\Delta t \\ -(\mathbf{Q}^w)^T\Delta t & \frac{-\theta}{\beta_1}[(\mathbf{H}^w+\mathbf{H}^{gw})^T\theta\Delta t+(\mathbf{S}^w+\mathbf{S}^{gw})^T] \end{bmatrix} \begin{Bmatrix} \Delta\ddot{\mathbf{u}}_n \\ \Delta\dot{\mathbf{p}}_n \end{Bmatrix} = \\ = \begin{Bmatrix} -\boldsymbol{\Psi}^u_{n+1} \\ \frac{\theta}{\beta_1}\boldsymbol{\Psi}^p_{n+1}+(\mathbf{Q}^{gw})^T\theta\Delta t\ddot{\mathbf{u}}_n \end{Bmatrix} \tag{7.102}$$

System (7.102) is solved iteratively, taking value $\Delta\ddot{\mathbf{u}}$ from the previous iteration.

The time integration method is unconditionally convergent if:

$$\beta_2 \geq \beta_1, \quad \beta_1 \geq 1/2, \quad \theta \geq 1/2.$$

7.8.3. Undrained case

In the case of an incompressible fluid, **S** matrix takes a value close to zero, compared with other matrices

$$\mathbf{S}^w = \mathbf{S}^{gw} \approx 0 \tag{7.103}$$

furthermore, in the case of very small permeability coefficients included in matrix **H** (e.g. in the case of silt, clay)

$$\mathbf{H}^w = \mathbf{H}^{gw} \approx 0 \tag{7.104}$$

leads to the undrained problem.

Equation (7.102) is transformed to the form

$$\begin{bmatrix} \mathbf{M}+\mathbf{K}_T\beta_2\Delta t^2 & -\mathbf{Q}^w\theta\Delta t \\ -(\mathbf{Q}^w)^T\Delta t & 0 \end{bmatrix} \begin{Bmatrix} \Delta\ddot{\mathbf{u}}_n \\ \Delta\dot{\mathbf{p}}_n \end{Bmatrix} = \begin{Bmatrix} -\boldsymbol{\Psi}^u_{n+1} \\ \frac{\theta}{\beta_1}\boldsymbol{\Psi}^p_{n+1}+(\mathbf{Q}^{gw})^T\theta\Delta t\ddot{\mathbf{u}}_n \end{Bmatrix} \tag{7.105}$$

and can be solved only if

$$n_u \geq n_p \tag{7.106}$$

where:

n_u – the number of displacements degree of freedom, number of elements in vector $\bar{\mathbf{u}}$,

n_p – number of pore pressures degree of freedom, number of elements in $\bar{\mathbf{p}}$ (Figure 7.19).

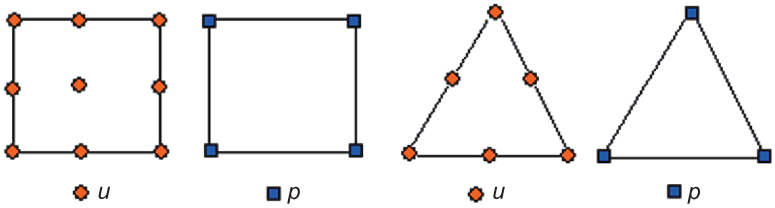

Fig. 7.19. Approximation nodes displacement **u** and pore pressures *p*

Figure 7.19 shows the interpolation functions for rectangular and triangular element nodes for displacements and pressures to ensure continuity class C_0.

If the inertia forces are omitted $\mathbf{M}\ddot{\mathbf{u}} = 0$, then the equation (7.105) describes the phenomenon of consolidation problem.

7.9. References to Chapter 7

Bathe K.J. (1996): *Finite Element Procedures*, Prentice Hall.

Belytschko T., Hughes T.J.R., editors (1983): *Computational Methods for Transient Analysis*. North-Holland, Amsterdam.

Bonelli A., Bursi O.S., Mancuso M. (2001*): Explicit predictor-multicorrector time discontinuous Galerkin methods for linear dynamics*, Journal of Sound and Vibration, 246(4), 625-652.

Bonelli A., Bursi O.S., Mancuso M. (2002): *Explicit predictor-multicorrector time discontinuous Galerkin methods for non-linear dynamics*, Journal of Sound and Vibration, 256(4), 659-724.

Cannillo V., Mancuso M. (2002): *On the behaviour of dissipative time integration methods near the resonance condition*, Letters to the Editor, Journal of Sound and Vibration, 249(3), 599-605

Clough R.W., Penzien J. (1995): *Dynamics of Structures*, Second edition, Mc Graw-Hill International.

Hilber H., T.J.R. Hughes, R.L. Taylor. (1977): *Improved numerical dissipation for the time integration algorithms in structural dynamics*, Earthquake Engineering and Structural Dynamics, 5, 283-292.

Hughes T.J.R. (1987): *The Finite Element Method, Linear Static and Dynamic Finite Element Analysis*, Prentice-Hall, Englewood Cliffs, NJ.

Hughes T.J.R., Hulbert G. (1988): *Space-time finite element methods for elastodynamics: formulation and error estimates*, Comput. Methods Appl. Mech. Eng. 66, 363-393.

Lacoma L.M., Romero I. (2007): *Error estimation for HHT method in non-linear solid dynamics*, Computers and structures, 85, 158-169.

Langer J. (1980): *Dynamika budowli*, Politechnika Wrocławska.

Lewandowski R. (2006): *Dynamika konstrukcji budowlanych*, Wydawnictwo Politechniki Poznańskiej.

Li X.D., Wiberg N.-E. (1996): *Structural dynamic analysis by a time-discontinuous Galerkin finite element method*, International Journal for Numerical Methods in Engineering 39, 2131-2152.

Newmark N.M. (1959): *A Method of Copulation for Structural Dynamics*, ASCE Journal of Engineering Mechanics Division, Vol. 85, 67-94.

Wilson E.L., Farhoomand I., Bathe K.J. (1973): *Nonlinear Dynamic Analysis of Complex Structures*, International Journal of Earthquake Engineering and Structural Dynamics, Vol. 1, 241-252.

Wrana B. (1996): *Problemy doboru modelu macierzy bezwładności oraz jej identyfikacji w dynamice*, Konf. Analiza Modalna, 9–13 grudnia 1996, Akademia Górniczo-Hutnicza w Krakowie.

Wrana B. (1997): *Metoda elementów spektralnych w zagadnieniach interakcji konstrukcji z podłożem*, II Ogólnopolskie Sympozjum „Wpływy Środowiskowe na budowle i ludzi – obciążenia, oddziaływania, interakcje, dyskomfort", 24–26 październik 1997, Lublin–Kazimierz Dolny, 359-363.

Wrana B. (1998): *Interakcja konstrukcji z podłożem w zakresie oddziaływań dynamicznych. Aproksymacja numeryczna*, X Jubileuszowa Konferencja Naukowa „Metody Numeryczne do Projektowania i Analizy Konstrukcji Hydrotechnicznych", Korbielów '98, 2–4 marca 1998, 29-35.

Wrana B. (1999): *Metoda krępych elementów spektralnych i jej zastosowanie do analizy dynamicznej fundamentów pod turbozespoły*, Monografia nr 253, Seria Inżynieria Lądowa, Politechnika Krakowska.

Wrana B. (2001): *Równania dynamiki obszaru gruntu*, XIII Konferencja Naukowa Korbielów 2001 „Metody Komputerowe w Projektowaniu i Analizie Konstrukcji Hydrotechnicznych*"* 5–8 marca 2001, Korbielów.

Wrana B., Borowiec A. (2004): *Zastosowanie transformaty falkowej do analizy wyników obliczeń dynamicznych nasyconej warstwy piasku*, Wydawnictwo Techniczne, Budownictwo, Politechnika Krakowska.

Wrana B., Borowiec A. (2004): *Transformaty falkowe w dynamice gruntów*, Wydawnictwo Techniczne, Budownictwo*,* Politechnika Krakowska.

Wrana B., Borowiec A. (2006): *Analiza dynamiczna wyników warstwy zagęszczonego piasku przy użyciu transformaty falkowej*, Wydawnictwo Techniczne, Budownictwo, Politechnika Krakowska.

Wrana B. (2007): *Identification of Damping by Means of Wavelet and Half Bandwidth Method*, CMM-2007 – Computer Methods in Mechanics, June 19–22, 2007, Łódź–Spała, Poland.

Wrana B., Czado B. (2007): *Identification of damping in soil*, V Symposium Environmental Effects on Buildings and People – actions, influences, interactions, discomfort, Kazimierz Dolny, Poland, October 24–27, 2007.

Wrana B. (2010): *Rozwiązywanie zadania rozchodzenia się fali naprężeniowej w gruncie przy zastosowaniu sformułowania nieciągłego w czasie Galerkina*, Górnictwo i geoinżynieria, AGH

Wrana B. (2011): *A Discontinuous Galerkin Finite Element Method for Dynamic of Fully Saturated Soil*, Archives of Civil Engineering, LVII, 1,119-134.

Wrana B. (2011): *Rozwiązywanie zadania rozchodzenia się fali naprężeniowej w gruncie przy zastosowaniu sformułowania nieciągłego w czasie Galerkina*, II Kongres Mechaniki Polskiej.

Zieliński T.P. (2002): *Od teorii do cyfrowego przetwarzania sygnałów*, Wydział Elektrotechniki, Automatyki, Informatyki i Elektroniki, Akademia Górniczo-Hutnicza w Krakowie.

Zienkiewicz O.C., Taylor R.L., Zhu J.Z. (2005): *Finite Element Method: Its Basis and Fundamentals*, Sixth edition, Elsevier.

APPENDIX A – Operations on vectors and matrices

A.1. Vectors, Matrices

Denotation:

A – matrix, tensor

a – vector

Displacement vector in the Voigt notation

$$\mathbf{u} = \{u_1, u_2, u_3\}^T \tag{A.1}$$

Stress vector in the Voigt notation

$$\boldsymbol{\sigma} = \{\sigma_{11}, \sigma_{22}, \sigma_{33}, \sigma_{12}, \sigma_{13}, \sigma_{23}\}^T \tag{A.2}$$

Strain vector in the Voigt notation

$$\boldsymbol{\varepsilon} = \{\varepsilon_{11}, \varepsilon_{22}, \varepsilon_{33}, \varepsilon_{12}, \varepsilon_{13}, \varepsilon_{23}\}^T =$$

$$= \left\{ \frac{\partial u_1}{\partial x_1},\ \frac{\partial u_2}{\partial x_2},\ \frac{\partial u_3}{\partial x_3}, \frac{1}{2}\left(\frac{\partial u_1}{\partial x_2} + \frac{\partial u_2}{\partial x_1}\right), \frac{1}{2}\left(\frac{\partial u_1}{\partial x_3} + \frac{\partial u_3}{\partial x_1}\right), \frac{1}{2}\left(\frac{\partial u_2}{\partial x_3} + \frac{\partial u_3}{\partial x_2}\right) \right\}^T \tag{A.3}$$

Rotation vector

$$\boldsymbol{\omega} = \{\omega_1,\ \omega_2,\ \omega_3\}^T = \left\{ \left(\frac{\partial u_3}{\partial x_2} - \frac{\partial u_2}{\partial x_3}\right),\ \left(\frac{\partial u_1}{\partial x_3} - \frac{\partial u_3}{\partial x_1}\right),\ \left(\frac{\partial u_2}{\partial x_1} - \frac{\partial u_1}{\partial x_2}\right) \right\}^T \tag{A.4}$$

Cauchy stress tensor

$$\boldsymbol{\Sigma} = \begin{bmatrix} \sigma_{11} & \sigma_{12} & \sigma_{13} \\ \sigma_{21} & \sigma_{22} & \sigma_{23} \\ \sigma_{31} & \sigma_{32} & \sigma_{33} \end{bmatrix} \tag{A.5}$$

Euler strain tensor

$$\mathbf{E} = \begin{bmatrix} \varepsilon_{11} & \varepsilon_{12} & \varepsilon_{13} \\ \varepsilon_{21} & \varepsilon_{22} & \varepsilon_{23} \\ \varepsilon_{31} & \varepsilon_{32} & \varepsilon_{33} \end{bmatrix} \tag{A.6}$$

Hamilton operator

$$\nabla = \left\{ \frac{\partial}{\partial x_1} \quad \frac{\partial}{\partial x_2} \quad \frac{\partial}{\partial x_3} \right\} \tag{A.7}$$

Laplace operator

$$\Delta = \nabla^2 = \left\{ \frac{\partial^2}{\partial x_1^2} \quad \frac{\partial^2}{\partial x_2^2} \quad \frac{\partial^2}{\partial x_3^2} \right\} \tag{A.8}$$

$$\Delta U = \frac{\partial^2 U}{\partial x_1^2} + \frac{\partial^2 U}{\partial x_2^2} + \frac{\partial^2 U}{\partial x_3^2}, \quad U = U(x_1, x_2, x_3) \tag{A.9}$$

$$\Delta \mathbf{u} = \begin{Bmatrix} \Delta u_1 \\ \Delta u_2 \\ \Delta u_3 \end{Bmatrix} = \begin{Bmatrix} \dfrac{\partial^2 u_1}{\partial x_1^2} + \dfrac{\partial^2 u_1}{\partial x_2^2} + \dfrac{\partial^2 u_1}{\partial x_3^2} \\ \dfrac{\partial^2 u_2}{\partial x_1^2} + \dfrac{\partial^2 u_2}{\partial x_2^2} + \dfrac{\partial^2 u_2}{\partial x_3^2} \\ \dfrac{\partial^2 u_3}{\partial x_1^2} + \dfrac{\partial^2 u_3}{\partial x_2^2} + \dfrac{\partial^2 u_3}{\partial x_3^2} \end{Bmatrix} \tag{A.10}$$

Scalar product of two vectors

$$\mathbf{u}^T \mathbf{v} = \{u_1,\ u_2,\ u_3\} \begin{Bmatrix} v_1 \\ v_2 \\ v_3 \end{Bmatrix} \tag{A.11}$$

Tensor product of two vectors

$$\mathbf{u}\mathbf{v}^{\mathrm{T}} = \begin{Bmatrix} u_1 \\ u_2 \\ u_3 \end{Bmatrix} \{v_1,\ v_2,\ v_3\} = \begin{bmatrix} u_1 v_1 & u_1 v_2 & u_1 v_3 \\ u_2 v_1 & u_2 v_2 & u_2 v_3 \\ u_3 v_1 & u_3 v_2 & u_3 v_3 \end{bmatrix} \tag{A.12}$$

Vector product of two vectors

$$\mathbf{u} \times \mathbf{v} = \begin{Bmatrix} u_2 v_3 - u_3 v_2 \\ u_3 v_1 - u_1 v_3 \\ u_1 v_2 - u_2 v_1 \end{Bmatrix} \tag{A.13}$$

A.2. Derivative operators

A.2.1. Cartesian coordinates

Gradient of scalar field $U = U(x_1, x_2, x_3)$

$$\nabla U = \text{grad} U = \begin{Bmatrix} \dfrac{\partial U}{\partial x_1} \\ \dfrac{\partial U}{\partial x_2} \\ \dfrac{\partial U}{\partial x_3} \end{Bmatrix} \tag{A.14}$$

Gradient of vector field $\mathbf{u} = \{u_1, u_2, u_3\}^T$

$$\mathbf{u}\nabla = \text{grad}\mathbf{u} = \begin{Bmatrix} u_1 \\ u_2 \\ u_3 \end{Bmatrix} \left\{ \frac{\partial}{\partial x_1}, \frac{\partial}{\partial x_2}, \frac{\partial}{\partial x_3} \right\} = \begin{bmatrix} \dfrac{\partial u_1}{\partial x_1} & \dfrac{\partial u_1}{\partial x_2} & \dfrac{\partial u_1}{\partial x_3} \\ \dfrac{\partial u_2}{\partial x_1} & \dfrac{\partial u_2}{\partial x_2} & \dfrac{\partial u_2}{\partial x_3} \\ \dfrac{\partial u_3}{\partial x_1} & \dfrac{\partial u_3}{\partial x_2} & \dfrac{\partial u_3}{\partial x_3} \end{bmatrix} \tag{A.15}$$

The gradient of vector field is characterized by the invariance with respect to translation and rotation, so a scalar invariance type.

Divergence of the vector field $\mathbf{u} = \{u_1, u_2, u_3\}^T$

$$\nabla \mathbf{u} = \text{div}\mathbf{u} = \left\{ \frac{\partial}{\partial x_1}, \frac{\partial}{\partial x_2}, \frac{\partial}{\partial x_3} \right\} \begin{Bmatrix} u_1 \\ u_2 \\ u_3 \end{Bmatrix} = \frac{\partial u_1}{\partial x_1} + \frac{\partial u_2}{\partial x_2} + \frac{\partial u_3}{\partial x_3} = \varepsilon_v \tag{A.16}$$

ε_v – volumetric strain, if the vector $\mathbf{u}$ is the displacement vector

Rotation of the vector field $\mathbf{u} = \{u_1, u_2, u_3\}^T$

$$\nabla \times \mathbf{u} = \text{rot}\,\mathbf{u} = \text{curl}\,\mathbf{u} = \begin{Bmatrix} \dfrac{\partial}{\partial x_1} \\ \dfrac{\partial}{\partial x_2} \\ \dfrac{\partial}{\partial x_3} \end{Bmatrix} \times \begin{Bmatrix} u_1 \\ u_2 \\ u_3 \end{Bmatrix} = \begin{Bmatrix} \dfrac{\partial u_3}{\partial x_2} - \dfrac{\partial u_2}{\partial x_3} \\ \dfrac{\partial u_1}{\partial x_3} - \dfrac{\partial u_3}{\partial x_1} \\ \dfrac{\partial u_2}{\partial x_1} - \dfrac{\partial u_1}{\partial x_2} \end{Bmatrix} = \begin{Bmatrix} \omega_1 \\ \omega_2 \\ \omega_3 \end{Bmatrix} = \boldsymbol{\omega} \tag{A.17}$$

Divergence of the tensor field or matrix

$$\mathrm{div}\mathbf{E} = \mathrm{div}\varepsilon_{ij} = \frac{\partial \varepsilon_{ij}}{\partial x_j} = \mathbf{E}\nabla^T = \begin{bmatrix} \varepsilon_{11} & \varepsilon_{12} & \varepsilon_{13} \\ \varepsilon_{21} & \varepsilon_{22} & \varepsilon_{23} \\ \varepsilon_{31} & \varepsilon_{32} & \varepsilon_{33} \end{bmatrix} \begin{Bmatrix} \dfrac{\partial}{\partial x_1} \\ \dfrac{\partial}{\partial x_2} \\ \dfrac{\partial}{\partial x_3} \end{Bmatrix} = \begin{Bmatrix} \dfrac{\partial \varepsilon_{11}}{\partial x_1} + \dfrac{\partial \varepsilon_{12}}{\partial x_2} + \dfrac{\partial \varepsilon_{13}}{\partial x_3} \\ \dfrac{\partial \varepsilon_{21}}{\partial x_1} + \dfrac{\partial \varepsilon_{22}}{\partial x_2} + \dfrac{\partial \varepsilon_{23}}{\partial x_3} \\ \dfrac{\partial \varepsilon_{31}}{\partial x_1} + \dfrac{\partial \varepsilon_{32}}{\partial x_2} + \dfrac{\partial \varepsilon_{33}}{\partial x_3} \end{Bmatrix} \tag{A.18}$$

$$\mathrm{div}\boldsymbol{\Sigma} = \mathrm{div}\sigma_{ij} = \frac{\partial \sigma_{ij}}{\partial x_j} = \boldsymbol{\Sigma}\nabla^{\mathrm{T}} = \begin{bmatrix} \sigma_{11} & \sigma_{12} & \sigma_{13} \\ \sigma_{21} & \sigma_{22} & \sigma_{23} \\ \sigma_{31} & \sigma_{32} & \sigma_{33} \end{bmatrix} \begin{Bmatrix} \dfrac{\partial}{\partial x_1} \\ \dfrac{\partial}{\partial x_2} \\ \dfrac{\partial}{\partial x_3} \end{Bmatrix} = \begin{Bmatrix} \dfrac{\partial \sigma_{11}}{\partial x_1} + \dfrac{\partial \sigma_{12}}{\partial x_2} + \dfrac{\partial \sigma_{13}}{\partial x_3} \\ \dfrac{\partial \sigma_{21}}{\partial x_1} + \dfrac{\partial \sigma_{22}}{\partial x_2} + \dfrac{\partial \sigma_{23}}{\partial x_3} \\ \dfrac{\partial \sigma_{31}}{\partial x_1} + \dfrac{\partial \sigma_{32}}{\partial x_2} + \dfrac{\partial \sigma_{33}}{\partial x_3} \end{Bmatrix} \tag{A.19}$$

A.2.2. Cylindrical coordinates

Gradient of scalar field $U = U(r, \theta, z)$

$$\nabla U = \mathrm{grad}U = \begin{Bmatrix} \dfrac{\partial U}{\partial r} \\ \dfrac{1}{r}\dfrac{\partial U}{\partial \theta} \\ \dfrac{\partial U}{\partial z} \end{Bmatrix} \tag{A.20}$$

Gradient of vector field $\mathbf{u} = \{u_r, u_\theta, u_z\}^T$

$$\mathbf{u}\nabla = \mathrm{grad}\mathbf{u} = \begin{Bmatrix} u_r \\ u_\theta \\ u_z \end{Bmatrix} \left\{ \frac{\partial}{\partial r}, \frac{\partial}{\partial \theta}, \frac{\partial}{\partial z} \right\} = \begin{bmatrix} \dfrac{\partial u_r}{\partial r} & \dfrac{1}{r}\left(\dfrac{\partial u_r}{\partial \theta} - u_\theta \right) & \dfrac{\partial u_r}{\partial z} \\ \dfrac{\partial u_\theta}{\partial r} & \dfrac{1}{r}\left(\dfrac{\partial u_\theta}{\partial \theta} + u_r \right) & \dfrac{\partial u_\theta}{\partial z} \\ \dfrac{\partial u_z}{\partial r} & \dfrac{1}{r}\dfrac{\partial u_z}{\partial \theta} & \dfrac{\partial u_z}{\partial z} \end{bmatrix} \tag{A.21}$$

Divergence of vector field $\mathbf{u} = \{u_r, u_\theta, u_z\}^T$

$$\nabla \mathbf{u} = \mathrm{div}\mathbf{u} = \left\{\frac{\partial}{\partial r},\ \frac{\partial}{\partial \theta},\ \frac{\partial}{\partial z}\right\}\begin{Bmatrix} u_r \\ u_\theta \\ u_z \end{Bmatrix} = \frac{1}{r}\frac{\partial}{\partial r}\left(r\,u_r\right) + \frac{1}{r}\frac{\partial u_\theta}{\partial \theta} + \frac{\partial u_z}{\partial z} = \varepsilon_v \qquad \text{(A.22)}$$

Rotation of vector field $\mathbf{u} = \{u_r, u_\theta, u_z\}^T$

$$\nabla \times \mathbf{u} = \mathrm{rot}\,\mathbf{u} = \mathrm{curl}\,\mathbf{u} = \begin{Bmatrix} \dfrac{\partial}{\partial r} \\ \dfrac{\partial}{\partial \theta} \\ \dfrac{\partial}{\partial z} \end{Bmatrix} \times \begin{Bmatrix} u_r \\ u_\theta \\ u_z \end{Bmatrix} = \begin{Bmatrix} \dfrac{1}{r}\dfrac{\partial u_z}{\partial \theta} - \dfrac{\partial u_\theta}{\partial z} \\ \dfrac{1}{r}\dfrac{\partial u_r}{\partial z} - \dfrac{\partial u_z}{\partial r} \\ \dfrac{1}{r}\dfrac{\partial\left(r\,u_\theta\right)}{\partial r} - \dfrac{1}{r}\dfrac{\partial u_r}{\partial \theta} \end{Bmatrix} = \begin{Bmatrix} \omega_r \\ \omega_\theta \\ \omega_z \end{Bmatrix} = \boldsymbol{\omega} \qquad \text{(A.23)}$$

A.2.3. Spherical coordinates

Gradient of scalar field $U = U(r, \theta, \varphi)$

$$\nabla U = \mathrm{grad}U = \begin{Bmatrix} \dfrac{\partial U}{\partial r} \\ \dfrac{1}{r}\dfrac{\partial U}{\partial \theta} \\ \dfrac{1}{r\sin\theta}\dfrac{\partial U}{\partial \varphi} \end{Bmatrix} \qquad \text{(A.24)}$$

Gradient of vector field $\mathbf{u} = \{u_r, u_\theta, u_\varphi\}^T$

$$\mathbf{u}\nabla = \mathrm{grad}\mathbf{u} = \begin{Bmatrix} u_r \\ u_\theta \\ u_\varphi \end{Bmatrix}\left\{\frac{\partial}{\partial r},\ \frac{\partial}{\partial \theta},\ \frac{\partial}{\partial \varphi}\right\} =$$

$$= \begin{bmatrix} \dfrac{\partial u_r}{\partial r} & \dfrac{1}{r}\left(\dfrac{\partial u_r}{\partial \theta} - u_\theta\right) & \dfrac{1}{r}\left(\sin\theta\dfrac{\partial u_r}{\partial \varphi} - u_\varphi\right) \\ \dfrac{\partial u_\theta}{\partial r} & \dfrac{1}{r}\left(\dfrac{\partial u_\theta}{\partial \theta} + u_r\right) & \dfrac{1}{r}\left(\dfrac{1}{\sin\theta}\dfrac{\partial u_\theta}{\partial \varphi} - \cot\theta u_\varphi\right) \\ \dfrac{\partial u_\varphi}{\partial r} & \dfrac{1}{r}\dfrac{\partial u_\varphi}{\partial \theta} & \dfrac{1}{r}\left(\dfrac{1}{\sin\theta}\dfrac{\partial u_\varphi}{\partial \varphi} - \cot\theta u_\theta + u_r\right) \end{bmatrix} \qquad \text{(A.25)}$$

Divergence of vector field $\mathbf{u} = \{u_r, u_\theta, u_\varphi\}^T$

$$\nabla \mathbf{u} = \operatorname{div} \mathbf{u} = \left\{ \frac{\partial}{\partial r}, \frac{\partial}{\partial \theta}, \frac{\partial}{\partial \varphi} \right\} \begin{Bmatrix} u_r \\ u_\theta \\ u_\varphi \end{Bmatrix} = \frac{1}{r^2} \frac{\partial (r^2 u_r)}{\partial r} + \frac{1}{r \sin\theta} \frac{\partial (\sin\theta \, u_\theta)}{\partial \theta} + \frac{1}{r \sin\theta} \frac{\partial u_\varphi}{\partial \varphi} = \varepsilon_v \tag{A.26}$$

Rotation of vector field $\mathbf{u} = \{u_r, u_\theta, u_\varphi\}^T$

$$\nabla \times \mathbf{u} = \operatorname{rot} \mathbf{u} = \operatorname{curl} \mathbf{u} = \begin{Bmatrix} \frac{\partial}{\partial r} \\ \frac{\partial}{\partial \theta} \\ \frac{\partial}{\partial \varphi} \end{Bmatrix} \times \begin{Bmatrix} u_r \\ u_\theta \\ u_\varphi \end{Bmatrix} = \begin{Bmatrix} \frac{1}{r \sin\theta} \left(\frac{\partial (\sin\theta \, u_\varphi)}{\partial \theta} - \frac{\partial u_\theta}{\partial \varphi} \right) \\ \frac{1}{r} \left(\frac{1}{\sin\theta} \frac{\partial u_r}{\partial \varphi} - \frac{\partial (r u_\varphi)}{\partial r} \right) \\ \frac{1}{r} \left(\frac{\partial (r u_\theta)}{\partial r} - \frac{\partial u_r}{\partial \theta} \right) \end{Bmatrix} = \begin{Bmatrix} \omega_r \\ \omega_\theta \\ \omega_\varphi \end{Bmatrix} = \boldsymbol{\omega} \tag{A.27}$$

A.3. Calculation formulas

$$\operatorname{div} c = 0 \tag{A.28}$$

$$\operatorname{rot} \operatorname{grad} U = 0, \quad U = U(x_1, x_2, x_3) \tag{A.29}$$

$$\operatorname{div} \operatorname{rot} \mathbf{u} = 0 \tag{A.30}$$

$$\nabla \mathbf{u} = \operatorname{div} \mathbf{u} = \operatorname{tr} (\operatorname{grad} \mathbf{u}) \tag{A.31}$$

$$\mathbf{v} \operatorname{grad} \mathbf{u} = \begin{bmatrix} \frac{\partial u_1}{\partial x_1} & \frac{\partial u_1}{\partial x_2} & \frac{\partial u_1}{\partial x_3} \\ \frac{\partial u_2}{\partial x_1} & \frac{\partial u_2}{\partial x_2} & \frac{\partial u_2}{\partial x_3} \\ \frac{\partial u_3}{\partial x_1} & \frac{\partial u_3}{\partial x_2} & \frac{\partial u_3}{\partial x_3} \end{bmatrix} \begin{Bmatrix} v_1 \\ v_2 \\ v_3 \end{Bmatrix} = \begin{Bmatrix} u_1 \\ u_2 \\ u_3 \end{Bmatrix} \left\{ \frac{\partial}{\partial x_1}, \frac{\partial}{\partial x_2}, \frac{\partial}{\partial x_3} \right\} = (\mathbf{u} \nabla) \mathbf{v} \tag{A.32}$$

$$\operatorname{rot} (c \mathbf{u}) = c \operatorname{rot} \mathbf{u} \tag{A.33}$$

$$\operatorname{div} (c \mathbf{u}) = c \operatorname{div} \mathbf{u} = \left\{ \frac{\partial}{\partial x_1}, \frac{\partial}{\partial x_2}, \frac{\partial}{\partial x_3} \right\} \left(c \begin{Bmatrix} u_1 \\ u_2 \\ u_3 \end{Bmatrix} \right) = c \left\{ \frac{\partial}{\partial x_1}, \frac{\partial}{\partial x_2}, \frac{\partial}{\partial x_3} \right\} \begin{Bmatrix} u_1 \\ u_2 \\ u_3 \end{Bmatrix} = c \nabla \mathbf{u} \tag{A.34}$$

$$\operatorname{div}(\mathbf{u}+\mathbf{v}) = \operatorname{div}\mathbf{u} + \operatorname{div}\mathbf{v} = \nabla(\mathbf{u}+\mathbf{v}) = \nabla\mathbf{u} + \nabla\mathbf{v} = \left\{\frac{\partial}{\partial x_1},\ \frac{\partial}{\partial x_2},\ \frac{\partial}{\partial x_3}\right\}\left(\begin{Bmatrix} u_1 \\ u_2 \\ u_3 \end{Bmatrix} + \begin{Bmatrix} v_1 \\ v_2 \\ v_3 \end{Bmatrix}\right) =$$

$$= \left\{\frac{\partial}{\partial x_1},\ \frac{\partial}{\partial x_2},\ \frac{\partial}{\partial x_3}\right\}\begin{Bmatrix} u_1 \\ u_2 \\ u_3 \end{Bmatrix} + \left\{\frac{\partial}{\partial x_1},\ \frac{\partial}{\partial x_2},\ \frac{\partial}{\partial x_3}\right\}\begin{Bmatrix} v_1 \\ v_2 \\ v_3 \end{Bmatrix} \tag{A.35}$$

$$\operatorname{rot}(\mathbf{u}+\mathbf{v}) = \operatorname{rot}\mathbf{u} + \operatorname{rot}\mathbf{v} \tag{A.36}$$

$$\operatorname{div}(\mathbf{u}\times\mathbf{v}) = \mathbf{v}^T\operatorname{rot}\mathbf{u} - \mathbf{u}^T\operatorname{rot}\mathbf{v} = \{v_1, v_2, v_3\}\begin{Bmatrix} \dfrac{\partial u_3}{\partial x_2} - \dfrac{\partial u_2}{\partial x_3} \\ \dfrac{\partial u_1}{\partial x_3} - \dfrac{\partial u_3}{\partial x_1} \\ \dfrac{\partial u_2}{\partial x_1} - \dfrac{\partial u_1}{\partial x_2} \end{Bmatrix} - \{u_1, u_2, u_3\}\begin{Bmatrix} \dfrac{\partial v_3}{\partial x_2} - \dfrac{\partial v_2}{\partial x_3} \\ \dfrac{\partial v_1}{\partial x_3} - \dfrac{\partial v_3}{\partial x_1} \\ \dfrac{\partial v_2}{\partial x_1} - \dfrac{\partial v_1}{\partial x_2} \end{Bmatrix} \tag{A.37}$$

$$\operatorname{rot}(\mathbf{v}\mathbf{u}) = \mathbf{v}\operatorname{rot}\mathbf{u} + \operatorname{grad}\mathbf{v}\times\mathbf{u} \tag{A.38}$$

$$\operatorname{rot}(\mathbf{u}\times\mathbf{v}) = (\mathbf{v}\operatorname{grad})\mathbf{u} - (\mathbf{u}\operatorname{grad})\mathbf{v} + \mathbf{u}\operatorname{div}\mathbf{v} - \mathbf{v}\operatorname{div}\mathbf{u} \tag{A.39}$$

The rotation of the field potential vanishes, i.e.

$$\operatorname{rot}\operatorname{grad}U(x_1, x_2, x_3) = 0 \tag{A.40}$$

$$\operatorname{div}(\operatorname{div}\sigma_{ij}) = (\nabla\boldsymbol{\Sigma})\nabla^T =$$

$$= \left(\left\{\frac{\partial}{\partial x_1},\ \frac{\partial}{\partial x_2},\ \frac{\partial}{\partial x_3}\right\}\begin{bmatrix} \sigma_{11} & \sigma_{12} & \sigma_{13} \\ \sigma_{21} & \sigma_{22} & \sigma_{23} \\ \sigma_{31} & \sigma_{32} & \sigma_{33} \end{bmatrix}\right)\begin{pmatrix} \dfrac{\partial}{\partial x_1} \\ \dfrac{\partial}{\partial x_2} \\ \dfrac{\partial}{\partial x_3} \end{pmatrix} = \begin{Bmatrix} \dfrac{\partial\sigma_{11}}{\partial x_1} + \dfrac{\partial\sigma_{12}}{\partial x_2} + \dfrac{\partial\sigma_{13}}{\partial x_3} \\ \dfrac{\partial\sigma_{21}}{\partial x_1} + \dfrac{\partial\sigma_{22}}{\partial x_2} + \dfrac{\partial\sigma_{23}}{\partial x_3} \\ \dfrac{\partial\sigma_{31}}{\partial x_1} + \dfrac{\partial\sigma_{32}}{\partial x_2} + \dfrac{\partial\sigma_{33}}{\partial x_3} \end{Bmatrix}\begin{pmatrix} \dfrac{\partial}{\partial x_1} \\ \dfrac{\partial}{\partial x_2} \\ \dfrac{\partial}{\partial x_3} \end{pmatrix} =$$

$$= \left(\frac{\partial^2\sigma_{11}}{\partial x_1^2} + \frac{\partial^2\sigma_{12}}{\partial x_2^2} + \frac{\partial^2\sigma_{13}}{\partial x_3^2}\right) + \left(\frac{\partial^2\sigma_{21}}{\partial x_1^2} + \frac{\partial^2\sigma_{22}}{\partial x_2^2} + \frac{\partial^2\sigma_{23}}{\partial x_3^2}\right) + \left(\frac{\partial^2\sigma_{31}}{\partial x_1^2} + \frac{\partial^2\sigma_{32}}{\partial x_2^2} + \frac{\partial^2\sigma_{33}}{\partial x_3^2}\right) \tag{A.41}$$

$$\operatorname{div}\left(\frac{\partial^2 u_i^m}{\partial t^2}\right) = \frac{\partial^2}{\partial t^2}\operatorname{div}\mathbf{u}^m = \frac{\partial^2}{\partial t^2}\nabla\mathbf{u}^m = \frac{\partial^2}{\partial t^2}\varepsilon_v^m \tag{A.42}$$

APPENDIX B – Gradient of potential function of the theory of plasticity

B.1. The first derivative of stress invariants p, q, θ

In the numerical algorithms for solving plasticity problem, such as the Backward Euler algorithm and the Consistent Tangent Matrix, one should to know the explicit form of the potential function derivatives. Explicit formulas for the derivatives of the yield surface function and plastic potential function are given below.

Function Q depends on stress σ_{ij}. Eeach stress state can be represented by three stress invariants – p, q and θ as:

$$p = -\frac{1}{3} I_1 \tag{B.1}$$

$$q = \sqrt{3J_2} = \sqrt{\frac{3}{2} s_{ij} s_{ij}} \tag{B.2}$$

$$\cos 3\theta = \frac{3\sqrt{3}}{2} \frac{J_3}{\sqrt{J_2^3}} = \frac{3\sqrt{3}}{2} \frac{\frac{1}{3} s_{ij} s_{jk} s_{ki}}{\sqrt{\left(\frac{1}{2} s_{ij} s_{ij}\right)^3}} \tag{B.3}$$

$$I_1 = \sigma_{kk} \tag{B.4}$$

$$J_2 = \frac{1}{2} s_{ij} s_{ij} \tag{B.5}$$

$$J_3 = \frac{1}{3} s_{ij} s_{jk} s_{ki} \tag{B.6}$$

$$s_{ij} = \sigma_{ij} - \frac{1}{3} \sigma_{kk} \delta_{ij} \tag{B.7}$$

It was assumed that the tensile stress is positive. Lode angle θ is defined as follows: $\theta = 0$ corresponds to the average value in CTE – *Conventional Triaxial Extension*, $\theta = \pi/3$ corresponds to the average value in CTC – *Conventional Triaxial Compression*.

Potential function can be written as $Q = Q(p,q,\theta)$, at which the derivatives are of the form

$$\frac{\partial Q}{\partial \sigma_{ij}} = \frac{\partial Q}{\partial p}\frac{\partial p}{\partial \sigma_{ij}} + \frac{\partial Q}{\partial q}\frac{\partial q}{\partial \sigma_{ij}} + \frac{\partial Q}{\partial \theta}\frac{\partial \theta}{\partial \sigma_{ij}}, \tag{B.8}$$

where the first derivatives of the stress invariants with respect to the stress are:

$$\frac{\partial p}{\partial \sigma_{ij}} = \frac{\partial\left(-1/3\sigma_{kk}\right)}{\partial \sigma_{ij}} = -\frac{1}{3}\delta_{ij} \tag{B.9}$$

$$\frac{\partial q}{\partial \sigma_{ij}} = \frac{\partial\sqrt{3J_2}}{\partial \sigma_{ij}} = \frac{\sqrt{3}}{2}\frac{1}{\sqrt{J_2}}\frac{\partial J_2}{\partial \sigma_{ij}} = \frac{\sqrt{3}}{2}\frac{1}{\sqrt{J_2}}s_{ij} = \frac{3}{2}\frac{1}{q}s_{ij} \tag{B.10}$$

$$\frac{\partial \theta}{\partial \sigma_{ij}} = \frac{1}{3}\frac{-1}{\sqrt{1-\left(\frac{3\sqrt{3}}{2}\frac{J_3}{J_2^{3/2}}\right)^2}}\frac{3\sqrt{3}}{2}\left(\frac{\partial J_3}{\partial \sigma_{ij}}\frac{1}{J_2^{3/2}} - \frac{3}{2}J_3\frac{\partial J_2}{\partial \sigma_{ij}}\frac{1}{J_2^{5/2}}\right) =$$

$$= \frac{1}{3\sqrt{1-\left(\frac{3\sqrt{3}}{2}\frac{J_3}{J_2^{3/2}}\right)^2}}\frac{3\sqrt{3}}{2}\left(-t_{ij}\frac{1}{J_2^{3/2}} + \frac{3}{2}J_3 s_{ij}\frac{1}{J_2^{5/2}}\right) =$$

$$= \frac{1}{\sin 3\theta}\frac{\sqrt{3}}{2}\left(\frac{3}{2}J_3\frac{1}{J_2^{5/2}}s_{ij} - \frac{1}{J_2^{3/2}}t_{ij}\right) = \frac{\sqrt{3}}{2}\frac{1}{\sin 3\theta}\left(\frac{\sqrt{3}\cos 3\theta}{q^2}s_{ij} - \frac{3\sqrt{3}}{q^3}t_{ij}\right) =$$

$$= \frac{3}{2}\frac{\cos 3\theta}{q^2 \sin 3\theta}s_{ij} - \frac{9}{2}\frac{1}{q^3 \sin 3\theta}t_{ij}. \tag{B.11}$$

B.2. The second derivatives of stress invariants *p*, *q*, θ

The second derivatives of the potential function Q can be written as:

$$\frac{\partial^2 Q}{\partial \sigma_{pq}\partial \sigma_{mn}} = \frac{\partial\left(\frac{\partial Q}{\partial \sigma_{pq}}\right)}{\partial \sigma_{mn}} = \frac{\partial\left(\frac{\partial Q}{\partial p}\frac{\partial p}{\partial \sigma_{pq}} + \frac{\partial Q}{\partial q}\frac{\partial q}{\partial \sigma_{pq}} + \frac{\partial Q}{\partial \theta}\frac{\partial \theta}{\partial \sigma_{pq}}\right)}{\partial \sigma_{mn}} =$$

$$= \frac{\partial\left(\frac{\partial Q}{\partial p}\right)}{\partial \sigma_{mn}}\frac{\partial p}{\partial \sigma_{pq}} + \frac{\partial Q}{\partial p}\frac{\partial^2 p}{\partial \sigma_{pq}\partial \sigma_{mn}} + \frac{\partial\left(\frac{\partial Q}{\partial q}\right)}{\partial \sigma_{mn}}\frac{\partial q}{\partial \sigma_{pq}} + \frac{\partial Q}{\partial q}\frac{\partial^2 q}{\partial \sigma_{pq}\partial \sigma_{mn}} +$$

$$+\frac{\partial\left(\dfrac{\partial Q}{\partial\theta}\right)}{\partial\sigma_{mn}}\frac{\partial\theta}{\partial\sigma_{pq}}+\frac{\partial Q}{\partial\theta}\frac{\partial^2\theta}{\partial\sigma_{pq}\partial\sigma_{mn}}=$$

$$=\left(\frac{\partial^2 Q}{\partial p^2}\frac{\partial p}{\partial\sigma_{mn}}+\frac{\partial^2 Q}{\partial p\partial q}\frac{\partial q}{\partial\sigma_{mn}}+\frac{\partial^2 Q}{\partial p\partial\theta}\frac{\partial\theta}{\partial\sigma_{mn}}\right)\frac{\partial p}{\partial\sigma_{pq}}+\frac{\partial Q}{\partial p}\frac{\partial^2 p}{\partial\sigma_{pq}\partial\sigma_{mn}}+$$

$$+\left(\frac{\partial^2 Q}{\partial p\partial q}\frac{\partial p}{\partial\sigma_{mn}}+\frac{\partial^2 Q}{\partial q^2}\frac{\partial q}{\partial\sigma_{mn}}+\frac{\partial^2 Q}{\partial p\partial\theta}\frac{\partial\theta}{\partial\sigma_{mn}}\right)\frac{\partial q}{\partial\sigma_{pq}}+\frac{\partial Q}{\partial q}\frac{\partial^2 q}{\partial\sigma_{pq}\partial\sigma_{mn}}+$$

$$+\left(\frac{\partial^2 Q}{\partial\theta\partial p}\frac{\partial p}{\partial\sigma_{mn}}+\frac{\partial^2 Q}{\partial\theta\partial q}\frac{\partial q}{\partial\sigma_{mn}}+\frac{\partial^2 Q}{\partial\theta^2}\frac{\partial\theta}{\partial\sigma_{mn}}\right)\frac{\partial\theta}{\partial\sigma_{pq}}+\frac{\partial Q}{\partial\theta}\frac{\partial^2\theta}{\partial\sigma_{pq}\partial\sigma_{mn}},\qquad\text{(B.12)}$$

where the second derivatives of the stress invariants with respect to the stress are:

$$\frac{\partial^2 p}{\partial\sigma_{pq}\partial\sigma_{mn}}=\frac{\partial^2\left(-\dfrac{1}{3}\sigma_{kk}\right)}{\partial\sigma_{pq}\partial\sigma_{mn}}=\frac{\partial\left(-\dfrac{1}{3}\delta_{kp}\delta_{qk}\right)}{\partial\sigma_{mn}}=0\qquad\text{(B.13)}$$

$$\frac{\partial^2 q}{\partial\sigma_{pq}\partial\sigma_{mn}}=\frac{\partial\left(\dfrac{\partial q}{\partial\sigma_{pq}}\right)}{\partial\sigma_{mn}}=\frac{\partial\left(\dfrac{\sqrt{3}}{2}\dfrac{1}{\sqrt{J_{2D}}}s_{pq}\right)}{\partial\sigma_{mn}}=\frac{\sqrt{3}}{2}\frac{1}{\sqrt{J_{2D}}}\frac{\partial s_{pq}}{\partial\sigma_{mn}}+\frac{\sqrt{3}}{2}\frac{\partial\dfrac{1}{\sqrt{J_{2D}}}}{\partial\sigma_{mn}}s_{pq}=$$

$$=\frac{\sqrt{3}}{2}\frac{1}{\sqrt{J_{2D}}}\left(\delta_{pm}\delta_{nq}-\frac{1}{3}\delta_{pq}\delta_{km}\delta_{nk}\right)+\frac{\sqrt{3}}{2}\left(\frac{-1}{2}\left(\frac{1}{\sqrt{J_{2D}}}\right)^3 s_{mn}\right)s_{pq}=$$

$$=\frac{\sqrt{3}}{2}\frac{1}{\sqrt{J_{2D}}}\left(\delta_{pm}\delta_{nq}-\frac{1}{3}\delta_{pq}\delta_{mn}\right)-\frac{\sqrt{3}}{4}\left(\frac{1}{\sqrt{J_{2D}}}\right)^3 s_{mn}s_{pq}=$$

$$=\frac{3}{2q}\left(\delta_{pm}\delta_{nq}-\frac{1}{3}\delta_{pq}\delta_{mn}\right)-\frac{9}{4q^3}s_{mn}s_{pq}\qquad\text{(B.14)}$$

and

$$\frac{\partial^2\theta}{\partial\sigma_{pq}\partial\sigma_{mn}}=\frac{\partial(S\cdot s_{pq})}{\partial\sigma_{mn}}+\frac{\partial(T\cdot t_{pq})}{\partial\sigma_{mn}}=-\frac{9}{2q^4}\frac{\cos 3\theta}{\sin 3\theta}\left(1+\frac{3}{2}\frac{1}{\sin^2 3\theta}\right)s_{pq}s_{mn}+$$

$$+\frac{81}{4q^5}\frac{1}{\sin^3 3\theta}s_{pq}t_{mn}+\frac{81}{4q^5}\frac{1}{\sin 3\theta}\left(1+\frac{\cos^2 3\theta}{\sin^2 3\theta}\right)t_{pq}s_{mn}-\frac{243}{4q^6}\frac{\cos 3\theta}{\sin^3 3\theta}t_{pq}t_{mn}+$$

$$+\frac{3}{2q^2}\frac{\cos 3\theta}{\sin 3\theta}p_{pqmn}-\frac{9}{2q^3}\frac{1}{\sin 3\theta}w_{pqmn}, \tag{B.15}$$

where:

$$S=\frac{3}{2q^2}\frac{\cos 3\theta}{\sin 3\theta} \tag{B.16}$$

$$T=-\frac{9}{2q^3}\frac{1}{\sin 3\theta} \tag{B.17}$$

$$t_{ij}=\frac{\partial J_3}{\partial \sigma_{ij}} \tag{B.18}$$

$$p_{pqmn}=\frac{\partial s_{pq}}{\partial \sigma_{mn}}=\delta_{mp}\delta_{nq}-\frac{1}{3}\delta_{pq}\delta_{mn} \tag{B.19}$$

$$w_{pqmn}=\frac{\partial t_{pq}}{\partial \sigma_{mn}}=s_{np}\delta_{qm}+s_{qm}\delta_{np}-\frac{2}{3}s_{qp}\delta_{nm}-\frac{2}{3}s_{pq}\delta_{mn}. \tag{B.20}$$

APPENDIX C – Dynamics of discrete systems

C.1. System with one degree of freedom

C.1.1. Free vibrations, eigenvalue problem

The following equation of motion is considered:

$$m\ddot{q}(t) + c\dot{q}(t) + kq(t) = f(t). \tag{C.1}$$

The characteristic equation is obtained after substituting the solution of the homogeneous equation $q(t) = Ge^{st}$,

$$s^2 + \frac{c}{m}s + \omega^2 = 0 \quad \text{with} \quad \omega^2 = \frac{k}{m}, \tag{C.2}$$

where:

ω [rad/s] – angular frequency,

$f\left[\frac{1}{s} = \text{Hz}\right] = \frac{\omega}{2\pi}$ – frequency,

$T[s] = \frac{1}{f}$ – period.

C.1.2. Damping free vibration

The solutions to the homogeneous equation depend on the roots of the characteristic equation (C.2):

$$s_{1,2} = -\frac{c}{2m} \pm \sqrt{\left(\frac{c}{2m}\right)^2 - \omega^2}. \tag{C.3}$$

Solution (C3) consists of three cases depending on the value of the square root, which can be negative, positive or zero.

C.1.3. Case of sub-critical damping

A case in which the value of the square root in equation (C.3) is negative, i.e.

$$\left(\frac{c}{2m}\right)^2 - \omega^2 < 0 \tag{C.4}$$

or a case where the damping is less than the critical value i.e.

$$c < c_c \quad \rightarrow \quad c < 2m\omega.$$

The critical damping coefficient ξ *is introduces as:*

$$\xi \equiv \frac{c}{c_c} = \frac{c}{2m\omega} \quad \rightarrow \quad \frac{c}{m} = 2\xi\omega. \tag{C.5}$$

Now the equation of motion (C.5) can be written as:

$$\ddot{q}(t) + 2\xi\omega\dot{q}(t) + \omega^2 q(t) = \frac{1}{m} f(t). \tag{C.6}$$

Solution (C.3) is of the form:

$$s_{1,2} = -\xi\omega \pm i\omega_d \tag{C.7}$$

where:

$$\omega_d \equiv \omega\sqrt{1-\xi^2} \tag{C.8}$$

is the eigenfrequency of the system with viscous damping.

The solution to the homogeneous equation, taking into account (C.8) is

$$q(t) = G_1 e^{-\omega t + i\omega_D t} + t\,G_2 e^{-\omega t - i\omega_D t} = [G_1 e^{i\omega_D t} + G_2 e^{-i\omega_D t}] \cdot e^{-\omega t}, \tag{C.9}$$

where $G_1 = G_R + iG_I$, $G_2 = G_R + iG_I$.

Solution (C.9) can be represented by the following trigonometric functions:

$$q(t) = [A\cos\omega_d t + B\sin\omega_d t] \cdot e^{-\xi\omega t} \tag{C.10}$$

where:

$$A = 2G_R, \quad B = -2G_I. \tag{C.11}$$

Constants A and B are determined from the initial conditions, hence:

$$q(t) = \left[q(0)\cos\omega_d t + \left(\frac{\dot{q}(t) + q(0)\xi\omega}{\omega_d} \right) \sin\omega_d t \right] \cdot e^{-\xi\omega t} \tag{C.12}$$

Solution (C.12) can be written in another form as:

$$q(t) = G\cos(\omega_d t + \theta) \cdot e^{-\xi\omega t} \tag{C.13}$$

where:

$$G = \left\{ q(0)^2 + \left[\frac{\dot{q}(0) + q(0)\xi\omega}{\omega_d q(0)} \right]^2 \right\}^{1/2}, \quad \theta = -\arctan\left[\frac{\dot{q}(0) + q(0)\xi\omega}{\omega_d q(0)} \right]. \quad \text{(C.14)}$$

In practical calculations, the most widely used model is the viscous damping model – this is because it well describes the nature of the free vibration.

Consider the ratio of displacement q_n / q_{n+1} in two following time points $n(2\pi / \omega_d)$ and $(n+1)(2\pi / \omega_d)$. Substituting for (C.12) obtained:

$$q_n / q_{n+1} = e^{2\pi\xi\omega/\omega_d}. \quad \text{(C.15)}$$

Logarithms on both sides (C.15) and taking into account, $\omega_d = \omega\sqrt{1-\xi^2}$, *the logarithmic decrement of damping* δ is defined as:

$$\delta = \ln\frac{q_n}{q_{n+1}} = \frac{2\pi\xi}{\sqrt{1-\xi^2}}. \quad \text{(C.16)}$$

We are expanding in power series the exponential function

$$\frac{q_n}{q_{n+1}} = e^{\delta} = 1 + \delta + \frac{\delta^2}{2!} + \ldots \quad \text{(C.17)}$$

The approximation value of the logarithmic decrement of damping can be given by two components of a series in the form:

$$\frac{q_n}{q_{n+1}} = e^{\delta} \approx 1 + \delta \quad \rightarrow \quad \delta \approx \frac{q_n - q_{n+1}}{q_{n+1}}. \quad \text{(C.18)}$$

Assuming further $\omega / \omega_D \approx 1 \rightarrow \delta \approx 2\pi\xi$, the approximate value of the critical damping coefficient can be obtained:

$$\xi \approx \frac{q_n - q_{n+1}}{2\pi q_{n+1}} = \frac{\delta}{2\pi}. \quad \text{(C.19)}$$

If we consider two displacements with *m* periods distance, the similar formula to (C.17) can be obtained:

$$\ln\frac{q_n}{q_{n+m}} = \frac{2\pi m\xi}{\sqrt{1-\xi^2}} \quad \text{(C.20)}$$

$$\xi \approx \frac{q_n - q_{n+m}}{2\pi m q_{n+m}}. \quad \text{(C.21)}$$

C.1.4. General solution with subcritical viscous damping

The solution of equation (C.6) is the sum of free vibration $q_s(t)$ (general integral differential equation) and forced vibration $q_w(t)$ (special integral differential equation):

$$q(t) = q_s(t) + q_w(t) \tag{C.22}$$

The case of sub-critical damping is considered with $\xi < 1$. According to (C.10)

$$q_s(t) = Ae^{-\xi\omega t}\cos\omega_d t + Be^{-\xi\omega t}\sin\omega_d t = Aq_1(t) + Bq_2(t). \tag{C.23}$$

The special integral can be calculated according to the method of variables of constants A and B

$$q_w(t) = A(t)q_1(t) + B(t)q_2(t). \tag{C.24}$$

Substituting (C.24) into the equations of motion one can obtained:

$$A(t) = \frac{1}{m\omega_d}\int_0^t f(\tau)e^{\xi\omega\tau}\cos(\omega_d\tau)\,d\tau + C_1 \tag{C.25}$$

$$B(t) = \frac{1}{m\omega_d}\int_0^t f(\tau)e^{\xi\omega\tau}\sin(\omega_d\tau)\,d\tau + C_2 \tag{C.26}$$

Substituting (C.25) and (C.26) to (C.24) obtained the following special integral:

$$q_w(t) = \frac{1}{m\omega_d}\int_0^t f(\tau)e^{-\xi\omega(t-\tau)}\sin\omega_d(t-\tau)\,d\tau. \tag{C.27}$$

The solution to the equation of motion consists of solutions (C.23) and (C.27)

$$q(t) = e^{-\xi\omega t}(C_1\sin\omega_d t + C_2\cos\omega_d t) + \frac{1}{m\omega_d}\int_0^t f(\tau)e^{-\xi\omega(t-\tau)}\sin\omega_d(t-\tau)\,d\tau. \tag{C.28}$$

Constants C_1 and C_2 are determined from the initial conditions, for $t = 0$:

$$q(t) = q_0, \quad \dot{q}(t) = \dot{q}_0 \;\rightarrow\; C_1 = \frac{\dot{q}_0 + \xi\omega q_0}{\omega_d}, \quad C_2 = q_0. \tag{C.29}$$

Finally, the displacement for $t \geq 0$ is:

$$q(t) = e^{-\xi\omega t}\left[q_0\left(\cos\omega_d t + \frac{\xi\omega}{\omega_d}\sin\omega_d t\right) + \frac{\dot{q}_0}{\omega_d}\sin\omega_d t\right] +$$

$$+ \frac{1}{m\omega_d}\int_0^t f(\tau)e^{-\xi\omega(t-\tau)}\sin\omega_d(t-\tau)\,d\tau. \tag{C.30}$$

The special case: $q_0 = \dot{q}_0 = 0$:

$$q(t) = \frac{1}{m\omega_d} \int_0^t f(\tau) e^{-\xi\omega(t-\tau)} \sin\omega_d (t-\tau)\, d\tau. \tag{C.31}$$

Equation (C.31) is known as the *Duhamel integral*.

The velocity was obtained by differentiating equation (C.30)

$$\dot{q}(t) = e^{-\xi\omega t}\left\{-\frac{\omega^2 q_0}{\omega_d}\sin\omega_d t + \dot{q}_0\left[\cos\omega_d t - \frac{\xi\omega}{\omega_d}\sin\omega_d t\right]\right\} +$$

$$+\frac{1}{m\omega_d}\int_0^t f(\tau) e^{-\xi\omega(t-\tau)}\left[\cos\omega_d (t-\tau) - \frac{\xi\omega}{\omega_d}\sin\omega_d (t-\tau)\right] d\tau. \tag{C.32}$$

Finally, acceleration, according to the equation of motion is:

$$\ddot{q}(t) = f(t) - 2\xi\omega\dot{q}(t) - \omega^2 q(t). \tag{C.33}$$

C.1.5. Solution in range of time step Δt

The following solution to equations of motion in the time interval is considered: $t_n \le t \le t_n + \Delta t$, where $\Delta t = t_{n+1} - t_n$. By substituting the initial conditions $q(t_n) = q_n$ and $\dot{q}(t_n) = \dot{q}_n$ to equation (C.30) and (C.32), one can obtain:

$$q(t) = e^{-\xi\omega(t-t_n)}\left\{q_n\left[\cos\omega_d (t-t_n) + \frac{\xi\omega}{\omega_d}\sin\omega_d (t-t_n)\right] + \frac{\dot{q}_0}{\omega_d}\sin\omega_d (t-t_n)\right\} +$$

$$+\frac{1}{m\omega_d}\int_0^t f(\tau) e^{-\xi\omega(t-\tau)}\sin\omega_d (t-\tau)\, d\tau \tag{C.34a}$$

$$\dot{q}(t) = e^{-\xi\omega(t-t_n)}\left\{-q_n\frac{\omega^2}{\omega_d}\sin\omega_d (t-t_n) + \dot{q}_n\left[\cos\omega_d (t-t_n) - \frac{\xi\omega}{\omega_d}\sin\omega_d (t-t_n)\right]\right\} +$$

$$+\frac{1}{m\omega_d}\int_0^t f(\tau) e^{-\xi\omega(t-\tau)}\left[\cos\omega_d (t-\tau) - \frac{\xi\omega}{\omega_d}\sin\omega_d (t-\tau)\right] d\tau. \tag{C.34b}$$

The displacement, velocity and acceleration at the end of time step $t = t_{n+1}$ are:

$$q(t_{n+1}) = e^{-\xi\omega\Delta t}\left\{q_n\left[\cos\omega_d \Delta t + \frac{\xi\omega}{\omega_d}\sin\omega_d \Delta t\right] + \frac{\dot{q}_n}{\omega_d}\sin\omega_d \Delta t\right\} +$$

$$+\frac{1}{m\omega_d}\int_{t_n}^{t_{n+1}} f(\tau) e^{-\xi\omega(t-\tau)}\sin\omega_d (t-\tau)\, d\tau \tag{C.35a}$$

$$\dot{q}(t_{n+1}) = e^{-\xi\omega\Delta t}\left\{-q_n\frac{\omega^2}{\omega_d}\sin\omega_d\Delta t + \dot{q}_n\left[\cos\omega_d\Delta t - \frac{\xi\omega}{\omega_d}\sin\omega_d\Delta t\right]\right\} +$$

$$+\frac{1}{m\omega_d}\int_{t_n}^{t_{n+1}} f(\tau)e^{-\xi\omega(t-\tau)}\left[\cos\omega_d(t-\tau) - \frac{\xi\omega}{\omega_d}\sin\omega_d(t-\tau)\right]d\tau. \qquad \text{(C.35b)}$$

Neglecting the damping, with $\xi = 0$ obtained:

$$q(t_{n+1}) = \left(q_n\cos\omega\Delta t + \frac{\dot{q}_n}{\omega}\sin\omega\Delta t\right) + \frac{1}{m\omega}\int_{t_n}^{t_{n+1}} f(\tau)\sin\omega(t-\tau)d\tau \qquad \text{(C.36a)}$$

$$\dot{q}(t_{n+1}) = \{-q_n\omega\sin\omega\Delta t + \dot{q}_n\cos\omega\Delta t\} + \frac{1}{m\omega}\int_{t_n}^{t_{n+1}} f(\tau)\cos\omega(t-\tau)d\tau. \qquad \text{(C.36b)}$$

or with matrix notation:

$$\begin{Bmatrix} q(t_{n+1}) \\ \dot{q}(t_{n+1}) \end{Bmatrix} = \begin{bmatrix} \cos\omega\Delta t & \frac{1}{\omega}\sin\omega\Delta t \\ -\omega\sin\omega\Delta t & \cos\omega\Delta t \end{bmatrix}\begin{Bmatrix} q(t_n) \\ \dot{q}(t_n) \end{Bmatrix} + \frac{1}{m\omega}\begin{Bmatrix} \int_{t_n}^{t_{n+1}} f(\tau)\sin\omega(t-\tau)\,d\tau \\ \int_{t_n}^{t_{n+1}} f(\tau)\cos\omega(t-\tau)\,d\tau \end{Bmatrix} \qquad \text{(C.37a)}$$

or

$$\begin{Bmatrix} q(t_{n+1}) \\ \dot{q}(t_{n+1}) \end{Bmatrix} = \mathbf{A}\begin{Bmatrix} q(t_n) \\ \dot{q}(t_n) \end{Bmatrix} + \mathbf{L}_n^{n+1}, \qquad \text{(C.37b)}$$

where:

$$\mathbf{A} = \begin{bmatrix} \cos\omega\Delta t & \frac{1}{\omega}\sin\omega\Delta t \\ -\omega\sin\omega\Delta t & \cos\omega\Delta t \end{bmatrix}, \quad \mathbf{L}_n^{n+1} = \frac{1}{m\omega}\begin{Bmatrix} \int_n^{n+1} f(\tau)\sin\omega(t-\tau)\,d\tau \\ \int_n^{n+1} f(\tau)\cos\omega(t-\tau)\,d\tau \end{Bmatrix}. \qquad \text{(C.37c)}$$

Eigenvalues of **A** matrix are complex numbers which module equal unity. This means that in calculation with **A** matrix, the transition from time t to time $t + \Delta t$ (with $\xi = 0$ and no-load dynamic $\mathbf{L} = 0$) displacement and velocity amplitude does not change regardless of the length of the time step Δt.

C.2. Basic equation of dynamics

C.2.1. Newton's second law

The change of momentum of a mass point is equal to the resultant force acting on that mass

$$\frac{\mathrm{d}}{\mathrm{d}t}\left(m\frac{\mathrm{d}\overline{q}}{\mathrm{d}t}\right)=\overline{f}, \tag{C.38}$$

where:

m – mass point,

$\overline{q}$ – the displacement vector,

$\overline{f}$ – the resultant force vector.

C.2.2. D'Alembert principle and the principle of virtual work

D'Alembert principle:

The system of masses with n degrees of freedom are always in equilibrium, if to the existing forces acting on the system $\overline{f}_i(t)$ will be added the inertia forces $\overline{b}_i(t)$:

$$\sum\nolimits_{i=1}^{n}\overline{f}_i(t)+\sum\nolimits_{i=1}^{n}\overline{b}_i(t)=0 \tag{C.39}$$

Principle of virtual work:

A system of n degrees of freedom will be in equilibrium if the total work done by external and internal forces on virtual displacements is zero:

$$\sum\nolimits_{i=1}^{n}[\overline{f}_i(t)+\overline{b}_i(t)]\delta\overline{q}_i=0, \tag{C.40}$$

where:

$\delta\overline{q}_i$ – the virtual displacement of i-th point.

C.2.3. Lagrange equation

Let $\overline{q}_i$ the physical coordinates of the n degrees of freedom does not explicitly depend on time and can be described by the generalized coordinates x_i defined as:

$$q_i=q_i(x_1,x_2,\ldots,x_n),\quad i=1,2,\ldots,n. \tag{C.41}$$

The system will be in balance when

$$\frac{\mathrm{d}}{\mathrm{d}t}\left(\frac{\partial L}{\partial\dot{x}_l}\right)-\frac{\partial L}{\partial x_l}=Q_l,\quad l=1,2,\ldots,n, \tag{C.42}$$

where:

$L=E_k-E_p$ – Lagrange function,

E_k – kinetic energy,

E_p – potential energy,
Q_l – generalized conservative force. In the case of conservative forces $Q_l = Q$.

C.2.4. Hamilton's principle

Variation of a integral with respect to the time of the Lagrangian function is zero in the case of real motion. If the virtual displacement $\delta\overline{q}_i(t)$ is equal to zero at the initial time $t = t_1$ and final time $t = t_2$, then:

$$\delta \int_{t_1}^{t_2} (E_k - E_p)\,\mathrm{d}t = 0 \tag{C.43a}$$

and

$$\delta\overline{q}_i(t_1) = \delta\overline{q}_i(t_2) = 0, \quad i = 1,2,\ldots,n. \tag{C.43b}$$

C.3. Equation of motion of discrete systems

A system with a finite number of degrees of freedom is called a discrete system. The process of replacing the continuous system with a discrete system is called the method of discretization.

The potential energy of structures built with the linear-elastic material is a quadratic function of the displacement and is given by:

$$E_s = \frac{1}{2}\sum_{i=1}^{n}\sum_{j=1}^{n} k_{ij} q_i(t) q_j(t) = \frac{1}{2}\mathbf{q}^T(t)\mathbf{K}\mathbf{q}(t), \tag{C.44}$$

where:
k_{ij} – are stiffness coefficients,
$\mathbf{K}$ – the stiffness matrix.

The kinetic energy of a discrete system is given by:

$$E_k = \frac{1}{2}\sum_{i=1}^{n} m_i \dot{q}_i^2(t) = \frac{1}{2}\dot{\mathbf{q}}^T(t)\mathbf{M}\dot{\mathbf{q}}(t), \tag{C.45}$$

where:
m_i – are discrete masses (lumped masses),
$\mathbf{M}$ – a mass matrix or inertia matrix.

The system may include discrete viscous dampers, which are damping forces $\mathbf{f}_d(t)$:

$$\mathbf{f}_d(t) = \sum_{i=1}^{n} c_i \dot{q}_i(t) = \mathbf{C}\dot{\mathbf{q}}(t), \tag{C.46}$$

where:

c_i – are the viscous damping coefficients,

$\mathbf{C}$ – the damping matrix.

Damping forces are not conservative, virtual work of these forces on virtual displacements $\delta\mathbf{q}(t)$ is given by:

$$\delta W_d = \delta\mathbf{q}^T(t)\mathbf{f}_d(t). \tag{C.47}$$

Work of excitation forces is given by:

$$\delta W_w = \delta\mathbf{q}^T(t)\mathbf{p}(t). \tag{C.48}$$

The potential energy of the system with excitation of the conservative forces is:

$$E_p = E_s - E_w. \tag{C.49}$$

Substituting equations (C.44)–(C.49) to the Lagrange equations (C.42) obtained the following equation of motion of the discrete system:

$$\mathbf{M}\ddot{\mathbf{q}}(t) + \mathbf{C}\dot{\mathbf{q}}(t) + \mathbf{K}\mathbf{q}(t) = \mathbf{p}(t) \tag{C.50}$$

with the initial conditions: $\mathbf{q}(t = t_0) = \mathbf{q}_0$, $\dot{\mathbf{q}}(t = t_0) = \dot{\mathbf{q}}_0$.

C.4. References

Argyris J., Mlejnek H.-P. (1991): *Dynamics of Structures*, North-Holland.

Clough R.W., Penzien J. (1995): *Dynamics of Structures*, Second edition, Mc Graw-Hill International.

Lewandowski R. (2006): *Dynamics of building structures*, Poznan University of Technology (in Polish).

Rao S.S. (2007): *Vibration of Continuous Systems*, John Wiley&Sons, Inc.

APPENDIX D – Dynamic parameters of soil, construction and building materials

D.1. Velocity of dilation waves v_L, shear waves v_S, and Rayleigh waves v_R in soil and materials

Table D.1

(Ciesielski, 1973)

Soil, Material	v_L [m/s]	v_S [m/s]	v_R [m/s]
Sand	200–1500	100–250	90–225
Fine sand	500	110	100
Medium sand	550	160	150
Gravel with sand	–	180–550	160–500
Gravel	760	180	160
Compacted gravel with sand	480	250	220
Clay	500–1500	150–200	150–180
Less	800	260	250
Sandstone not weathered		1100	1050
Sandstone weathered		500	460
Rocks	2000–6000	1000–2000	960–1960
Simple steel	5000		
Concrete (average)	1700		
Wood parallel to fibres	3000		
Cork	130		
Water	1440		
Air	340		

D.2. Values of dynamic modulus of soil elasticity

Table D.2

(Lipiński, 1985)

Type of soil	E_{dyn} [MPa]
Cohesionless soils	
Loose sands	1.5–3.0
Medium dense sands	2.0–5.0
Gravel, rubble	3.0–8.0
Cohesive soils	
Solid clay	1.0–5.0
Semi-solid clay	0.4–1.5
Plastic clay	0.3–0.8
Silt	0.3–1.0
Mud	0.1–0.3

D.3. Modulus of elasticity of construction materials used in calculation of dynamic structures

Table D.3

(Lipiński, 1985)

Type of material	Modulus of elasticity E [GPa]	Shear modulus G [GPa]	Poisson coefficient
Reinforced concrete, with concrete class: – C12/15 – C16/20 – C20/25 – C25/30 – C30/37	 23.1 27.0 30.0 32.4 34.4	0.45E	1/6
Steel	205	80	0,30
Brick wall: – full regular brick on cement mortar of strength 8 MPa – clinker brick on cement mortar of strength 8 MPa	 3 to 5 8 to 13	 0.8 to 2.5 2 to 6.5	 0.16 to 0.30
Wood: – along the fibre – across the fibre	 8 to 11.5 0.35 to 0.48	0.5 to 0.7	–
Natural cork with a static pressure: – 50 GPa – 100 GPa – 200 GPa	 150 200 230	~0.4 E	0.00

D.4. Factors determining of damping

The fundamental relationship

$$\xi = \frac{\delta}{\pi},$$

where:

δ [–] – logarithmic decrement of damping,
ξ [–] – coefficient of critical damping.

Table D.4

Value $\xi \cdot 100$ [%] of different constructions (Ciesielski, 1973)

Type of construction	Value $\xi \cdot 100$ [%]		
	Maximum	Average	Recommended
1	2	3	4
Steel structures			
Beams and steel frames	1.0–4.0	1.2–2.0	1.5
Trusses	2.0–8.0	3.1–4.7	3.5
Thin-wall structures	1.0–2.5	1.0–1.6	1.2
Concrete structures			
Reinforced concrete beams and frames	2.5–12.5	4.1–7.8	4.5
Reinforced concrete floors, ribs	5.1–12.5	7.0–8.8	6.0
Ceilings big plates	3.2–9.5	3.5–8.3	5.5
Compressed elements	to 4.8	1.6–2.5	1.6
Foundations and concrete blocks	9.5–20.0	12.0	10
Buildings made of reinforced concrete frame with brick filling	5.0–10.0	7.5	8.0
Masonry (only compressive stress)			
Brick walls	3.2–10.0	6.0–8.0	8.0
Ceilings and brick pillars	1.5–10.0	4.5	4.5
Brick masonry buildings with a height of 7 to 25 m	7.5–12.0	9.5	9.5
Stone walls in lime-cement mortar or cement	4.0–10.0	7.5	9.5
Wooden structures			
Ordinary wooden beams and glulam	1.0–6.5	1.5–4.5	3.0
Beams complex and nail beams	3.0–6.5	4.5	4.5
Wood floors	3.5–7.5	5.0–6.5	4.5

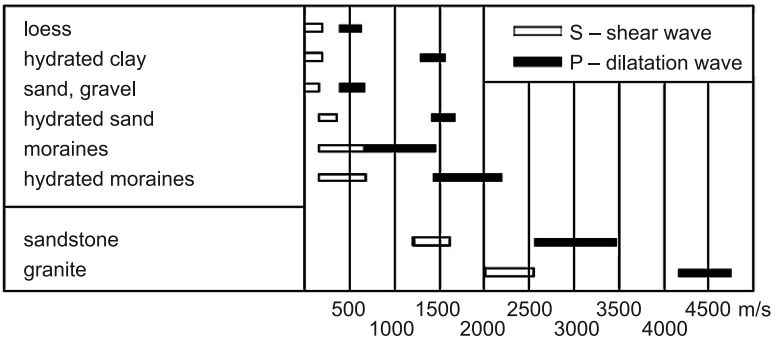

Fig. D.1. Wave velocity of dilatation and shear wave for different kind of soil (CEB, 1991)

D.5. Dynamic characteristics of soil

Table D.5 shows the values of Poisson's ratio ν for different soils. Next, Table D.6 shows the values of shear modulus G at small shear strain $\gamma \approx 10^{-6}$ for various soils.

Table D.5

Poisson's ratio ν for different soils

Type of soil	Poisson's ratio ν
Clay	0.40–0.45
Sand	0.30–0.40
Rock	0.15–0.25

Table D.6

Shear modulus G for different soils

Type of soil	G [MN/m^2]
Cohesionless soils	
Loose sand	50–120
Medium compacted sand	70–170
Gravel and sand compacted	100–300
Cohesive soils	
Mud, marine silt	3–10
Clay	20–50
Silt with clay	80–300
Rock	
Layered, fragile	1 000–5 000
Solid rock	4 000–20 000

The value of the dynamic shear modulus G_d and the critical damping coefficient ξ depends on the value of the shear strain of soil γ. When the shear strain of soil tends to $\gamma \rightarrow 10^{-2}$, then the dynamic shear modulus goes to zero $G_d \rightarrow 0$, and the critical damping ratio tends to unity $\xi \rightarrow 1$ (see Figure D.2).

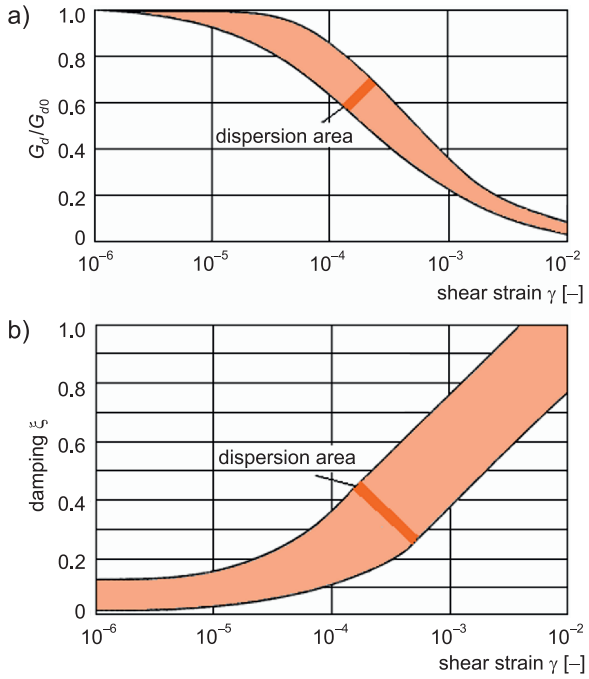

Fig. D.2. Effect of change of shear strain γ on: a) dynamic shear modulus G_d, b) critical damping ratio ξ (Smoltczyk, 2002)

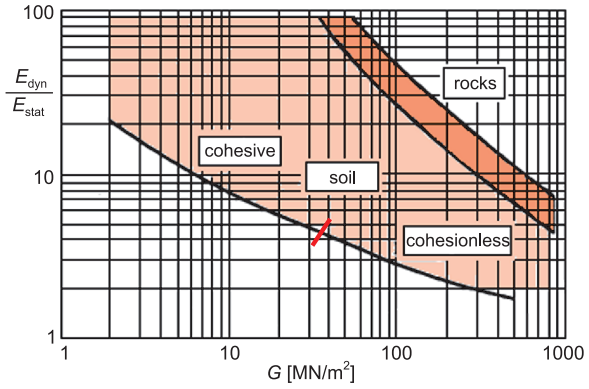

Fig. D.3. The ratio of dynamic modulus of elasticity to static modules E_{dyn}/E_{stat} depending on the shear modulus G (Alpen, 1970)

Figure D3 shows the ratio of dynamic to static elasticity modulus E_{dyn}/E_{stat}, depending on the shear modulus G (Alpen, 1970).

The elasticity modulus in the case of a static load is smaller than in the case of dynamic loads. Table D.7 shows the values of both modules for different types of soil.

Table D.7

Elasticity modulus in the case of dynamic loads for various soil types

Soil type	E – elasticity modulus [MN/m^2]	
	E_{static}	$E_{dynamic}$
Cohesionless soil		
Grainy smooth loose sand	40–80	150–300
Grainy sharp loose sand	50–80	150–300
Average compacted of grainy smooth sand	80–160	200–500
Average compacted of grainy sharp sand	100–200	200–500
Gravel without sand	100–200	300–800
Grainy sharp broken stone	150–300	300–800
Cohesive soil		
Solid clay	3–50	100–500
Semi-solid clay	6–20	40–150
Plastic clay	3–6	30–80
Silt, glacial clay	6–50	100–500
Clay, loess	4–8	50–150
Rare mule	3–8	30–100
Mule, drift sea, organic soil	2–5	10–30

D.6. Soil liquefaction

During earthquakes in ground consisting of fine sands, the liquefaction phenomenon takes place which is manifested by a shear strength decrease. The threat of liquefaction increases with the intensity and duration of the earthquake, it also depends on ground water table level – as this decreases, soil compaction increases. In Part 5 of Eurocode 8, the conditions under which liquefaction may occur are considered. Specified actions are as follows:

1. Identifying the soil grading curve position on a grading diagram as shown in Figure D.4.
2. Determination of F_t factor according to the formula:

$$F_t = r_d \frac{\sigma}{\sigma'} \; [-] \tag{D.1}$$

where:

- σ – total load stress from building and irrigation soil up to t depth,
- σ' – effective load stress from building and irrigation soil up to t depth,
- r_d – reduction factor according to Figure D.5.

3. Determination of the possibility of the occurrence of liquefaction based on $I_D - F_t$ chart shown in Figure D.6.

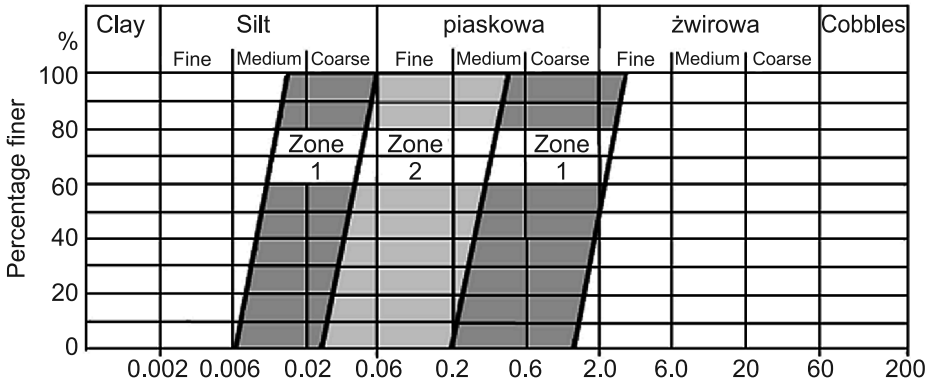

Fig. D.4. Areas of the grain size distribution curve

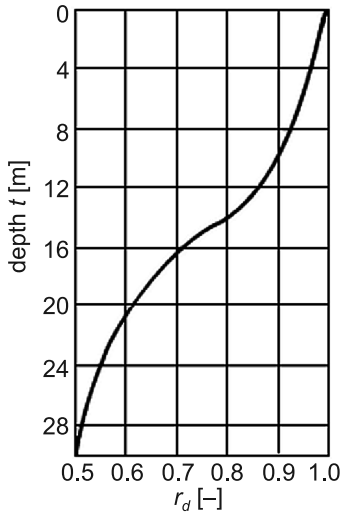

Fig. D.5. Reduction factor r_d dependent on depth t

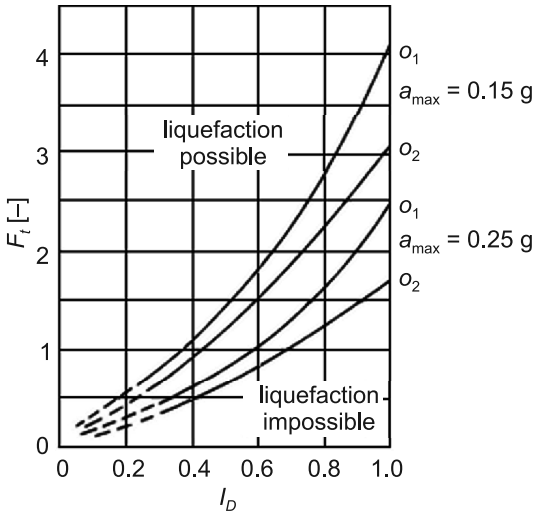

Fig. D.6. Possibility of soil liquefaction occurrence during an earthquake

D.7. Wave velocity in two phase soil model

Below, diagrams of velocity and damping of slow and fast dilatational wave depending on the excitation frequency are shown (Young, 2000), in the case of sand (Figure D.7) and in the case of clay (Figure D.8).

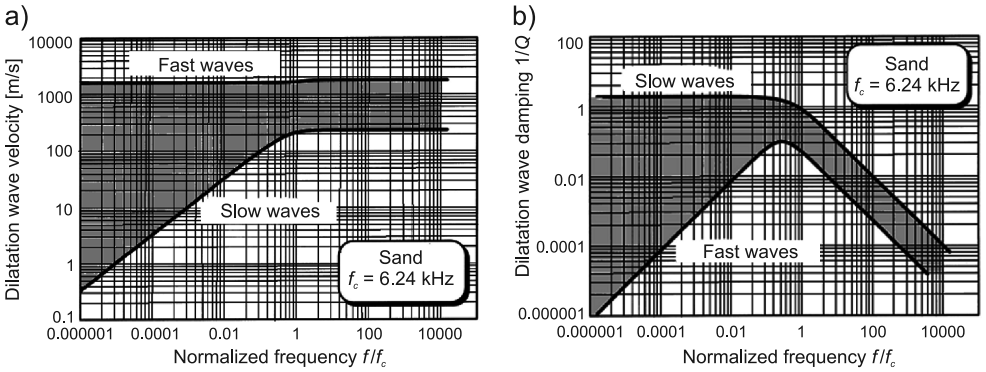

Fig. D.7. Velocity and damping of slow and fast dilatational waves in sand (Yang, 2000)

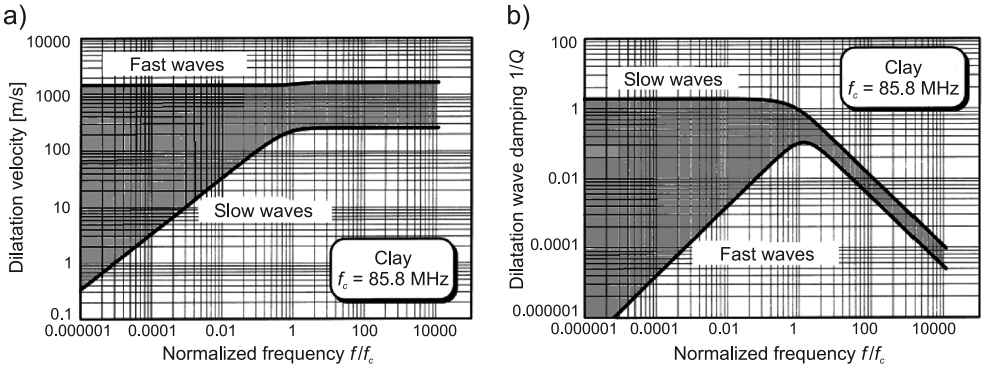

Fig. D.8. Velocity and damping of slow and fast dilatational waves in clay (Yang, 2000)

D.8. References

Alpen I. (1970): *The Geotechnical Properties of Soils*, *Earth-Science Proceedings*.

CEB (1991): *Vibration Problems in Structures*, Lausanne, CEB Bulletin d'Information, No. 209.

Ciesielski R. (1973): *Estimation of influence of dynamic load in buildings*, Arkady, Warszawa (in Polish).

Lipiński J. (1985): *Foundations for machines*, Arkady, Warszawa (in Polish).
Smoltczyk U. (2002): *Geotechnical Engineering Handbook*, John Wiley & Sons, Berlin.
Yang J., Sato T. (2000): *Comparison of individual contributions of two compression waves in vibration of water-saturated soils*, Computers and Geotechnics, 27, 79-100.